UNIVERSIDADE FEDERAL DO RIO GRANDE DO SUL
INSTITUTO DE GEOCIÊNCIAS
PROGRAMA DE PÓS-GRADUAÇÃO EM GEOCIÊNCIAS

CONTROLES DEPOSICIONAIS SOBRE OS PADRÕES DIAGENÉTICOS DOS ARENITOS DO CRETÁCEO INFERIOR DA BACIA DE JEQUITINHONHA, MARGEM SUDESTE DO BRASIL

Celso Moura Jardim

Orientador: Prof. Dr. Luiz Fernando De Ros – UFRGS / IG

Co-Orientador: Prof. Dr. João Marcelo Medina Ketzer - PUCRS

Banca examinadora:

Dr. Almério Barros França – PETROBRAS E&P
Dr. Claiton Marlon dos Santos Scherer – UFRGS / IG
Dr. Rogério Schiffer de Souza – PETROBRAS CENPES

Dissertação de mestrado apresentada como requisito parcial para obtenção do título de Mestre em Geociências

Porto Alegre - 2008

Jardim, Celso Moura
Controles deposicionais sobre os padrões diagenéticos dos arenitos do cretáceo inferior da Bacia de Jequitinhonha, margem sudeste do Brasil. / Celso Moura Jardim. - Porto Alegre : IGEO/UFRGS, 2008.
[175 f.] il.

Dissertação (Mestrado). - Universidade Federal do Rio Grande do Sul. Instituto de Geociências. Programa de Pós-Graduação em Geociências. Porto Alegre, RS - BR, 2008.

1. Estratigrafia de Seqüências. 2. Diagênese Clástica. 3. Qualidade de Reservatório. 4. Petrofácies . 5. Exploração de Petróleo. I. Título.

_____
Catalogação na Publicação
Biblioteca Geociências - UFRGS
Renata Cristina Grun CRB 10/1113

Agradecimentos

Agradeço à PETROBRAS por ter me proporcionado esta oportunidade de crescimento profissional, em especial ao Dr. Paulo de Tarso Guimarães e Marcos V. Galvão, pela aprovação e concessão para dedicação em tempo integral para o desenvolvimento dessa dissertação de mestrado. Agradeço também aos meus gerentes imediatos, Dr. José Antonio Cupertino e Alexandre Grassi, pelo apoio durante o desenvolvimento do projeto de pesquisa que antecedeu a minha ida para Porto Alegre.

Aos colegas da gerência de Sedimentologia e Estratigrafia da UN-BA, em especial a Nadja Fisher, Lucia Freire e Rita Koga, pelo apoio durante as atividades de descrição e coleta de material nos testemunhos utilizados nesse estudo. Aos colegas da gerência de Sedimentologia e Estratigrafia de Macaé, em especial a Helga Volker, pela confecção de material utilizado nessa dissertação.

Aos colegas do CENPES, em especial ao Dr. Rogério Schiffer e Dra. Dolores Carvalho, pela liberação de lâminas petrográficas utilizadas nesse estudo.

Aos colegas Viviane Santos, Rangel dos Santos Filho e Roberto D'Ávila, pelo apoio prestado na discussão de alguns resultados, bem como nas sugestões e críticas construtivas que ajudaram a elaborar o projeto de estudo.

Aos colegas Álvaro Arouca e Glauco Bragança pelas sugestões durante o desenvolvimento dessa dissertação, e.

Aos amigos e funcionários do Programa de Pós-Graduação em Estratigrafia, por toda a gentileza e presteza com que me receberam e atenderam durante esses dois anos em Porto Alegre.

Aos meus orientadores, com muita gratidão pelos ensinamentos e dedicação ao meu projeto, mesmo quando obrigados a trabalhar nas férias. Agradeço também a Magali Abel, pela paciência e compreensão.

Durante esse tempo foram muitas as pessoas que contribuíram para esta dissertação. Peço desculpas para aquelas pessoas que esqueci de citar aqui.

Resumo

O estudo de arenitos, calcarenitos e arenitos híbridos do Cretáceo Inferior (Neo-Aptiano ao Meso-Albiano) da Bacia de Jequitinhonha, margem leste Brasileira, compreendendo depósitos continentais fluvio-deltaicos a lacustres da fase rifte, e fluvio-deltaicos costeiros e de plataforma mista siliciclástico-carbonática da fase transicional a drifte, demonstra que a distribuição das alterações diagenéticas e correspondente evolução da qualidade de reservatório podem ser preditas dentro de um contexto de estratigrafia de seqüências. Dados de poços (descrições de testemunhos e perfis elétricos), descrição petrográfica de laminas delgadas, e análises petrofísicas de porosidade e permeabilidade, foram integrados de modo a identificar e avaliar os aspectos genéticos dos parâmetros que controlam os padrões diagenéticos, e, por conseguinte, a qualidade de reservatório dos intervalos estudados. Os resultados desse estudo são relevantes para a exploração de bacias de margem passiva do tipo Atlântico. Foi demonstrada a influëncia de fatores deposicionais (i.e fácies sedimentares) e composição detrítica original (i.e. proveniência) na evolução diagenética, permitindo estimar e predizer a distribuição da qualidade e heterogeneidade de reservatório dos intervalos estudados. A integração dos dados e posterior avaliação da qualidade de reservatório desenvolvida nesse estudo foi baseada no conceito de *petrofácies de reservatório*, o qual consiste no agrupamento de amostras com base nos principais atributos responsáveis pela qualidade de reservatório, tais como composição primária, estruturas deposicionais, granulometria, seleção, alterações diagenéticas mais influentes na redução ou preservação da porosidade e permeabilidade originais, tipos e distribuição de poros, etc.. Essa dissertação demonstra que o conceito de petrofácies de reservatório que permite o reconhecimento sistemático dos atributos petrográficos que controlam as características (i.e. assinaturas) petrofísicas e geofísicas, bem como a redução dos riscos exploratórios.

Palavras-chave: sistemas deposicionais, estratigrafia de seqüências, diagênese clástica, qualidade de reservatórios, petrofácies, exploração de petróleo

Abstract

A study of the fluvial, deltaic, and shallow-marine siliciclastic sandstones, calcarenites and hybrid arenites of Lower Cretaceous (Late Aptian to Early Albian) rift to early drift phase from the Jequitinhonha Basin, eastern Brazilian margin, reveals that the distribution of diagenetic alterations and of related reservoir quality evolution can be constrained within a sequence stratigraphic framework. Description of cores, wireline logs, thin sections, and petrophysical porosity and permeability analyses were integrated in order to unravel the genetic aspects that controlled the complex patterns of diagenesis of these rocks, and hence their reservoir quality evolution. The results of this study are relevant to the exploration of rift and an early drift phase of Atlantic-type passive margin basins, and demonstrate the influence of depositional factors such as sedimentary facies and detrital composition (provenance) on diagenetic and reservoir evolution, with application to the prediction of reservoir quality and heterogeneity during exploration. The data integration and reservoir quality assessment performed in this paper was accomplished using the concept of reservoir petrofacies, defined by the combination of the main attributes affecting the quality of petroleum reservoirs (such as depositional structures, textures, composition, diagenetic processes and products, pore types and distribution, etc.). This paper demonstrate that the reservoir petrofacies concept is a tool for the systematic recognition of the petrographic attributes that control the petrophysical and geophysical properties, as well as the practical use of this approach in reducing exploration risks.

Keywords: depositional systems, sequence stratigraphy, clastic diagenesis, reservoir quality, petrofacies, petroleum exploration

Sumário

Sobre a estrutura desta dissertação:

Esta dissertação de Mestrado está estruturada em torno de dois artigos submetidos a periódicos internacionais. Sua organização compreende as seguintes partes principais:

a) **Introdução**: contendo objetivos, revisão conceitual sobre o tema influência de parâmetros e fácies deposicionais sobre a evolução de padrões diagenéticos em arenitos e arenitos híbridos, com ênfase nas fases eodiagenéticas, a descrição da metodologia utilizada, e análise integradora onde são apresentados, de forma condensada, a interpretação dos resultados obtidos;

b) **Corpo principal**: artigos "*Depositional controls on the diagenetic patterns of Lower Cretaceous sandstones from the Jequitinhonha Basin, Eastern Brazil*" e "*Reservoir quality assessment and petrofacies of the Lower Cretaceous siliciclastic, carbonate and hybrid arenites from the Jequitinhonha Basin, Eastern Brazil*", submetidos à publicação nos periódicos Sedimentology e Journal of Petroleum Geology, respectivamente, elaborados durante o desenvolvimento do Mestrado;

c) **Anexos**: compreendendo documentação pertinente de natureza numérica (tabelas) e fotográfica que, por sua dimensão e/ou natureza, não foram incluídos nos artigos.

1. Introdução e objetivos

A análise estratigráfica desenvolvida com os conceitos da Estratigrafia de Seqüências (cf. Mitchum et al., 1977a, 1977b; Vail et al., 1977a, 1977b; Van Wagoner et al., 1988; Posamentier et al., 1988; Posamentier & Vail, 1988) permitiu a predição da distribuição espacial das fácies deposicionais e, por conseguinte, da porosidade e permeabilidade deposicionais, cuja distribuição é função de fatores como a geometria dos reservatórios, as estruturas sedimentares, a granulometria, seleção, etc... Posteriormente, a integração da estratigrafia de seqüências com os processos e padrões diagenéticos (cf. Morad et al., 2000; Ketzer et al., 2002; 2003a; 2003b; Al-Ramadan, 2006) permitiu prever a distribuição espacial e temporal de alterações diagenéticas superficiais (eodiagênese), e, por conseguinte, a evolução pós-deposicional da porosidade e permeabilidade, ou seja, da qualidade de reservatório.

O objetivo dessa dissertação é integrar, dentro de um arcabouço estratigráfico elaborado conforme os conceitos de estratigrafia de seqüências, análises faciológicas (fácies sedimentares e ambientes deposicionais) e petrográficas (tipos e distribuições espacial e temporal de processos diagenéticos e composição detrítica original), dos arenitos, calcarenitos e arenitos híbridos do intervalo do Aptiano Superior ao Albiano da Bacia de Jequitinhonha. A meta central é determinar os fatores deposicionais que controlam os padrões diagenéticos, e, por conseguinte, a qualidade de reservatório, bem como avaliar a aplicação desses estudos visando à redução dos riscos exploratórios. A linha de pesquisa aplicada nessa dissertação tem como referência os conceitos apresentados por Morad et al. (2000), Ketzer et al. (2002; 2003a; 2003b) e Al-Ramadan (2006).

A qualidade de reservatório dos intervalos estudados foi avaliada com a aplicação do conceito de *petrofácies de reservatório* (DeRos & Goldberg, 2007) (ARTIGO II). Essa metodologia se baseia na identificação de grupos de amostras definidos pela combinação dos principais fatores que afetam a qualidade de reservatório, i.e., porosidade e permeabilidade: (i) características deposicionais (estruturas sedimentares, granulometria, seleção, composição detrítica, etc.); (ii) processos diagenéticos e seus produtos (volume, intensidade, hábitos e distribuição das fases autigênicas); e (iii) tipos e distribuição de poros. Grupos de amostras definidos

pela combinação destes fatores mostram faixas de valores de porosidade e permeabilidade, assinaturas características nos perfis elétricos e na sísmica de reflexão, permitindo o reconhecimento desses atributos petrográficos e correspondente qualidade de reservatório em escala exploratória.

A aplicabilidade desses conceitos foi testada nessa dissertação na área proximal da Bacia de Jequitinhonha, amostrado por dois poços *onshore* e um poço *offshore* raso (Fig. 1), compreendendo o intervalo de tempo geológico correspondente aos Andares Aptiano (Superior) e Albiano. As unidades estudadas (formações Mariricu, São Mateus e Regência), constituem uma sucessão complexa depositada em ambientes continentais siliciclásticos a litorâneos mistos (plataforma siliciclástico-carbonática). Os objetivos finais deste estudo foram de:

a) Estudar os aspectos genéticos relacionados aos padrões diagenéticos, e respectiva qualidade de reservatório, e demonstrar a importância desse tipo de estudo na redução dos riscos exploratórios; e

b) Demonstrar o uso prático, como ferramenta de trabalho na fase de exploração, da caracterização dos processos diagenéticos (tipos, distribuição e evolução), e respectivas relações entre padrões diagenéticos e fácies sedimentares, dentro dos conceitos de estratigrafia de seqüências e petrofácies de reservatório, visando maior eficiência dos processos exploratórios.

2. Contexto geológico

A Bacia de Jequitinhonha tem sua origem relacionada à ruptura do paleocontinente de Gondwana e conseqüente formação do oceano Atlântico Sul durante o Eo-Cretáceo (cf. Asmus & Ponte, 1973; Ojeda, 1982; Chang et al., 1990), e está localizada na margem leste da plataforma continental brasileira, entre os paralelos de latitudes 18º 05' S e 14º 47' S (Fig. 1), limitada a Sul pelo Alto Vulcânico de Royal Charlotte, que a separa da Bacia de Cumuruxatiba, e a Norte pelo Alto de Olivença, que a separa da Bacia de Almada, ocupando uma área de aproximada de 7.200 Km^2, sendo a parte emersa da bacia de cerca de 500 Km^2.

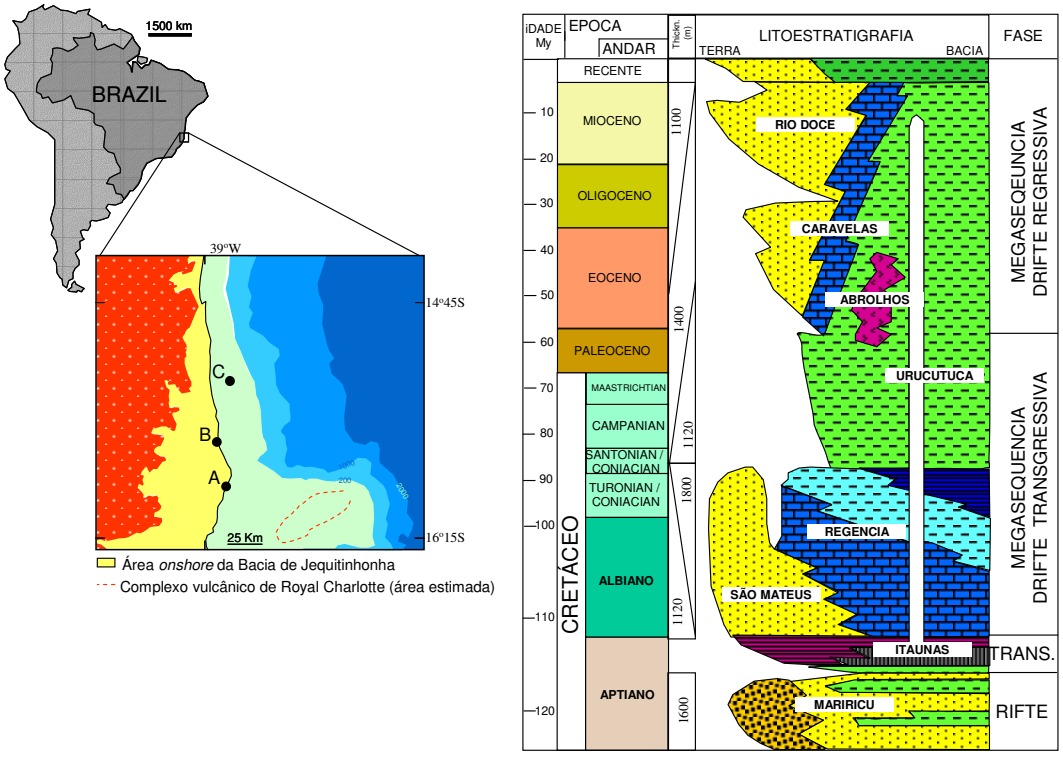

Fig.1. Mapa de localização da área de estudo e resumo da carta estratigráfica da Bacia de Jequitinhonha (fonte: ANP – Agência Nacional do Petróleo).

O embasamento na Bacia de Jequitinhonha é constituído por terrenos pré-cambrianos do Cráton do São Francisco (Almeida, 1977), consistindo em rochas granítico-gnáissicas e metassedimentos de baixo grau. O processo de separação dos continentes sul-americano e africano, com conseqüente implantação de um ambiente do tipo margem passiva, pode ser diferenciado em três estágios tectono-sedimentares distintos (Fig. 1) (cf. Chang et al, 1988; Santos et al, 1995): (i) rifte, representado por rochas de idades aptiana e neocomiana, as quais consistem em sedimentos siliciclásticos continentais, interpretados como sistemas de leques aluviais, fluviais e lacustres; (ii) transicional, representado por cunhas clásticas proximais compostas por conglomerados, arenitos e pelitos, e por evaporitos; e (iii) drifte (deriva continental), consistindo em sedimentos albo-cenomanianos terrígenos fluvio-deltáicos e carbonatos depositados em ambientes parálico e nerítico em um contexto de mar semi-restrito, passando para um contexto de mar aberto e estreito, do Albiano ao Coniaciano, com deposição de folhelhos anóxicos e margas (cf. Chagas, 2003), e marinho franco a partir do

Coniaciano. Com o progressivo resfriamento térmico e basculamento da bacia, processos halocinéticos estruturam intensamente a cobertura sedimentar pós-sal.

O pacote sin-rifte é conhecido como Formação Mariricu, correspondendo a conglomerados e arenitos continentais fluvio-deltáicos, associados a folhelhos lacustres ricos em matéria orgânica. A seqüência acomodou-se em grabens de orientação geral N-S ou SW-NE. O seu topo é definido por uma importante superfície de discordância, sobre a qual apóiam-se os sedimentos de natureza transicional, consistindo em siliciclásticos fluvio-deltaicos, recobertos por um pacote de evaporitos e folhelhos negros conhecidos como Membro Itaúnas.

O primeiro registro sedimentar da fase marinha na Bacia engloba os sedimentos albo-cenomanianos depositados diretamente sobre o pacote evaporítico, consistindo em arenitos grossos de fáceis transicional e marinha marginal (leques deltáicos) da Formação São Mateus. Esta unidade totaliza cerca de 1800 metros de espessura estimada, gradando no sentido da bacia para os carbonatos de alta e baixa energia da Formação Regência. O Cretáceo Superior registra um rápido afogamento da bacia, indicada pelo recobrimento de fácies carbonáticas por uma sedimentação pelítica de talude e bacia profunda, representada pela Formação Urucutuca.

Durante o Terciário a bacia registra uma típica seqüência de plataforma continental progradacional formada por fácies arenosas proximais, representada pela Formação Rio Doce, intercalada com carbonatos da Formação Caravelas, que grada no sentido da bacia para fácies pelíticas (Fm. Urucutuca). Um importante episódio magmático corresponde à Formação Abrolhos, consistindo em rochas vulcânicas e vulcaniclásticas alcalinas e sub-alcalinas extrudidas durante o intervalo Paleoceno-Eoceno (cf. Almeida et al., 1996).

3. Metodologia de trabalho

A metodologia de trabalho empregada nessa dissertação compreendeu:

1) A descrição de testemunhos, incluindo a análise de fácies sedimentares (*sensu* Miall, 1996), com a descrição de texturas, estruturas primárias (deposicionais, deformativas e biogênicas), e identificação de associações e sucessões faciológicas verticais (*sensu* Walker, 1992), visando reconhecer processos e sistemas deposicionais (geneticamente relacionados) e suas respectivas assinaturas em perfis elétricos e seções sísmicas (ARTIGO I).

2) A elaboração de um arcabouço estratigráfico, com base em dados bioestratigráficos, e sucessão vertical de sistemas deposicionais (ARTIGO I), com o suporte da descrição sistemática de lâminas petrográficas (microscopia ótica) de amostras selecionadas nos testemunhos. Face à baixa resolução bioestratigráfica, não foram interpretados limites cronoestratigráficos precisos.

3) A análise petrográfica quantitativa da composição essencial, realizada com uso do software Petroledge® (De Ros et al., 2007), via contagem de 300 pontos por lâmina delgada, segundo o método Gazzi-Dickinson (*sensu* Zuffa, 1985). A análise petrográfica quantitativa visou determinar: (a) a composição detrítica original, de forma a permitir considerações sobre a proveniência; (b) a assembléia de minerais autigênicos, sua evolução paragenética, e relações texturais com os constituintes detríticos e a compactação, para análise do impacto dos processos diagenéticos na porosidade e permeabilidade; (c) a classificação das rochas analisadas (*sensu* Folk, 1968 e Zuffa, 1980), e (d) a determinação da porosidade (macroporosidade) atual, para estimar a influência da compactação e da cimentação na redução da porosidade original (cf. Ehrenberg, 1989).

4) análises adicionais das principais fases diagenéticas responsáveis pela redução ou preservação da porosidade primária (cimentos carbonáticos, sulfatos e argilo-minerais), consistindo em (ARTIGO I):

a) estudos de composição isotópica (isótopos estáveis) de carbono, oxigênio e enxofre, com análises em rocha total ou método *microdrilling* sobre lâminas espessas (50 µm), para determinar as condições geoquímicas de precipitação de cimentos carbonáticos e sulfatos (cf. Al-Aasm et al., 1990). Os resultado dessas analises são apresentados no formato de δ relativo aos padrões SMOW (Craig, 1961), PDB (Craig, 1957) e CDT (Thode et al, 1961). As temperaturas de precipitação dos cimentos de

dolomita foram calculadas com base nas curvas de fracionamento isotópico segundo Friedman & O'Neil (1977); enquanto que os valores istópicos do sulfato autigênico e deposicional (Membro Itaúnas) foram comparados com os valores de referência segundo Claypool et al. (1980);

b) análises de difratometria de raios-x da fração argila (< 10 μm), utilizando difratômetro Siemens Bruker AXS, modelo D5000 (Laboratório de Difratometria de Raios-X da UFRGS), em amostra natural (*air dried*), glicolada (*ethylene glycol*) e calcinada (*heated*) a 550^{o}C por 2 horas; e

c) microscopia eletrônica de varredura (MEV), em microscópio Phillips XL-30, com o recurso de imagens de elétrons primários retroespalhados (*backscattering - BSE*), sobre lâminas selecionadas, polidas e revestidas com carbono, visando a determinação de morfologias, hábitos e relações paragenéticas entre minerais detríticos e autigênicos, com o suporte de espectômetro de energia dispersada (*energy-dispersive spectrometer - EDS)*, visando identificação química dos minerais autigênicos.

5) A classificação dos intervalos amostrados em lâmina petrográfica em *petrofácies de reservatório* (*sensu* De Ros & Goldberg, 2007) (ARTIGO II), definidas pelo agrupamento das amostras com base nas características deposicionais primárias (composição primária, estruturas, seleção, granulometria), as quais condicionam as características permo-porosas originais, e nas alterações diagenéticas mais influentes na redução, geração ou preservação da porosidade e permeabilidade. Tal procedimento permite agrupar as amostras com características permo-porosas e evolução diagenética semelhantes, e, conseqüentemente, com características petrofísicas e assinaturas sísmicas e em perfis elétricos similares. Medidas petrofísicas (porosidade e permeabilidade) foram utilizadas, quando coincidentes com os pontos amostrados em lâminas delgadas.

6) A análise dos padrões diagenéticos dos intervalos estudados em relação ao contexto do ambiente deposicional previamente interpretado, e ao contexto da estratigrafia de seqüências, visando avaliar a existência de controles deposicionais e estratigráficos sobre as variações nos constituintes originais (i.e. proveniência) e evolução diagenética (ARTIGO I). As relações com a estratigrafia de seqüências foram feitas em escala de tratos de sistemas e seqüências deposicionais. Não foi possível analisar a assinatura diagenética de superfícies-chaves face à amostragem descontínua em subsuperfície.

7) A análise integrada das características definidoras de cada *petrofácies de reservatório*, e por extensão dos intervalos de rocha representados por elas, em relação ao contexto de qualidade de reservatório *versus* ambiente deposicional e estratigrafia de seqüências (ARTIGO II).

8) A elaboração de modelos conceituais de predição de qualidade de reservatório, em relação à evolução de porosidade e permeabilidade dos reservatórios (ARTIGOS I e II).

9) A elaboração de artigos científicos descrevendo os resultados e sua interpretação.

4. Controles deposicionais sobre os padrões diagenéticos - Revisão conceitual

A diagênese engloba os processos físicos e químicos que afetam os sedimentos após a sua deposição e durante os primeiros milhares de metros de soterramento, ocorrendo a baixas temperaturas (< 200º C) e pressões (< 2000 kg/cm²), e na presença de grande quantidade de soluções aquosas, com diferentes valores de salinidade. As alterações diagenéticas são classificadas com base em limites de temperatura e soterramento (*sensu* Morad et al., 2000), conforme segue:

(i) **Eodiagênese –** engloba as alterações que ocorrem a profundidades de soterramento inferiores a 2 km e temperaturas inferiores a 70^{o}C, onde a química das águas intersticiais é controlada pelas águas do ambiente deposicional e/ou circulação das águas superficiais, onde as características deposicionais (textura, estruturas, geometria dos sedimentos) influem no fluxo de fluidos. É também a fase principal de expulsão da água e perda de porosidade por compactação;

(ii) **Mesodiagênese** – engloba as alterações que ocorrem a profundidades de soterramento superiores a 2 km e temperaturas superiores a 70^{o}C, caracterizado por um efetivo isolamento da superfície e dos fluidos superficiais, onde os fluidos diagenéticos são modificados pelas reações com os minerais; e

(iii) **Telodiagênese** – engloba alterações decorrentes de soerguimento (*uplift*) ou da infiltração profunda de águas meteóricas, comumente sob influência de águas meteóricas, com o retorno às condições superficiais de rochas anteriormente submetidas às alterações mesodiagenéticas. Comumente associadas à formação de discordâncias.

As alterações eodiagenéticas têm forte controle por parte de fatores relacionados ao ambiente deposicional, tais como a textura, composição detrítica, conteúdo de matéria orgânica, composição de fluidos intersticiais deposicionais, clima e características hidrológicas da bacia (cf. Morad, 1998). Essas alterações promovem a interação entre sedimentos e fluidos superficiais. A intensidade da eodiagênese é função da taxa de sedimentação: quando alta, os sedimentos são rapidamente soterrados e isolados dos efeitos superficiais; quando baixa, ocorre prolongada exposição às influencias superficiais (cf. De Ros, 1996).

As alterações mesodiagenéticas, em virtude do restrito fluxo de fluidos durante a diagênese profunda, são muito influenciadas pela porosidade e permeabilidade remanescentes, apresentando menor relação com fácies deposicionais, e abrangência espacial que transpassa os limites entre fácies, face à maior correlação com padrões de circulação de fluidos em escala regional (Stonecipher, 2000). Desta forma, bruscas variações verticais e laterais na suíte de alterações diagenéticas são mais comumente relacionadas a controles deposicionais, e associadas a reações eodiagenéticas. As alterações mesodiageneticas são comumente, entretanto, produzidas ou favorecidas pela presença de fases eodiagenéticas específicas, estas ultimas com forte influencia deposicional.

4.1. Estruturas, texturas e trama (*fabric*) deposicionais

As estruturas e trama deposicionais, e características texturais como granulometria, arredondamento, esfericidade e seleção influenciam na dinâmica do fluxo de fluidos intersticiais, e, por sua vez, na distribuição e grau das alterações diagenéticas promovidas por esses fluidos, e na intensidade da compactação e cimentação na alteração do espaço intergranular original. Quanto melhor a seleção e menor o conteúdo de argila, melhor será a circulação de fluidos, resultando em uma

maior probabilidade desses intervalos serem objeto de extensas cimentação e/ou dissolução de grãos e cimentos durante o soterramento (Aktas & Cocker, 1994).

As propriedades hidrológicas de uma bacia sedimentar estão relacionadas com suas características litológicas (cf. Van De Graaf & Ealey, 1989; Hiatt & Dalrymple, 2003). Complexas distribuições laterais e verticais de litofácies podem gerar heterogeneidades (compartimentalização) no perfil de porosidade e permeabilidade, controlando a o fluxo de fluidos intersticiais através dos pacotes sedimentares, e influindo nas alterações diagenéticas subseqüentes (cf. Stonecipher, 2000).

Depósitos fluviais, por exemplo, comumente mostram variações na porosidade e permeabilidade relacionadas à intercalação entre arenitos grossos, porosos e permeáveis (fácies de preenchimento de canal) e lutitos com alta microporosidade e baixa permeabilidade (fácies de transbordamento de canal). Seqüências com padrões de *fining-upward* tendem a corresponder a melhores valores de permeabilidade e porosidade nas fácies mais grossas e com estratificações de maior porte na base, e piores nas fácies finas com estratificações tipo *climbing-ripples* do topo (cf. Van De Graaf & Ealey, 1989). Fácies deposicionais com elevado percentual em finos, bem como fácies muito bioturbadas, fluidizadas, deformadas (*slumps*), etc., tendem a impor maior restrição ao fluxo de fluidos, refletindo em alterações diagenéticas menos intensas (cf. Aktas & Cocker, 1994).

Sedimentos grossos (p.ex.: arenitos), por outro lado, tendem a apresentar variado espectro de porosidades e permeabilidades originais, dependendo de fatores como seleção e composição detrítica (cf. De Ros, 1996). A manutenção de elevados valores de porosidade e permeabilidade durante a eodiagênese torna esses intervalos vias preferenciais para o fluxo de fluidos durante a mesodiagênese. A amalgamação dos canais aumenta a conectividade das seqüências permitindo um maior fluxo de fluidos responsáveis pelas alterações diagenéticas (Van De Graaf & Ealey, 1989).

4.2. Composição detrítica - Proveniência

Estudos têm demonstrado que as alterações diagenéticas têm forte controle da composição detrítica original (e.g. Surdam et al., 1989; Amorosi, 1995; De Ros, 1996).

A composição química e mineralógica das rochas é função da interação de fatores como a composição das áreas-fonte (litologia), intensidade e processos de intemperismo, transporte, ambiente deposicional, idade e profundidade de soterramento, refletindo condicionantes tectônicos e climáticos (cf. De Ros et al., 1994; Morad et al., 2000; Harris, 2000).

O tempo, distância e os processos de transporte promovem o aumento do grau de maturidade pela seleção dos minerais com diferente resistência mecânica e química, resultando em depósitos com assembléias de minerais detríticos particulares, os quais apresentarão padrões de evolução diagenética distintos (cf. De Ros, 1996). O fator clima também influi no grau de maturidade composicional. Sedimentos imaturos com baixa resistência ao intemperismo químico (feldspatos) tendem a serem mais preservados sob ação de climas semi-áridos (cf. De Ros, 1996). A concentração de minerais estáveis favorece a preservação de porosidade primaria (cf. Burley, 1993), enquanto que sedimentos ricos em constituintes imaturos e instáveis (p. ex.: feldspatos, fragmentos líticos vulcânicos, grãos intrabaciais carbonáticos, intraclastos lamosos) tendem a apresentar limitada preservação de porosidade primária ao longo da sua historia de soterramento e diagenética, pela pronunciada alteração destes constituintes e geração de fases diagenéticas (cimentos) especificas, tais como a intensa cimentação intergranular por argilo-minerais esmectíticos e/ou cloríticos promovida pela alteração de fragmentos vulcânicos (cf. De Ros, 1996).

A presença de grãos carbonáticos, muito reativos e instáveis frente à compactação mecânica e química, favorece a cimentação carbonática precoce pela sua dissolução e/ou pela nucleação de cimentos derivados da água do mar (cf. Cavazza & Gandolfi, 1992; Amorosi, 1995; Morad et al, 2000; Ketzer et al, 2002). Face à cimentação precoce, esses intervalos sofrem menos compactação mecânica do que arenitos não cimentados.

4.3. Composição e fluxo dos fluidos

As alterações diagenéticas são controladas pela composição química dos fluidos intersticiais (cf. McKay et al, 1995). Sedimentos mais permeáveis (i.e. que permitem maior circulação de fluidos) tendem a sofrer processos diagenéticos mais intensos (Harrison, 1989).

O fluxo de fluidos intersticiais ocorre em virtude da existência de gradientes de pressão em subsuperfície (p. ex.: expulsão de água de lutitos durante a compactação), tectonismo (i.e. falhamentos) e correntes (células) de convecção impulsionadas por gradientes de densidade devidos a variações de salinidade e/ou de temperatura (cf. Bjørlykke et al., 1989; Morad et al., 2000). O fluxo de fluidos nas bacias sedimentares é comumente associado aos seguintes regimes ou sistemas (cf. De Ros, 1996) (Fig. 2):

(i) o regime meteorico, o qual é caracterizado por baixa salinidade, sendo bastante influenciado pela paleogeografia, em especial por áreas tectonicamente soerguidas, que forneçam adequado gradiente hidráulico, bem como pela continuidade de corpos arenosos com propriedades permo-porosas adequadas (cf. Bjørlykke et al., 1989); (ii) o regime marinho caracterizado por grande extensão, mas pequena penetração, mais influente em áreas de baixas taxas de aporte sedimentar; (iii) o regime compactacional, caracterizado e limitado pelo volume de fluídos intersticiais expulsos durante o soterramento; e (iv) o regime termobárico, caracterizado por limitado volume de fluidos intersticiais, relacionado às reações desencadeadas pela geração de hidrocarbonetos e desidratação de argilo-minerais, sob condições de elevada P e T, bem como pelo fluxo de fluidos através de falhas.

Os padrões de fluxo de fluidos intersticiais são controlados pela distribuição espacial dos intervalos de maior permeabilidade, a qual é função de características deposicionais, tais como: geometria externa, textura, estruturas e fábrica (cf. Beard & Weyl, 1973; De Ros, 1996). Intervalos com intensa cimentação, e evaporitos, atuam como barreiras à circulação de fluidos (cf. Morad, 1998), influindo diretamente nos padrões de fluxo dos fluídos e nas alterações diagenéticas por eles induzidas (cf. Worden & Burley, 2003).

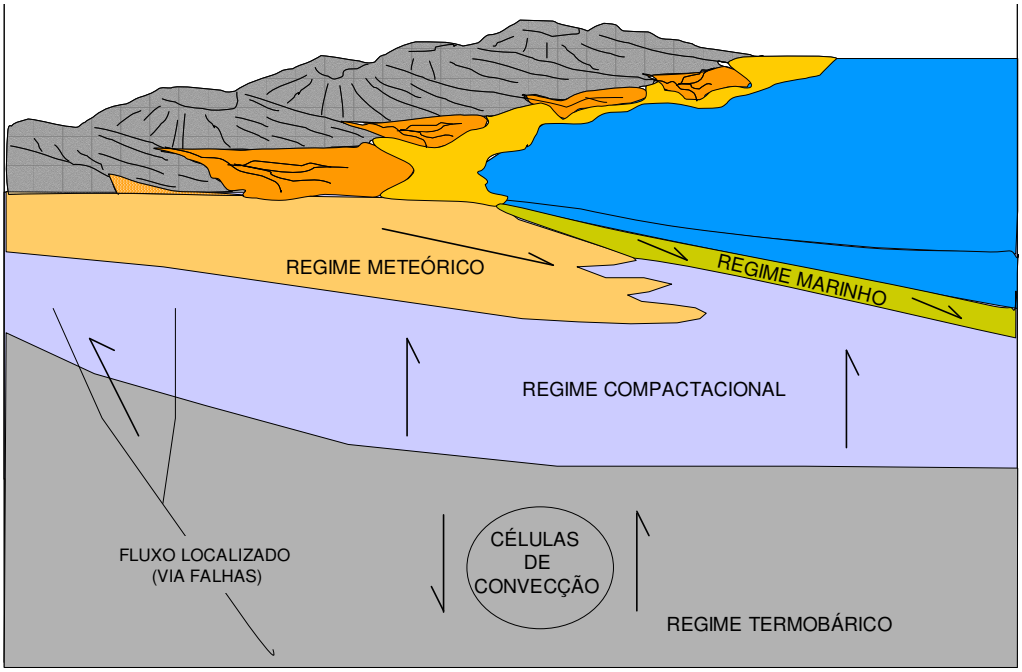

Fig. 2. Regimes hidrológicos de fluxo de fluidos intersticiais em bacias sedimentares (adaptado de De Ros, 1996).

4.4. Composição dos constituintes diagenéticos anteriores

As alterações eodiagenéticas podem controlar diretamente a porosidade e permeabilidade, influir na evolução dos processos mesodiagenéticos. Isto ocorre particularmente porque fases precoces muito reativas como argilo-minerais ou carbonatos sofrem expressivas alterações durante o soterramento (cf. De Ros, 1996). Cimentos carbonáticos eodiagenéticos tendem a ser substituídos por cimentos carbonáticos mesodiageneticos, comumente com granulação mais grossa. Cutículas ou franjas de argilas esmectíticas autigênicas ou mecanicamente infiltradas tendem a ser cloritizadas ou ilitizadas, e/ou a ser recobertas por franjas mesodiageneticas de clorita ou ilita (cf. De Ros, 1996), que reduzem a permeabilidade pela obstrução das gargantas dos poros, mas contribuem para preservar a porosidade pela inibição dos crescimentos secundários de quartzo (cf. Harrison, 1989).

4.5. Diagênese versus estratigrafia de seqüências

A estratigrafia de seqüências, surgida com base nos estudos de caráter sismoestratigráficos efetuados pelos profissionais da Exxon, forneceu uma importante ferramenta para a análise estratigráfica de bacias, bem como para a correlação e análise de fácies em diferentes escalas de trabalho (cf. Mitchum et al., 1977a, 1977b; Vail et al., 1977a, 1977b; Van Wagoner et al., 1988; Posamentier et al., 1988; Posamentier & Vail, 1988).

A estratigrafia de seqüências baseia-se em definições como: (i) **seqüência deposicional**, unidade estratigráfica básica, constituída por uma sucessão contínua de estratos geneticamente relacionados, limitados por discordâncias erosivas e suas concordâncias relativas, correspondendo a um ciclo completo de variação relativa do nível de base; e (ii) **tratos de sistemas**, como conjunto de sistemas deposicionais que coexistem e são característicos a determinados intervalos da curva de variações relativas do nível de base. Sua aplicação revolucionou a análise de bacias em face de sua capacidade preditiva quanto à distribuição das fácies, e a seu referencial na correlação estratigráfica entre diferentes bacias a partir da proposição de variações eustáticas de caráter global.

Trabalhos subseqüentes (e.g. Galloway, 1989; Lomando & Harris, 1991; Schlager, 1991; Hunt & Tucker, 1992; Posamentier & James, 1993; Loucks & Sarg, 1993; Miall, 1997; Catuneanu, 2002) questionaram o modelo original em questões controversas como: (i) definição das superfícies estratigráficas aptas para atuar como limite de seqüência, (ii) influência das quedas eustáticas na gênese das discordâncias em bacias com diferentes regimes tectônicos, e (iii) influência do aporte sedimentar e uso da estratigrafia de seqüências na correlação entre bacias com histórias evolutivas distintas. Isto permitiu a revisão e aperfeiçoamento do modelo original, e o fornecimento de novos conceitos e aplicações, tais como na estratigrafia de seqüências para ambientes mistos carbonáticos-siliciclásticos e tratos de sistemas de regressão forçada.

A abordagem integrada entre estratigrafia de seqüências e diagênese consiste em uma prática recente (cf. Morad et al, 2000; Ketzer et al, 2002; Ketzer et al, 2003a;

Ketzer et al, 2003b; Al-Ramadan, 2006), que tem demonstrado que as distribuições espacial e temporal das alterações diagenéticas podem ser previstas dentro de um contexto de estratigrafia de seqüências. A análise estratigráfica convencional permite a predição da distribuição de fácies, que controla a porosidade e permeabilidade deposicionais (geometria dos corpos sedimentares, tamanhos e seleção dos grãos, etc.), enquanto a abordagem integrada entre estratigrafia de seqüências e diagênese permite avaliar a evolução pós-deposicional da porosidade e permeabilidade, dentro de um contexto espacial e temporal, uma vez que muitos dos parâmetros que governam os processos diagenéticos podem ser obtidos a partir do contexto da estratigrafia de seqüências.

Dentre os parâmetros que influenciam a evolução diagenética, e que podem ser relacionados com a estratigrafia de seqüências, destacam-se:

(i) mudanças no quimismo das águas intersticiais (cf. McKay et al, 1995; Carvalho et al., 1995; Morad et al, 2000) - superfícies estratigráficas que definam significativas mudanças no quimismo dos fluidos intersticiais, tais como mudança de composição marinha para meteórica, ou mista marinho-metórica, ao delimitar importantes eventos transgresivos ou regressivos, tais como superfícies transgressivas, limites de paraseqüências e limites de seqüências. Estes últimos, por exemplo, no caso de rebaixamento do nível do mar, implicam na substituição de fluidos intersticiais marinhos por meteóricos em amplas áreas.

(ii) taxa de acumulação sedimentar (cf. Morad et al, 2000; Ketzer et al, 2003b; Al-Ramadan, 2006) - superfícies estratigráficas relacionadas com baixas taxas de acumulação sedimentar correspondem a uma longa permanência dos sedimentos em contato com fluidos intersticiais específicos. Isto ocorre em limites de paraseqüências e, principalmente, superfícies de máxima inundação, caracterizadas por significativo hiato não deposicional, o que favorece a ocorrência de alterações diagenéticas intensas, particularmente de cimentação carbonática, pela difusão de Ca^{2+} a partir da água do mar.

(iii) variação na composição primária (cf. Amorosi, 1995; Morad et al, 2000; Ketzer et al, 2002) **–** mais especificamente, na variação da distribuição de constituintes

intrabaciais, tais como bioclastos carbonáticos, intraclastos lamosos e grãos de glauconita, a qual varia significativamente com os tratos de sistemas preditos pela ES. Esses constituintes são altamente reativos, promovendo processos diagenéticos responsáveis tipicamente por substancial redução de porosidade e permeabilidade.

5. Resultados obtidos

A caracterização dos fatores determinantes da qualidade dos reservatórios, bem como sua distribuição espacial e temporal, e relação com o ambiente deposicional, foi obtida a partir da integração e interpretação de descrições de testemunhos, perfis elétricos, dados petrológicos, isotópicos, petrofísicos e geofísicos .

Descrições de 32 testemunhos distribuídos ao longo dos 3 poços foram utilizadas como base para elaboração do arcabouço estratigráfico (Figs. 3, 3a), a partir da correlação dos perfis de poços e sucessões faciológicas verticais (ARTIGO I). Essas descrições resultaram na diferenciação de 18 litofácies, seguindo um modelo adaptado de Miall (1996), as quais foram agrupadas em 14 associações de fácies de caráter genético, seguindo o modelo proposto por Walker (1992), representando os seguintes sistemas deposicionais:

(i) **Sistemas continentais fluvio-deltáicos** (e.g. Galloway & Hobday, 1983; Collinson, 1996) - **Associação de fácies CD** e **FD** (Fig. 4A), depositados em meio-grabens assimétricos, sob tectonismo distencional ativo (cf. Küchle et al., 2005), diferenciados em fácies com granulometria média a grossa (CD), interpretados como proximais em relação às bordas de falha da bacia, e fácies com granulometria média a fina (FD), interpretados como distais em relação às bordas de falha da bacia e/ou relativos a drenagens longitudinais (axiais) em relação à calha rifte. Ambos sistemas fluvio-deltáicos são diferenciados em fácies subaquosas: frente deltaicas e prodelta-lacustrino; e fácies subaérea: planície deltaicas, localmente intercalados com lutitos pró-deltaicos a lacustres.

(ii) **Sistemas de leques deltáicos costeiros** (e.g. Bhattacharya, 2006) **- Associação de fácies SD (*shallow-water* deltas)** (Figs. 4B-C), caracterizados por granulometria média

a grossa, relacionados a plataformas rasas em ambiente marinho restrito – golfo, diferenciado em fácies subaquosas de frente deltaicas (*shoreface* inferior e superior) e localmente subaéreas de planície deltaicas (*shoreface* superior a *foreshore*).

(iii) **Sistemas fluviais tipo entrelaçado - *braided*** (e.g. Steel & Thompson, 1983) - **Associação de fácies BR** (Figs. 4A, 4C)**,** caracterizados por granulometria média a grossa, relacionados a fácies proximais aos sistemas fluvio-deltáicos em tratos de sistemas de mar baixo ou progradações de tratos de sistema de mar alto sobre os sistemas deltáicos.

(iv) **Sistemas de sabkha costeira** (e.g. Handford & Loucks, 1993) - **Associação de fácies SC** (Fig. 4B), interpretadas no topo das progradações deltaicas (fácies SD), como depósitos de tratos de sistemas de mar alto tardio, formando ambientes de sabkha costeira (*sabkha and coastal salina supratidal flats*);

(v) **Sistemas estuarinos** (e.g. Weimer et al., 1982) **- Associação de fácies ES** (Fig. 4C), caracterizados por granulometria grossa a fina, relacionados às fácies transgressivas de ambientes de plataforma interna; e

(vi) **Sistema misto (carbonático-siliciclástico) de plataforma interna** (e.g. Wright & Burchette, 1996) - **Associação de fácies MR** (Fig. 4C), depositados em ambiente do tipo rampa carbonática rasa (cf. Córdoba, 1994; Küchle et al., 2005), marcada por uma sedimentação mista siliciclástica, nas porções proximais da bacia (fácies SD/BR) e carbonática nas porções mais distais (fácies MR). Estes últimos consistindo em arenitos híbridos (*sensu* Zuffa, 1980) e calcarenitos. Os intervalos siliciclásticos são aqui interpretados como preferencialmente depositados nos tratos de sistema de mar baixo (*LST*), transgressivos (*TST*) inicial e mar alto (*HST*) tardio (progradações de fácies costeiras/continentais), enquanto que os tratos de sistemas transgressivos (*TST*) e mar alto (*HST*) favorecem a deposição dos intervalos carbonáticos (Handford & Loucks, 1993).

Os testemunhos que serviram de base para a interpretação dos sistemas deposicionais acima citados, contendo as principais estruturas sedimentares diagnósticas, são discutidos a seguir (Figs. 5 a 11):

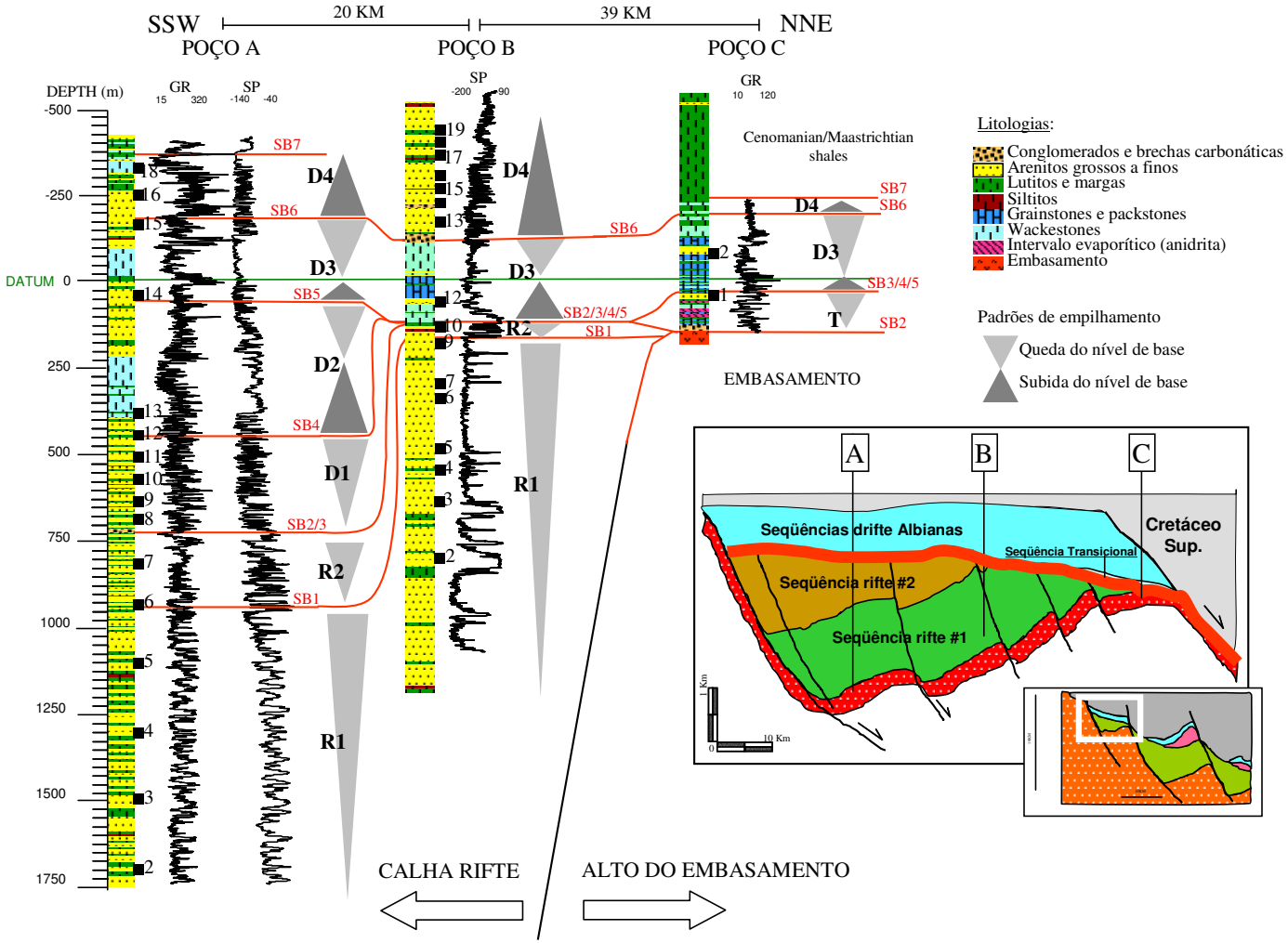

Fig. 3. Seção de correlação entre perfis de poços (raios gama e potencial espontâneo) dos poços estudados, com indicação das seqüências deposicionais (simbologia indicando a posição dos testemunhos não está em escala).

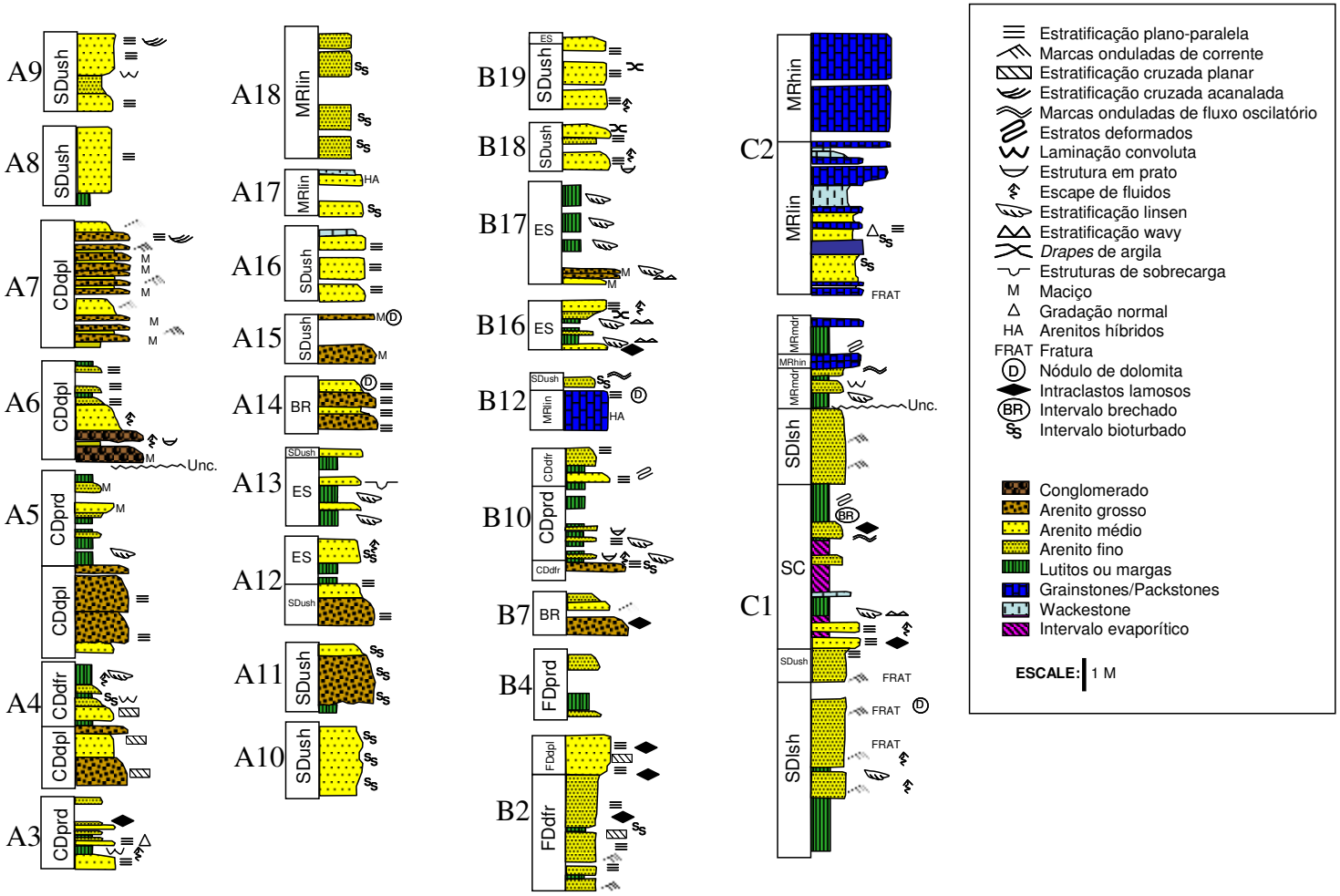

Fig. 3a. Seleção dos testemunhos mais diagnósticos com interpretação das associações de fácies.

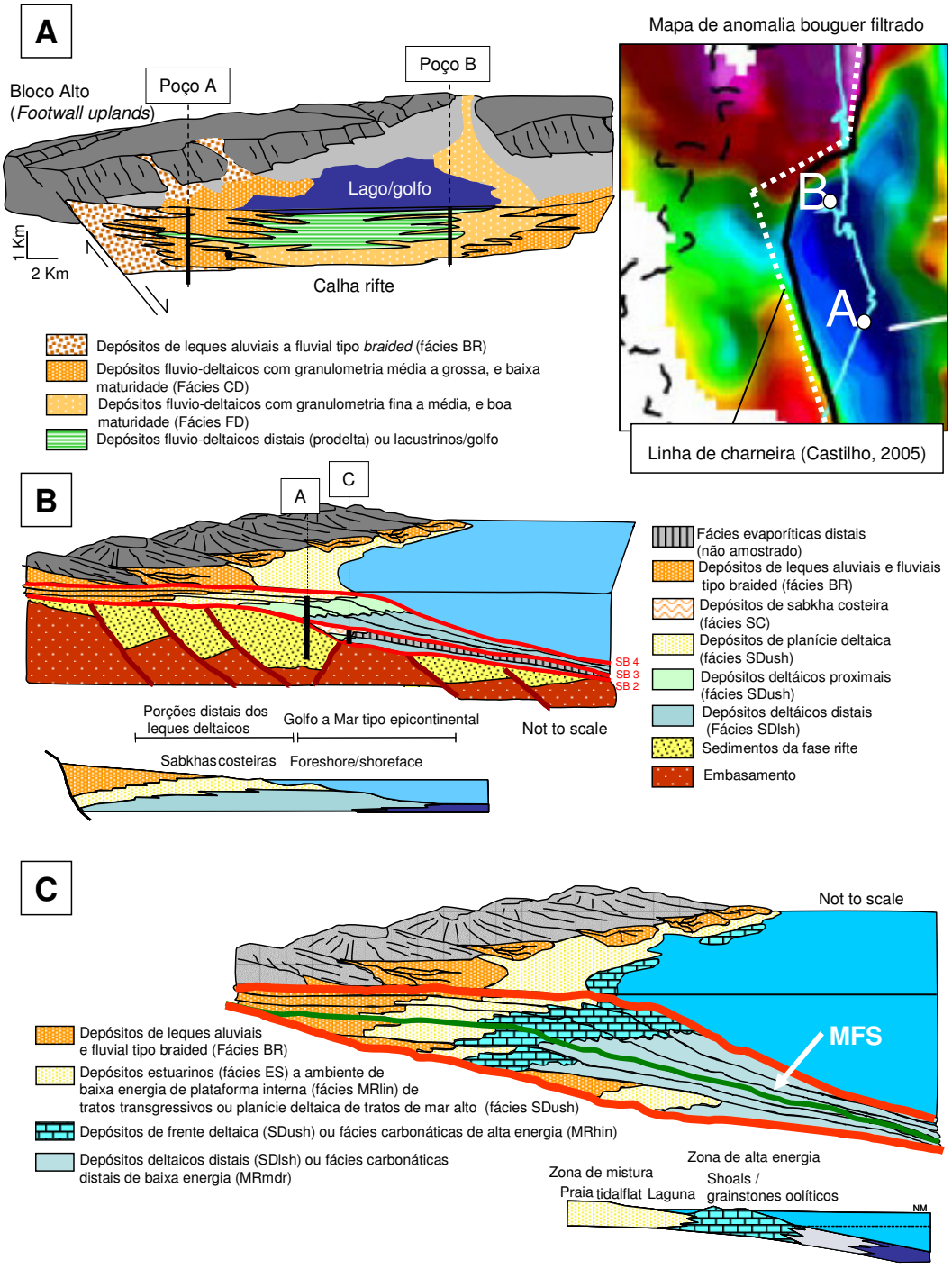

Fig. 4. Representação esquemática da interpretação paleo-geográfica dos ambientes deposicionais para as seqüências rifte (A), transicional e drifte siliciclástica D1 (B) e plataforma mista (siliciclástica-carbonática) albiana – Seqüências D2-D4 (C).

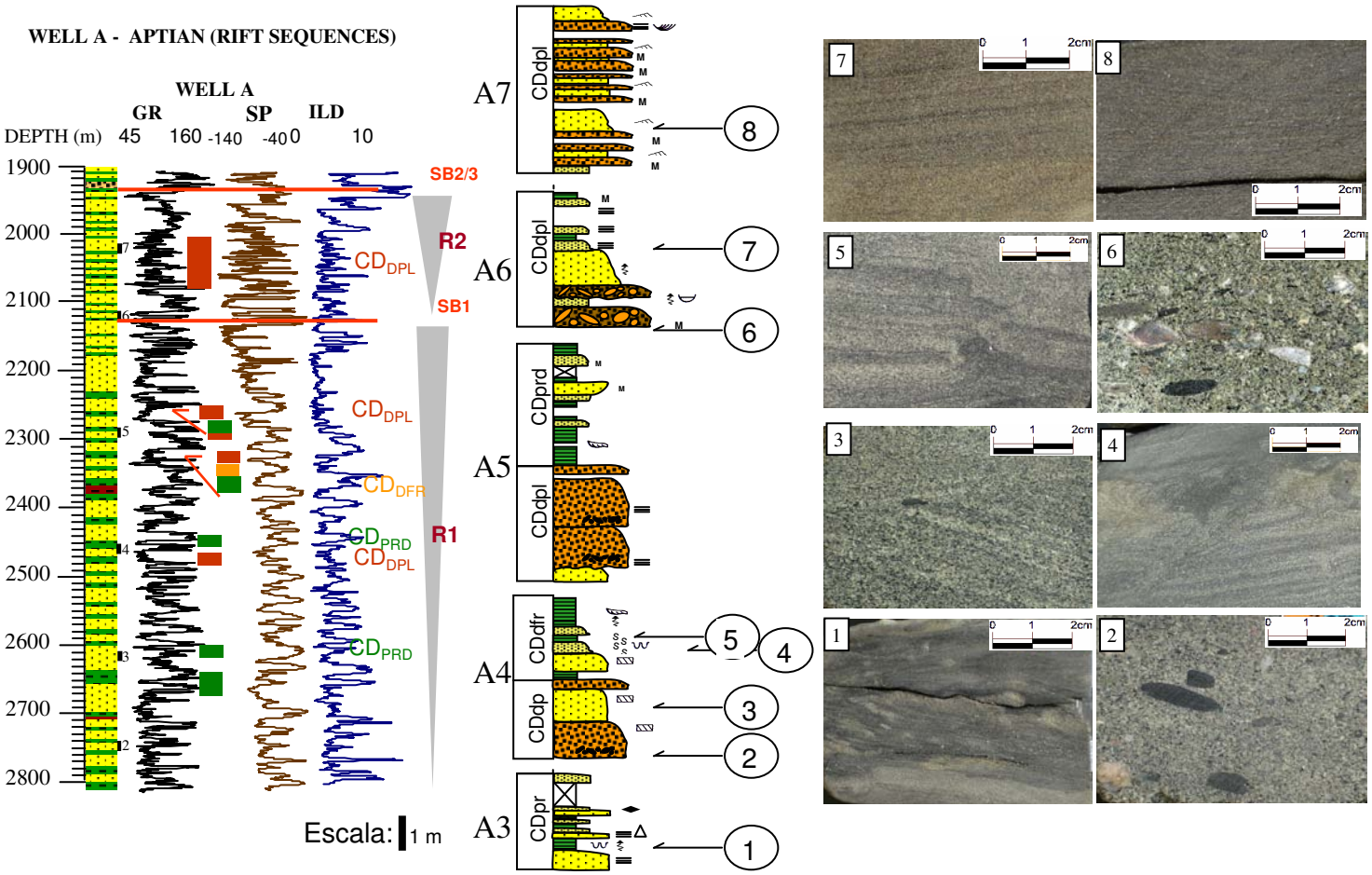

Fig. 5. Associação de fácies CD. Fotografias digitais de testemunhos mostrando: 1) lutitos a arenitos finos, com estratificações plano-paralelas (Fl) a plano-onduladas (dobras convolutas e/ou fluidização), representando registro de fácies de prodelta; 2 a 3) Arenitos grossos (localmente com grânulos), arcósios, mal selecionados, com estratificações cruzada planares (Sp), representando o registro de planícies/frentes deltaicas; 4 e 5) Arenitos médios a finos com dobras convolutas por fluidização (Sc) – bioturbação(?) de frente deltaica; 6) Conglomerados suportados pelos clastos, representando registro de canais de planície deltaica (Gmt); 7) Arenitos finos a médios, micáceos, com estratificações plano-paralela (Sl) de planície deltaica; 8) Arenitos médios com estratificações cruzadas de marca onduladas – *ripples de corrente* (Sr).

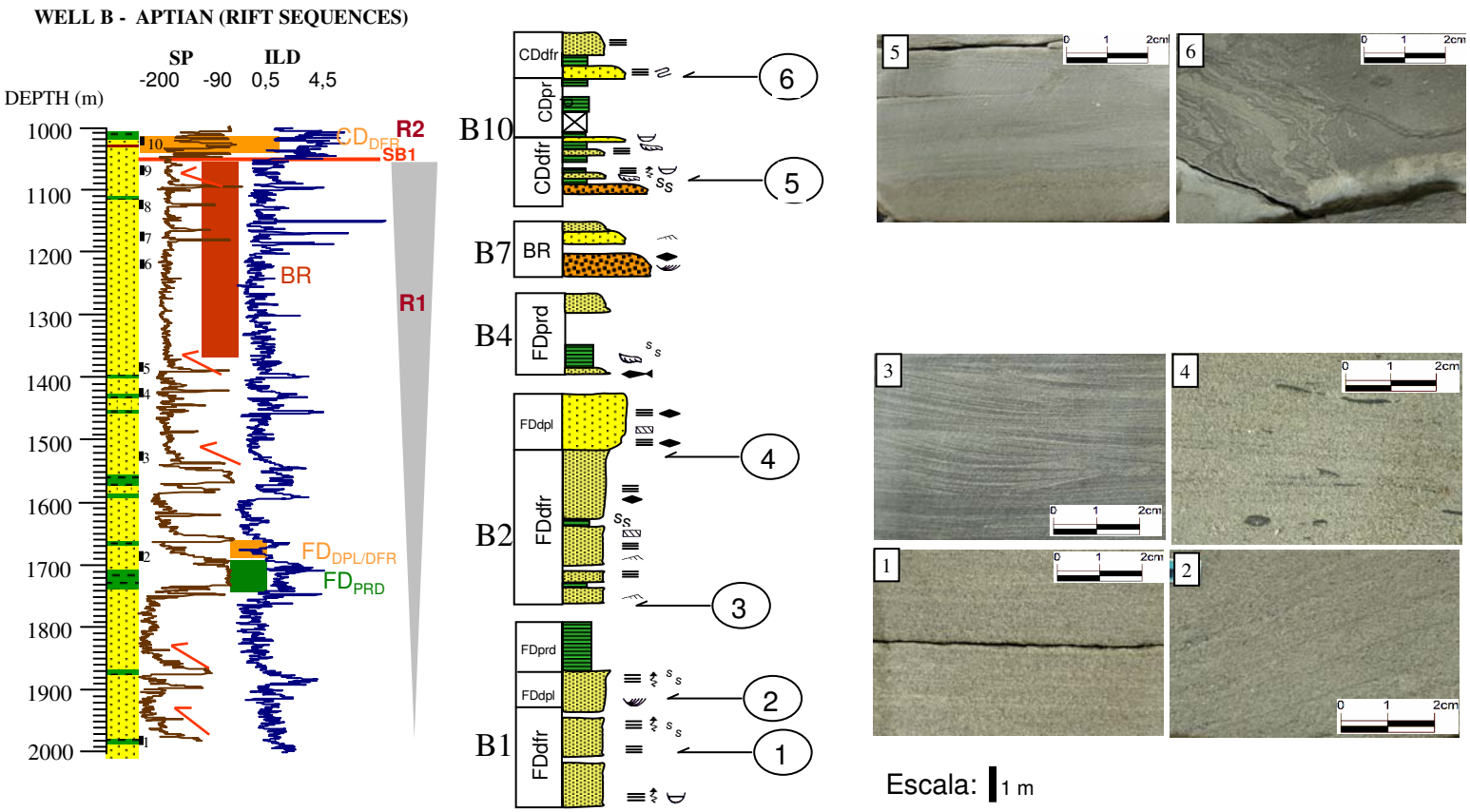

Fig. 6. Associação de fácies FD e CD. Fotografias digitais de testemunhos mostrando: 1) Arenitos finos a médios, bem selecionados, quartzosos, com estratificações plano-paralelas de transição frente deltaica a planície deltaica; 2) Arenitos finos a médios, quartzosos, com estratificações cruzadas tabulares ou acanaladas (St), representando o registro de canais distributários de planície deltaica; 3) arenitos finos com estratificações de marcas onduladas – ripples de *corrente* (Sr) representando o registro de fácies distais de frente deltaica; 4) arenitos finos a médios com estratificações plano-paralelas de frente deltaica a planície deltaicas, com presença de intraclastos lamosos; 5) arenitos finos com estratificações plano-paralelas (Sl); 6) arenitos finos a médios com dobras convolutas (Sc) por fluidização, representando o registro de frentes deltaicas distais de fácies CD.

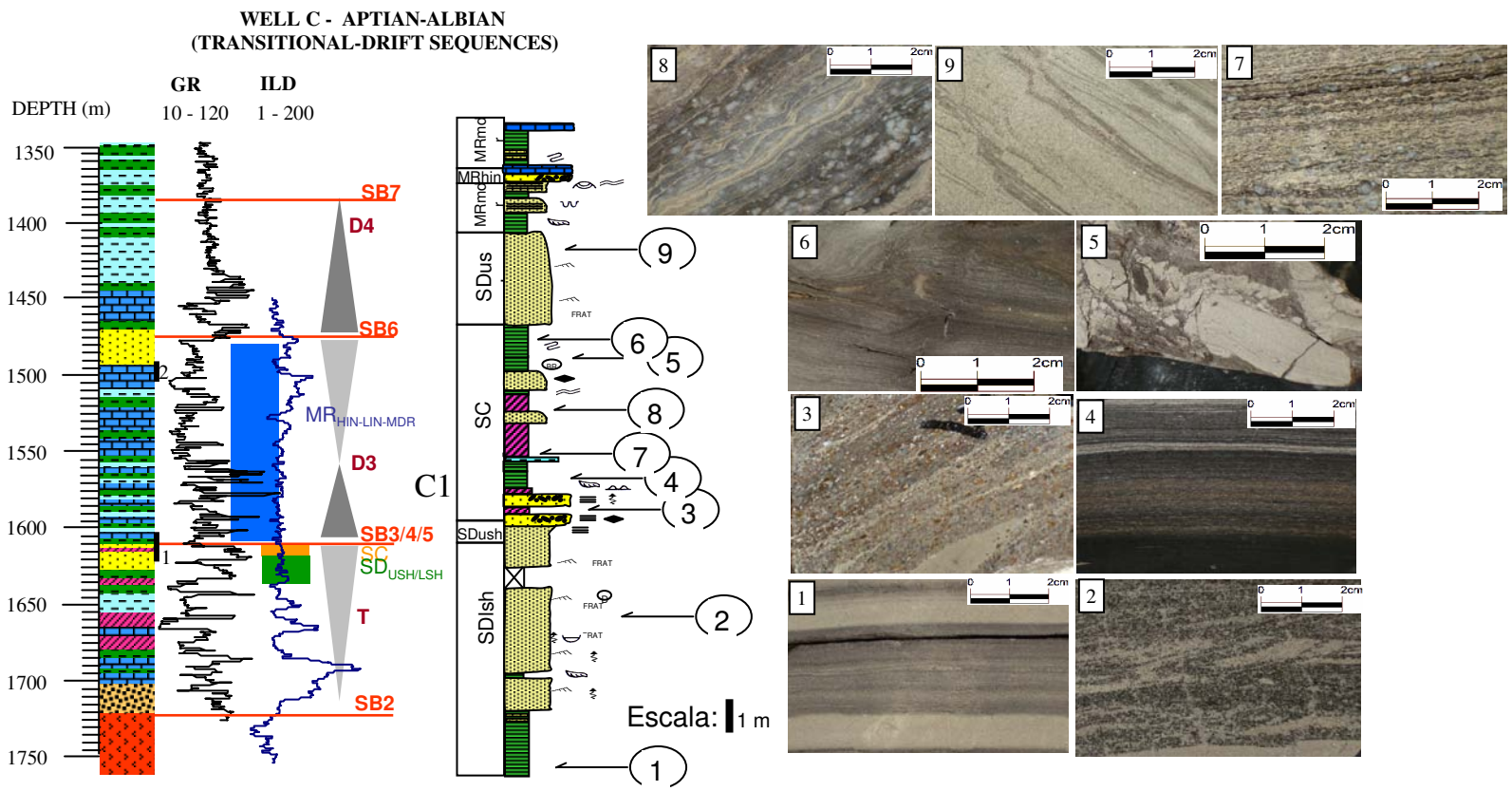

Fig. 7. Associações de fácies SD (fase pré-sal) e SC (intervalo evaporítico). Fotografias digitais de testemunhos mostrando: 1) registro de facies prodeltaicas consistindo de intervalo heterolítico com alternância entre camadas de arenitos muito finos cinza e calcilutito creme (Hc); 2) Arenito médio com estratificações cruzadas de marcas onduladas – *ripples de corrente* (Sr) com impregnação de óleo residual (manchas escuras); 3) arenito fino a médio com estratificações plano-paralelas intercalado com lentes de calcilutito creme; 4 a 6) Litofacies heterolítica (He), consistindo em interlaminados de folhelho preto com calcilutito creme (algálico?) ou interlaminados de lutito e calcilutito creme, fluidizados, dobrados e microfalhados, com aspecto brechado (*tepee structures?*), sugerindo eventos de exposição subaérea, e lutito com laminação convoluta (algálico?), representando o registro de planícies tipo *mudflat* associadas aos ambientes de sabkha; 7 e 8) alternância entre lâminas de lutitos carbonáticos (*algal-laminated dolomudstones*) e anidrita nodular (*chicken-wire*) - litofacies Ec; 9) fácies de frente deltaica com estratificações de marcas onduladas – *ripples de corrente* (Sr), localmente com possível interpretação de influência de ondas (*ripples de oscilação* – Sw), sugerindo ambiente tipo *shoreface* superior a *foreshore.*

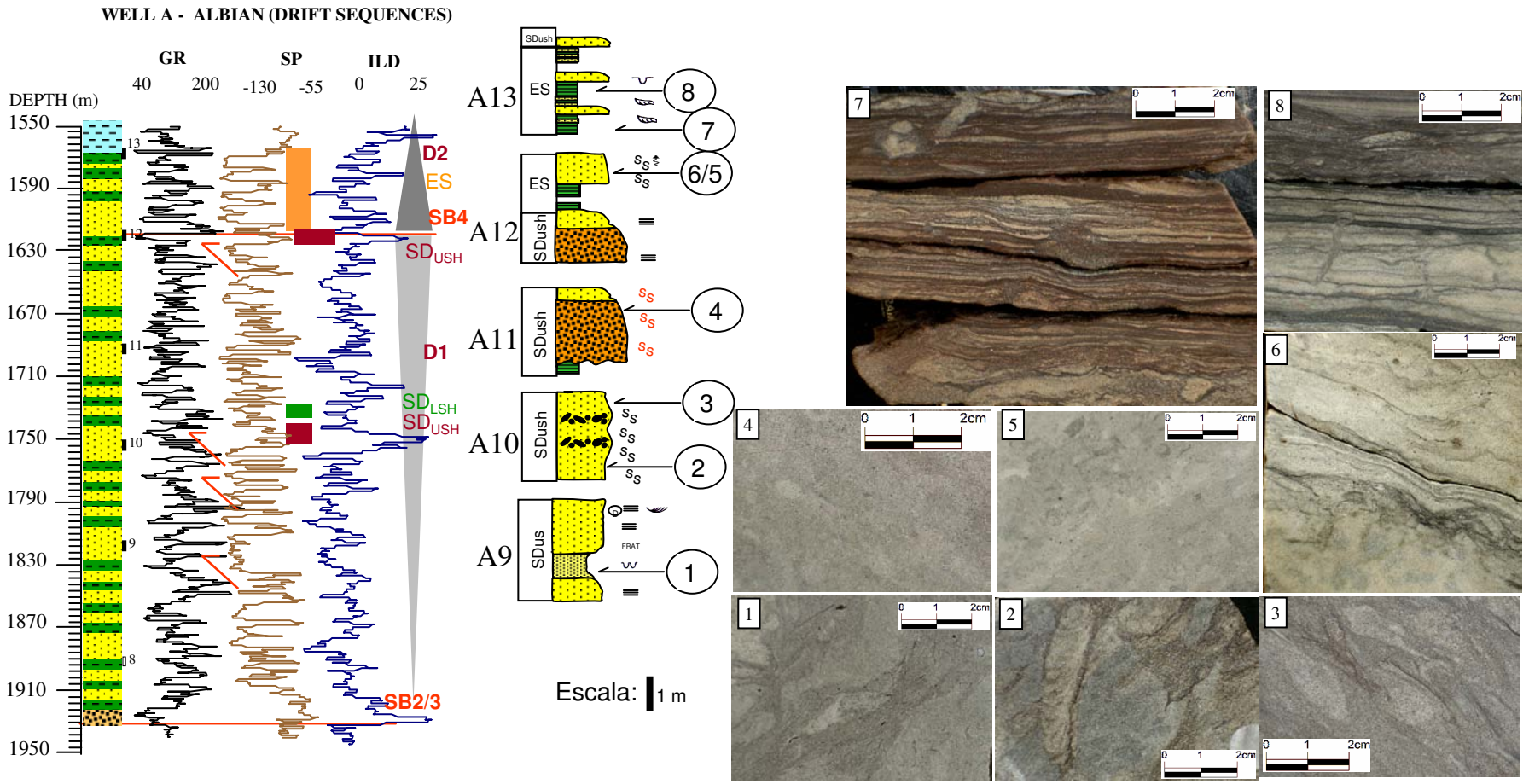

Fig. 8. Associações de fácies SD (pré-implantação plataforma carbonática) e ES. Fotografias digitais de testemunhos mostrando: 1) Arenito fino a médio, mal selecionado, arcósio, com laminação convoluta (Sc) e freqüente mistura (argila-silte-areia); 2 a 5) fácies de frente deltaica a planície deltaica (*foreshore to upper shorface*) com intensa bioturbação (Sb). Traço fóssil de Diplocraterion? (foto 2), Icnofácies Skolithos, ambiente raso (frente deltaica/*upper shoreface*); 6 e 8) fácies heterolíticas (H) com alternância entre intervalos com predominância de lutitos (*silty laminated mudstones*), com < 25% de grãos tamanho areia, e intervalos com predominância de arenitos (*muddy sandstones)*, com < 25% de grãos tamanho argila, representando o registro de ambientes estuarino, lateralmente associados aos ambientes de leques deltaicos. Fotos 6 e 8 com feições tipo *crinckled laminae* (finas lâminas de argila em conformidade com prováveis marcas onduladas de corrente (*ripples*). Traços fósseis de thalassinoides ou ophiomorphas(?) (foto 7), Icnofácies Cruziana, e skolithos(?) (foto 8), Icnofácies Skolithos, sugerindo mistura de fósseis de ambas as icnofácies.

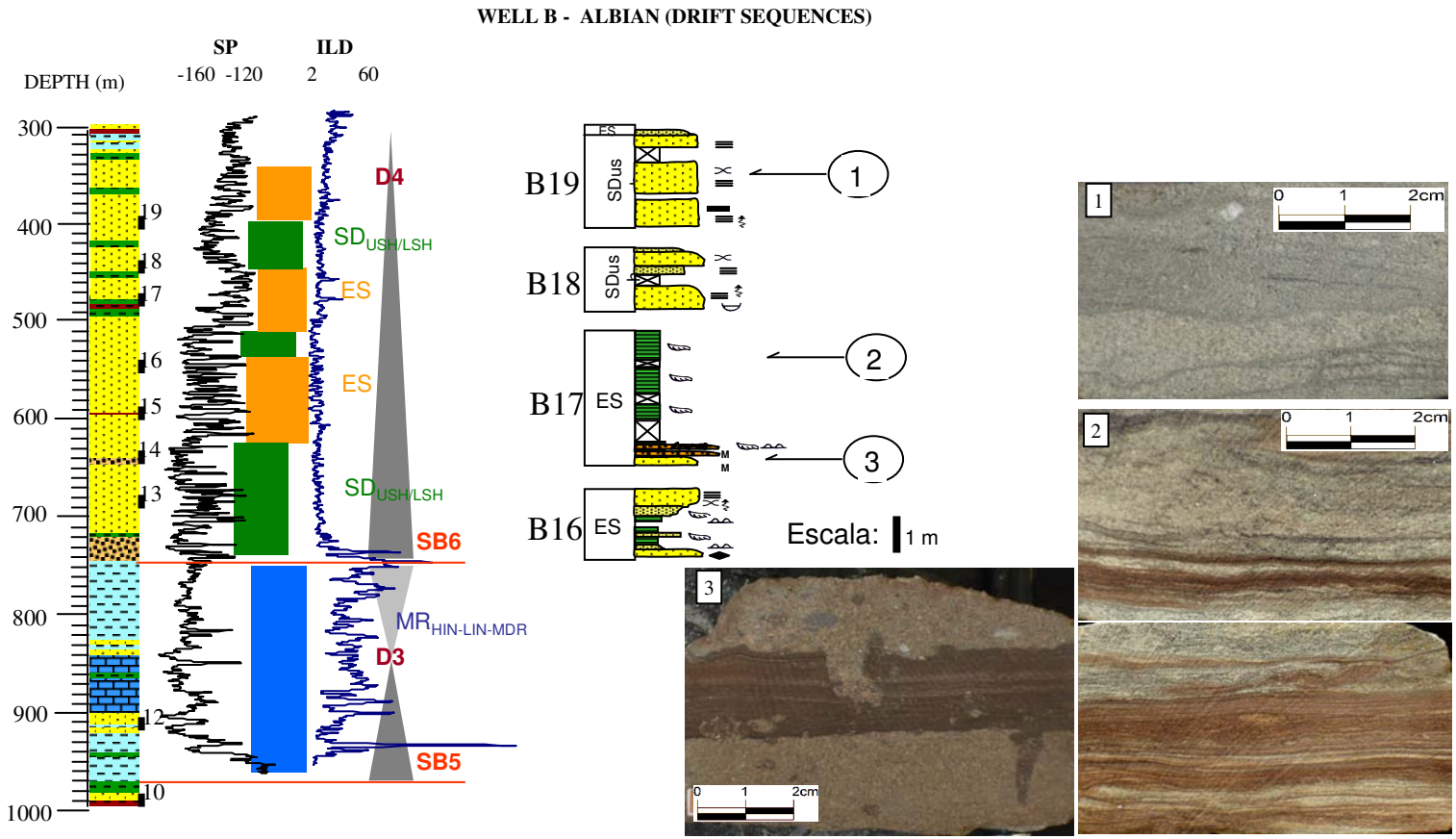

Fig. 9. Associações de fácies SD e ES. Fotografias digitais de testemunhos mostrando: arenitos médios a grossos, mal selecionados, arcósios líticos, alternando entre (foto 1) fácies cinza claras com estratificações plano-paralelas e lutitos cinza escuros (possíveis *mud drapes*), interpretadas como registro de leques deltaicos (fácies SD) na forma de fácies de frente deltaicas ou planícies deltaicas, intercaladas com depósitos de ambiente estuarino (fotos 2 a 3) a planície de maré (*tidal flat*) (fácies ES), localmente possível fácies fluvial (proximal) (foto 3?). Laminações finas (argila) interpretadas como *crinkled laminae* em conformidade com estruturas tipo marcas onduladas, possivelmente corrente (*current ripples*). Intervalos arenosos grossos (foto 3), mas selecionados, intercalados com lutitos avermelhados, com contatos abruptos, localmente com feições de carga (*load casts* - parte superior do intervalo argiloso), interpretados como depósitos de canais de maré (ou possíveis canais distributários de planície deltaica). Observa-se a presença de possíveis traços fósseis (*planolites*? - metade inferior do intervalo argiloso, e marcas de raízes - topo do intervalo arenoso inferior).

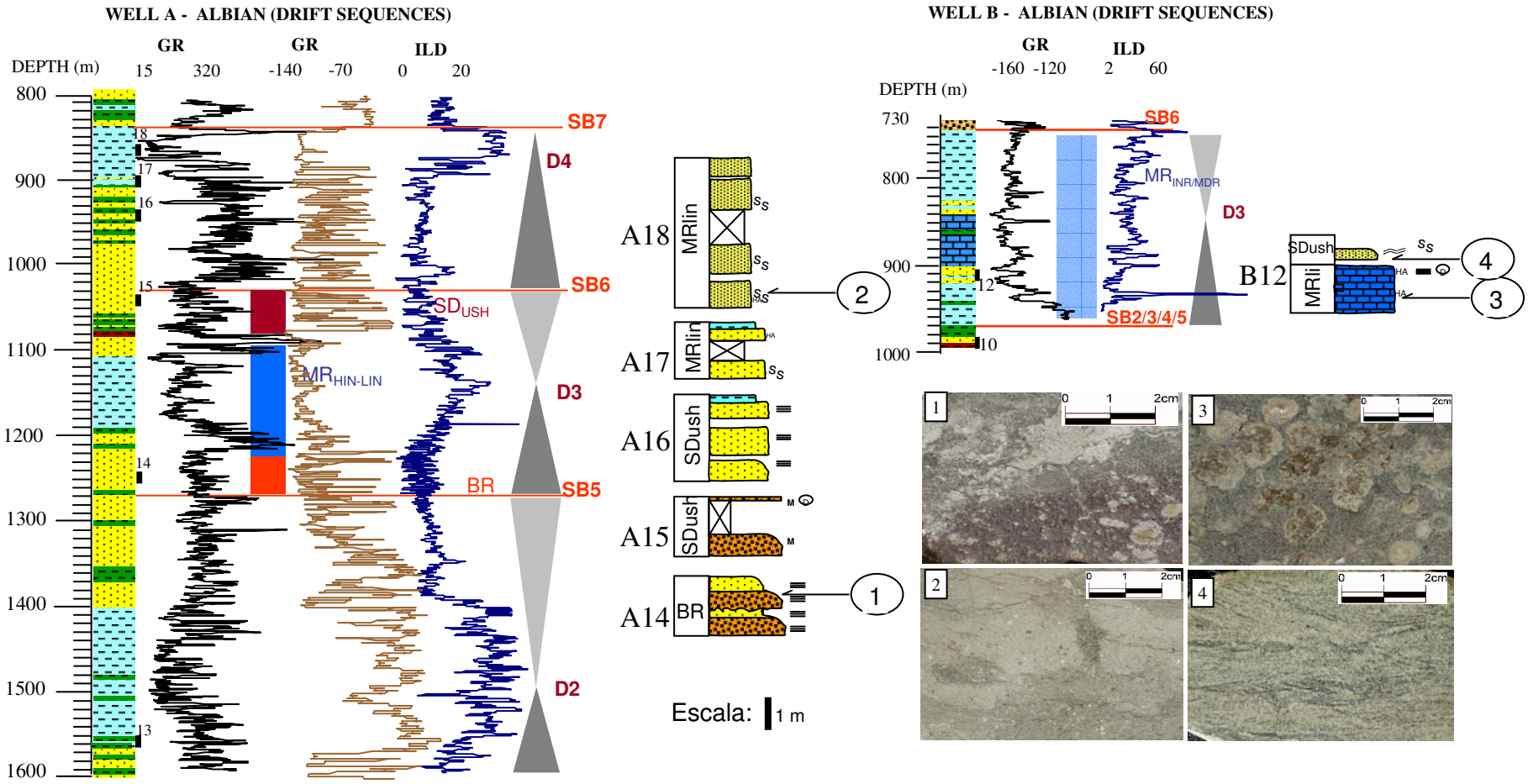

Fig. 10. Associações de fácies BR, SD e MR. Fotografias digitais de testemunhos mostrando: 1) Arenitos médios a grossos com estratificações plano-paralelas e cimentação deslocante carbonática (dolomita) localizada, interpretada como fácies fluviais (tipo *braided* – entrelaçado) de canal ativo; 2) arenito híbrido (> 30% grãos carbonáticos), localmente bioturbado (Sbh); 3) calcirrudito oncolítico (oncolitos centimétricos) micrítico? (imersos em matriz carbonática dolomitizada?), consistindo em dolopackstone oncolítico bioclástico, com substituição parcial dos oncolitos (núcleo) por cimentação dolomita e anidrita; 4) arenito médio a fino, micáceo, com estratificações cruzadas onduladas *ripples de oscilação* (Sw), interpretado como registro de ambiente costeiro com maior influência de ondas ao longo do ambiente de plataforma interna.

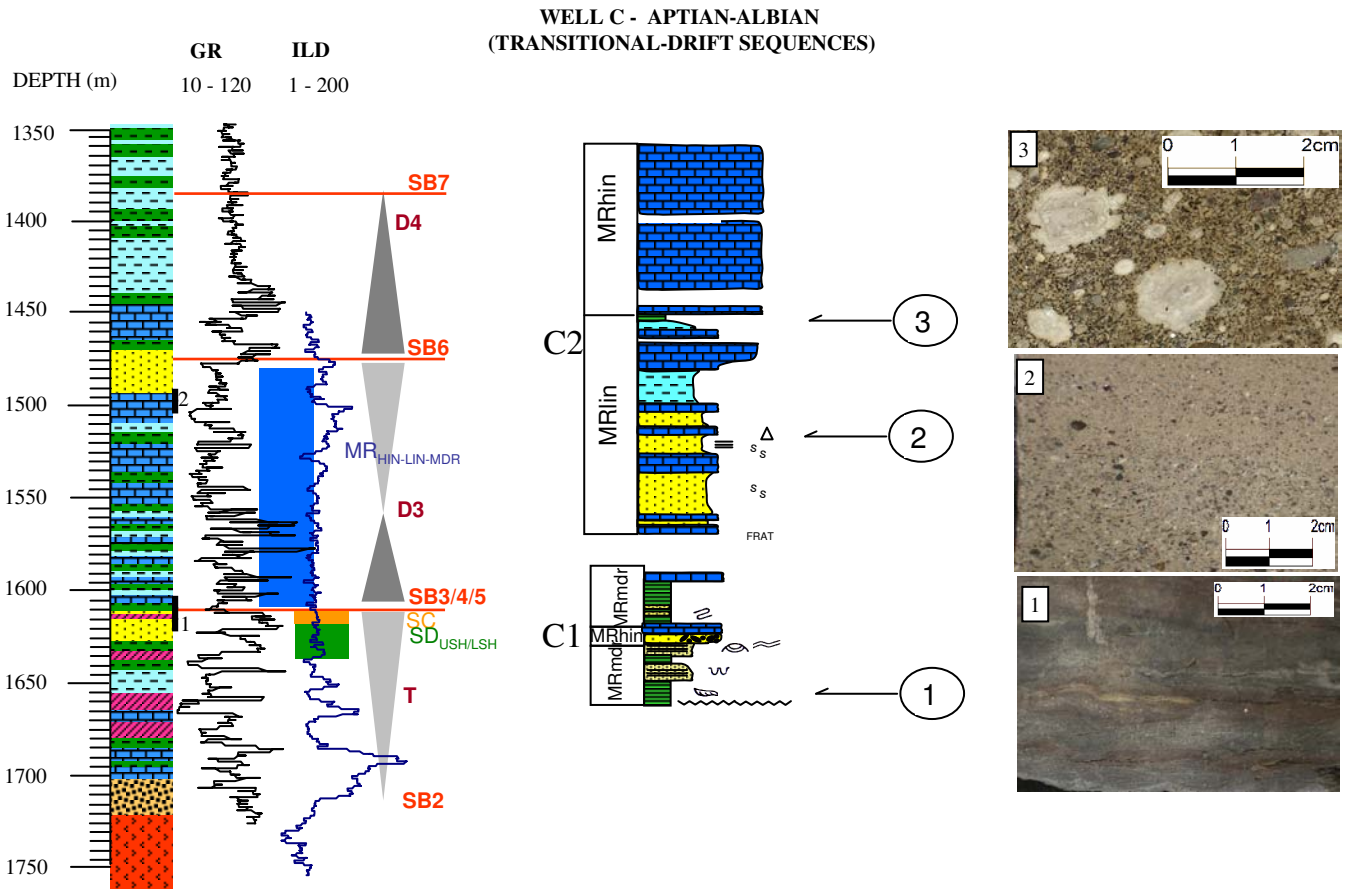

Fig. 11. Associação de fácies MR. Fotografias digitais de testemunhos mostrando: 1) lutitos cinza escuros, localmente ricos em carbonatos (litofácies Flc), consistindo em lâminas de calcilutitos cinza claras e lutitos cinza escuros, localmente deformados (fluidização?); 2) arenitos híbridos com gradação normal; 3) packestones oncolítico e bioclástico, interpretado como associado a zona de transição entre fácies de mais baixa energia (plataforma interna) e fácies de mais alta energia (sotoposta ao ponto fotografado), caracterizada por *grainstones* oolíticos.

As descrições de testemunhos foram aprimoradas com a descrição petrográfica de 67 lâminas delgadas (ANEXO A), cujos resultados estão sumarizados em duas tabelas de análise petrográfica quantitativa (percentuais médios relativos ao volume total – *bulk rock volume*) com as amostras agrupadas conforme os tratos de sistemas e/ou seqüências deposicionais (ARTIGO I) e conforme a classificação em *petrofácies reservatório* (ARTIGO II). Fotomicrografias óticas e imagens de elétrons retro-espalhados (BSE), com suporte de análises de espectrometria de energia dispersada (EDS), de parte das lâminas, são apresentadas nos ANEXOS B e C, respectivamente, evidenciando fases autigênicas, suas relações paragenéticas e seu impacto na qualidade de reservatório do intervalo estudado. Análises de difratometria de raios-X foram realizadas em 5 amostras contendo percentual significativo de argilo-minerais autigênicos, identificados via petrografia óptica, de modo a dar suporte às análises petrográficas. Os difratogramas e interpretações são apresentados no ANEXO D.

Apenas os dados geofísicos (sísmica de reflexão) referentes aos poços A e C foram integrados à caracterização das *petrofácies de reservatório* (ARTIGO II) por possuírem amarração com seções sísmicas com qualidade adequada para avaliação de sismofácies (Fig. 12). Os resultados mais favoráveis foram obtidos no poço A, em virtude da limitada dimensão temporal (vertical) do intervalo de estudo no poço C. Entretanto, o caráter *strike* da linha sísmica ao longo do poço A não permitiu a aplicação robusta das técnicas sismoestratigráficas, tais como a identificação de terminações de reflectores.

A integração dos dados geofísicos no poço A permitiu: (i) identificar limites superiores e inferiores dos intervalos carbonáticos (alto contraste de impedância); (ii) delimitar intervalos com alto contraste de amplitude sísmica, correlacionáveis com intervalos litológicos com alto percentual de cimentação, permitindo aferir intervalos (seqüências deposicionais) com bom controle da assinatura geofísica sobre a qualidade de reservatório; e (iii) delimitar intervalos com respostas sísmicas similares, porém com composição detrítica e/ou evolução diagenética distintas, com impacto nos parâmetros de porosidade e permeabilidade, permitindo aferir intervalos com baixo controle da assinatura geofísica sobre a qualidade de reservatório. Os resultados da integração desses dados e interpretação de sismofácies foram incorporados na caracterização das *petrofácies de reservatório.*

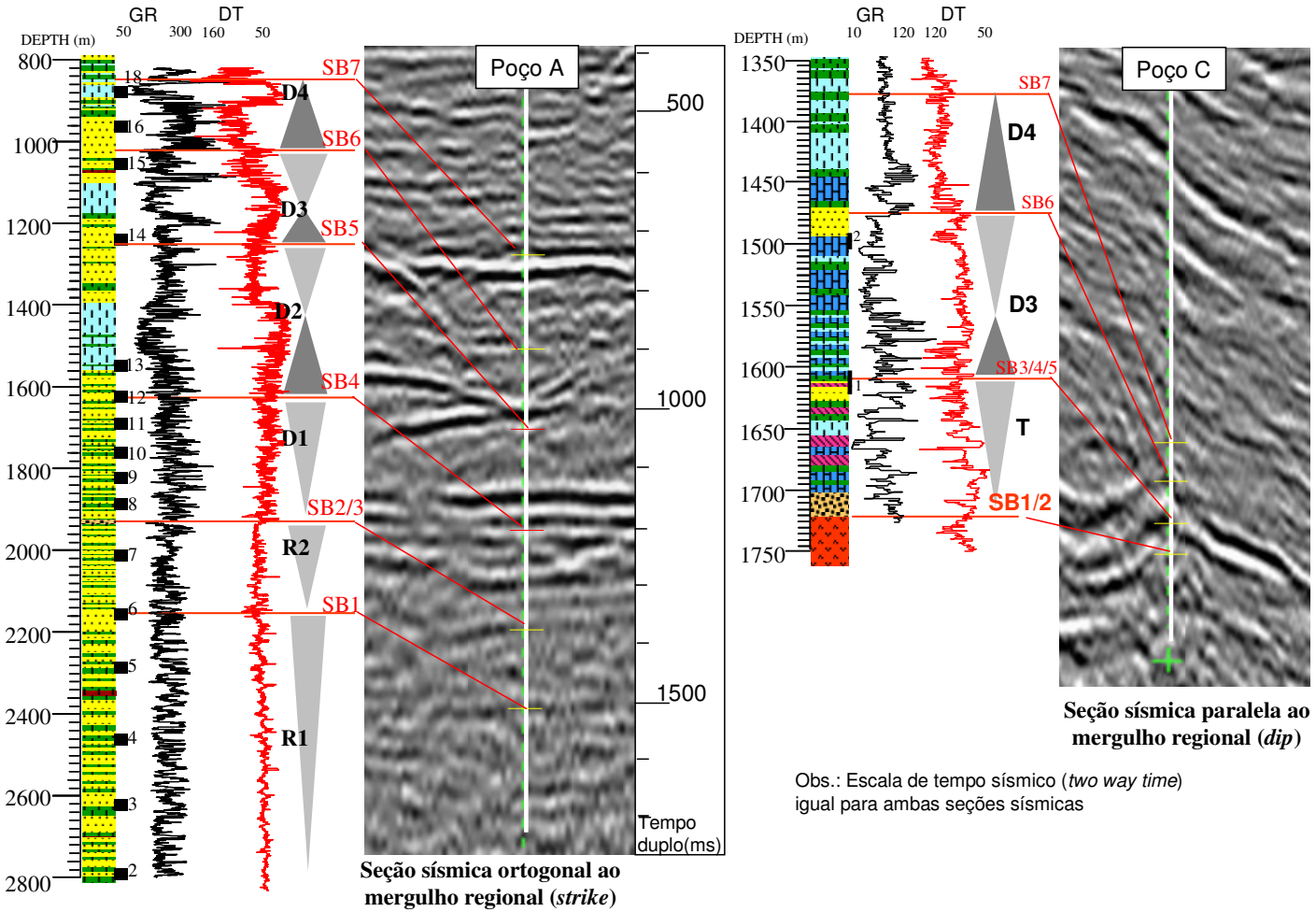

Fig. 12. Amarração sísmica-poço referente aos poços A e C.

Foram realizadas análises isotópicas (isótopos de carbono, oxigênio e enxofre) em 14 amostras representativas, distribuídas ao longo do arcabouço estratigráfico, objetivando determinar as condições geoquímicas de precipitação de cimentos eodiagenéticos de dolomita e mesodiagenéticos de anidrita, e do intervalo evaporítico Aptiano. Os resultados das análises são apresentados no ARTIGO I, bem como a sua interpretação (i.e. relação com o ambiente deposicional).

Na elaboração do arcabouço estratigráfico (Fig. 3) foram utilizados os perfis elétricos (poço) de raios-gama (GR), potencial espontâneo (SP) e sônico (DT), visando estimar a argilosidade e a qualidade do reservatório, tecer inferências sobre ambientes deposicionais, identificar as discordâncias mais significativas, estabelecer a correlação litológica com os testemunhos e sua extrapolação para o intervalo não testemunhado (ARTIGO I). Para a caracterização das *petrofácies de reservatório*, além das curvas anteriores, foi utilizado o perfil de resistividade por indução (ILD), para estimativas do grau de cimentação (ARTIGO II). Face à ausência de medidas petrofísicas em diversos dos pontos amostrados por lâminas petrográficas, porosidade e permeabilidade foram estimadas, onde necessário, com base nas características petrográficas observadas via microscopia ótica e eletrônica (ARTIGO II).

6. Discussão resumida

6.1. Classificação em *Petrofácies de Reservatório*

A determinação da qualidade de reservatório ao longo do intervalo Aptiano-Albiano se deu pela integração dos dados discutidos no item anterior, de modo a classificar as litologias amostradas (arenitos siliciclásticos, híbridos e carbonáticos) em *petrofácies de reservatório*, segundo as definições e procedimentos sugeridos em De Ros e Goldberg (2007). A grande variação na composição primária e diagenética, bem como nas assinaturas petrofísicas e geofísicas, refletindo a complexidade e a diversidade de ambientes deposicionais e contextos tectônico-estratigráficos (tratos de sistemas e/ou seqüências deposicionais) amostrados, resultou na caracterização de 14 *petrofácies de reservatório* (ARTIGO II), apresentadas de forma esquemática ao longo das próximas páginas:

MEGAESCALA

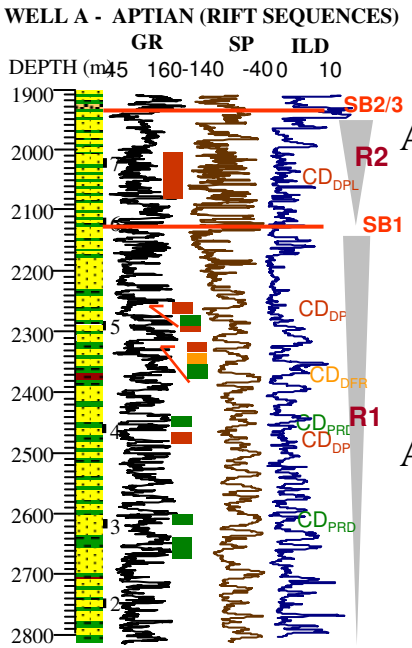

Características & controles:
- Fácies CD (poço A)/ FD (poço B)
- Baixos valores de SP-GR-ILD
- Resposta sísmica de baixo contraste de amplitude

MACROESCALA

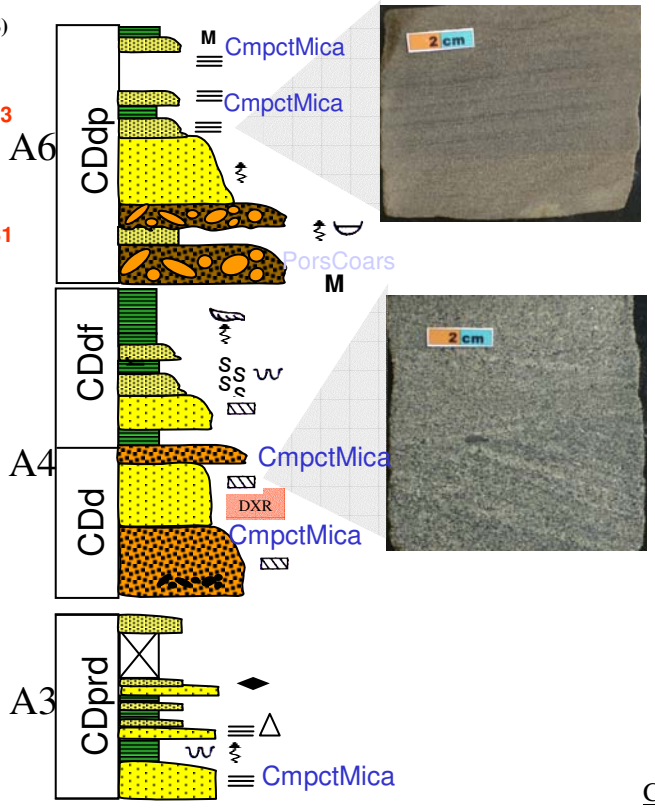

Características & controles :
- Composição detrítica – Fácies deposicionais fluvio-deltaicas de baixa energia; alto conteúdo em mica (orientação ao longo do acamamento)

MICROESCALA

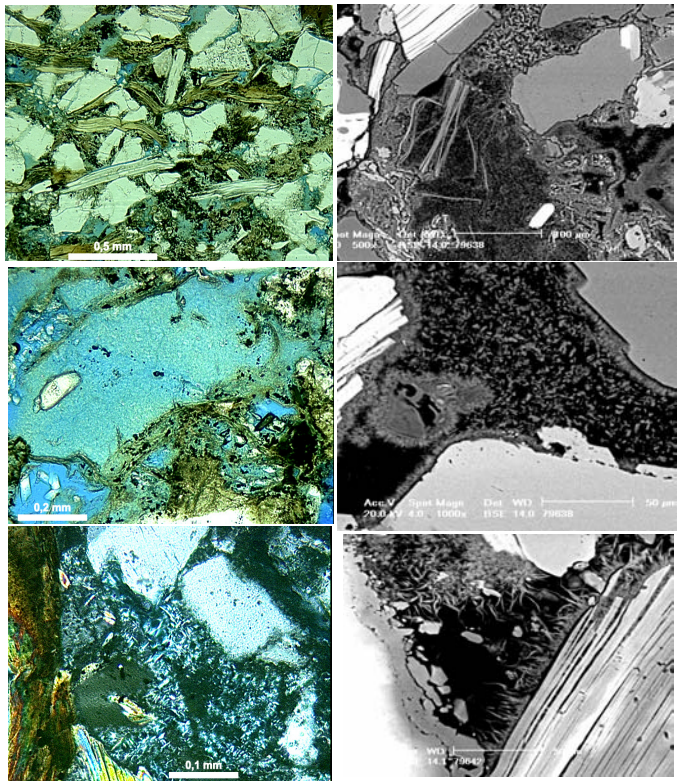

Características & controles :
- Composição detrítica – Arcósios a arcósios líticos, com granulometria media a grossa, mal selecionados, com alto conteúdo em grão dúcteis (pseudomatrix) e instáveis - alteração de intraclastos lamosos e fragmentos de rocha
- Diagênese - franjas de Mg-clorita e I-S; pseudomatrix alterada a mica, clorita, I-S e/ou dickita; quartzo outgrowths
- Compactação moderada – orientação micas e deformação grãos
- Macroporosidade variável (8-20%) – função do percentual em mica (3-28%) e deformação de líticos
- Permeabilidade estimada: Baixa

PF CmpctMica

MEGAESCALA

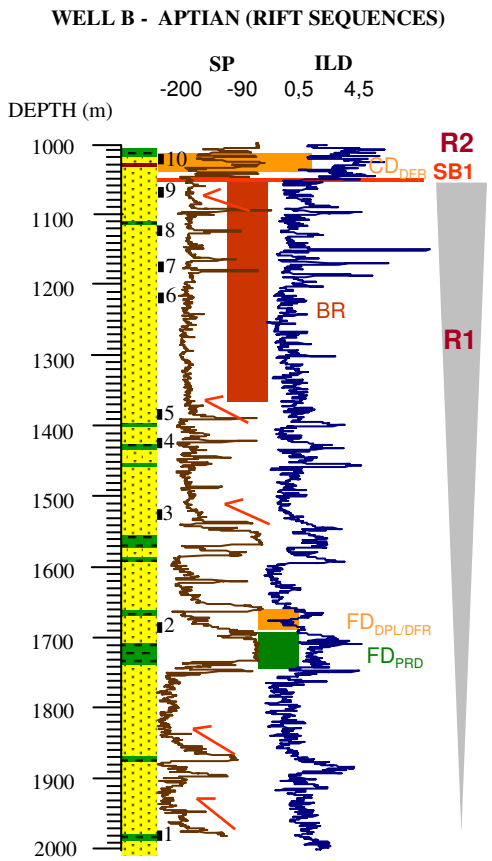

Características & controles:

• Fácies FD/BR

• Baixos valores SP-ILD e relativamente alto DT (fácies arenosas e porosas)

MACROESCALA

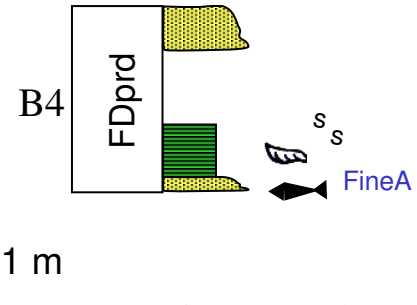

Características & controles :

• Deposicionais - fácies fluvio-deltaicas de baixa energia com baixo percentual de grãos líticos e micáceos (boa maturidade) e com seleção moderada (relativo transporte)

MICROESCALA

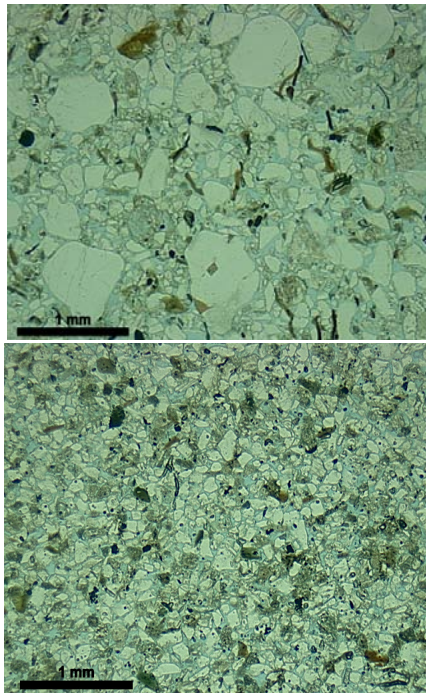

Características & controles :

• Composição detrítica – Arcósios finos a médios, mal a moderadamente selecionados

• Diagênese – cimentação intergranular pouco expressiva

• Compactação moderada

• Macroporosidade variável (av. 19%) face à seleção variável e, em menor escala, percentual de fragmentos de rocha metamórfica

• Permeabilidade estimada: Moderada a boa

PF FineA

MEGAESCALA

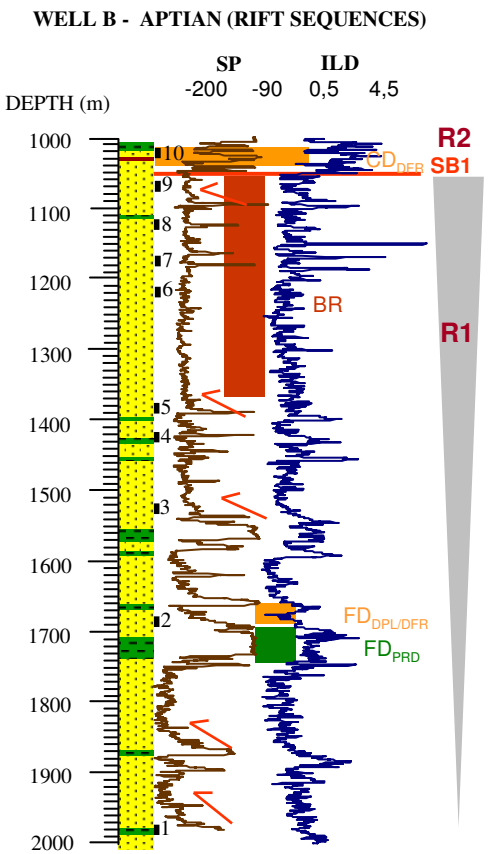

Características & controles:

- Fácies BR
- Padrão regular (reto) em perfil SP com baixos valores (fácies arenosas)
- Altos valores de resistividade (cimentação)
- Sem relação a ciclos de *coarsening-upward* (sistema *braided* amalgamado)

MACROESCALA

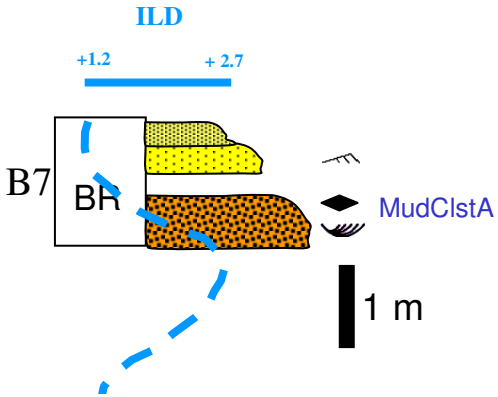

Características & controles :

- Deposicionais - facies de canais fluviais (alta energia) com alto percentual em intraclastos lamosos

MICROESCALA

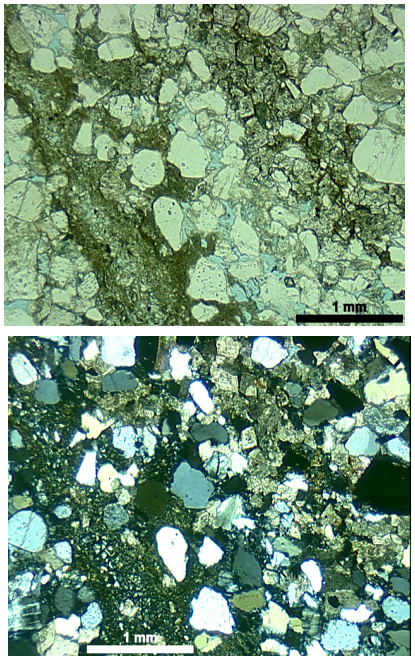

Características & controles :

- Composição detrítica – Arcósios grossos, mal selecionados, com alto percentual de intraclastos lamosos
- Diagênese – intensa dolomitização (preferencialmente intraclastos e pseudomatrix) e presença de *saddle dolomite*
- Compactação variável e diferenciada com base na presença de intraclastos (pseudomatrix)
- Macroporosidade moderada (13%)
- Permeabilidade estimada: Moderada

PF MudClstA

MEGAESCALA

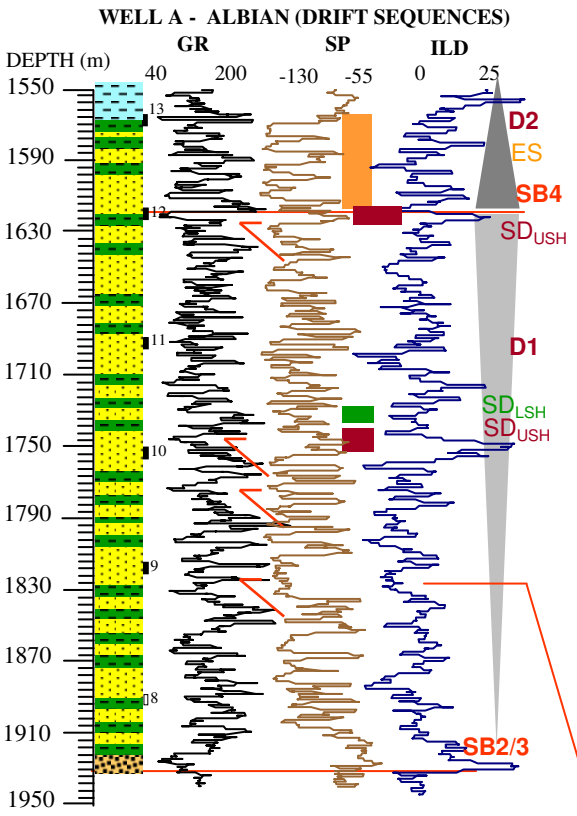

Características & controles:
- Fácies SD
- Baixos valores de GR-SP-ILD
- Resposta sísmica de baixo contraste de amplitude

MACROESCALA

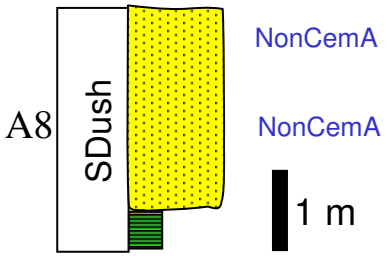

Características & controles :
- Deposicionais - facies fluvio-deltaicas de média a alta energia (*shoreface to foreshore*)

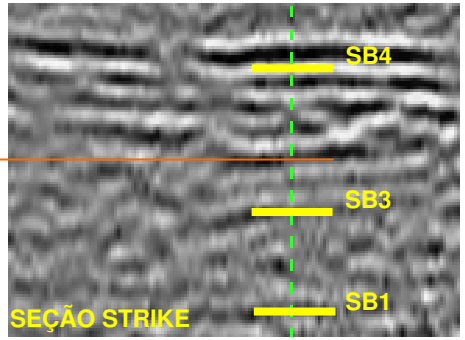

MICROESCALA

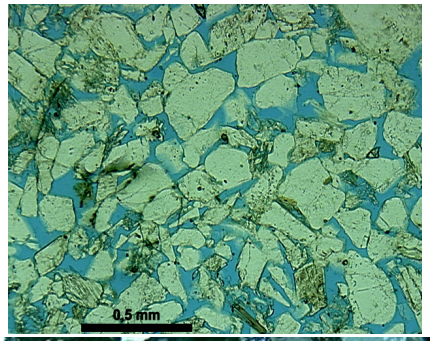

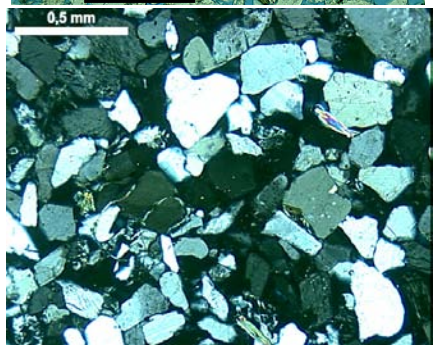

Características & controles :
- Composição detrítica – Arcósios médios, mal selecionados
- Diagênese – pouco expressiva
- Compactação moderada
- Macroporosidade moderada (14 a 17%)
- Permeabilidade estimada: moderada a alta

PF NonCemA

MEGAESCALA

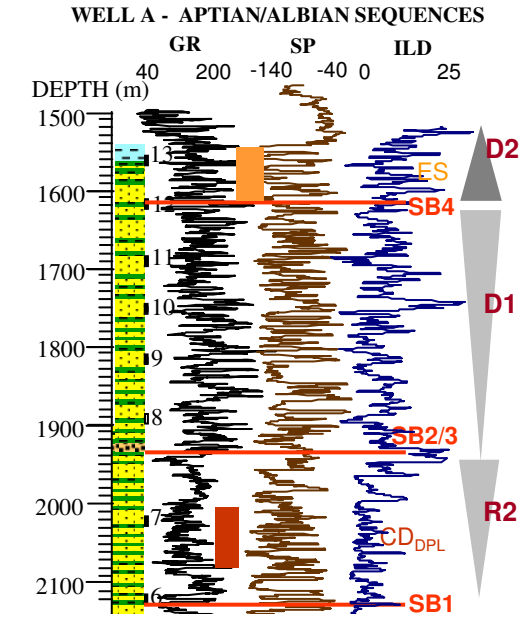

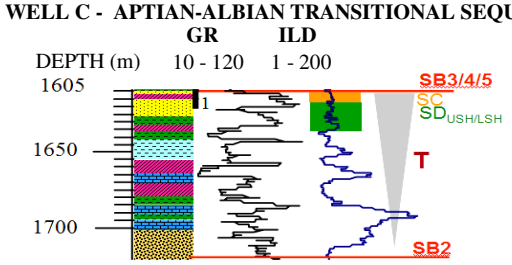

Características & controles:
- Fácies CD/SD
- Baixos valores de GR-SP e altos valores de ILD
- Resposta sísmica de alto contraste de amplitude quando intercalada com fácies porosas

PF CemA

MACROESCALA

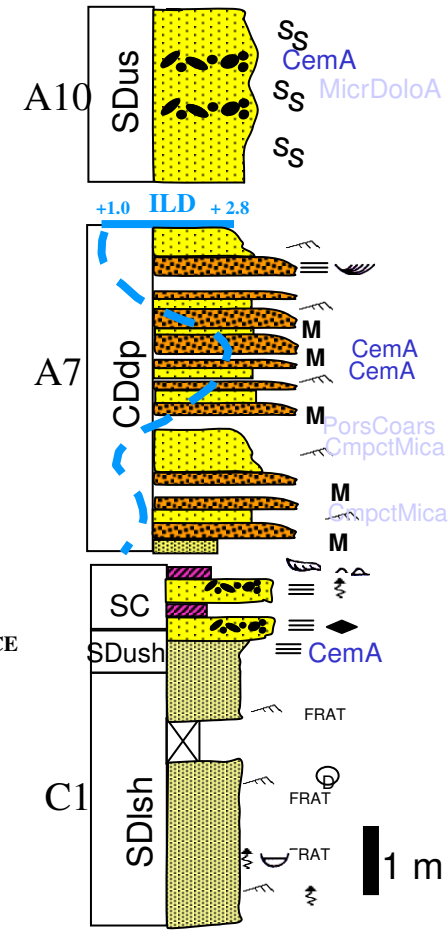

Características & controles :
- Deposicionais - Fácies fluvio-deltaicas de média a alta energia (*shoreface to foreshore*) com alta porosidade deposicional

MICROESCALA

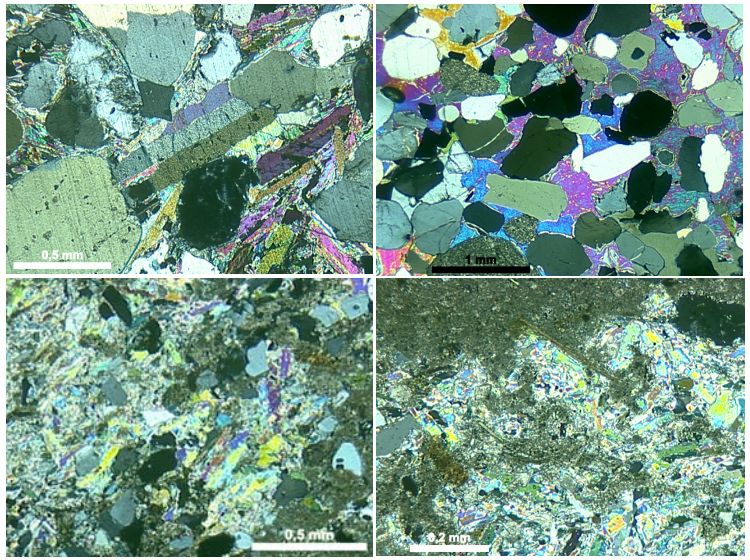

Características & controles :
- Composição detrítica – Arcósios finos (Seq. Transicional) a grossa (Seq. D1), mal selecionados, com baixo percentual grãos dúcteis (micas e fragmentos de rocha)
- Diagênese – intensa cimentação pré-compactacional por anidrita tipo feltro e dolomita microcristalina, ou pós-compactação por anidrita poiquilotópica; Siderita em intraclastos lamosos (solos?)
- Compactação frouxa a moderada
- Macroporosidade baixa (<3%) *f.* cimentação
- Permeabilidade estimada: baixa

MEGAESCALA

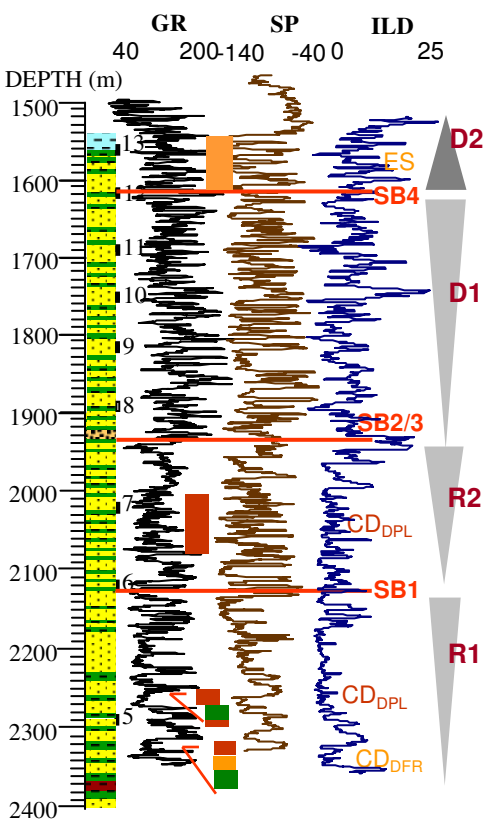

Características & controles:
- Fácies CD/SD
- Baixos valores de SP-GR-ILD
- Resposta sísmica de alto contraste de amplitude na Seq. D1

MACROESCALA

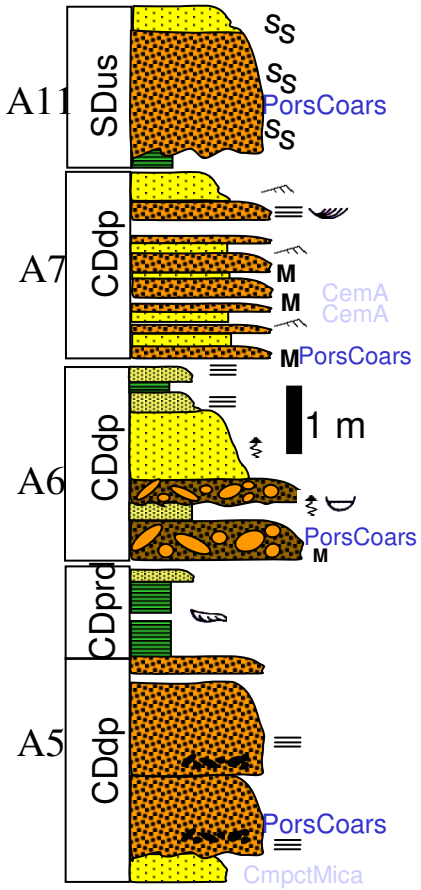

Características & controles :
- Deposicionais - fácies fluvio-deltaicas de alta energia com alta porosidade deposicional estimada

MICROESCALA

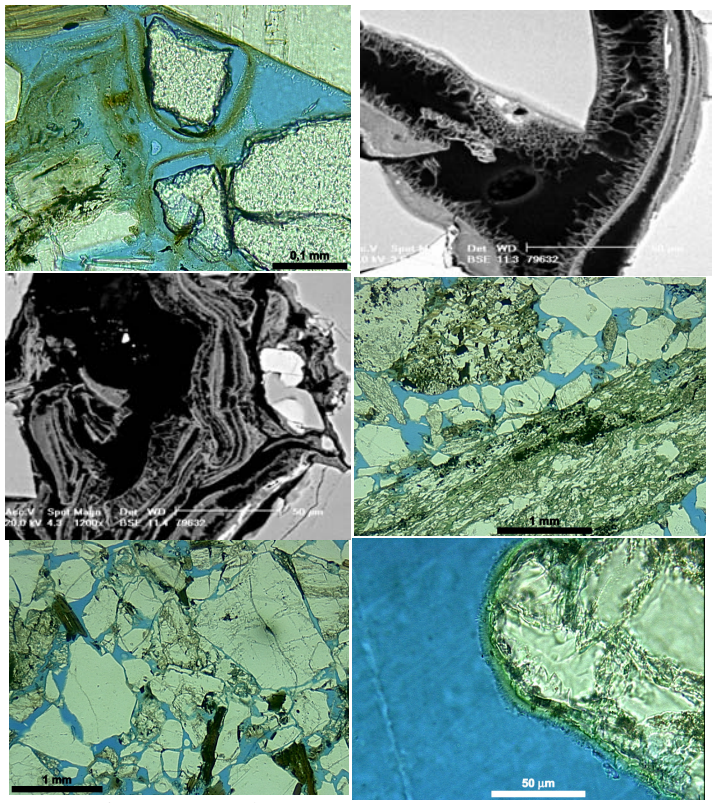

Características & controles :
- Composição detrítica – Arcósios e arcósios líticos com granulometria grossa a conglomerática, mal selecionados
- Diagênese - cimento anidrita pouco expressivo; cutículas esmectita pré-compactação (sin-dissolução de min. pesados), neoformação para corrensita ou Mg-Clorita, e recobrimento por respectivas franjas
- Compactação moderada a frouxa
- Macroporosidade alta (av. 18.3%)
- Permeabilidade estimada: variável (função da presença de franjas ao longo dos contatos entre grãos)

PF PorsCoars

MEGAESCALA

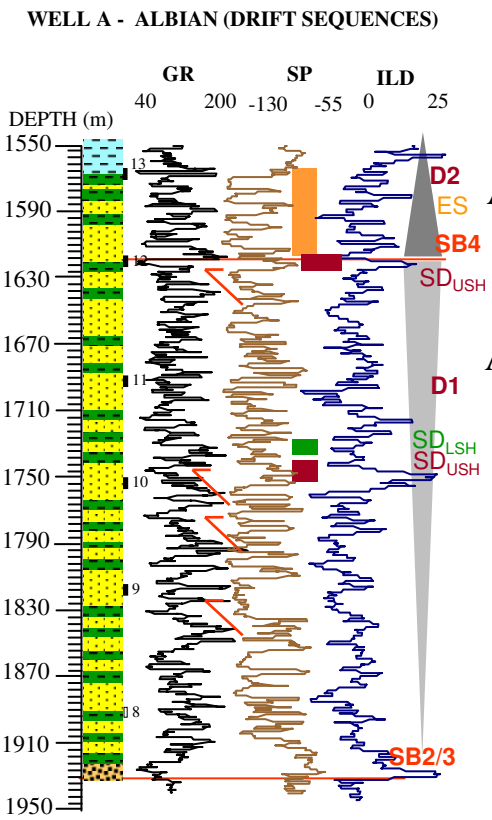

Características & controles:
• Fácies SD/ES: Padrão regular em perfil GR-SP; Ciclos de *coarsening-upward* bem desenvolvidos
• Resposta sísmica de alto contraste de amplitude face à associação vertical com as petrofácies PorsCoars e CemA

MACROESCALA

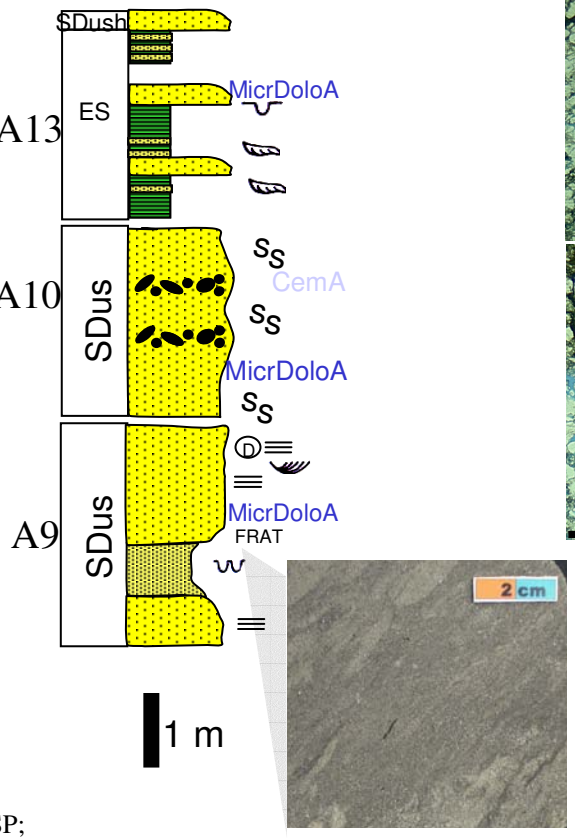

Características & controles :
• Deposicionais - facies fluvio-deltaicas de média a alta energia (*shoreface to foreshore*) com moderada a intensa bioturbação e/ou fluidização

MICROESCALA

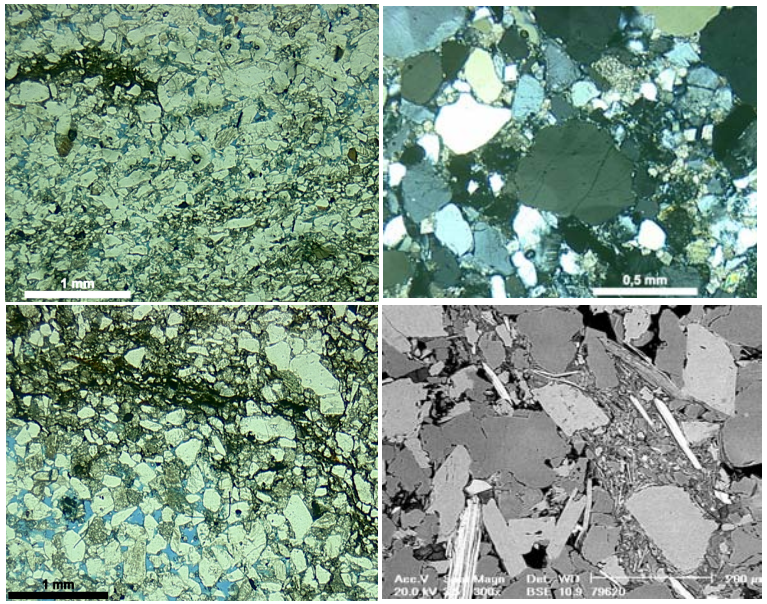

Características & controles :
• Composição detrítica – Arcósios médios a grossos, moderadamente a mal selecionados, localmente com intraclastos lamosos
• Diagênese – variável percentual de cimento intergranular de dolomita (eo- & mesodiag.)
• Compactação moderada
• Macroporosidade variável (av.12.5%) *f.* conteúdo de intraclastos lamosos e cimentação dolomita e anidrita
• Permeabilidade estimada: moderada a alta

MicrDoloA

MEGAESCALA

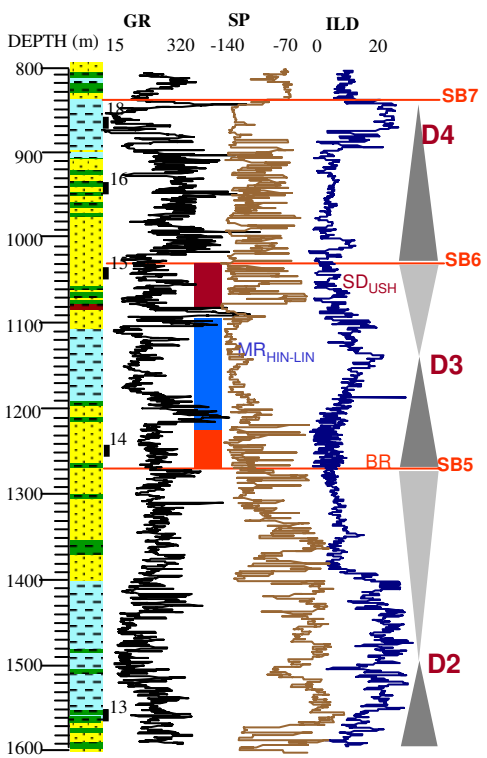

Características & controles:
- Fácies BR
- Baixos valores de SP-GR-ILD (padrão tipo *box)*
- Resposta sísmica de baixo contraste de amplitude

MACROESCALA

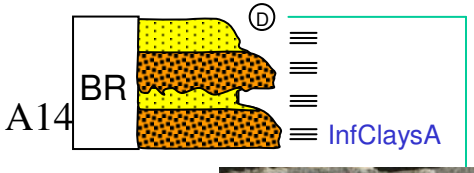

Características & controles :
- Deposicionais - facies fluviais (*braided*) de alta energia

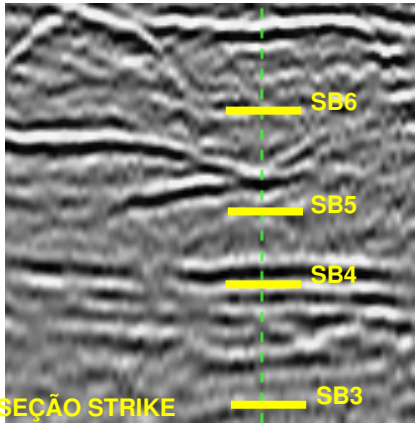

MICROESCALA

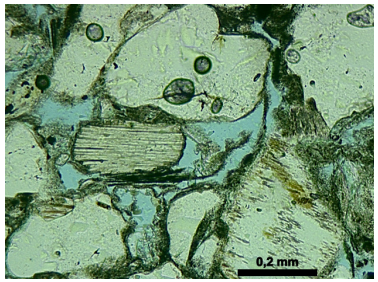

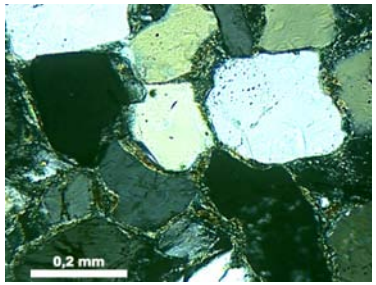

Características & controles :
- Composição detrítica – Arcósios grossos, mal selecionados
Diagênese – infiltração mecânica de esmectitas detríticas desfavorecendo cimentações posteriores
- Compactação moderada
- Macroporosidade baixa (10%) – alta microporosidade e porosidade secundária pelo descolamento das cutículas
- Permeabilidade estimada: Baixa

PF InfClaysA

MEGAESCALA

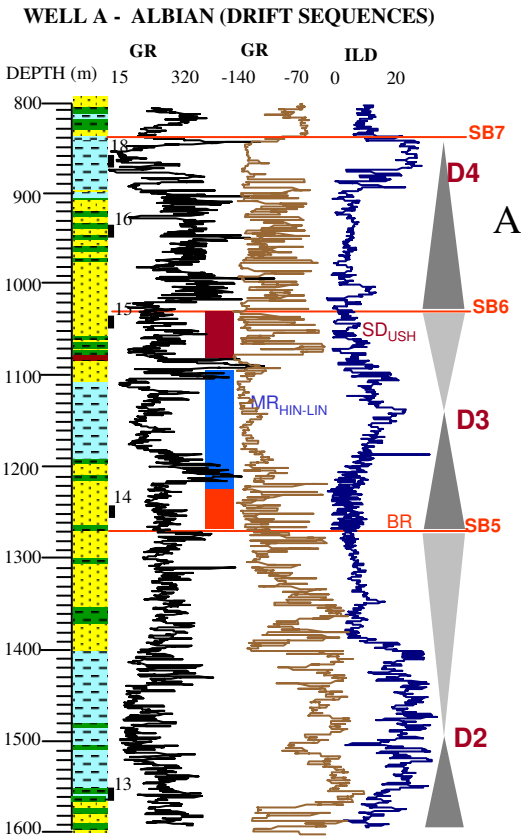

Características & controles:
- Fácies SD
- Baixos valores de GR-SP-ILD

MACROESCALA

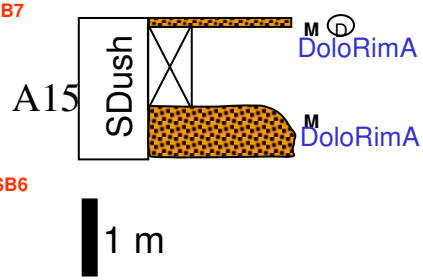

Características & controles :
- Deposicionais - facies frente deltaica a *foreshore* de alta energia

MICROESCALA

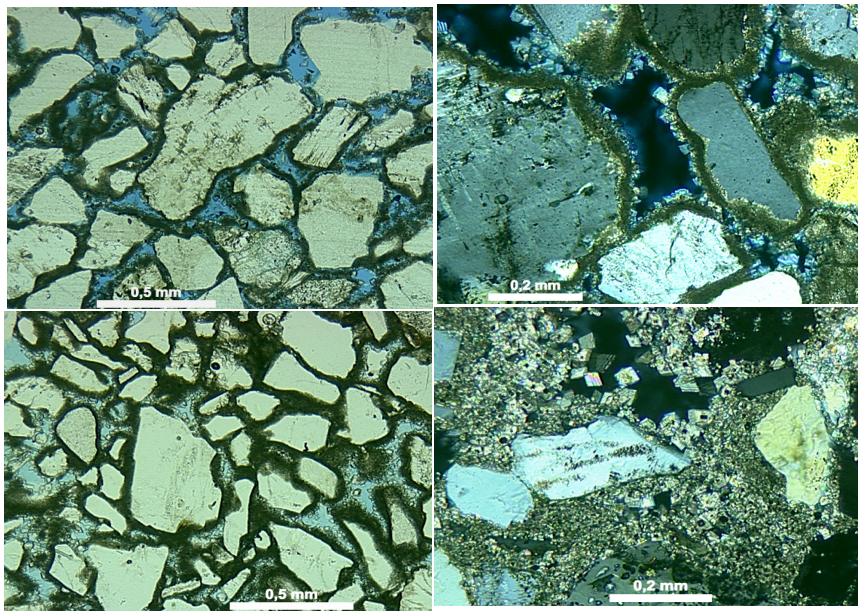

Características & controles :
- Composição detrítica – Arcósios grossos, moderadamente selecionados
- Diagênese – cimentação marinha freática precoce com micritização e franjas de dolomita (substituição Mg-calcita?) e dolomita intraporos nodular/deslocante
- Compactação frouxa
- Macroporosidade moderada (8-17%) função do percentual de cimento dolomita intergranular intraporos
- Permeabilidade estimada: moderada a alta

PF DoloRimA

MEGAESCALA

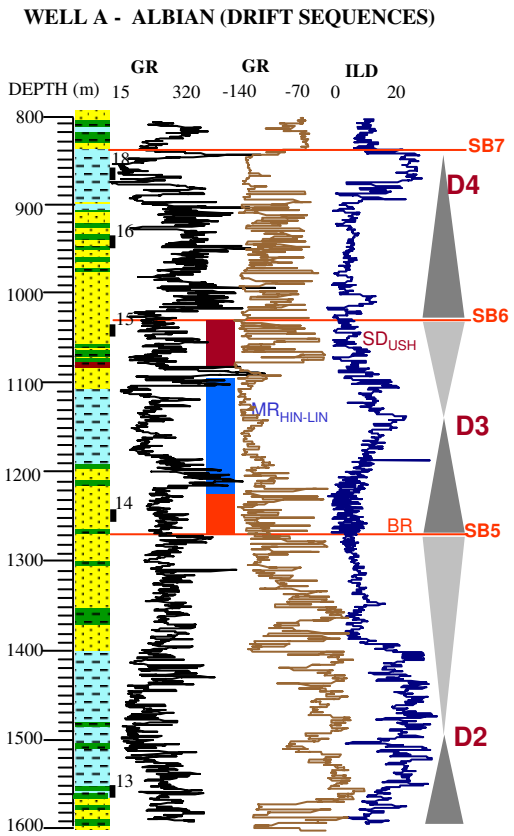

Características & controles:
- Fácies SD
- Padrão irregular em perfil: baixos valores de GR-SP-ILD

MACROESCALA

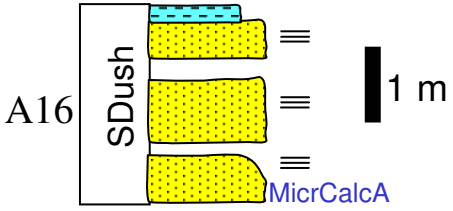

Características & controles :
- Deposicionais - facies fluvio-deltaicas de média a alta energia (*shoreface to foreshore*)

MICROESCALA

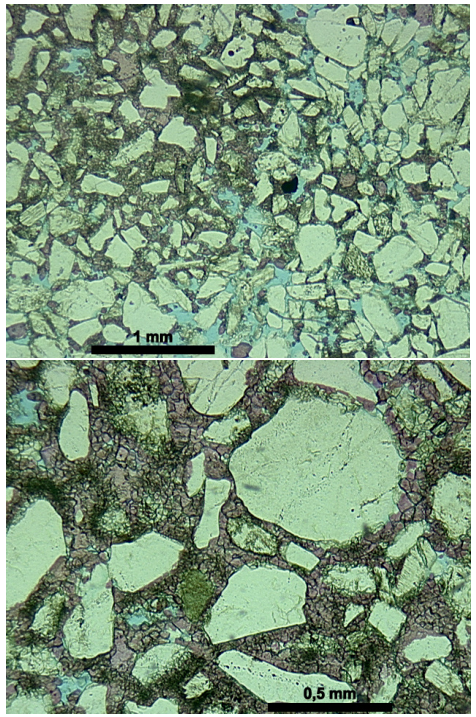

Características & controles :
- Composição detrítica – Arcósios médios, mal selecionados
- Diagênese - cimentação calcita marinha freática precoce (franja microcristalina) e posterior cimentação nodular e deslocante
- Compactação frouxa
- Macroporosidade moderada (15%)
- Permeabilidade estimada: moderada a alta

PF MicrCalcA

MEGAESCALA

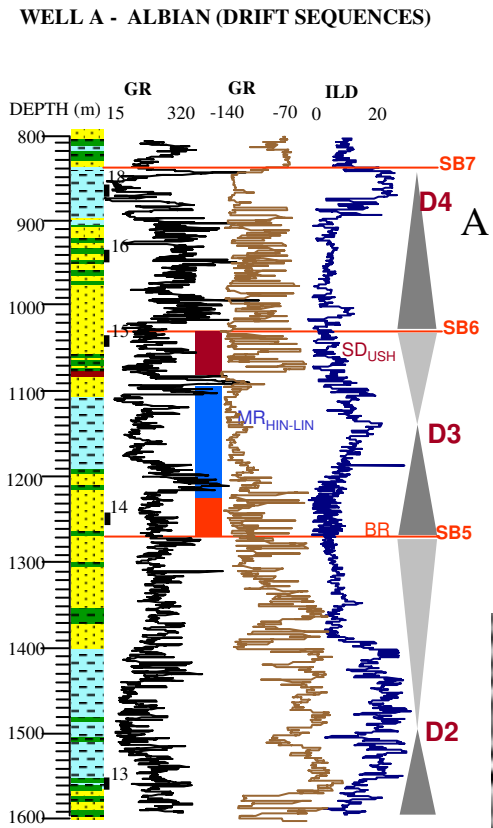

Características & controles:
- Fácies MR
- Baixos valores de GR-SP (tipo *box*) e altos valores de resistividade
- Resposta sísmica de alto contraste de amplitude

MACROESCALA

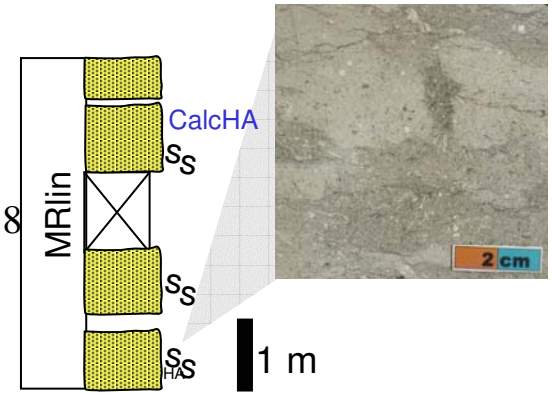

Características & controles :
- Deposicionais – ambiente de plataforma interna de baixa energia com oncolitos e bioclastos

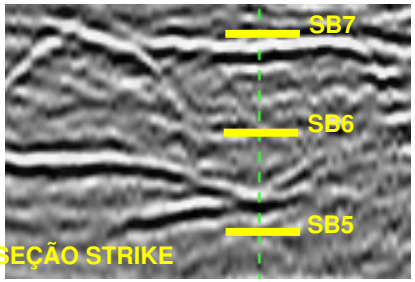

MICROESCALA

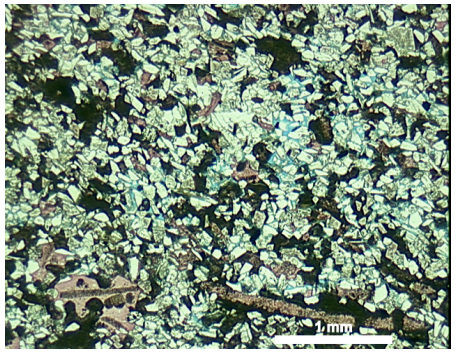

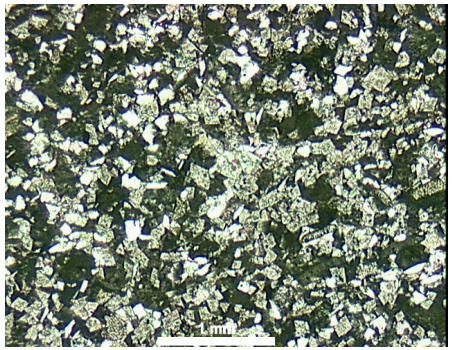

Características & controles :
- Composição detrítica - arenitos híbridos (zona de mistura), com oóides e bioclastos, e grãos extrabaciais quartzo-feldspáticos, finos e mal selecionados
- Diagênese – cimento marinho freático (micritização); crescimento sintaxial calcita (equinodermas)
- Compactação frouxa
- Macroporosidade baixa (1-5%)
- Permeabilidade estimada: Baixa

PF CalcHA

MEGAESCALA

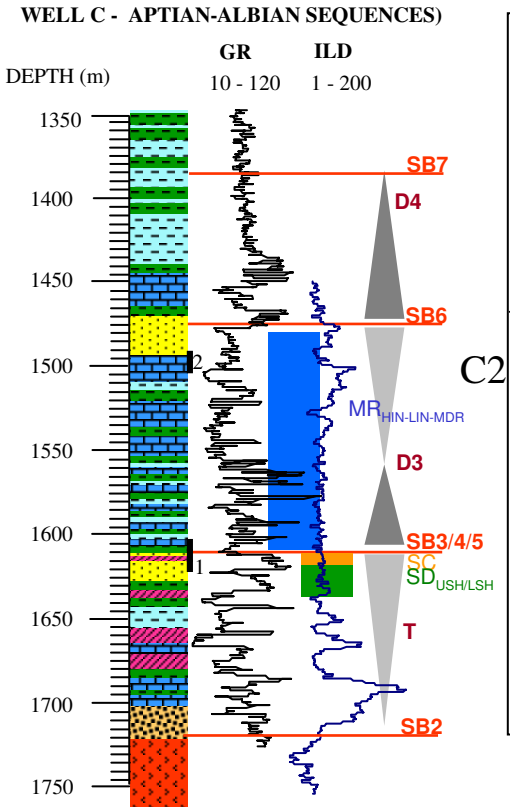

Características & controles:
- Fácies MR
- Padrão regular em perfil GR-SP tipo *box* com baixos valores de resistividade moderados
- Resposta sísmica de alto contraste de amplitude

MACROESCALA

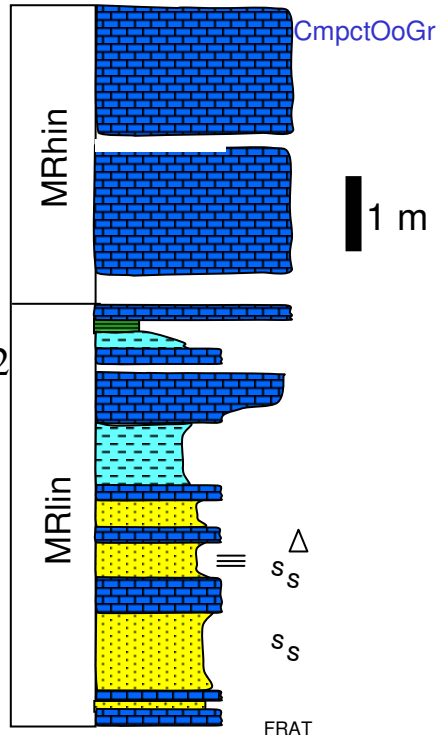

Características & controles :
- Deposicionais – ambiente de plataforma interna de alta energia com oólitos e bioclastos

MICROESCALA

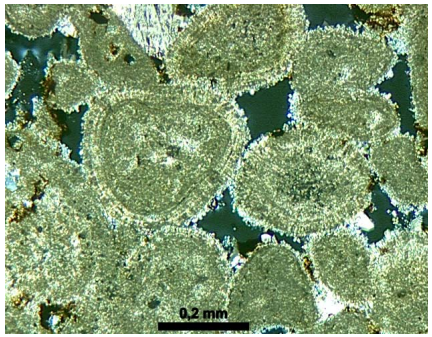

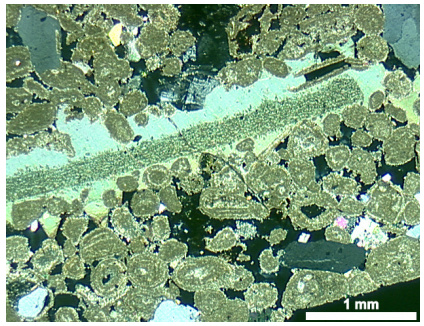

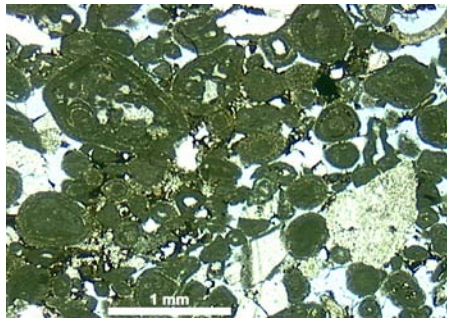

Características & controles :
- Composição detrítica – grainstone oolítico-bioclástico
- Diagênese – cimentação marinha freática menos intensa (em relação à petrofácies CalcHA). Localmente cresc. Sintaxial calcita (equinodermas)
- Compactação moderada - face pouca cimentação
- Macroporosidade baixa (8%)
- Permeabilidade estimada: moderada a alta

PF CmpctOoGr

MEGAESCALA

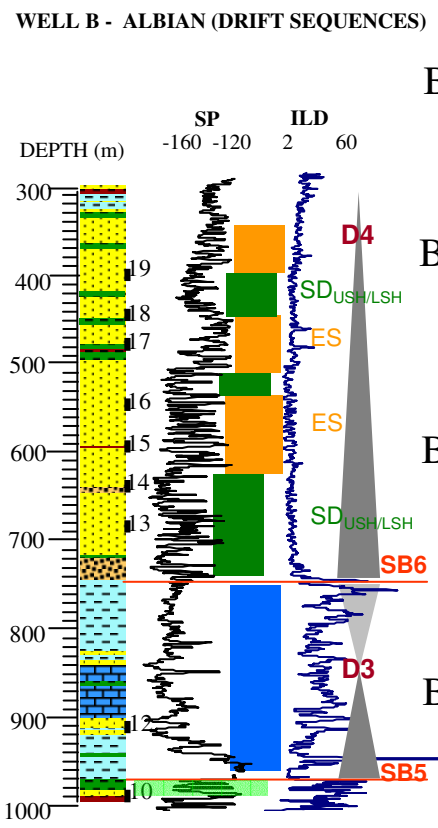

Características & controles:
- Fácies CD/SD/ES
- Baixos valores de SP-ILD

MACROESCALA

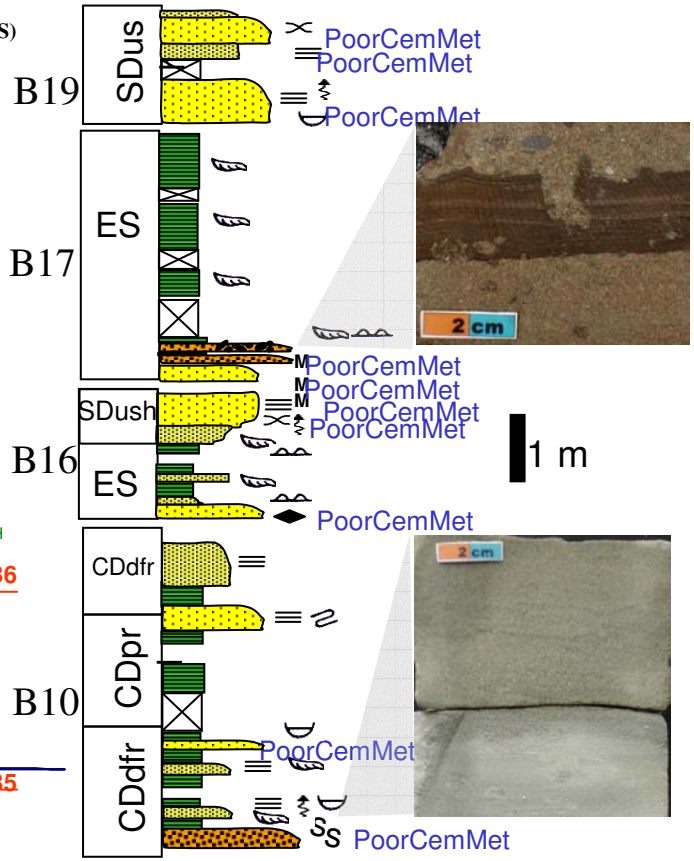

Características & controles :
- Deposicionais - facies fluvio-deltaicas (planície deltaica e frente deltaica) intercaladas com fácies heterolíticas de ambiente estuarino (Seq. D4)

MICROESCALA

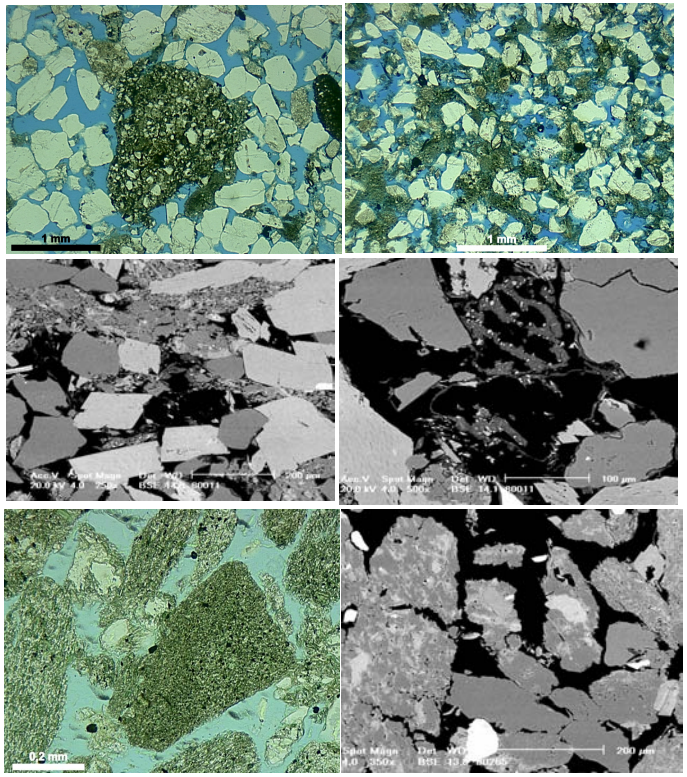

Características & controles :
- Composição detrítica – Arcósios líticos a litarenitos feldspáticos, médios a grossos, mal selecionados, com alto percentual em fragmentos de rochas metamórficas de baixo grau e arenitos (litificação incipiente) – pouco transporte
- Diagênese – cimentação intergranular pouco expressiva e cutículas de esmectitas (minerais pesados dissolvidos)
- Compactação frouxa (pouco soterramento?)
- Macroporosidade alta (13-22%; av. 17%)
- Permeabilidade estimada: alta

PF PoorCemMet

MEGAESCALA

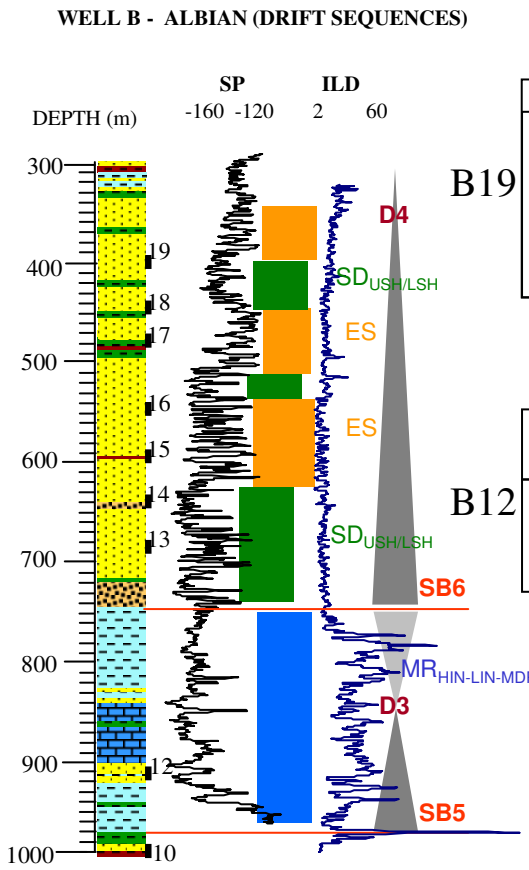

Características & controles:
- Fácies ES-MR
- Baixos valores de SP e altos valores de resistividade

MACROESCALA

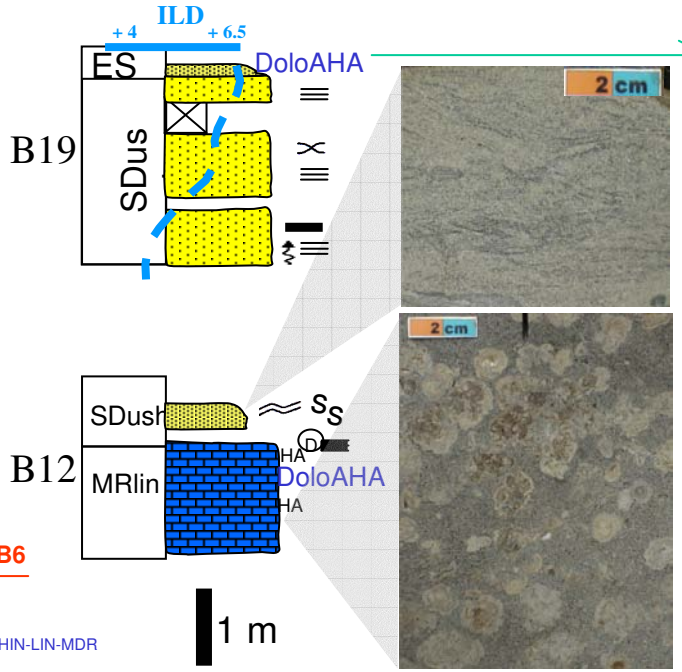

Características & controles :
- Deposicionais – Fácies de plataforma interna de baixa energia com oncolitos e bioclastos ou heterolíticas de ambiente estuarino a planície deltaica

MICROESCALA

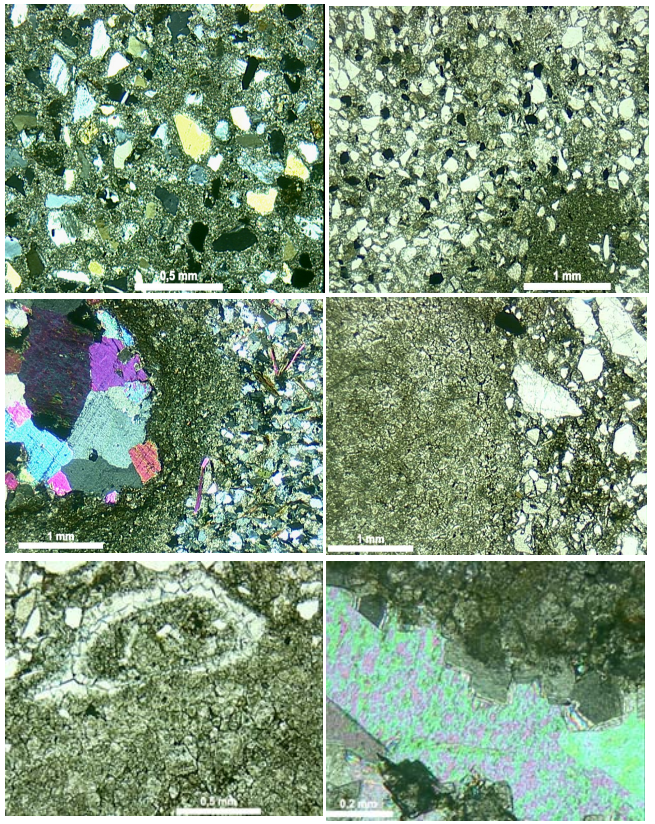

Características & controles :
- Composição detrítica – Arcósios e arenitos híbridos (dolopackstone oncolitico bioclastico), com intraclastos lamosos (pesudomatriz) e micas
- Diagênese – dolomitização intensa; substituição de grãos carbonáticos por dolomita & anidrita
- Compactação frouxa – intensa cimentação precoce
- Macroporosidade baixa (< 1%)
- Permeabilidade estimada: Baixa

PF DoloAHA

6.2. Integração dos dados

A distribuição das amostras (i.e. *petrofácies de reservatório*) com base nos processos mais atuante na redução da porosidade primaria se dá na forma de cinco agrupamentos bem destacados (Fig. 13):

(1) grupo com IGV moderado e com baixa porosidade, referente as petrofácies: (i) com abundante cimento intergranular carbonático eodiagenético, em tratos transgressivos, associadas à fácies de plataforma interna de baixa energia (CalcHA e DoloAHA), ou associadas à fácies estuarinas (DoloAHA); (ii) com abundante cimento intergranular eodiagenético por dolomita microcristalina, em tratos de mar alto, associados à fácies de planície/frente deltaicas (MicrDoloA); ou (iii) com abundante cimento de anidrita mesodiagenética, localmente com a presença de fases eodiagenéticas, em tratos de mar alto a mar alto tardio, associadas à fácies de planície e frente deltaicas (CemA).

(2) grupo com IGV alto e baixa porosidade, referente a petrofácies com abundante cimento intergranular eodiagenético (CemA), localmente deslocante, de dolomita e/ou anidrita, em trato de mar alto tardio, associadas à fácies de planície/frente deltaicas, sotopostas por fácies de sabkha costeiras (intervalo evaporítico).

(3) grupo com baixos valores de IGV e porosidade, referente a petrofácies com escasso cimento intergranular eodiagenético: (i) com alto percentual de grãos dúcteis, consistindo em sedimentos fluviais a fluvio-deltaicos do trato de sistema de mar alto (fase final preenchimento rifte), em especial fácies de energia relativamente menor, com alto percentual em micas (CmpctMica); (ii) com alto conteúdo de cutículas de argila precoces, de trato de sistema de mar baixo (InfClaysA); ou (iii) associado as fácies carbonáticas com reduzida cimentação marinha precoce (CmpctOoGr), de trato de sistemas de mar alto, resultando na compactação do arcabouço carbonático.

(4) grupo com alto IGV e baixa porosidade, referente a petrofácies com alto conteúdo em cimento carbonático eodiagenético, localmente deslocante, em tratos transgressivos, associados à fácies de frente deltaica (MicrCalcA).

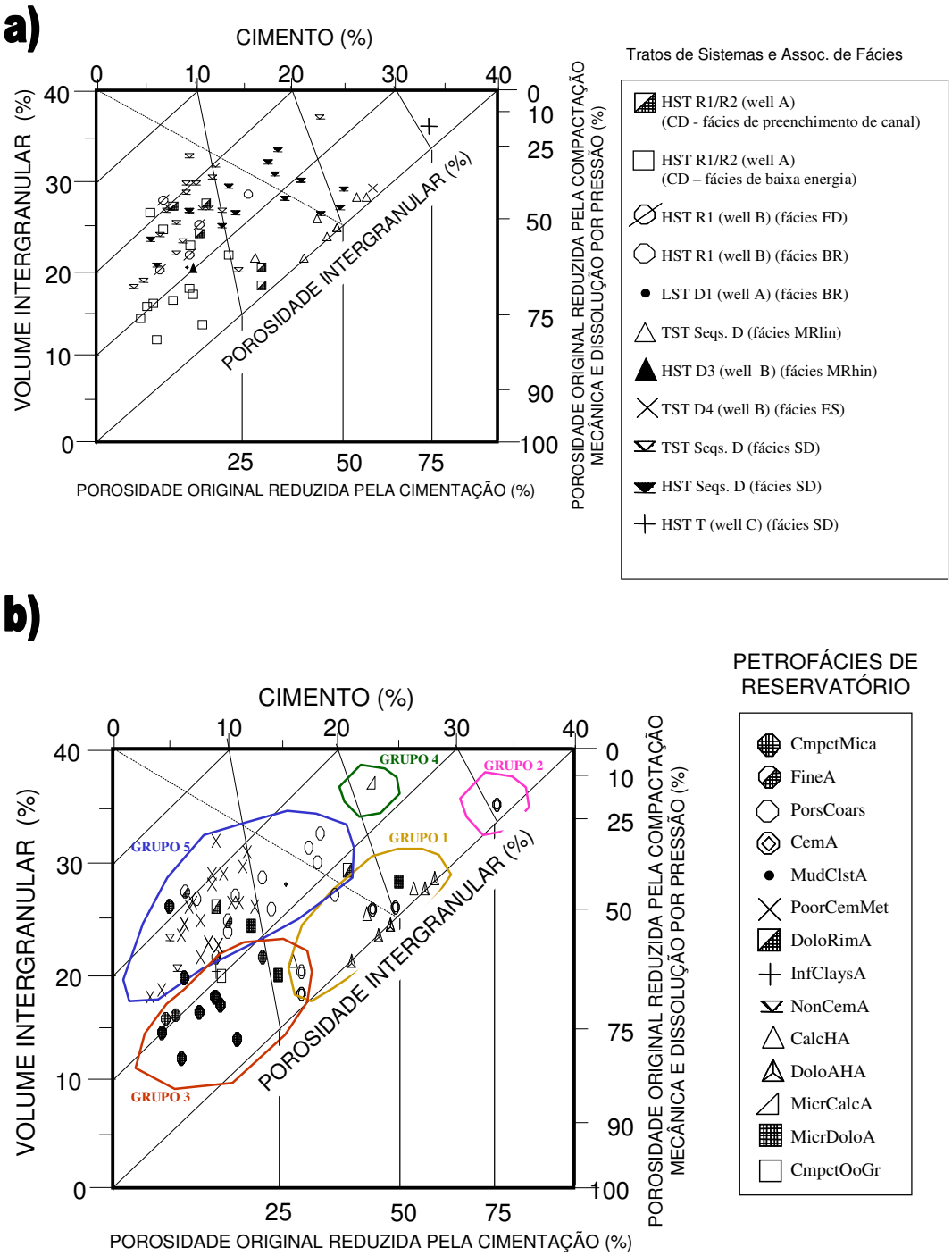

Fig. 13. Diagramas de volume intergranular versus volume de cimento (cf. Ehrenberg, 1989) para agrupamento das amostras de acordo com o ambiente deposicional interpretado (a) e com *petrofácies de reservatório* (b).

(5) grupo com valores moderados a alto de IGV e porosidade, referentes a petrofácies: (i) com baixo a moderado conteúdo em cimento intergranular carbonático (dolomita)

eodiagenético, em geral na forma de concreções ou nódulos localizados, localmente inibindo a compactação, em tratos de mar alto, associados à fácies de planície/frente deltaicas (NonCemA, PorsCoars e DoloRimA), ou fácies fluvio-deltaicas (planície deltaica) de preenchimento de canal (PorsCoars); (ii) com empacotamento frouxo, relacionadas a intervalos com pouco soterramento (PoorCemMet); ou (iii) com cimentação eodiagenética pouco expressiva, relacionada à fácies de mar alto com seleção moderada e baixo conteúdo de grãos dúcteis (FineA).

Os depósitos da fase final de preenchimento rifte (*highstand system tract*), com a continuada redução do espaço de acomodação, face ao rápido aporte sedimentar, sofreram rápido isolamento em relação aos efeitos superficiais, resultando em pouca cimentação precoce (cf. De Ros, 1996). Nesses depósitos, as variações composicionais (proveniência) foram mais atuantes sobre as variações de qualidade de reservatório (Fig. 14). Os intervalos com granulometria grossa e seleção moderada a pobre, e ricos em grãos rígidos (quartzo-feldspáticos), apresentam melhores características de reservatório, face à menor deformação do arcabouço frente à compactação (petrofácies PorsCoars), mas exibem precipitação tardia de franjas de clorita magnesiana ou ilita-esmectita, relacionadas com a presença de cutículas precursoras de esmectita. Por outro lado, as fácies de menor energia de fluxo, com menor granulometria e, principalmente, pior seleção, enriquecidas em micas (petrofácies CmpctMica), apresentam maior compactação mecânica, e piores valores de porosidade e permeabilidade (cf. Van De Graaf & Ealey, 1989; Stonecipher, 2000). Exceção apenas a petrofácies FineA, cuja melhor seleção e menor conteúdo em grãos dúcteis resulta em valores de porosidade similares a petrofácies PorsCoars.

A variação composicional entre as seqüências rifte do poço A, na comparação entre a petrofácies CmpctMica (Seqüência R1) e PorsCoars (Seqüência R2), além do fator energia do ambiente deposicional, é igualmente interpretada como produto de variação de proveniência, onde os depósitos da Seqüência R1 têm qualidade de reservatório inferior, em virtude do maior percentual em fragmentos de rochas metamórficas de baixo grau. Estas foram as possíveis fonte de Fe e Mg para a precipitação eodiagenética por cutículas de esmectita, posteriormente transformada para corrensita ou clorita magnesiana, e recobertas por franjas de corrensita, clorita-magnesiana ou ilita-esmectita (I-S) (ARTIGO I).

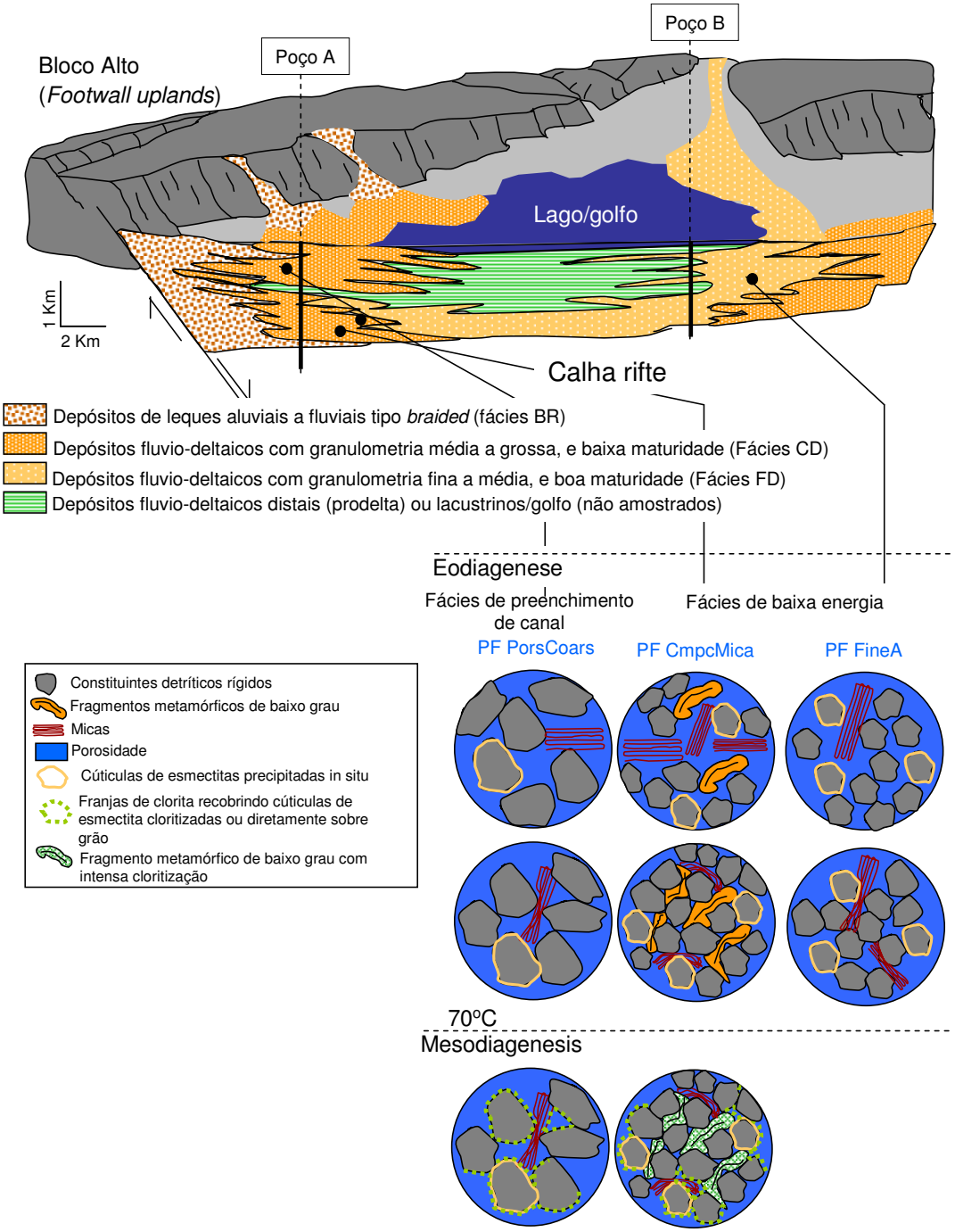

Fig. 14. Modelos esquemáticos mostrando a distribuição especial e temporal das alterações diagenéticas com base nas fácies deposicionais e *petrofácies de reservatório* (discutido a seguir) interpretados para as seqüências rifte aptianas.

As petrofácies rifte não apresentam assinatura em perfil de poço ou sísmica que sejam distinguíveis entre si, e mostram assinatura sísmica caracterizada por fraco contraste de impedância. Logo, os dados de proveniência obtidos das *petrofácies reservatório* permitem interpretar a discordância SB1 como importante superfície

limítrofe de intervalos estratigráficos com características de qualidade de reservatório distintas.

A intensa cimentação eodiagenética por dolomita microcristalina e anidrita tipo feltro (petrofácies CemA) na Seqüência Transicional (Fig. 13a), com alta deterioração da porosidade deposicional, em fácies deltaicas sotopostas ao intervalo evaporítico, é interpretada como produto de extensa exposição a condições superficiais caracterizadas por altas taxas de evaporação (Fig. 15).

As petrofácies associadas ao trato de mar alto da Seqüência D1 (NonCemA, MicrDoloA e PorsCoars), e de mar alto tardio (PorsCoars e CemA), apresentam grande variação no teor de cimentação eo- e mesodiagenética carbonática e sulfática (Fig. 15), na forma de concreções e nódulos, resultando na dispersão das amostras nos plotes de volume intergranular *versus* cimento (Fig. 13b). Uma vez que esse tipo de cimentação atua mais fortemente sobre a porosidade do que sobre a permeabilidade, estima-se uma qualidade de reservatório intermediária a boa para esses depósitos.

A tendência de maior influência relativa da cimentação por anidrita precoce em relação à cimentação por dolomita para o topo da seqüência, ou seja, em direção as fácies de trato de sistemas de mar alto tardio (planície deltaica a depósitos fluviais), é, tal qual observado na Seqüência Transicional, interpretada como produto de uma maior exposição às influencias superficiais, com crescente aridez, evidenciado pelo alto conteúdo em feldspatos detríticos, crescimentos secundários de K-feldspato e cimentação precoce por dolomita microcristalina e andrita (cf. De Ros, 1996), como observado nas amostras da petrofácies CemA em direção ao topo da Seqüência D1.

A maior intensidade da cimentação tardia por anidrita observada nas amostras com maior granulometria e/ou com melhor seleção (petrofácies CemA) reflete a maior probabilidade desses intervalos serem objeto de extensa cimentação e/ou dissolução durante o soterramento pela maior circulação de fluidos permitida pela porosidade e permeabilidade deposicionais (cf. Aktas & Cocker, 1994). Pelo mesmo motivo, fácies bioturbadas, fluidizadas e deformadas (slumps), interpretadas como depósitos de frente deltaica (petrofácies MicrDoloA), apresentam melhor qualidade de reservatório e menor cimentação, interpretada como produto de maior restrição ao fluxo de fluidos.

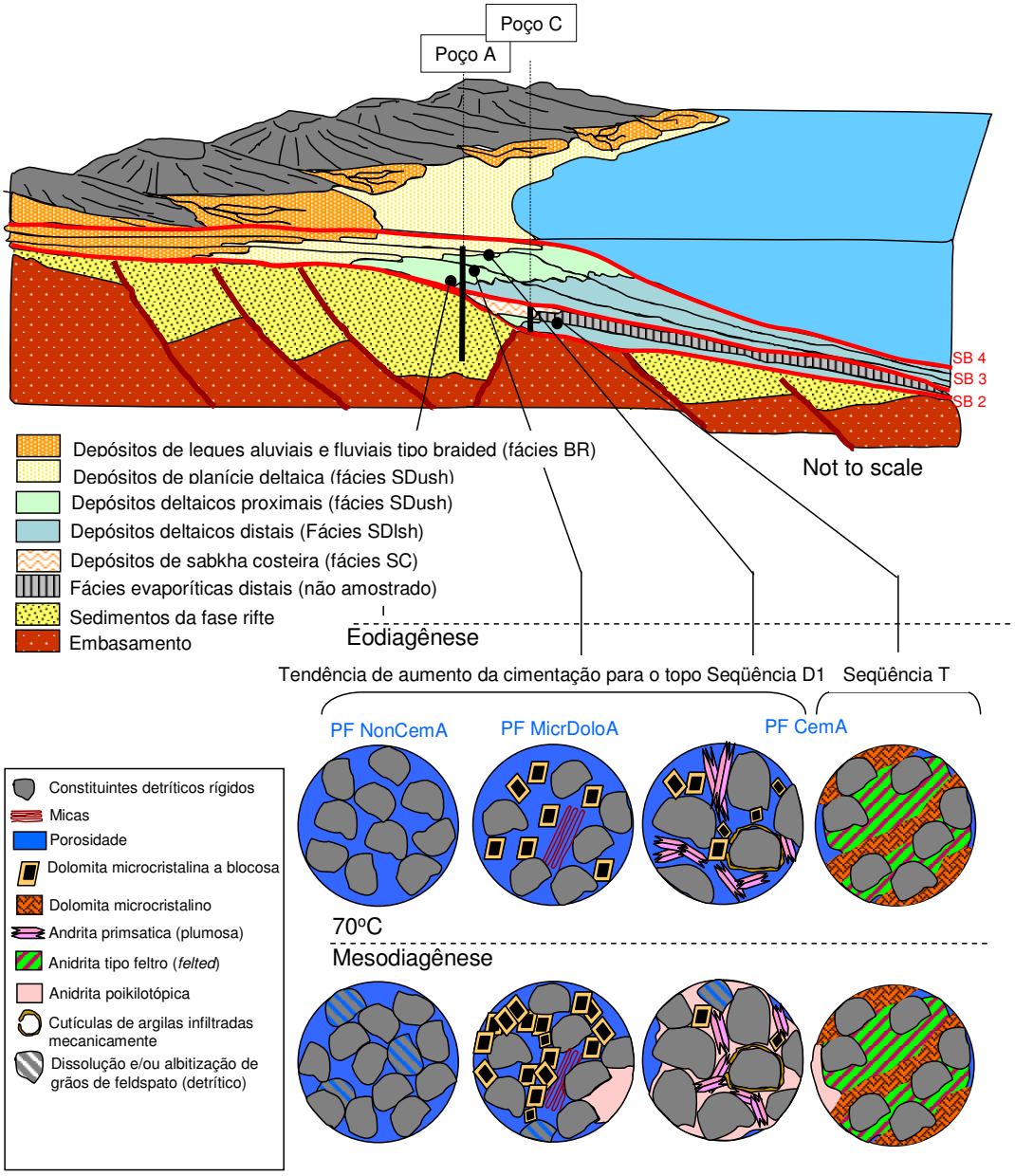

Fig. 15. Modelos esquemáticos mostrando a distribuição especial e temporal das alterações diagenéticas, com base nas fácies deposicionais e *petrofácies de reservatório* (discutido a seguir) interpretados para as seqüências transicional e drifte siliciclástica D1 (transição Aptiano Superior e Albiano Inferior).

Nas seqüências drifte Albianas observa-se uma progressiva deterioração da qualidade de reservatório nos tratos transgressivos em direção às seções condensadas, como observado na comparação entre as petrofácies MicrCalcA e CalcHA (Fig. 16). Tal fato é aqui associado à intensa cimentação carbonática marinha precoce (cf. Spadafora et al, 1998), favorecida pela disponibilização de íons, fornecidos pela água do mar por grãos intrabaciais carbonáticos (cf. De Ros, 1996; Ketzer et al., 2002; Ketzer et al.,

2003b). Com o distanciamento em relação às seções condensadas, e o baixo aporte de íons para cimentação carbonática precoce, o padrão de cimentação e de qualidade de reservatório torna-se mais característico de fácies dominantemente-siliciclásticas, como observado nas petrofácies de tratos de sistemas de mar alto (DoloRimA e CmpctOoGr), as quais apresentam menor oclusão do espaço poroso por cimentação marinha carbonática, resultando em maior preservação da porosidade primária (petrofácies DoloRimA), porém localmente mais compactada, face à maior ductibilidade do arcabouço (petrofácies CmpctOoGr) (Fig. 16).

As fácies carbonáticas e híbridas associadas a ambientes de alta energia (e.g. *shoals*) apresentam melhores valores de porosidade e permeabilidade, em relação as fácies de baixa energia, interpretadas como ambientes lagunares restritos de plataforma interna (petrofácies CalcHA e DoloAHA), em virtude dessas últimas se mostrarem preferencialmente cimentadas (calcita e/ou dolomita com forte influencia meteórica), com completa oclusão da porosidade primaria (Fig. 16).

Os depósitos transgressivos associados a alto aporte sedimentar da Seqüência D4 (poço B), interpretados como fácies de planície deltaica à frente deltaica (*shoreface-foreshore*), alternando com fácies estuarinas transgressivas (produto de oscilações de mais alta freqüência), mostram boa qualidade de reservatório (petrofácies PoorCemMet), a qual é interpretada principalmente como produto de soterramento pouco profundo. Por outro lado, os intervalos associados aos depósitos estuarinos (fácies ES) apresentam cimentação precoce e deslocante por dolomita microcristalina (petrofácies DoloAHA), com acentuada redução da porosidade primária, atribuída à mistura de fluidos marinhos e meteóricos.

As fácies permeáveis de arenitos de sistemas fluviais entrelaçados associados a tratos de sistemas de mar baixo, face ao clima seco vigente durante o Albiano, podem localmente apresentar intensa infiltração mecânica de argilas detríticas (petrofácies InfClaysA), resultando em intervalos com baixa qualidade de reservatório, face à intensa compactação pela inibição da cimentação, e à redução da permeabilidade promovida pelas cutículas argilosas (Fig. 16).

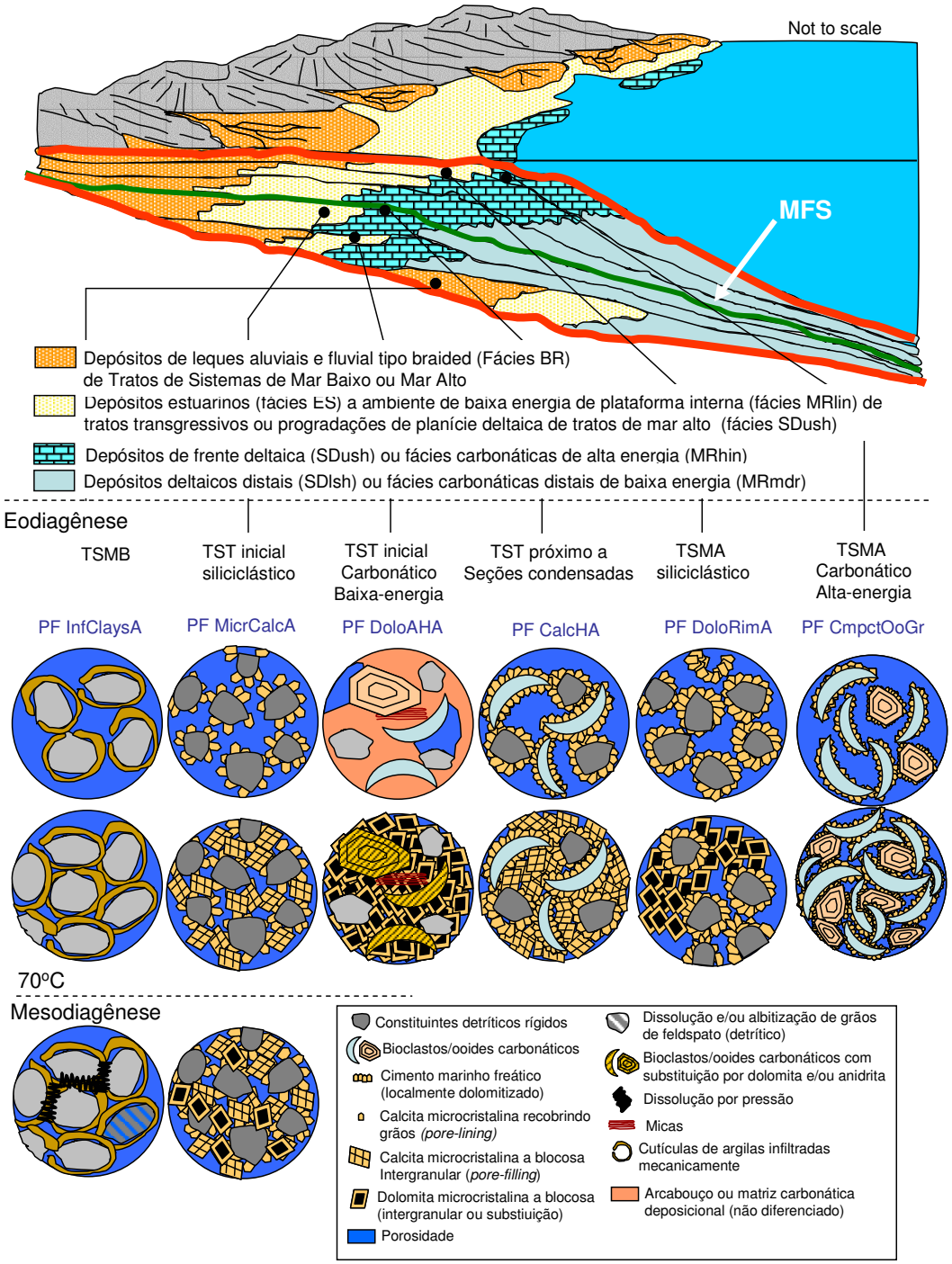

Fig. 16. Modelos esquemáticos mostrando a distribuição especial e temporal das alterações diagenéticas, evolução diagenética dos reservatórios com base nas fácies deposicionais e *petrofácies reservatório* (discutido a seguir) interpretados para as seqüências drifte mistas (siliciclásticas-carbonáticas) D2 a D4 (Meso a Eo-Albiano).

7. Conclusões

Não obstante a complexidade do controle exercido por parte das alterações diagenéticas sobre a porosidade e permeabilidade, essa dissertação mostra que estudos integrados estratigráfico-petrológicos da qualidade de reservatório no âmbito exploratório são factíveis e podem fornecer informações significativas, direcionando e otimizando as atividades de exploração subseqüentes.

A analise do intervalo estratigráfico com base na caracterização de *petrofácies de reservatório* permitiu identificar sistemas deposicionais (i.e. fácies sedimentares) e tratos de sistemas e/ou seqüências deposicionais (i.e. contexto de tectono-sedimentar) favoráveis e não favoráveis à preservação da porosidade primaria, bem como suas estimativas de permeabilidade.

Os resultados obtidos com a integração entre a análise estratigráfica, caracterização de textura e composição primárias e diagênese, através da aplicação do conceito de *petrofácies de reservatório*, forneceram seguintes conclusões:

(i) as alterações diagenéticas identificadas nos depósitos das seqüências rifte (fase final de preenchimento - *highstand system tract*) são compatíveis com alto aporte de sedimentos (intenso assoreamento), correspondente à cimentação eodiagenética pouco significativa. Nesses intervalos, a classificação dos reservatórios em *petrofácies de reservatório* permitiu salientar a importância de fatores como as fácies sedimentares e, em especial, a composição primária na qualidade de reservatório, o que deve ampliar de modo significativo à eficiência dos esforços de exploração nas seqüências rifte.

(ii) o ranqueamento dos intervalos (e seqüências) rifte em grupos de diferentes graus de qualidade de reservatório permitiu contrastar características de porosidade e respostas em perfis elétricos (GR-SP-ILD) e sísmica (amplitudes sísmicas e sismofácies), de onde se conclui haver pouca sensibilidade desses métodos frente às variações de qualidade de reservatório nas seqüências rifte.

(iii) as alterações diagenéticas identificadas nos depósitos das seqüências Transicional e drifte (D1 a D4), diversamente do que foi observado nas seqüências rifte, apresentam

maior influência dos volumes expressivos de cimentação eodiagenética, que influem diretamente na qualidade de reservatório e nas assinaturas em perfis (em na de resistividade) e geofísicas (amplitudes sísmicas e sismofácies).

(iv) O padrão nodular, concrecional e descontínuo da cimentação eo- e/ou mesodiagenética por calcita (petrofácies MicrCalcA), dolomita (petrofácies MicrDoloA) e anidrita (petrofácies CemA), apresenta localmente um forte impacto na porosidade, como evidenciado pela grande dispersão das amostras nos plotes de volume intergranular *versus* cimento, porém com menor impacto no fator permeabilidade. Face ao maior impacto na deterioração da porosidade promovido pela cimentação tardia por anidrita, a caracterização das petrofácies a partir das suas assinaturas em perfis elétricos permitiu identificar os intervalos com intensa cimentação (altos valores de resistividade).

(v) Apesar da grande variação dos valores de porosidade, as petrofácies associadas ao trato de sistema de mar alto da Seqüência D1 (petrofácies NonCemA, PorsCoars, MicrDoloA e CemA), apresentam progressivo aumento da cimentação intergranular em direção ao topo das seqüências, com uma assinatura geofísica caracterizada pelo aumento do contraste de amplitude (intervalo com alternância entre as petrofácies PorsCoars e CemA), o que permitiu associar a assinatura sísmica à qualidade de reservatório, diferentemente do observado nas seqüências rifte.

(vi) as seqüências siliciclásticas Transicional e drifte siliciclástica (D1) apresentam depósitos de tratos de sistemas de mar alto tardios caracterizados por expressiva cimentação eodiagenética por anidrita (petrofácies CemA), não observada nas demais seqüências drifte, consistindo em alterações diagenéticas relacionáveis a um ambiente deposicional árido com altas taxas de evaporação, com maior intensidade na primeira seqüência drifte (i.e. piores qualidades de reservatório).

(vii) A caracterização das *petrofácies de reservatório* permitiu identificar uma progressiva deterioração da qualidade de reservatório nos tratos transgressivos e de mar alto inicial em direção às zonas de inundação máximas, com equivalente assinatura dos perfis de raios gama e/ou potencial espontâneo, velocidade e resistividade, como notado na comparação entre as petrofácies MicrCalcA, CalcHA e DoloRimA, interpretado

como produto de expressiva cimentação carbonática precoce. Tal qual observado em perfil, o incremento nos contrastes de impedância acústica também permite associar uma resposta geofísica à perda de qualidade de reservatório em direção às seções condensadas.

(viii) Apesar de não distinguíveis em sísmica ou perfis, ao menos em relação aos dados utilizados nessa dissertação, a caracterização das petrofácies carbonáticas e/ou híbridas, e sua relação com o ambiente deposicional permitiu interpretar que as fácies associadas a ambientes de alta energia - *shoreface* e *shoals* (petrofácies CmpctOoGr) apresentam melhores valores de porosidade (e por analogia, permeabilidade) do que as fácies de baixa energia - ambientes lagunares, restritos (petrofácies DoloAHA e CalcHA), em virtude destes últimos apresentarem maior cimentação carbonática, permitindo a predição de qualidade de reservatório com base na interpretação sismoestratigráfica (i.e. tratos de sistemas).

8. Referências bibliográficas

Aktas, G; Cocker, J.D., 1994. **Diagenetic and depositional controls on reservoir quality in Khuff and Unayzah Sandstones, Hawtah Trend, Central Saudi Arabia**. GEO´94. Middle East Petroleum Geosciences Conference, p.44-52.

Al-Aasm, I.S., Taylor, B.E., South, B., 1990. Stable isotope analysis of multiple carbonate samples using selective acid extraction. **Chemical Geology, 80**, 119-125.

Al-Ramadan, K., 2006. Impact of diagenetic alterations on reservoir quality and heterogeneity of paralic and shallow marine sandstones: link to depositional facies and sequence stratigraphy. **Acta Universitatis Upsaliensis. Digital Comprehensive Summaries of Uppsala Dissertations from the Faculty of Science and Technology, 195**, 57pp.

Almeida, F.F.M., Hasui, Y., Neves, B.B.B, Fuck, R.A., 1977. **Províncias estruturais brasileiras**. Anais do I Simpósio de Geologia do Nordeste, p.363-391.

Almeida, F.F.M., Carneiro, C.D.R., Mizusaki, A.M.P., 1996. Correlação do magmatismo das bacias da margem continental brasileira com o das áreas emersas adjacentes: **Revista Brasileira de Geociências, 26**(3), p.125-138.

Amorosi, A., 1995. Glaucony and sequence stratigraphy: a conceptual framework of distribution in siliciclastic sequences. **Journal of Sedimentary Research, B65**, p.419-425.

Asmus, H.E., Ponte, F.C., 1973. The Brazilian marginal basins. In Nairm, A.E.M.; Stehili, F.G. (eds.) The ocean basins and margins. New York, **Plenum, 1**, p.87-133.

Beard, D.C., Weyl, P.K., 1973. Influence of texture on porosity and permeability of unconsolidated sand. **The American Association of Petroleum Geologists Bulletin, 57**, p.349-369.

Bjørlykke, K., M. Ramm and G. C. Saigal, 1989. Sandstone diagenesis and porosity modification during basin evolution. **Geologische Rundschau, 78**, p. 243-268.

Bhattacharya, J.P. 2006. Deltas. In: H.W. Posamentier e R.G. Walker (Eds.), Facies models revisited. **SEPM, Special Publication, 84**, 237-292.

Burley, S. D., 1993. **Models of burial diagenesis for deep exploration plays in Jurassic fault traps of the Central and Northern North Sea**. In: J. R. Parker (Ed.), Petroleum Geology of Northwest Europe: Proceedings of the 4th Conference, London, UK, The Geological Society, p. 1353-1375.

Castilho, J.G. 2005. **Integração de dados de métodos potenciais e de sensoriamento remoto como subsídio a exploração petrolífera offshore das bacias de Cumuruxatiba e Jequitinhonha**. Rio de Janeiro, 176p. tese de Mestrado em Geociências, COPPE, Universidade Federal do Rio de Janeiro.

Catuneanu, O., 2002. **Principles of sequence stratigraphy**. Oxford, Elsevier, 375p.

Carvalho, M.V.F., De Ros, L.F., Gomes, N.S., 1995. Carbonate cementation patterns and diagenetic reservoir facies in the Campos Basin Cretaceous turbidites, offshore eastern Brazil, **Marine and Petroleum Geology, 12** (7), p.741-758.

Cavazza, W. and G. Gandolfi, 1992. Diagenetic processes along a basin-wide marker bed as function of burial depth. **Journal of Sedimentary Petrology, 62**, p. 261-272.

Chagas, L.S., 2003. Bacia de Jequitinhonha. **Fundação Paleontológica Phoenix, 59** website: *www.phoenix.org.br.*

Chang, H.K., Kowsmann, R.O. and Figueiredo, A.M.F., 1988. New concepts on the development of East Brazilian marginal basins. **Episodes, 11** (3), p.194-202.

Chang, H.K., Kowsmann, R.O., Figueiredo, A.M.F., 1990. **Novos conceitos sobre o desenvolvimento das bacias marginais do leste brasileiro**. In: Raja Gabaglia, G.P., Milani, E.J. (Eds.) Origem e evolução de bacias sedimentares, Rio de Janeiro, Gávea, p. 269-290.

Claypool, G.E., Holser, W.T., Kaplan, I.R., Sakai, H., Zak, I., 1980. The age curves of sulfur and oxygen isotopes in marine sulfate and their mutual interpretation. **Chemical Geology, 28**, p.199-260.

Collinson, J.D., 1996. **Alluvial sediments**. In: Reading, H.G. (Ed.), Sedimentary environments: processes, facies and stratigraphy, London, Blackwell, p. 37-82.

Córdoba, V.C., 1994. **The Development of an Albian-Cenomanian Carbonate ramp as a first marine record in the Jequitinhonha Basin.** In: 14th International Sedimentological Congress, Recife, 2pp.

Craig, H., 1957. Isotopic standards for carbon and oxygen correction factors for mass spectrometric analysis of carbon dioxide. **Geochimica Cosmochimica Acta, 12**, p.133-149.

Craig, H., 1961. Standards for reporting concentrations of deuterium and oxygen-18 in natural waters. **Science, 133**, p. 1833-1934.

De Ros, L.F.S., Morad, S., Paim, P.S.G., 1994. The role of detrital composition and climate on the diagenetic evolution of continental molasses: evidence from the Cambro-Ordovician Guaritas Sequence, southern Brazil. **Sedimentary Geology, 92**, p.197-228.

De Ros, L.F., 1996. Compositional controls in sandstones diagenesis. **Acta Universitatis Upsaliensis, Comprehensive Summaries of Uppsala Dissertations from the Faculty of Science and Technology, 198**, 24 pp.

De Ros, L.F., Goldberg, K., 2007.**Reservoir petrofácies: a tool for quality characterization and prediction**. AAPG Annual Conference and Exhibition: The American Association of Petroleum Geologists, Long Beach, CA, USA, Extended Abstracts CD, 6pp.

De Ros, L.F., Goldberg, K., Abel, M., Victorinetti, F., Mastella, L. and Castro, E., 2007. **Advanced Acquisition and Management of Petrographic Information from Reservoir Rocks Using the PETROLEDGE® System**. AAPG Annual Conference and Exhibition: The American Association of Petroleum Geologists, Long Beach, CA, USA, Extended Abstracts CD, 6pp.

Ehrenberg, S.N., 1989. Assessing the relative importance of compaction processes and cementation to reduction of porosity in sandstones: discussion; Compaction and porosity evolution of Pliocene sandstones, Ventura Basin, California: discussion. **The American Association of Petroleum Geologists Bulletin, 73**, 1274-1276.

Folk, R.L., 1968. **Petrology of sedimentary rocks**. Austin, Texas, Hemphill's Pub., 107p.

Friedman, I. & O'Neil, J.R., 1977.Compilation of stable isotopic fractionation factors of geochemical interest. **United States Geological Survey, U.S.G.S. Professional Paper 440-KK**, 12pp.

Galloway, W.E., Hobday, D.K., 1983. **Terrigenous clastic depositional systems: applications to petroleum, coal, and uranium exploration**. Springer-Verlag Inc., Heidelberg, 489pp.

Galloway, W. E., 1989. Genetic stratigraphic sequences in basin analysis, I. Architecture and genesis of flooding-surface bounded depositional units. **The American Association of Petroleum Geologists, 73**, p.125-142.

Harris, N.B., 2000. Evolution of the Congo rift basin, West Africa: an inorganic geochemical record in lacustrine shales. **Basin Research, 12,** p.425-445.

Harrison, W.J., 1989. **Modeling fluid/rock interactions in sedimentary basins**. In: Cross, T.A. (ed.) Quantitative dynamic stratigraphy. Prentice Hall, p.195-231.

Handford, C.R., Loucks, R.G., 1993. Carbonate depositional sequences and systems tracts – responses of carbonate platforms to relative sea-level changes. In: Loucks, R.G., and J.F. Sarg (Eds.), Carbonate sequence stratigraphy: recent developments and applications. **The American Association of Petroleum Geologists, Memoir, 57**, p.3-41

Hiatt, E.E., Hyser, K., Dalrymple, R.W., 2003. Relationships among sedimentology, stratigraphy, and diagenesis in the Proterozoic Thelon Basin, Nunavut, Canada: implications for paleoaquifers and sedimentary-hosted mineral deposits. **Journal of Geochemical Exploration, 80**, p.221-240.

Hunt, D. Tucker, M.E., 1992. Stranded parasequences and the forced regressive wedge systems tract: deposition during base level fall. **Sedimentary Geology, 81**, p.1-9.

Ketzer, J.M., Morad, S., Evans, R., AL-Aasm, I.S., 2002. Distribution of diagenetic alterations in fluvial, deltaic and shallow marine sandstones within a sequence stratigraphic framework: evidence from the Mullaghmore Formation (carboniferous), NW Ireland. **Journal of Sedimentary Research, 72**, No 6, p.760-774.

Ketzer, J. M., Morad, S., Amorosi, A., 2003a. Predictive diagenetic clay-mineral distribution in siliciclastic rocks within a sequence stratigraphic framework. In: Worden, R., Morad, S. (Eds.): Clay Mineral Cementation in Sandstones, **Special**

Publication of International Association of Sedimentologists, 34, p. 42-59.

Ketzer, J.M., Holz, M., Morad, S., 2003b. Sequence stratigraphic distribution of diagenetic alterations in coal-bearing, paralic sandstones: evidence from the Rio Bonito Formation (early Permian), southern Brazil. **Sedimentology, 50**, p.855-877.

Kuchle, J., Holz, M., Brito, A.F., Bedregal, R.P., 2005. Análise estratigráfica de bacias rifte: aplicação de conceitos genéticos nas bacias de Camamu-almada e Jequitinhonha (Tr. Stratigraphic analysis of rift basins: applications of genetic concepts in Camamu-Almada and Jequitinhonha basins). **Boletim de Geociências da Petrobrás, 13**(1), p.227-244.

Lomando, A.J., Harris, P.M., 1991. **Mixed Carbonate-Siliciclastic Sequences** (eds.), Dallas, TX, SEPM (Society for Sedimentary Geology), 569 pp.

Loucks, R.G., Sarg, J.F. (eds.) Carbonate Sequence Stratigraphy – Recent Developments and Applications. **American Association of Petroleum Geologists, Memoir 57**, 545p.

McKay, J.L., Longstaffe, F.J., Plint, A.G., 1995. Early diagenesis and its relationship to depositional environment and relative sea-level fluctuations (Upper Cretaceous Marshybank Formation, Alberta and British Columbia). **Sedimentology, 42**, p.161-190.

Miall, A. D., 1996. **The geology of fluvial deposits: sedimentary facies, basin analysis and petroleum geology**. Springer-Verlag Inc., Heidelberg, 582p.

Miall, A. D., 1997. **The geology of stratigraphic sequences**. Springer-Verlag Inc., Heidelberg, 433p.

Mitchum, R.M., Vail, P.R., Thompson, S., 1977a. Seismic stratigraphy and global changes of sea level, part 2: the depositional sequence as a basic unit for stratigraphic analysis. In: Payton, C. E. (Ed.) Seismic Stratigraphy Applications to Hydrocarbon Exploration. **The American Association of Petroleum Geologists, Memoir 26** p.53-62.

Mitchum, R.M., Vail, P.R., Sangree, J.B., 1977b. Seismic stratigraphy and global changes of sea level, part 6: Stratigraphic Interpretation of Seismic Reflection Patterns in Depositional Sequences. In: Payton, C. E. (Ed.) Seismic stratigraphy applications to hydrocarbon exploration. **The American Association of Petroleum Geologists, Memoir 26,** p.117-134.

Morad, S., 1998. Carbonate cementation in sandstones: distribution patterns and geochemical evolution, In: Morad, S. (Ed.), 1998. Carbonate cementation in

sandstones. **International Association of Sedimentologist Special Publication, 26**. p.1-26.

Morad, S., Ketzer, J.M., De Ros, L.F., 2000. Spatial and temporal distribution of diagenetic alterations in siliciclastic rocks: implication for mass transfer in sedimentary basins. **Sedimentology, 47**, p.95-120.

Ojeda, H.A., 1982. Structural framework, stratigraphy and evolution of Brazilian marginal basins. **American Association of Petroleum Geologists Bulletin, 66**, p.732-749

Posamentier, H.W., James, D.P., 1993. Sequence stratigraphy – uses and abuses. In: Posamentier, H.W. , Sumerhayes, C.P. , Haq, B.U. , Allen, G.P. (Eds.) Sequence Stratigraphy and Fácies Associations. **International Association of Sedimentologists Special Publications, 18**, p. 3-18.

Posamentier, H.W., Jervey, M. T., Vaill, P.R., 1988. Eustatic controls on clastic deposition-I – Conceptual framework. In: Wilgus, C.K.; Kendall, C.G.St.C.; Posamentier, H.W.; Ross, C.A. e Van Wagoner, J.C. (eds.), Sea-level changes: an integrated approach. **SEPM, Special Publication, 42**, p 125-154.

Posamentier, H.W., Vaill, P.R., 1988. Eustatic controls on clastic deposition-II – Sequence and systems tract models. In: Wilgus, C.K.; Kendall, C.G.St.C.; Posamentier, H.W.; Ross, C.A. e Van Wagoner, J.C. (eds.), Sea-level changes: an integrated approach. **SEPM, Special Publication, 42**, p 125-154.

Reading, H.G., Collinson, J.D., 1996. **Clastic coasts**. In: Reading, H.G. (Ed.), Sedimentary environments: processes, facies and stratigraphy, London, Blackwell, p. 154-231.

Santos, C. F., Gontijo, R. C., Feijó, F. J., 1995. Bacias de Cumuruxatiba e Jequitinhonha. **Boletim de Geociências da Petrobrás, 8**(1), p.185-190.

Schlager, W., 1991. Depositional bias and environmental change-important factors in sequence stratigraphy. **Sedimentary Geology, 70**, p.109-130.

Spadafora, E., De Ros, L.F., Zuffa, G.G., Morad, S., Al-Aasm, I.S., 1998. Diagenetic evolution of synorogenic hybrid and lithic arenites (Miocene), northern Apennines, Italy, In: Morad, S. (Ed.), Carbonate cementation in sandstones. **Special Publication of the International Association of Sedimentologists, 26**, p. 241-260.

Steel, R.J., Thompson, D.B., 1983. Structures and textures in Triassic braided stream conglomerates (Bunter pebble beds) in the Sherwood Sandstone Group, North Staffordshire, England. **Sedimentology, 30**, p.341-367

Stonecipher, S.A., 2000. Applied sandstone diagenesis: Practical petrographic solutions for a variety of common exploration, development, and production problems, **SEPM Short Course Notes, 50,** 143p.

Surdam, R. C., Dunn, T.L., Heasler, H.P. e MacGowan, D.B., 1989. **Porosity evolution in sandstone/shale systems**. In: Hutcheon, I.E. (Ed.), Short Course on Burial Diagenesis: Montreal, Mineralogical Association of Canada, p. 61-133

Thode, H.G., Monster, J. & Dunford, H.B., 1961. Sulphur isotope geochemistry. **Geochimica et Cosmochimica Acta, 25**, p. 150-174.

Vail, P.R., Mitchum, R.M. Jr., Thompson, S., III, 1977a. Seismic stratigraphy and global changes of sea level, part 3: relative changes of sea level from coastal onlap. In: Payton, C.E. (Ed.) Seismic stratigraphy applications to hydrocarbon exploration. **The American Association of Petroleum Geologist, Memoir 26,** p.63-81.

Vail, P.R., Mitchum, R.M. Jr., Thompson, S., III, 1977b. Seismic stratigraphy and global changes of sea level, part 4: Global cycles of relative changes of sea level. In: Payton, C.E. (Ed.) Seismic stratigraphy applications to hydrocarbon exploration. **The American Association of Petroleum Geologist, Memoir 26,** p.83-98.

Van De Graaf, W.J.E., Ealey, P.J., 1989. Geological modeling for simulation studies: **The American Association of Petroleum Geologist Bulletin, 73**, p. 1436-1444.

Van Wagoner, J. C., Posamentier, H. W., Mitchum, R. M., Vail, P. R., Sarg, J. F., Loutit, T. S., Hardenbol, J., 1988. An overview of the fundamentals of the sequence stratigraphy and key definitions . In: Wilgus, C.K.; Kendall, C.G.St.C., Posamentier, H.W.; Ross, C.A. e Van Wagoner, J.C. (eds.), Sea-level changes: an integrated approach. **SEPM, Special Publication, 42**, p 39-46.

Walker, R.G., 1992. **Fácies, facies models and modern stratigraphic concepts**. In: Walker, R.G. e James, N.P. (Eds.), Fácies models: Response to sea level change: Geological Association of Canada, p. 1-14.

Weimer, R.J., Howard, J.D. and Lindsay, D.R., 1982. **Tidal flats**. In: Scholle, P.A. e Spearing, D. (eds.) Sandstones depositional environments. The American Association of Petroleum Geologists, Tulsa, Oklahoma, 191-246.

Worden, R.H., Burley, S.D., 2003. **Sandstone diagenesis: evolution of sand to stone**. In: Worden, R.H., Burley, S.D. (Eds.), Sandstone diagenesis: Recent and ancient, London, Blackwell, p.3-44.

Wright, V.P., Burchette, T.P., 1996. **Shallow-water carbonate environments**. In: Reading, H.G. (Ed.). Sedimentary environments: processes, facies and stratigraphy, London, Blackwell, p. 325-394.

Zuffa, G. G., 1980 Hybrid arenites: their composition and classification. **Journal of Sedimentary Petrology, 50**, p. 21-29.

Zuffa, G. G., 1985. Optical analysis of arenites: influence of methodology on compositional results. In: Zuffa, G.G. (Ed.), Provenance of Arenites. **NATO-ASI Series C: Mathematical and Physical Sciences, 148**, p. 165-189.

Data:	Thu, 28 Feb 2008 15:10:03 -0500 (EST)
De:	E.Richardson@soton.ac.uk
Para:	celsomourajardim@yahoo.com.br
Assunto:	Sedimentology - Manuscript ID SED-2008-OM-033

28-Feb-2008

Dear Mr. Jardim:

Your manuscript entitled "Depositional controls on the diagenetic patterns of Lower Cretaceous sandstones from the Jequitinhonha Basin, Eastern Brazil" has been successfully submitted online and is presently being given full consideration for publication in Sedimentology.

Your manuscript ID is SED-2008-OM-033.

Please quote the above manuscript ID in all future correspondence. If you have an existing user account for Sedimentology and there have been any changes to your contact details since you last used the website, please log in to Manuscript Central at http://mc.manuscriptcentral.com/sed and edit your user information as appropriate.

You can also view the status of your manuscript at any time by checking your Author Center after logging in to http://mc.manuscriptcentral.com/sed .

Thank you for submitting your manuscript to Sedimentology.

Yours sincerely
Elaine Richardson
Editorial Office Manager
Sedimentology

Depositional controls on the diagenetic patterns of Lower Cretaceous sandstones from the Jequitinhonha Basin, Eastern Brazil

Short title: Lower Cretaceous Jequitinhonha Sandstones, Brazil

Celso Moura Jardim[1], João Marcelo Ketzer[2] and Luiz Fernando De Ros[3]

[1] PETROBRAS, Av. Republica do Chile, 65/1302 Rio de Janeiro, RJ, 20031-975, Brazil; celsomj@petrobras.com.br

[2] Instituto do Meio-Ambiente, Pontifícia Universidade Católica do Rio Grande do Sul - PUC-RS, Av. Ipiranga, 6681, Porto Alegre, RS, 90619-900, Brazil; marcelo.ketzer@pucrs.br

[3] Instituto de Geociências, Universidade Federal do Rio Grande do Sul, Av. Bento Gonçalves, 9500, Porto Alegre, RS, 91501-970, Brazil; lfderos@inf.ufrgs.br

ABSTRACT

A study of fluvial, deltaic, and shallow-marine Lower Cretaceous (Upper Aptian to Lower Albian) sandstones, hybrid arenites and calcarenites from the Jequitinhonha Basin, eastern Brazilian margin, reveals that the distribution of their diagenetic alterations and of related reservoir quality evolution can be constrained within a sequence stratigraphic framework. Description of cores, wireline logs, quantitative petrographic, and petrophysical porosity and permeability analyses were integrated in order to unravel the genetic aspects that controlled the complex patterns of diagenesis of these reservoirs, and hence of reservoir quality, as well as to demonstrate the practical use of this approach in reducing exploration risks. The results of this study are relevant to the exploration of rift and an early drift phase of Atlantic-type passive margin settings, and demonstrate the influence of depositional factors such as sedimentary facies and detrital composition (provenance) on diagenetic and reservoir evolution, with application to reservoir quality and heterogeneity prediction during exploration.

Keywords: depositional systems, sequence stratigraphy, clastic diagenesis, reservoir quality, petroleum exploration

INTRODUCTION

The distribution of reservoirs, seals and source rocks (i.e. depositional facies) and depositional-related reservoir quality can be constrained within a sequence stratigraphic context. This approach is based on the interplay between sediment supply, basin-floor physiography and changes in the relative sea level (cf. Van Wagoner et al., 1990; Posamentier and Allen, 1993). Similarly, the spatial and temporal distribution of near-surface diagenetic alterations in siliciclastic rocks can be constrained within a sequence stratigraphic context (sequence stratigraphic surfaces and systems tracts), based on variations in depositional

facies, climatic conditions and significant changes in detrital composition, residence time under specific geochemical conditions, and pore water chemistry (cf. Morad et al., 2000; Ketzer et al., 2002; Ketzer et al., 2003a/b). These, in turn, may exert significant and complex controls on burial diagenetic alterations, resulting in an improvement or deterioration of primary porosity (cf. Al-Ramadan, 2006). An integrated approach between diagenesis and sequence stratigraphy enables the prediction of post-depositional evolution of reservoir quality in sandstones, which ultimately is the goal of petroleum exploration.

The present study aims to integrate, within a sequence stratigraphic framework, the depositional facies and the types and distribution of diagenetic processes that affected the Lower Cretaceous (Late Aptian to Early Albian) reservoirs from the Jequitinhonha Basin, eastern Brazilian margin. This integration is developed in order to unravel the genetic aspects that controlled the complex patterns of diagenesis of these sandstones, and to demonstrate the practical use of this approach in reducing exploration risks.

The characterization of types, distribution and evolution of the diagenetic processes of siliciclastic sandstones and hybrid arenites (*sensu* Zuffa, 1980), and the determination of their relationships with depositional facies and sequence stratigraphic surfaces and systems tracts were performed through description of cores, borehole logs, thin sections, and petrophysical porosity and permeability analyses on core samples from three onshore and shelf wells drilled in the Jequitinhonha Basin (Fig.1). The basin has potential for oil and natural gas, with several blocks under exploration.

Insert Fig.1

Diagenetic stages are defined in this paper *sensu* Morad et al. (2000), including: (i) eodiagenesis (i.e. 0-2 km of burial depth; < 70°C), with pore-water chemistry controlled mainly by depositional and/or meteoric waters; and (ii) mesodiagenesis (i.e. > 2 km of burial depth; > 70°C), with diagenetic alterations mediated mainly by formation waters evolved through water-rock interactions.

GEOLOGICAL SETTING

The origin and evolution of the Jequitinhonha basin, located at the Eastern Brazilian continental margin, was a result of rifting of Gondwana and opening of the South Atlantic Ocean during Mesozoic and Cenozoic times (cf. Asmus and Ponte, 1973; Ojeda, 1982; Chang et al, 1988) (Fig. 1). The basement of the Jequitinhonha basin is composed mostly of pre-Cambrian granites, gneisses, granulites and low grade meta-sediments. The stratigraphic section of this basin can be divided into four units (cf. Chang et al, 1988; Cainelli & Mohriak, 1999):

(i) Neocomian to Early Aptian sin-rift unit, consisting of continental fluvial to lacustrine-deltaic conglomerates and sandstones associated with organic-rich lacustrine shales of the Mariricu Formation. These rocks were deposited under rapid subsidence, filling N-S to SW-NE half-grabens. The uppermost limit of this unit is represented by an unconformity that marks the onset of a tectonic

quiescence, showing the cessation of stretching and rifting of the continental crust (Cainelli & Mohriak, 1999).

(ii) Late Aptian to Early Albian transitional unit consists of fluvial-deltaic sandstones deposited in a shallow-water, narrow proto-oceanic environment, capped by evaporitic beds of the Itaunas Member (Mariricu Formation). There is an upward increase in marine influence and in an arid to semi-arid climate conditions. At the end of the Aptian (period of high aridity), the presence of volcanic barriers to the south (cf. Kumar and Gamboa, 1979) formed a restricted gulf area, allowing the deposition of an evaporite package along the Brazilian continental margin, composed of mainly halite at the base and anhydrite at the top.

(iii) Albian to Paleocene drift transgressive unit, characterized by marine deposits. During the Albian-Cenomanian, coarse-grained alluvial and coastal sandstones of the São Mateus Formation were deposited, grading offshore into shallow-water carbonates and basinal marls and shales of the Regência Formation. During the Senonian transgression, the Regência carbonates were covered by basinal shales and turbidites of the Urucutuca Formation. The Aptian evaporites were extensively deformed and slided downslope by halokynetic movements, promoting lystric faulting of the post-salt sequences.

(iv) Paleocene to Recent drift regressive sequence, characterized by the progradation of coarse-grained coastal sandstones of the Rio Doce Formation grading offshore towards shallow-water carbonates of the Caravelas Formation. Paleocene-Eocene volcanic/volcaniclastic sediments of the Abrolhos Formation occur at the Royal Charlotte Volcanic Complex at south of the basin (Fig. 1).

SAMPLES AND METHODS

The studied Late Aptian to Early Albian succession was cored irregularly in three wells drilled in the onshore and shelf part of the basin (Fig. 2). The study was carried out on 140 m, discontinuous well core data of the three wells (Fig. 3), representing the late rift phase and the passage from evaporitic (transitional) to the onset of the drift phase. The cores were described in detail (lithologies, textures, structures, vertical trends) in order to identify lithofacies (adapted from Miall, 1996) and to interpret facies associations and their successions (*sensu* Walker, 1992), which were compared with well-recognized sedimentary models (e.g. Galloway and Hobday, 1983; Collinson, 1996; Johnson & Baldwin, 1996; Kendall & Harwood, 1996; Reading & Collinson, 1996; Bhattacharya, 2006), and used as the building blocks for the reconstruction of depositional environments and sequence stratigraphic framework. The cores were sampled within a depth range of 400 to 2800 m. Sixty-seven thin sections of sandstone samples were prepared from blue epoxy resin-impregnated samples were described in detail with polarized light microscopes. Petrographic modal analyses were performed using the Petroledge® system (De Ros et al., 2007), by counting 300 points per thin section, recording the relationships between detrital and authigenic components and porosity. The percentage of detrital and diagenetic constituents and types of pores is expressed in relation to bulk rock volume. Sorting was estimated by comparison with the standard charts of Beard

and Weyl (1973). Carbonate cements were stained with Alizarin red-S in order to distinguish calcite from other carbonate cements. Available petrophysical porosity and permeability data from the analyzed cores were integrated to the stratigraphic and petrologic data.

The paragenetic sequence of diagenetic processes and products was interpreted from the textural relationships obtained from optical and electronic microscopy, aided by oxygen isotopic composition of carbonate and sulphate cements. Scanning electron microscopy (SEM) was performed in a Phillips XL-30 microscope, equipped with an EDAX (energy-dispersive x-ray spectrometer), to characterize the major chemical composition, morphology and paragenetic relation among diagenetic constituents. X-ray diffraction analyses of the < 10 μm fraction were performed in 5 oriented samples in a Siemens Bruker AXS D5000 diffractometer, in order to identify the clay mineralogy. The oriented samples were air-dried, ethylene glycol-saturated and heated at 550°C for 2 hours. Carbon, oxygen and sulphur isotope analyses were carried out on 14 selected samples (cf. Al-Aasm et al., 1990), in order to determine the geochemical conditions under which dolomite and anhydrite were formed. Oxygen, carbon and sulphur isotope data are presented in the normal δ notation relative to SMOW (Craig, 1961), PDB (Craig, 1957) and CDT (Thode et al, 1961) standards, respectively. The precipitation temperatures of dolomite cements informed in this paper were calculated using the fractionation equation of Friedman and O'Neil (1977).

Insert Fig.2

FACIES ASSOCIATIONS AND DEPOSITIONAL SYSTEMS

The stratigraphic framework of the Late Aptian to Albian stratigraphic succession of Jequitinhonha basin discussed in this paper was based on the interpretation of wireline logs, facies successions from core lithological descriptions, and supported by petrographic analysis. The description of the selected cores resulted in eighteen non-genetic lithofacies (Table 1), with facies codes modified from Miall (1996). Theses lithofacies were grouped into fourteen facies associations (Table 2) *sensu* Walker (1992), i.e. groups of facies genetically related which have environmental significance, reflecting distinct interpreted depositional systems. The interpreted stratigraphic framework consists of seven sequences (Fig. 2): two rift phase sequences (R1 and R2), one transitional sequence (T) and four drift phase sequences (D1 to D4).

The clastic continental deposits of the Aptian rift phase sequences are interpreted as a complex interplay of fluvial-deltaic (e.g. Galloway and Hobday, 1983; Collinson, 1996) and lacustrine depositional environments. Three distinct depositional settings were interpreted (Fig. 4):

(1) Medium- to coarse-grained, locally conglomeratic, poorly- to very poorly-sorted braided-stream and coarse-grained deltaic deposits, corresponding to successions of lacustrine deposits (rift-lake / prodelta) that pass upwards to delta front and delta plain/fluvial (braided) deposits. These deposits are well preserved at Sequence R1 in well A, and are assigned here to coarse-grained deltaic – CD facies associations (Figs. 5a-c), being differentiated into three

facies associations (Table 2): delta plain, delta front and prodelta/rift lake. These deposits are characterized by a poorly developed *Spontaneous potential* (SP) – *gamma ray* (GR) coarsening-upward log pattern.

Insert Fig.3

(2) Fine- to medium-grained, poorly- to moderately-sorted deltaic deposits, corresponding to successions of lacustrine deposits (rift-lake / prodelta) that pass upwards to delta front and sandy delta plain facies, with occasional slight thinning-upward trend at the top, suggesting fluvial systems. These deposits are well represented at Sequence R1 in well B, and are assigned here to fine-grained deltaic - FD facies associations (Figs. 5d-f), being differentiated into three facies associations (Table 2): delta plain, delta front and prodelta/rift lake. These deposits are characterized by a typical deltaic progradation SP log signature, with a coarsening-upward pattern (funnel-shaped log signature). The estimated deltaic progradation thickness is up to 150m, based upon SP logs.

(3) Fining-upward successions of coarse- to fine-grained, poorly- to very poorly-sorted sandstones, interpreted as high-energy fluvial braided – BR facies association (Table 2). Thick (> 100m) sandy intervals are interpreted as stacking of channel deposits in the braided plain. The log signature is characterized by a box SP/GR response (low values), with high sonic (DT) log values, such as at Sequences R1 of well B.

Insert Table 1

Insert Table 2

Insert Fig. 4

The interpreted depositional environments for the Aptian/Albian transition and Albian stage correspond to an extensive, shallow water, restricted marine, homoclinal ramp, showing an interplay of four differentiated depositional settings (Figs. 6, 7):

(1) Shallow-water, coarse-grained deltaic deposits (e.g. Bhattacharya, 2006), assigned here to SD facies associations, being differentiated into two facies associations (Table 2): delta plain to delta front (upper shoreface) and delta front (lower shoreface) (Figs. 8a-b). This clastic coastal system intertongues basiward and along strike with carbonatic deposits of open-shelf environments (mixed ramp facies discussed below), and landward with fluvial braided facies. This facies locally show a coarsening-upward GR and SP log pattern from delta front (lower to upper-shoreface) to delta plain (foreshore) facies.

(2) Fining upward deposits consisting of coarse-grained sandstone layers alternating with heterolithic (sand/mud) layers (Figs. 8c-f), showing an irregular GR and SP log signature (Figs. 6, 7). This facies occurs vertically associated with SD facies, and are interpreted as brackish water environments (estuaries, lagoons, bays or tidal flats) of low relief and relatively low energy and protected areas along the coast. This facies are assigned here to estuarine – ES facies association (e.g. Weimer et al., 1982).

Insert Fig.5

Insert Fig.6

Insert Fig.7

Insert Fig.8

(3) Supratidal-coastal sabkha evaporative deposits (Figs. 9a-d) developed in response to increasing marine influence and arid climatic conditions (e.g. Kendall & Harwood, 1996) during the transition of Late Aptian to Early Albian stage. These deposits, overlying SD facies, are assigned here to supratidal coastal sabkha – SC facies association (Table 2). This facies show low SP and GR log values, and high resistivity-log (ILD) and sonic (DT) values.

(4) Hybrid arenites (*sensu* Zuffa, 1980) or calcarenite deposits (Figs. 9e-f), assigned here to mixed ramp – MR deposits, reflecting the development of extensive shallow water restricted marine mixed siliciclastic-carbonatic ramp depositional environment (e.g. Wright & Burchette, 1996), with coeval supply (intertongue landward) of coarse-grained siliciclastic sources (SD facies). This Albian drift phase deposits were differentiated into three facies associations (Table 2): high-energy inner ramp (MRhin), low-energy inner ramp (MRlin), and mid ramp (MRmdr). The GR and SP show an irregular high-frequency log response, mostly with an upward decrease of GR (and SP) log values, indicating an upward trend of increasing sand content, showing the transition from distal low energy facies to proximal high energy facies.

DETRITAL TEXTURE, COMPOSITION AND PROVENANCE

The studied samples range from fine to conglomeratic sandstones (up to granule size), with predominance of medium to coarse-grained sandstones, to hybrid arenites (*sensu* Zuffa, 1980) and calcarenites. The sorting is usually poor and grains are mostly subrounded. Quantitative petrographic results of the studied samples (Table 3) were grouped according to interpretation of deposicional facies, system tracts and depositional sequence. The sandstones are dominantly arkoses (av. $Q_{38}F_{56}L_{6}$) and subordinately lithic arkoses (av. $Q_{33}F_{46}L_{21}$) and feldspathic litharenites (av. $Q_{18}F_{30}L_{52}$) (*sensu* Folk, 1968; Fig. 10). The dominant immature feldspathic and lithic detrital composition indicate provenance from uplifted basement terrains (blocks uplifted along the rift margins), characterized by plutonic magmatic and high-grade metamorphic rocks, and from recycled orogenic terrains of sedimentary and low-grade meta-sedimentary rocks (cf. Dickinson, 1985; Fig. 11).

The quartz grains are essentially monocrystalline (av. 18%) and detrital feldspars are dominantly orthoclase (av. 17%). Plutonic (av. 4.7%) and metamorphic (av. 4.2 %) rock fragments are more common in the poorer-sorted, coarser-grained and conglomeratic facies. Sedimentary rock fragments (av. 1.7%) consist mainly of dolostones and monocrystalline dolomite grains.

Biotite (av. 3.4%) is the main accessory detrital constituent. Garnet (av. 2%) is the second most abundant. Intrabasinal grains of siliciclastic samples (av. 2.3%) are dominantly of mud intraclasts and carbonaceous fragments (plant debris); whereas hybrid arenites and calcarenite samples show high content of carbonate intrabasinal grains (ooids/oncoids and bioclasts). Bioclasts consist mostly of benthic foraminifers, echinoderms and molluscs (bivalves and gastropods); with increasing number and variety towards the younger drift sequences (cf. Cordoba, 1994). Pre-salt sandstones of the Transitional Sequence (well C) contain dolomitized ostracodes bioclasts and possibly ooids.

Insert Fig. 9

Insert Fig.10

Insert Fig.11

Insert Table 3

STRATIGRAPHIC FRAMEWORK

Sequences R1 and R2

The rift phase sediments were deposited in deep, asymmetric half-grabens under active rift tectonism and increasing marine influence (cf. Kuchle et al., 2005; Fig. 12a). Aptian braided streams and lacustrine-deltaic deposits present in wells A and B are interpreted as rift sequences R1 and R2 (Fig. 4), separated by sequence boundary 1 (SB1).

Sequence R1 in well A presents coarse-grained fluvial-deltaic deposits (CD facies) that are compositionally and texturally less mature than equivalent finer-grained fluvial-deltaic deposits (FD facies) present in well B, showing high content of ductile metamorphic rock fragments and detrital mica (Fig. 13). Such differences are interpreted as resulted from diverse relative position to basin margin faults and distinct source terrains (cf. De Ros et al., 2005). CD facies (well A) deposits are interpreted as proximal to basin margin faults, showing significant content of ductile grains and poorer sorting sediments, preferentially at finer-grained lower-energy, delta front or overbank/floodplain facies (Fig. 3; cores A3-7). Coarser-grained, channel-related delta plain facies (Fig. 3; cores A4-7), on the other hand, show minor content of these ductile detrital constituents. The more mature and quartz-feldspathic composition of FD facies (well B) reflect more developed transport and erosion, showing a homogeneous detrital composition along deltaic and fluvial-braided (BR facies) sandstones.

SB1 implies in little change of sedimentary regime and subsidence patterns, but its time is marked by a sharp shift of facies (mainly primary detrital composition; i.e. source area). The base of Sequence R2 in well A is characterized by an important basal conglomeratic interval with high content of large metamorphic rock fragments. However, this sequence shows a sharp decrease of ductile grains (mainly metamorphic rock fragments) in comparison with Sequence R1

(Table 3). SB1 shows a clear shift between wells A and B. The transition of Sequence R1 to R2 in well B, conversely to well A, shows a sharp increase of metamorphic rock fragments (decrease maturity of sediments, regarding Sequence R1), with large meta-sandstone and sandstone fragments (Fig. 13). The sharp increase of lithic constituents at Sequence R2 in well B is interpreted as a significant shift of drainage patterns, with increase supply of sediments associated with basin margin faults.

Facies succession from sequences R1 to R2 in well A, and along Sequence R1 in well B shows a thickening-upward delta front/delta plain facies corresponding to a coarsening-upward SP trend, with continuous trend of sedimentation rate exceeding creation of accommodation space, locally overlain by braided river systems (continuous low SP signature), such as in the uppermost interval Sequence R1 of well B (Fig. 4). Such trend supports a highstand system tract for Sequence R1. Sequence R2 is poorly preserved in well B, and, therefore rendering a precise stacking pattern interpretation.

Insert Fig.12

Insert Fig.13

Sequences T and D1

The Late Aptian to Early Albian gradual transition from continental (fluvial-lacustrine) to marine settings, are characterized by the Transitional sequence - T (well C) and early Drift Sequence D1 (well A), consisting of prograding coarse-grained coastal-deltaic systems (SD facies), which were deposited into a basinal environment grading from a narrow gulf into a progressively open marine conditions, and under arid climatic conditions, capped by sabkha and coastal salina supratidal facies environments (Fig. 12b), as observed at Sequence T.

The Transitional Sequence is preserved only in well C (Fig. 7), directly overlying basement rocks (SB2), indicating paleo-high settings for well C during rift phase. Sequence T is characterized by the alternation of siliciclastic (SD facies) and evaporative (SC facies) deposits. Deposition and preservation of platform evaporites generally occur during highstand conditions (Handford & Loucks, 1993). SB2 is not preserved in well A.

The lower limit of Sequence D1 (SB3) displays a marked change in sedimentary regime in well A from continental fluvial-deltaic deposits to highly-bioturbated and deformed coarse-grained deltaic deposits. The facies succession of this sequence reflects the high supply of siliciclastics (no indication of coeval carbonate deposition during Sequence D1). The lack of muddy sediments (prodeltaic facies) observed in the coarse-grained coastal deposits is herein interpreted as a consequence of the very shallow-water depositional setting (cf. Reading & Collinson, 1996), resulting in high-energy conditions with widespread dispersal of suspended sediment by wave-reworking (cf. Galloway and Hobday, 1983). The occurrence of plant fragments is probably related to the proximal fluvial sediment supply. The SD facies deposits of Sequence D1 show high

content (up to 4%) of detrital plagioclase. The high average K-feldspar content (47-50%) suggests rapid erosion and transportation from mountainous source-areas, under arid or semiarid climate.

The compositional trends of wells A and B show a gradual decrease of lithic contribution towards Albian samples (Fig. 13). This is especially clear in well A from a lithic composition of rift sequences (R1 and R2) to feldspathic drift Sequence D1, with corresponding decrease of average grain size.

The upper limit of Sequence D1 (SB4) marks a change in sedimentary regime, with the onset of significant carbonatic deposition (carbonate package of Sequence D2).

Sequences D2 to D4

Albian drift Sequences D2 to D4 reflect the gradual onset of less restricted marine conditions, consisting of high-energy, shallow water, wave-reworked, mixed siliciclastic-carbonatic ramp (Fig. 12c). These sequences show a vertical succession of siliciclastic and carbonate deposition (Figs. 6, 7). The deposition of carbonatic and siliciclastic sediments tends to be mutually exclusive, with siliciclastic-dominated sediments interpreted as preferably deposited during regressive (highstand and lowstand) system tracts, and carbonate-dominated sediments preferably deposited during transgressive to early highstand system tracts (cf. Handford & Loucks, 1993). The observed cyclicity of siliciclastic and carbonate intervals (well presented in well A) is herein interpreted as product of relative eustatic sea-level changes and/or variations in sediment supply (cf. Shew, 1991), as well as local product of alongshore currents, which is attested by the lower limit of sequences D3 and D4 (SB5 and SB6, respectively), which display no significant change in sedimentary regime.

Regressive siliciclastic deposits were interpreted mostly as highstand, interpreted as fluvial-braided/delta plain deposits prograding over delta front (foreshore to upper shoreface facies), as indicated by the coarsening-upward GR log response (Sequence D3, for instance; Fig. 6). Lowstand system tract successions, resulting in typical “box” GR well log response intervals (Sequence D3, for instance; Fig. 6) are herein poorly developed due to the interpreted shallow ramp and proximal settings of the studied wells.

The interval comprising the maximum flooding surfaces of Sequences D2 to D4 (not sampled) were interpreted by wireline GR/SP log responses and facies succession, when suggesting higher carbonate/siliciclastic ratio, interpreted as indicative of maximum landward shift of shallow marine facies. Conversely to the other wells, the transgressive system tract of Sequence D4 in well B is characterized by an alternation of siliciclastic-dominated deltaic succession of shoreface to foreshore deposits (SDush facies) and restricted estuarine-lagoonal deposits (ES facies). This interval shows distinct detrital composition from other drift sequences, consisting of high content of meta-sedimentary rocks, and plant fragments, suggesting fast and short transportation from source areas, and higher sediment supply in comparison with transgressive

system tract of wells A and C, resulting unfavourable conditions for carbonate deposition.

Cordoba (1994) identified two coastal shoal systems: (i) oolitic/oncolitic shoals, continuously active during sedimentation); and (ii) bioclastic shoals, formed during later stages of ramp evolution during Albian times. Such trend is observed in wells A and B, where oolitic/oncolitic intrabasinal grains occur along all drift sequences (D2 to D4); whereas the bioclasts content is significant along drift sequences D3 and D4 only. Such trend was used to correlate the drift sequences between the wells.

DIAGENETIC CONSTITUENTS

Dolomite. This is the most abundant diagenetic constituent in the studied sandstones (av. 7.0% of bulk volume). Dolomite occurs as intergranular pore-filling or grain rimming microcrystalline to coarsely-crystalline rhombs (20 to 450 μm, av. 120 μm), as cement locally displacive, and pre-dating other intergranular pore-filling cements, except K-feldspar overgrowths. Microcrystalline rhombs (< 60 μm) replace mud intraclasts and high-Mg calcite rim marine cement (Fig. 14a). Coarsely-crystalline dolomite replaces feldspars, micas and rock fragments, as well as the microcrystalline phase. Euhedral crystals up to 450 μm with wavy extinction, characteristic of the “baroque” or “saddle” dolomite types, occur as intergranular pore-filling cement, as well as replacing previous dolomitized constituents (mainly mud intraclasts). Bulk-rock, carbon and oxygen isotopes of dolomite reveal a range of $\delta^{13}C_{PDB}$ between -5.98‰ and 0.15‰, $\delta^{18}O_{PDB}$ between -8.36‰ and 2.67‰ (Table 4).

Calcite. This cement (av. 1.5 % of bulk volume) occurs as microcrystalline, grain-rimming and pore-filling cement in sandstones (Fig. 14b), and replacing early, pore-filling micritic cement in hybrid arenites and calcarenites, as well as syntaxial overgrowths on echinoid bioclasts (Fig. 14c). Post-compaction, coarsely-crystalline (av. 150 μm), intergranular pore-filling and grain-replacive calcite cement is patchily distributed in arkose and lithic arkose sandstones.

Anhydrite. This is the second most abundant diagenetic constituent in the studied sandstones (av. 2.5 % of bulk volume). Anhydrite occurs with two diverse distribution modes: Pre- to syn-compaction, lamellar or prismatic/ plumose (divergent) crystals (from 120 to 500 μm; av. 170 μm; Fig. 14d), or as felted (fibrous) crystals, engulf and thus post-date K-feldspar overgrowths and microcrystalline dolomite. Post-compactional, poikilotopic pore-filling cement (Fig. 14e) with crystal size from 0.3 to 2.4mm (av. 0.9mm) is the common habit (absent along grain contacts – post-compaction?), occurring in some samples mixed with earlier lamellar phase. Large crystals (up to 4.2mm wide) of anhydrite replace large carbonate bioclasts and oncoliths. Anhydrite cement distribution is commonly heterogeneous and patchy, locally pervasive. Bulk-rock, sulfur isotopes reveal a range of $\delta^{34}S_{CDT}$ between -0.4‰ and 21.3‰ (Table 4).

Insert Fig.14

K-feldspar. Potassic feldspar overgrowths are conspicuous in the studied sandstones (av. 1.6 % of bulk volume). The overgrowths are euhedral (sanidine habit), epitaxial, thick (up to 200 μm) and continuously cover detrital orthoclase and microcline grains, and are covered by, thus pre-dating all other intergranular pore-filling authigenic phases, except mechanically infiltrated smectite coatings (syn-precipitated).

Quartz. This cement (av. 0.5%) occurs as euhedral, syntaxial, up to 60 μm thick overgrowths on quartz grains. Quartz overgrowths engulf K-feldspar overgrowths and clay coatings, and are covered by anhydrite poikilotopic cement. Some samples with discontinuous clay coatings show expressive precipitation of prismatic crystals (outgrowths) with average size of 30 μm, locally occupying moldic pores (thus post-dating grain dissolution). However, deepest samples of Sequence R1 (well A) show large percentual of discrete, pore-filling quartz outgrowths, while adjacent quartz grains surfaces show neither clay coatings, nor overgrowths. Significant volume (> 2%) of quartz overgrowths and outgrowths is only observed in some of the deeper samples (rift phase sequences of well A).

Smectite. Smectite clays occur in the following habits: (i) as discontinuous coatings, thicker (up to 15 μm) along the concave portion of grain surfaces (scattered occurrence, in most sequences); (ii) as thin (av. 5 μm), pre-compaction, continuous and isopachous coatings; (iii) as thick (up to 60 μm; av. 12 μm) continuous and anisopachous, pre-compaction coatings (Fig. 14f), and; (iv) as rims of honeycombed aggregates, covering the coatings. Shrinkage and fragmentation features are commonly observed. X-ray diffraction analyses indicate the preservation of smectite in samples presently buried deeper than 1200 m.

Corrensite. Corrensite clays (regular mixed-layer chlorite-smectite) occur in one sample in the following habits: (i) thick (av. 8 μm), locally multiple (concentric) anisopachous coatings, displaying shrinkage and fragmentation features; and (ii) well developed rims covering the coatings. Multiple corrensite coatings are observed around dissolved heavy minerals (mainly garnet) indicating recurrent precipitation and dissolution (thicker around completely dissolved heavy mineral grains). Corrensite rims post-date the shrinkage of coatings and the expansion of micaceous grains, and pre-date grain dissolution (thicker along intergranular space).

Chlorite. Chlorite clays occur replacing detrital biotite and ferromagnesian heavy mineral grains, mud intraclasts and metamorphic rock fragments, smectite coatings (transformation), as well as partially to totally dissolved (locally transformed into pseudomatrix) metamorphic rock fragments (Fig. 15a). It was directly precipitated (neoformed) as continuous, isopachous (up to 10 μm thick; av. 7 μm) rims made of thin platelets arranged perpendicularly to grains surfaces. Double rims were formed along both sides of coatings detached due to shrinkage or grain dissolution.

Insert Fig.15

Other diagenetic minerals. Illite-Smectite (I-S) irregular mixed-layers occur in few samples, as intergranular pore-lining or pore-filling, radiated aggregates of fibrous crystals (up to 15 μm), locally covering chloritized coatings or chlorite rims, and also bridging across pores. Pyrite occurs as disseminated intergranular and intraparticle (within bioclasts) pore-filling framboidal aggregates (< 20 μm), and also replacing carbonaceous fragments, micas, clay coatings mud intraclasts and pseudomatrix. Siderite occurs as microcrystalline or spherulitic aggregates (up to 20 μm; av. 9 μm), commonly replacing mud intraclasts. Kaolinite replaces micaceous grains as large booklets (up to 80 μm) and pseudomorphic, lamellar crystals. Small, prismatic crystals of diagenetic titanium oxides (av. 25 μm) replace heavy mineral and biotite grains, and occur also as discrete, intergranular pore-filling cement. Diagenetic albite heterogeneously replaces feldspar grains in all depositional facies and systems tracts (av. 1.0% of bulk volume).

COMPACTION AND POROSITY

The degree of compaction undergone by the studied sandstones, as well as the evaluation of the relative role played by compaction and cementation in porosity reduction, were analysed in a diagram of intergranular volume versus intergranular cements (cf. Ehrenberg, 1989; Fig. 16). The wide range of intergranular volume (12 to 38%; av. 24.2%) reflect the variable timing and intensity of cementation and compaction of studied samples. Conversely to lithic and poorly-cemented rift samples, sandstones with abundant pre-compaction carbonate or sulphate cementation, such as in transgressive deltaic (SDush) facies of drift sequences or highstand system tracts of transitional sequence, suffered limited compaction, as indicated by their larger intergranular volume. However, pervasive eodiagenetic carbonate and/or sulphate cementation, with minor porosity preservation, was favoured in hybrid arenites of low-energy settings (MRlin) and deltaic (SDush) facies underlying evaporative supratidal sandstones (Sequence T).

Secondary intragranular porosity (av. 4.3%) is volumetrically subordinate in relation to total porosity resulted mainly from the dissolution of detrital feldspar grains (av. 2.1%) and subordinately from metamorphic rock fragments, heavy minerals and intrabasinal carbonate grains, being more significant in the

coarser-grained sandstones of rift sequences and transgressive siliciclastic (SD/TST) samples of drift Sequence D4 of well B (Table 3).

DISCUSSION

The diagenetic evolution of the sandstones is influenced by depositional parameters, such as the composition of framework grains, grain-size, sorting, sedimentary structures, and pore-water chemistry (e.g. De Ros, 1996; Morad et al., 2000). The variable original composition and depositional settings of the studied sandstones is reflected by the diversity of diagenetic evolution pathways, which are discussed below, within their sequence stratigraphic context (system tracts and depositional sequences), as shown in Fig. 17.

Insert Fig.16

Diagenetic alterations associated with rift sequences R1 and R2

Sandstones from rift sequences R1 and R2 (Fig. 17a) are characterized by a small content of early, pore-filling cementation (mainly microcrystalline to coarsely-crystalline dolomite), which is herein interpreted as possibly product of intense sediment accumulation rates, resulting in unfavourable conditions for significant eodiagenetic cementation (cf. De Ros, 1996). Consequently, the main diagenetic alterations associated with this tectonic system tract refer to post-compaction phases, and are directly related to the detrital composition.

Coarse-grained, channel-fill delta plain to braided fluvial sediments (Figs. 4, 3; cores A3-7) show large content of mud and soil intraclasts, interpreted as product of floodplain erosion by extensive lateral channel avulsion (cf. Ketzer et al., 2003a), resulting in moderately compacted intervals with intergranular porosity partially filled by pseudomatrix. Conversely, samples from low-energy, shallow/small channels, delta front to prodelta facies, or overbank and floodplain settings, are enriched in micas and low-rank metamorphic rock fragments. These samples, despite similar packing of channel-fill facies, show lower macroporosity values due to more intense compaction of ductile grains (Figs. 15a-b).

Insert Figs.17a-d

The scattered, intergranular and replacive microcrystalline to coarsely-crystalline dolomite cement, observed at Sequence R2 (well A) samples, are the product of mixing of eodiagenetic microcrystalline and mesodiagenetic coarsely-crystalline (including saddle dolomite) phases, as attested by its isotopic composition. Assuming an average value of -5.0 ‰ $\delta^{18}O_{SMOW}$ value for meteoric precipitating fluids (cf. Lloyd, 1982), expected for a continental setting at the paleolatitude of the basin during Lower Cretaceous, the precipitation temperatures calculated for the dolomite cement in these samples (Table 4; Fig. 18) range from 43.1 to 54.3°C. The late (syn- to post-compaction) character of dolomite cementation of rift sandstones agrees with their tight packing. The $\delta^{13}C_{PDB}$ values of -5.98 ‰ and –1.47‰) are compatible with derivation from organic matter oxidation.

Insert Fig.18

The relationship of late diagenetic alterations of rift sequences with provenance and depositional environment (Fig. 19) is attested by the conspicuous pore-lining chlorite, corrensite and illite-smectite cementation shown by low-energy facies samples, which is herein interpreted as developed through complete transformation of eodiagenetic smectite coatings, product of alteration of ferromagnesian silicates, such as biotite (e.g. Bjørlykke et al., 1989) and low-rank metamorphic rock fragments (Fig. 15a). This is supported by the good correlation between chlorite content and detrital biotite and metamorphic rock fragments (Fig. 13). The coarser, channel sandstones, with minor content of Fe-Mg detrital grains (Table 3), show limited chloritization, except for the local occurrence of chlorite rims or multiple and thick corrensite coatings, interpreted as the product of transformation of eodiagenetic smectite precursors.

Diagenetic alterations associated with Transitional Sequence

Sandstones of highstand delta plain (SDush) deposits of the Sequence T of well C (Figs. 7a, 3; core C1) show eodiagenetic pore-filling, locally displacive, microcrystalline dolomite and felted anhydrite cementation (Fig. 17b), which are interpreted as associated with to the supratidal-coastal sabkha facies (Fig. 20). Deposition and preservation of platform evaporites are favoured at late highstand conditions due to seawater influx to replenish the evaporation, which is not usually available during signicant sea-level falls (Handford and Loucks, 1993). The sulphur isotopic composition for eodiagenetic felted anhydrite cement of delta plain facies and overlying anhydrite of salt formations yielded $\delta^{34}S_{CDT}$ values between 19.8 to 21.5‰, higher than expected for Aptian-Albian marine-derived anhydrite (cf. Claypool et al., 1980). The observed high $\delta^{34}S$ values (up to 6‰ above global averages) could be interpreted as product of restricted replenishment, with minor supply of oceanic water enriched in light isotopes flowing into the evaporate. Progressive reduction of a limited sulfate reservoir continuously modifies the isotopic composition of the remaining sulfate towards more positive, heavier $\delta^{34}S$ values (cf. Strauss, 1997).

Insert Fig.19

Insert Table 4

Diagenetic alterations associated with drift Sequence D1 and D2

Sandstones of transgressive to highstand delta front to delta plain (SDush) deposits of the Sequence D1 and D2 of well A (Figs. 6, 3; cores A9 to13) show a coarsening-upward succession that is characterized by an upward increase in anhydrite and decrease in dolomite cementations (Figs. 13). Delta front facies due to mixing of sand and mud through bioturbation (Fig. 8a) and higher content of mud intraclasts were preferentially cemented by eodiagenetic dolomite, and consequently, coarsely-crystalline mesodiagenetic dolomite, locally engulfing early phases. Assuming a $\delta^{18}O_{SMOW}$ value of –3‰ for mixed meteoric-marine precipitating fluids expected for a coastal setting, a precipitation temperature range of 42.7 to 46°C is calculated for eodiagenetic dolomite cements with

$\delta^{18}O_{PDB}$ values between –5.37 to –4.85‰ (Table 4; Fig. 18). These temperatures are high for near-subsurface cementation, as observed in rift samples, and may be reflecting the mixing of pre-compaction microcrystalline dolomite with syn- to post-compaction coarsely-crystalline mesodiagenetic dolomite. Stable carbon isotope data of eodiagenetic dolomite cement around 0‰ ($\delta^{13}C_{PDB}$ values from –1.9 to 0.15‰) suggest direct supply of dissolved carbon from seawater (cf. Morad, 1998). Coarser-grained facies (mainly delta plain facies), On the other hand, show minor dolomite cementation, being preferentially and pervasively cemented by mesodiagenetic (and locally eodiagenetic) anhydrite. The upward increase in early anhydrite cementation observed in Sequence D1 of well A is herein associated with more intense evaporitic conditions towards the top of this sequence.

Insert Fig.20

The highstand system tract deposits of Sequence D1 and Sequence R1 (well A) show mesodiagenetic anhydrite cementation with $\delta^{34}S_{CDT}$ values ranging from –2.9 to 1.9‰. Such low values may be interpreted as resulting from: (i) thermal degradation of organic sulphur originated from deeply buried (up to 4km) Early Aptian lacustrine shales; or (ii) juvenile sulphur-rich fluids originated from Paleocene-Eocene near-surface volcanism of Royal Charlotte Volcanic Complex (c. 40 km to southeast of the studied wells). The single occurrence of a large (~1mm) evaporite intraclast in a coarse-grained highstand deposit of Sequence D1 with isotopic composition similar to Early Aptian evaporites ($\delta^{34}S_{CDT}$ = 21.3‰), attests the reworking of evaporite layers of the Itaunas Member (Mariricu Formation), deposited on top of the Transitional Sequence.

Diagenetic alterations associated with drift Sequence D3

Sandstones of lowstand braid plain channel-fill deposits of Sequence D3 of well A (Figs. 6, 3; core A14) display thick clay coatings, which are herein interpreted as abundant mechanical infiltration of detrital smectitic clays under subaerial, hot and arid depositional conditions (cf. Moraes & De Ros, 1992), as irregular coatings (Fig. 14f). The clay coatings unfavoured later cementation (Fig. 17d), as suggested by the lack of any volumetrically significant pore-filling cement (Fig. 21).

Hybrid arenites of transgressive system tract of Sequence D3 of well B (Figs. 7b, 3; core B12) with large carbonate bioclasts and oncoids, plant fragments, and high biotite content (Fig. 17d), herein interpreted as restricted (internal platform) lagoonal, possibly associated with intertital to supratidal settings (Fig. 21). This facies shows pervasive eodiagenetic intergranular pore-filling dolomite cement, as well as dolomitization of carbonate grains and well-developed K-feldspar overgrowths. The O^{18} enrichment of such dolomite cement relative to seawater (Table 4; Fig. 18; B-D3(a)) is possibly a product of evaporative conditions. Carbonate allochems show intense coarsely-crystalline dolomite and anhydrite replacement (Fig. 15c). The isotopic analysis of anhydrite cement yielded $\delta^{34}S_{CDT}$ values of 16.8‰, i.e. within the range of $\delta^{34}S_{CDT}$ = +14 to +18‰ for Albian anhydrite with marine origin (cf. Claypool et al., 1980), suggesting an Albian sea water origin of dissolved Ca^{+2} and SO_4^{-2}. A precipitation temperature of 75°C is calculated for the replacive dolomite, assuming a $\delta^{18}O_{SMOW}$ value of

1‰ for the evolved formation waters, consistent with a mesodiagenetic interpretation (Table 4; Fig. 18; B-D3(b)).

Sandstones of highstand delta front/delta plain (SDush) deposits of Sequence D3 of well A (Figs. 6, 3; core A15), show microcrystalline, pre-compaction dolomite rim cementation (Fig. 17c), derived from the dolomitization of high-Mg calcite marine rims (Fig. 14a). The relatively good sorting of this petrofacies is interpreted as a product of wave reworking. Locally, poorer-sorted samples show intergranular pore-filling, locally displacive, dolomite precipitation (Fig. 21). This could be interpreted as product of sea-water flow through the coastal sediments in an intertidal depositional setting, with the resulting mixing with meteoric waters, favouring eodiagenetic intergranular dolomite precipitation (cf. Ketzer et al., 2002).

Assuming a $\delta^{18}O_{SMOW}$ value of –3‰ for precipitating fluids originated by mixing of marine and meteoric waters, as expected for the continued progradation of highstand deposits towards SB6, a precipitation temperature of 31°C is calculated. Assuming a $\delta^{18}O_{SMOW}$ value of –5‰ for precipitating brackish pore waters with high meteoric contribution (cf. Lloyd, 1982), the precipitation temperature approximates 20°C, what is probably more compatible to near-surface precipitation (Table 4; Fig. 18). The $\delta^{13}C_{PDB}$ value of –2.1‰ is consistent with eodiagenetic precipitation of dolomite cement at oxic phreatic conditions (cf. Morad, 1998).

Calcarenites of highstand high-energy oolithic shoals (MRhin facies) of Sequence D3 of well C (Fig. 7a; core C2), consisting of oolithic grainstones (Fig. 15f), show less marine carbonate cementation than transgressive deposits in the vicinity of condensed sections (Figs. 17b, 21).

Diagenetic alterations associated with drift Sequence D4

The transgressive system tract delta plain-delta front (upper shoreface) deposits and inner ramp hybrid arenites of Sequence D4 of well A (Fig. 17b) are characterized by abundant pore-filling and pore-lining calcite cementation (Fig. 21). This occurred in response to the source and nucleation provided by the large amount of carbonate intrabasinal grains, such as ooids and bioclasts (cf. Morad et al., 2000; Ketzer et al., 2002; Ketzer et al., 2003b; Al-Ramadan et al., 2006). Early transgressive deltaic (SDush) sandstones (Figs. 6, 3; core A16) are characterized by scattered nodular calcite cementation (Fig. 14b), which pre-compactional nature is attested by the large intergranular volumes, whereas hybrid arenites and calcarenites (Figs. 6, 3; core A18), located in the vicinity of the condensed section, show pervasive, stratabound, microcrystalline calcite cementation that completely fill the pores (Fig. 14c).

Conversely to carbonate-dominated transgressive interval of well A, the transgressive system tract in well B (Figs. 7b, 3; cores B16-18) is characterized by a siliciclastic-dominated deltaic delta plain to delta front deposits (SDush) showing high sediment supply and lack of intergranular cementation (Figs. 15d, 17b), alternating with estuarine deposits showing pervasive microcrystalline dolomite cementation (Figs. 15e, 17d). This pervasive dolomite cementation is

herein interpreted as product meteoric and sea-water mixing, favouring eodiagenetic intergranular dolomite precipitation (cf. Ketzer et al., 2002). Assuming temperatures from 15 to 25°C for surface precipitation, the depositional water isotopic composition range from -3.5 to -1.2‰ would agree with the mixing zone interpretation. $\delta^{13}C_{PDB}$ values of –3.26 and -3.42‰ are consistent with eodiagenetic precipitation at oxic phreatic conditions (cf. Morad, 1998).

Insert Fig.21

Porosity evolution and reservoir quality prediction in a sequence-stratigraphic framework

The reservoir quality of the studied sandstones reflects the nature of their facies associations and sequence stratigraphic-related diagenetic evolution. The original porosity, controlled by depositional facies and provenance was modified during diagenesis owing mostly to carbonate and/or sulphate cementation, or to compaction. The samples with best reservoir quality correspond to early transgressive and highstand intervals. These samples show scattered patches of calcite and/or dolomite cement, which were apparently enough to prevent significant compaction of the framework grains, and minor amounts of mesodiagenetic (dolomite or sulphate) pore-filling cements. The discontinuous, patchy character of dolomite and anhydrite cementation observed in most intervals is expected not to any major impact on permeability reduction. In some Sequence R2 (well A) sandstones porosity was favoured by better sorting and/or minor content of highly altered and deformed (pseudomatrix) low-grade metamorphic grains.

The rift highstand and drift lowstand system tract samples (fluvial-deltaic facies) show compaction as the main process of porosity reduction, which can be attributed to rapid burial (high sediment supply), inhibiting significant volume of eodiagenetic precipitation. For these samples, the provenance control of original detrital composition is the key factor. Facies with better sorting and smaller content of ductile grains (i.e. biotite, mud intraclasts and metamorphic rock fragments), such as channel facies of well A and mica-poor samples of well B, show better reservoir quality (Fig. 16).

SB1 is a key surface for reservoir quality prediction for rift sequences in areas with provenance similar to well A, considering the distribution of metamorphic rock fragments (Fig. 13), because it separates lithic sandstones of Sequence R1, with poor reservoir quality (porosity < 12% and low permeability), from lithic-poor sandstones of Sequence R2, with better porosity (12 to 20%) and permeability values (Fig. 16).

On the other hand, a comparison between sequences R1 and R2 in well B shows an opposite trend (Fig. 13), from fluvial-deltaic (FD) and fluvial (BR) facies of Sequence R1, showing small content of metamorphic grains, minor mechanical compaction and good reservoir quality (Fig. 16), and CD facies of Sequence R2 displaying high content of metamorphic rock fragments. Surprisingly, the feldspathic litharenites of Sequence R2 (Fig. 4; core B10) show an anomalously high porosity preservation, interpreted as a probable product of

the limited maximum burial of Sequence R2 in well B area. The high content of low-grade meta-sedimentary rock fragments (av. 29.5%), including large (5.6 mm) meta-sandstone fragments suggests a rapid erosion and short transportation of old orogenic sequences (De Ros et al., 2005).

Eodiagenetic, pervasive, pore-filling cementation was observed at (Fig. 16): (i) transgressive system tract hybrid arenites and calcarenites of mixed ramp (MR) facies, preferentially lying in the vicinity of condensed sections or at low-energy, internal platform settings; (ii) estuarine sandstones in the transgressive system tract of Sequence D4 (well B); and (iii) late highstand sandstones underlying the supratidal sabkha evaporites of the Transitional Sequence (well C). The poorer reservoir quality of low-energy mixed-ramp facies comparing with high-energy facies results from abundant dolomite intergranular cementation, resulting unconnected pore space, pore throats and biomoldic porosity, which is herein interpreted as product of intense marine-meteoric mixing at intertidal to supratidal internal platform settings.

The observed trend from scattered, nodular calcite cementation in delta plain-delta front sandstones (distant from flooding surfaces) towards pervasive intergranular pore-filling cementation of inner-ramp hybrid arenites and calcarenites (near flooding surfaces) attests the deterioration of reservoir quality towards the vicinity of the condensed sections owing to increase bioclast content (Fig. 21). Such trend is characterized by a slight increase of induction-log resistivity values, and decrease of SP-GR log values, related to the larger carbonatic content (Figs. 6, 7).

The studied transgressive sandstones and hybrid arenites show cementation as the main process in porosity reduction, with the exception of transgressive deltaic (delta front to delta plain) sandstones of Sequence D4 (well B) (Fig.16), which show high porosity (≥ 20%), herein attributed to the combination of limited burial and lack of significant intergranular pore-filling cementation.

Conversely to the transgressive samples, the studied highstand sandstones and calcarenites show compaction or cementation as the main process in porosity reduction. Such varying impact is well demonstrated in the shallowing-upward succession of highstand sandstones of Sequence D1 (Fig. 13). In these sandstones, the poor depositional reservoir quality of delta front (upper/lower-shoreface) facies, due to higher bioturbation and mud intraclast content, favoured eodiagenetic dolomite cementation, resulting in moderate to good reservoir quality (Fig. 16). On the other hand, coarser-grained sandstones (mainly delta plain facies), with better original porosity and permeability, and minor eodiagenetic dolomite cementation, were preferentially cemented by mesodiagenetic anhydrite. Because of the greater impact on porosity reduction of anhydrite cementation in comparison with dolomite cementation, the coarser-grained sandstones show poorer reservoir quality. The highest amounts of late poikilotopic anhydrite is observed in coarser-grained and better-sorted samples, reflecting the control of depositional texture on fluid flow (Fig. 20).

CONCLUSIONS

This paper demonstrates that spatial and temporal distribution of eodiagenetic alterations (and associated mesodiagenetic alterations), as well as their impact on porosity and permeability of siliciclastic, hybrid and carbonate successions, are directly influenced by the depositional systems (i.e. sedimentary facies), which can be constrained within a sequence stratigraphic framework and related tectonic settings.

The preservation of porosity observed in channel-related facies of proximal fluvial-deltaic highstand deposits or distal (more mature) fluvial-deltaic highstand deposits of rift sequences R1 (well B) and R2 (well A) is attributed to a stable and rigid detrital framework, combined with the absence of pervasive pore-filling cementation. Conversely, low-energy facies of the proximal fluvial-deltaic deposits, with high content of micaceous and ductile rock fragments, show poorer preservation of porosity. In such reservoirs, as observed at Sequence R1 (well A), type of cementation and the degree of mechanical compaction are the major controls on porosity and permeability. Intense plastic deformation of ductile grains, combined with eodiagenetic, pre-compaction, smectite coatings precipitation, and their transformation into chlorite or illite-smectite phases (coatings and/or rims) directly influenced the pore network elements (pore size, pore throat size, and pore connectivity - tortuosity), with authigenic illite severely reducing the permeability.

The highstand system tracts reservoirs, spatially and temporally related with salt formations (evaporite layers) of Transitional Sequence, show intense microcrystalline dolomite and felted anhydrite eodiagenetic cementations, with complete deterioration of depositional porosity. Similar characteristics are observed at highstand deposits of early siliciclastic-dominated Albian drift sequence D1 (well A). Such paragenetic suite is not observed along the following drift sequences, probably reflecting the progressively less arid climatic conditions.

The onset of a mixed siliciclastic-carbonate platform depositional setting observed at Albian drift sequences, resulted in a diversity of reservoir quality. In such sequences, the variations in the carbonate intrabasinal content played a significant role in the distribution of eodiagenetic dolomite and calcite cements, with transgressive system tract reservoirs showing moderate to pervasive carbonate cementation, with poorer reservoir quality towards condensed sections due to higher content of carbonate cement, as expected due increasing carbonate intrabasinal content.

Highstand system tracts deposits of Albian drift sequences, conversely to transgressive deposits, show distinct eodiagenetic alterations depending on the depositional system. Wave-dominated deposits, such as sequences D2 (well C) and D3 (well A), show eodiagenetic, marine, carbonate cementation, with good porosity preservation. On the other hand, fluvial-dominated deltaic deposits, such as Sequence D1 (well A) are mostly affected by mechanical compaction and pore-filling mesodiagenetic cementations rather than early ones, resulting varying porosity preservation values. The deposits of Sequence D1 attest the

influence of depositional features (i.e. detrital composition, geometry, texture, and interconnectivity of the sandbodies) in the course of diagenetic evolution, determining the flow path and rate of the migrating fluids. Samples with high mud content in less clean sandstones show low extent of post-compaction cementation. This is attributed to increasing restrictions in the diagenetic fluid flow paths.

Fluvial (braided) lowstand sandstones (lowstand system tracts deposits of Sequence D3), likewise fluvial-dominated deltaic highstand deposits, show minor intergranular pore-filling cementation, with exception of high content of mechanical infiltration of smectite clays. Such coatings have resulted more intense influence of mechanical compaction in porosity reduction and permeability deterioration.

ACKNOWLEDGEMENTS

The authors thank PETROBRAS, in special M. V. Galvao, A. Grassi, J. A. Cupertino and Paulo de Tarso Guimarães, for access to samples, data, information, and for the license to publish this work. We acknowledge the support of the Institute of Geosciences of Rio Grande do Sul Federal University – UFRGS, and of the Environmental Institute of the Pontifical Catholic University of Rio Grande do Sul - PUC-RS. Suggestions of reviewers ..... and ..... helped improve the manuscript. Special thanks to Dr S. Morad, from Uppsala University, for improving the original manuscript. K. Goldberg, C.M. Scherer and L.A.C. Lopez are also acknowledged for commenting on previous versions of the manuscript.

REFERENCES

Al-Aasm, I.S., Taylor, B.E., South, B. (1990) Stable isotope analysis of multiple carbonate samples using selective acid extraction. *Chem. Geo.*, **80**, 119-125.

Al-Ramadan, K. (2006) Impact of diagenetic alterations on reservoir quality and heterogeneity of paralic and shallow marine sandstones: link to depositional facies and sequence stratigraphy. Acta Universitatis Upsaliensis, Digital Comprehensive Summaries of Uppsala Dissertations from the Faculty of Science and Technology 195, 57pp.

Asmus, H.E. and **Ponte, F.C.** (1973) The Brazilian marginal basins. In: The ocean basins and margins (Eds. A.E.M. Nairm and F.G. Stehili). New York, Plenum, v.1, 87-133.

Beard, D.C. and **Weyl, P.K.** (1973) Influence of texture on porosity and permeability of unconsolidated sand. *AAPG Bull.*, **57**, 349-369.

Bhattacharya, J.P. (2006) Deltas. In: Facies models revisited (Eds. H.W. Posamentier and R.G. Walker). *SEPM Spec. Publ.*, **84**, 237-292.

Bjørlykke, K., Ramm, M and **Saigal, G.C.** (1989) Sandstone diagenesis and porosity modification during basin evolution. *Geol. Rundsch.*, **78**, 243-268.

Cainelli, C. and **Mohriak, W.U.** (1999) Some remarks on the evolution of sedimentary basins along the Eastern Brazilian continental margin. Episodes, **22 (3)**, 206-216

Chang, H.K., Kowsmann, R.O. and **Figueiredo, A.M.F.** (1988) New concepts on the development of East Brazilian marginal basins. *Episodes*, **11 (3)**, 194-202.

Claypool, G.E., Holser, W.T., Kaplan, I.R., Sakai, H. and **Zak, I.** (1980) The age curves of sulfur and oxygen isotopes in marine sulfate and their mutual interpretation. *Chem. Geo.*, **28**, 199-260.

Collings, J.D. (1996) Alluvial sediments. In: Sedimentary environments: processes, facies and stratigraphy (Ed. H.G. Reading) 3rd edn, pp.37-82. Blackwell Science, Oxford.

Córdoba, V.C. (1994) The Development of an Albian-Cenomanian Carbonate ramp as a first marine record in the Jequitinhonha Basin In: 14th International Sedimentological Congress, Recife, Abstracts, 2pp.

Craig, H. (1957) Isotopic standards for carbon and oxygen correction factors for mass spectrometric analysis of carbon dioxide. *Geochim. Cosmochim. Acta*, **12**, 133-149.

Craig, H. (1961) Standards for reporting concentrations of deuterium and oxygen-18 in natural waters. *Science*, **133**, 1833-1934.

De Ros, L.F.S., Morad, S. and **Paim, P.S.G.** (1994) The role of detrital composition and climate on the diagenetic evolution of continental molasses: evidence from the Cambro-Ordovician Guaritas Sequence, southern Brazil. *Sed. Geol.*, **92**, 197-228.

De Ros, L.F., Remus, M.V.D., Vignol-Lelarge, M.L.M., Chemale Jr., F. and **Baitelli, R.** (2005) Sandstone provenance of BM-J-3 Block, Jequitinhonha Basin, BA. Petrobras-Statoil unpublished report.

De Ros, L.F. (1996) Compositional controls in sandstones diagenesis. Acta Universitatis Upsaliensis, Comprehensive Summaries of Uppsala Dissertations from the Faculty of Science and Technology 198, 24pp.

De Ros, L.F., Goldberg, K., Abel, M., Victorinetti, F., Mastella, L. and **Castro, E.** (2007) Advanced Acquisition and Management of Petrographic Information from Reservoir Rocks Using the PETROLEDGE® System, AAPG Anual Conference and Exhibition. AAPG, Long Beach, CA, USA, Extended Abstracts CD, 6pp.

Dickinson, W. R. (1985) Interpreting provenance relations from detrital modes of sandstones. In: Provenance of Arenites (Ed. G.G. Zuffa). *NATO Advanced Science Series C*, 148, 333-361.

Ehrenberg, S.N. (1989) Assessing the relative importance of compaction processes and cementation to reduction of porosity in sandstones: discussion; Compaction and porosity evolution of Pliocene sandstones, Ventura Basin, California: discussion. *AAPG Bull.*, **73**, 1274-1276.

Folk, R.L. (1968) Petrology of sedimentary rocks. Austin, Texas, Hemphill's Pub., 107pp.

Friedman, I. and **O'Neil, J.R.** (1977) Compilation of stable isotopic fractionation factors of geochemical interest. *US Geol. Surv. Prof. Pap.* 440-KK, 12pp.

Galloway, W.E. and **Hobday, D.K.** (1983) Terrigenous clastic depositional systems: applications to petroleum, coal, and uranium exploration. Springer-Verlag Inc., Heidelberg, 489pp.

Handford, C.R. and **Loucks, R.G.** (1993) Carbonate depositional sequences and systems tracts – responses of carbonate platforms to relative sea-level changes. In: Carbonate sequence stratigraphy: recent developments and applications (Eds. R.G. Lucks and J.F. Sarg). *AAPG Mem.*, **57**, 3-41.

Johnson, H.D. and **Baldwin, J.T.** (1996) Shallow clastic seas. In: Sedimentary environments: processes, facies and stratigraphy (Ed. H.G. Reading) 3rd edn, pp.232-280. Blackwell Science, Oxford.

Kendall, A.C. and **Harwood, G.M.** (1996) Marine evaporates: arid shorelines and basins. In: Sedimentary environments: processes, facies and stratigraphy (Ed. H.G. Reading) 3rd edn, pp.281-324. Blackwell Science, Oxford.

Ketzer, J.M., Morad, S., Evans, R. and **AL-Aasm, I.S.** (2002) Distribution of diagenetic alterations in fluvial, deltaic and shallow marine sandstones within a sequence stratigraphic framework: evidence from the Mullaghmore Formation (carboniferous), NW Ireland. *J. Sed. Res.,* **72**, 760-774.

Ketzer, J. M., Morad, S. and **Amorosi, A.** (2003a) Predictive diagenetic clay-mineral distribution in siliciclastic rocks within a sequence stratigraphic framework. In: Clay Mineral Cementation in Sandstones (Eds. R. Worden and S. Morad). *Int. Assoc. Sedimentol. Spec. Publ.,* **34**, 42-59.

Ketzer, J.M., Holz, M. and **Morad, S.** (2003b) Sequence stratigraphic distribution of diagenetic alterations in coal-bearing, paralic sandstones: evidence from the Rio Bonito Formation (early Permian), southern Brazil. *Sedimentology*, **50**, 855-877.

Kuchle, J., Holz, M., Brito, A.F. and **Bedregal, R.P.** (2005) Análise estratigráfica de bacias rifte: aplicação de conceitos genéticos nas bacias de Camamu-almada e Jequitinhonha (Tr. Stratigraphic analysis of rift basins: applications of genetic concepts in Camamu-Almada and Jequitinhonha basins). *Boletim de Geociências da Petrobrás*, **13(1)**, 227-244.

Kumar, N. and **Gamboa, L.A.P.** (1979) Evolution of the São Paulo plateau (southeastern Brazilian margin) and the implications for the early history of the South Atlantic. *Geol. Soc. Am. Bull.,* **90**, part 1, 281-293.

Lloyd, C.R. (1982) The mid-Cretaceous earth: paleogeography, ocean circulation and temperature, and atmospheric circulation. *J. Geol.*, **90**, 393-413.

Miall, A. D. (1996) The geology of fluvial deposits: sedimentary facies, basin analysis and petroleum geology. Springer-Verlag Inc., Heidelberg, 582pp.

Moraes, M.A.S. and **De Ros, L.F.** (1990) Infiltrated clays in fluvial Jurassic sandstones of Reconcavo basin, northeastern Brazil. *J. Sed. Petrol.*, **60**, 809-819.

Moraes, M.A.S. and **De Ros, L.F.** (1992) Depositional, infiltrated and authigenic clays in fluvial sandstones of the Jurassic Sergi Formation, Reconcavo basin, northeastern Brazil. *SEPM Spec. Publ.*, **47**, 197-208.

Morad, S. (1998) Carbonate cementation in sandstones: distribution patterns and geochemical evolution, In: Carbonate cementation in sandstones (Ed. S. Morad). *Int. Assoc. Sedimentol. Spec. Publ.,* **26**, 1-26.

Morad, S., Ketzer, J.M. and **De Ros, L.F.** (2000) Spatial and temporal distribution of diagenetic alterations in siliciclastic rocks: implication for mass transfer in sedimentary basins. *Sedimentology*, **47**, 95-120.

Ojeda, H.A. (1982) Structural framework, stratigraphy and evolution of Brazilian marginal basins. *AAPG Bull.,*, **66**, 732-749.

Posamentier, H.W. and **Allen, G.P.** (1993) Variability of the sequence stratigraphic model: effects of local basin factors. *Sed. Geol.*, **86**, 91-109.

Reading, H.G. and **Collins, J.D.** (1996) Clastic coasts. In: Sedimentary environments: processes, facies and stratigraphy (Ed. H.G. Reading) 3rd edn, pp.154-231. Blackwell Science, Oxford.

Shackleton, N.J. and **Kennett, J.P.** (1975) Late Cenozoic oxygen Late Cenozoic oxygen and carbon isotopic changes at DSDP site 284: implications for the glacial history of the Northern Hemisphere and Antarctica. In: Initial Reports of the Deep Sea Drilling Project 29 (Eds. J.P. Kennett and R.E. Houtz). U.S. Government Printing Office, Washington, D.C, 743-755.

Shew, R. D., 1991. Upward-shoaling sequence of mixed siliciclastics and carbonates from the Jurassic Smackover Formation of Central Mississippi, In: Mixed Carbonate-Siliciclastic Sequences (Eds. A.J. Lomando and P.M. Harris). Dallas, TX, SEPM (Society for Sedimentary Geology), 135-167.

Strausss, H. (1997) The isotopic composition of sedimentary sulfur through time. Palaeogeogr., Palaeoclimatol., Palaeoecol., **132**, 97-118.

Thode, H.G., Monster, J. and **Dunford, H.B.** (1961) Sulphur isotope geochemistry. *Geochim. Cosmochim. Acta*, **25**, 150-174.

Van Wagoner, J. C., Mitchum, R. M., Campion, K.M. and **Rahmanian, V.D.** (1990) Siliciclastic sequence stratigraphy in well logs, cores and outcrops: concepts for high resolution correlation of time and facies. AAPG Methods in Exploration Series, **7**, 55pp.

Walker, R.G. (1992) Facies, facies models and modern stratigraphic concepts. In: Facies models: Response to sea level change (Eds. R.G. Walker and N.P. James). Geological Association of Canada, 1-14.

Weimer, R.J., Howard, J.D. and **Lindsay, D.R.** (1982) Tidal flats. In: Sandstones depositional environments (Eds. P.A. Scholle and D. Spearing). *AAPG Mem.*, **31**, 191-246.

Wright, V.P. and **Burchette, T.P.** (1996) Shallow-water carbonate environments. In: Sedimentary environments: processes, facies and stratigraphy (Ed. H.G. Reading). London, Blackwell, 325-394.

Zuffa, G. G. (1980) Hybrid arenites: their composition and classification. *J. Sed. Petrol.*, **50**, 21-29.

FIGURE CAPTIONS

Figure 1. Location map of the studied wells, and stratigraphic summary of Jequitinhonha sedimentary basin (source Brazilian National Petroleum Agency).

Figure 2. Wireline log (gamma-ray and spontaneous potential) stratigraphic section of studied wells, with indication of depositional sequences and sequence boundaries (cored intervals not to scale).

Figure 3. Selected cores with identified facies associations (cores without thin sections were omitted here).

Figure 4. Wireline log signatures of Aptian rift sequences and their facies associations (core details are shown in Fig. 3). Red arrows indicate interpreted fluvio-deltaic coarsening-upward successions.

Figure 5. Core photographs showing: **A)** Fluvial-deltaic delta front deposits (CDdfr facies), with planar cross-laminated sands (Sp lithofacies), locally with granule-rich levels. **B)** Fluvial-deltaic delta plain to braid-plain deposits (CDdpl facies) with conglomeratic layers (Gmt lithofacies) and **C)** CDdpl facies with parallel-laminated micaceous sands (Sl lithofacies). **D)** Distal, fine-grained fluvial-deltaic delta front deposits (FDdfr facies) with parallel-laminated sands (Sl lithofacies) of upper planar bed flow, and **E)** FDdfr facies with climbing-ripple-laminated sands (Sr lithofacies) of lower planar bottom flow. **F)** Distal fine-grained fluvial-deltaic delta plain deposits (FDdpl facies) with parallel-laminated sands (Sl lithofacies), locally showing mud intraclasts.

Figure 6. Wireline log signatures of transitional and drift sequences of well A and interpreted facies associations, with their core position (core details are shown in Fig. 3). Red arrows indicate interpreted deltaic coarsening-upward successions.

Figure 7. Wireline log signatures of transitional and drift sequences of well C (a) and drift sequences of well B (b), and their interpreted facies associations, with their core positions (core details are shown in Fig. 3). Red arrows indicate interpreted deltaic coarsening-upward successions.

Figure 8. Core photographs showing: A) Shallow-water delta, delta front sandstones (SDush facies) with intense bioturbation (Sb lithofacies), and B) Delta front/upper shoreface sandstones (SDush facies) with slumped features (Sc lithofacies). C and D) Mud flat heterolithic deposits (ES facies) of Sequence D2 of well A. Alternation of silty mudstones (< 25% of sand) and muddy sandstones (< 25% of mud). Possible trace fossils thalassinoides or ophiomorphas (photo C) and skolithos (photo D). E and F) Mud flat heterolithic deposits (ES facies) of Sequence D4 of Well B. Possible trace fossils at photo F: planotites (bottom-half of clay interval) and root marks (top of lower sandy interval).

Figure 9. Core photographs showing: **A)** Shallow-water delta, delta front (SDlsh facies) with climbing-rippled cross laminated sandstones of Transitional Sequence (Sr – lithofacies). **B)** Prodeltaic/lower shoreface (SDlsh facies) with carbonate-rich laminated mudstones of Transitional Sequence (Hc lithofacies). **C)** Supra-tidal flat deposits (SC facies) with parallel-laminated sand with carbonatic lenses (Sl lithofacies). **D)** Sabkha deposits (SC facies) with nodular bedded anhydrite alternating with thin layers of carbonate mud (Ec lithofacies). **E)** Basinward mixed carbonatic-siliciclastic deposits (MRmdr facies) of Sequence D3 of well C, with wavy-rippled cross-laminated sands (Sw lithofacies), and **F)** lower-energy platform internal (MRlin) dolomitized hybrid arenite (Sbh lithofacies) of Sequence D3 of well B.

Figure 10. The original detrital composition of 67 representative samples of Jequitinhonha Basin sandstones plotted on Folk (1968) classification diagram.

Figure 11. Compositional indication of the tectonic provenance setting of the studied sandstones plotted on Dickinson (1985) diagram.

Figure 12. Interpreted depositional environments and paleogeographic settings for (a) Aptian rift sequences; (b) Late Aptian to Early Albian transitional to early drift (D1) sequences; and (c) Albian drift sequences.

Figure 13. Compositional trends of wells A and B regarding selected diagnostic detrital and diagenetic constituents.

Figure 14. Optical micrographs showing: **A)** Highstand drift sample with microcrystalline pore-lining dolomite cementation probably after Mg-calcite rims. Uncrossed polarizers (//P). **B)** Transgressive upper-shoreface sands with patchy, pre-compaction calcite cementation (//P). **C)** Transgressive samples in the vicinity of flooding zone (Seq. D3), with abundant calcite cementation, including syntaxial overgrowths around echinoid bioclasts (//P). **D)** Displacive, lamellar “plumose” eodiagenetic anhydrite cementation. Crossed polarizers (XP). **E)** Highstand Sequence D1 sample with intense burial anhydrite cementation and low porosity (c. 2%) (XP). **F)** Lowstand sample with mechanically infiltrated smectite coatings, unfavouring later cementation, resulting in intense compaction and limited porosity preservation (c.11%) (//P).

Figure 15. Optical micrographs showing: **A)** Rift fluvial deltaic low-energy sandstone with finely-crystalline rock fragment replaced by microcrystalline chlorite (//P). **B)** Rift, low-energy facies, micaceous sample with intense mechanical compaction (//P). **C)** Sequence D3 transgressive internal platform sample with mesodiagenetic anhydrite replacing oncoliths and intraclasts within a strongly dolomitized framework, with high biotite content (XP) **D)** Sequence D4 transgressive sample with moderate values of macroporosity (c. 17%) (//P). **E)** Sequence D4 transgressive, estuarine sample, with abundant intergranular, locally displacive, microcrystalline dolomite cementation (XP). **F)** Early highstand sample with microcrystalline calcite rim cementation and compaction of carbonate ooliths (XP).

Figure 16. Plot of cement volume versus intergranular volume (cf. Ehrenberg, 1989), illustrating the preferential mechanisms of porosity reduction in the studied samples.

Figures 17a-d. Diagrams with interpreted paragenetic evolution with main diagenetic alterations, system tracts and depositional facies.

Figure 18. Plot showing the equilibrium fractionation relationship between temperature and $\delta^{18}O$ values of pore fluids calculated on the basis of the obtained oxygen isotopes for dolomite cement, using the fractionation equation of Friedman and O’Neil (1977).

Figure 19. Schematic model showing the spatial and temporal distribution of diagenetic alterations and variations in the diagenetic evolution pathways of rift sequences sandstones.

Figure 20. Schematic model showing the spatial and temporal distribution of diagenetic alterations and variations in the diagenetic evolution pathways of Transitional and early drift (D1) sequences.

Figure 21. Schematic model showing the spatial and temporal distribution of diagenetic alterations and variations in the diagenetic evolution pathways of drift sequences.

Table 1. Lithofacies (LF) types. Facies codes are modified from Miall (1996).

Table 2. Facies Associations (FA) of studied Jequitinhonha Basin successions.

Table 3. Statistical summary of the petrographic parameters of studied sandstones.

Table 4. Isotopic ratios of representative carbonate and sulphate cements and depositional sulphate phases (salt formations).

FIG. 1

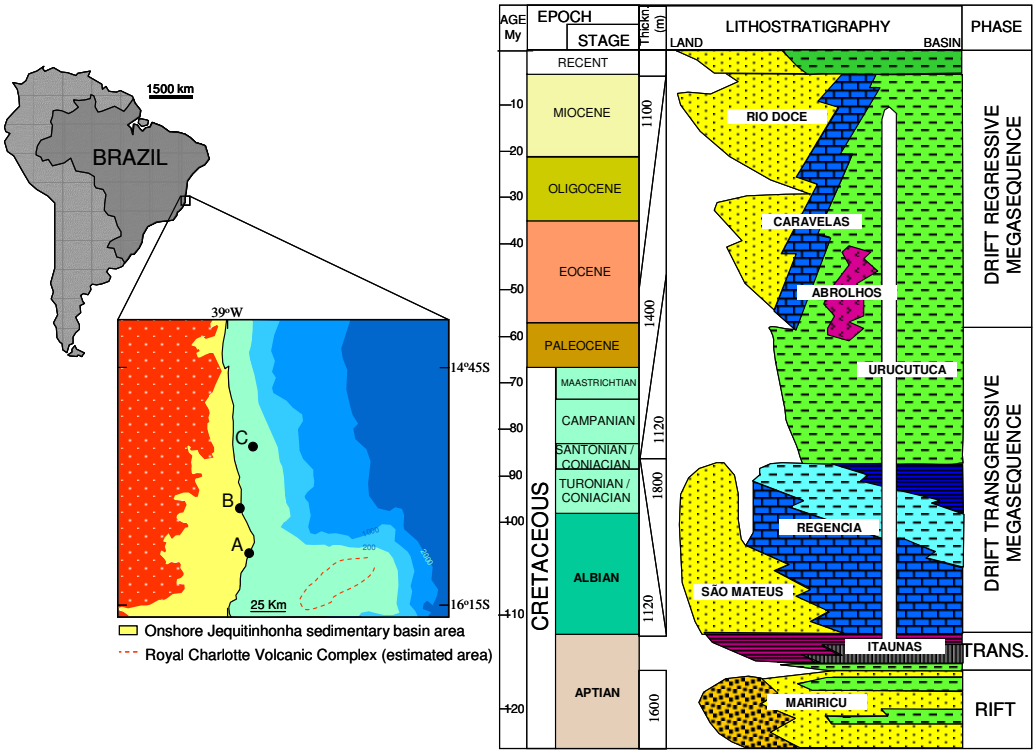
1500 km
BRAZIL
39°W
14°45S
16°15S
25 Km
A
B
C
Onshore Jequitinhonha sedimentary basin area
Royal Charlotte Volcanic Complex (estimated area)
AGE My
EPOCH
STAGE
Thickn. (m)
LITHOSTRATIGRAPHY
LAND
BASIN
PHASE
RECENT
MIOCENE
OLIGOCENE
EOCENE
PALEOCENE
MAASTRICHTIAN
CAMPANIAN
SANTONIAN / CONIACIAN
TURONIAN / CONIACIAN
CRETACEOUS
ALBIAN
APTIAN
1100
1400
1120
1800
1120
1600
RIO DOCE
CARAVELAS
ABROLHOS
URUCUTUCA
REGENCIA
SÃO MATEUS
ITAUNAS
MARIRICU
DRIFT REGRESSIVE MEGASEQUENCE
DRIFT TRANSGRESSIVE MEGASEQUENCE
TRANS.
RIFT

FIG. 2

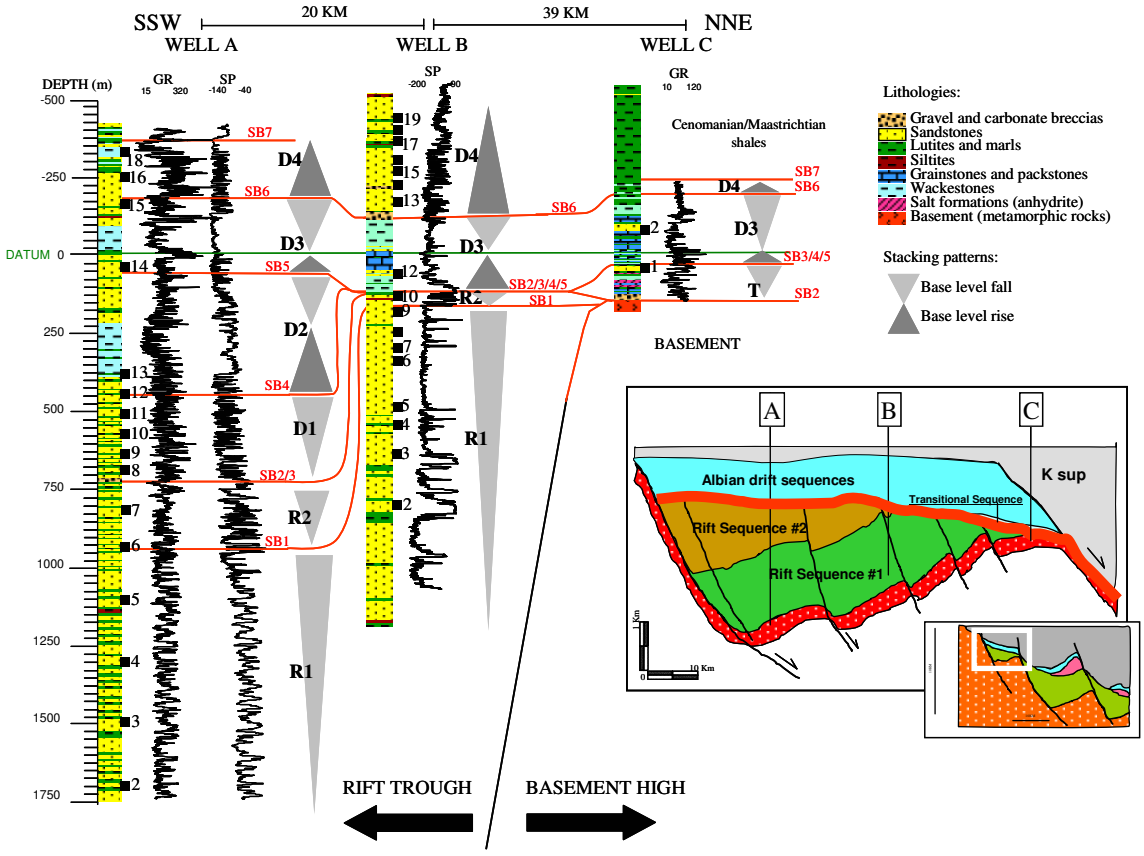
SSW
20 KM
39 KM
NNE
WELL A
WELL B
WELL C
DEPTH (m)
GR
SP
DATUM 0
SB7
SB6
SB5
SB4
SB2/3
SB1
SB2/3/4/5
SB3/4/5
SB2
D1
D2
D3
D4
R1
R2
T
Cenomanian/Maastrichtian shales
BASEMENT
Lithologies:
Gravel and carbonate breccias
Sandstones
Lutites and marls
Siltites
Grainstones and packstones
Wackestones
Salt formations (anhydrite)
Basement (metamorphic rocks)
Stacking patterns:
Base level fall
Base level rise
Albian drift sequences
Transitional Sequence
K sup
Rift Sequence #2
Rift Sequence #1
RIFT TROUGH
BASEMENT HIGH

FIG. 3

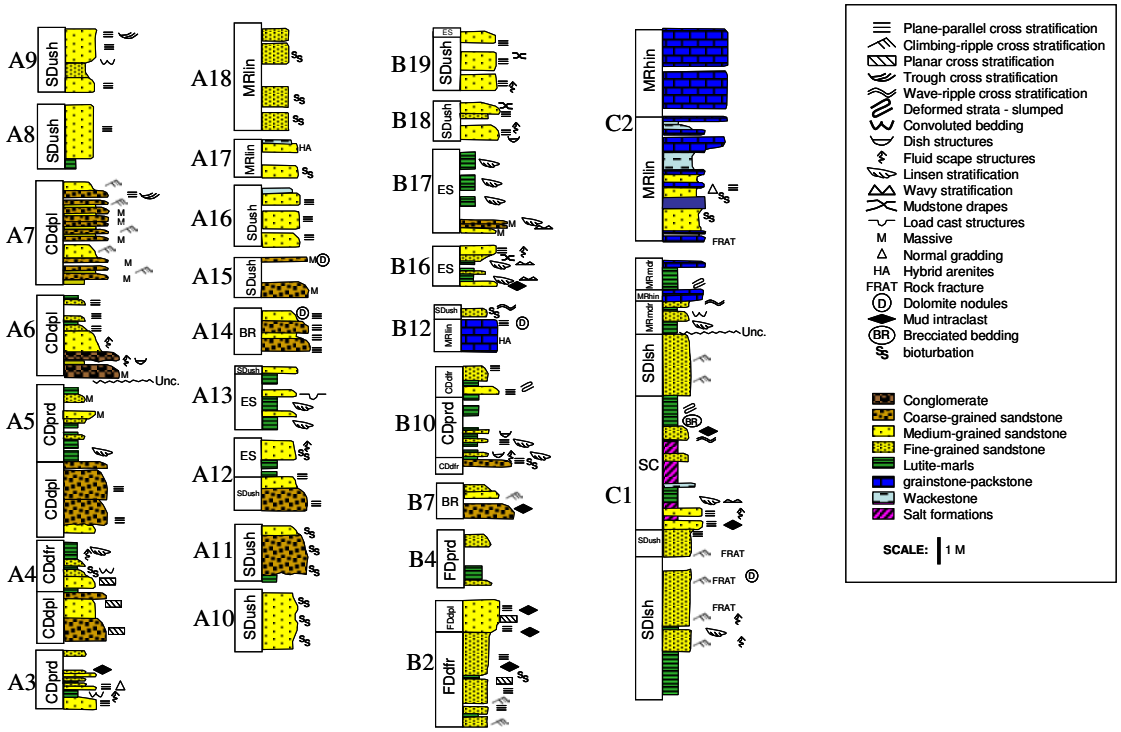
A9
A8
A7
A6
A5
A4
A3
A18
A17
A16
A15
A14
A13
A12
A11
A10
B19
B18
B17
B16
B12
B10
B7
B4
B2
C2
C1
SDush
CDdpl
CDprd
CDdfr
MRlin
MRhin
ES
BR
FDprd
FDdfr
SDlsh
SC
Unc.
FRAT
Plane-parallel cross stratification
Climbing-ripple cross stratification
Planar cross stratification
Trough cross stratification
Wave-ripple cross stratification
Deformed strata - slumped
Convoluted bedding
Dish structures
Fluid scape structures
Linsen stratification
Wavy stratification
Mudstone drapes
Load cast structures
M Massive
Normal gradding
HA Hybrid arenites
FRAT Rock fracture
Dolomite nodules
Mud intraclast
Brecciated bedding
bioturbation
Conglomerate
Coarse-grained sandstone
Medium-grained sandstone
Fine-grained sandstone
Lutite-marls
grainstone-packstone
Wackestone
Salt formations
SCALE: 1 M

FIG. 4

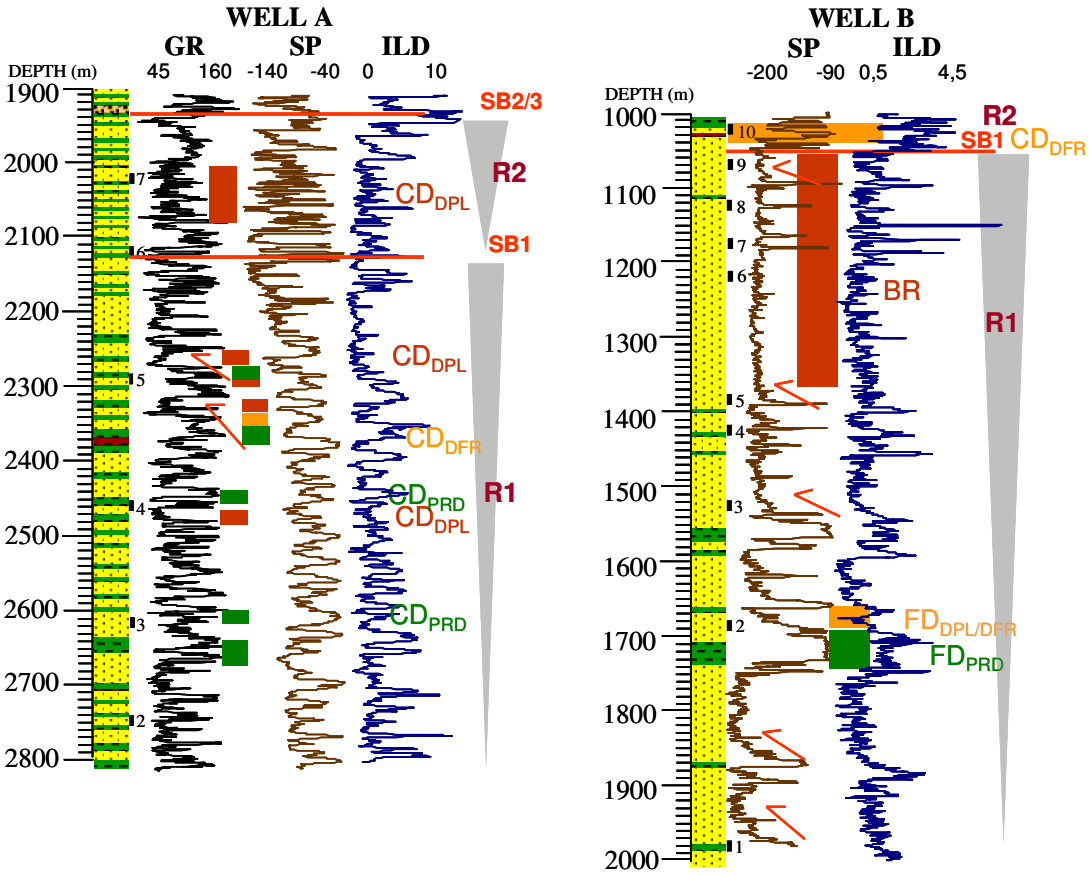
WELL A
GR
SP
ILD
DEPTH (m)
45 160 -140 -40 0 10
1900
2000
2100
2200
2300
2400
2500
2600
2700
2800
SB2/3
R2
CDDPL
SB1
CDDPL
CDDFR
R1
CDPRD
CDDPL
CDPRD
WELL B
SP
ILD
-200 -90 0,5 4,5
DEPTH (m)
1000
1100
1200
1300
1400
1500
1600
1700
1800
1900
2000
R2
SB1
CDDFR
BR
R1
FDDPL/DFR
FDPRD

FIG. 5

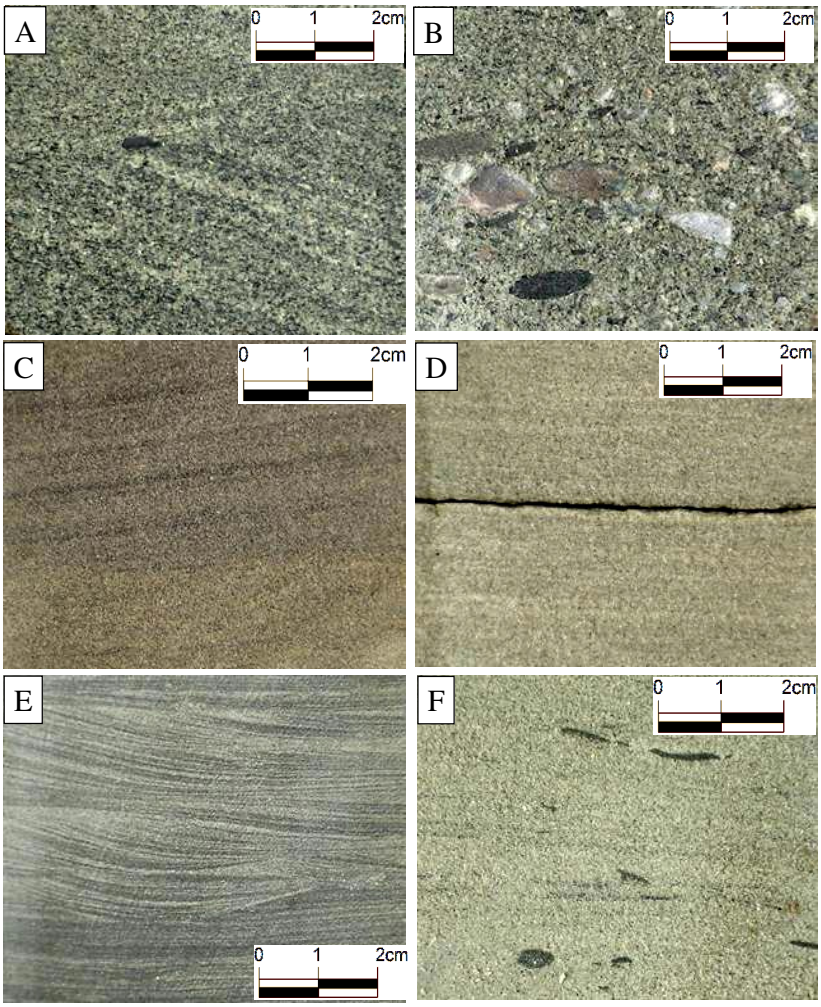
A
B
C
D
E
F
0 1 2cm

FIG. 6

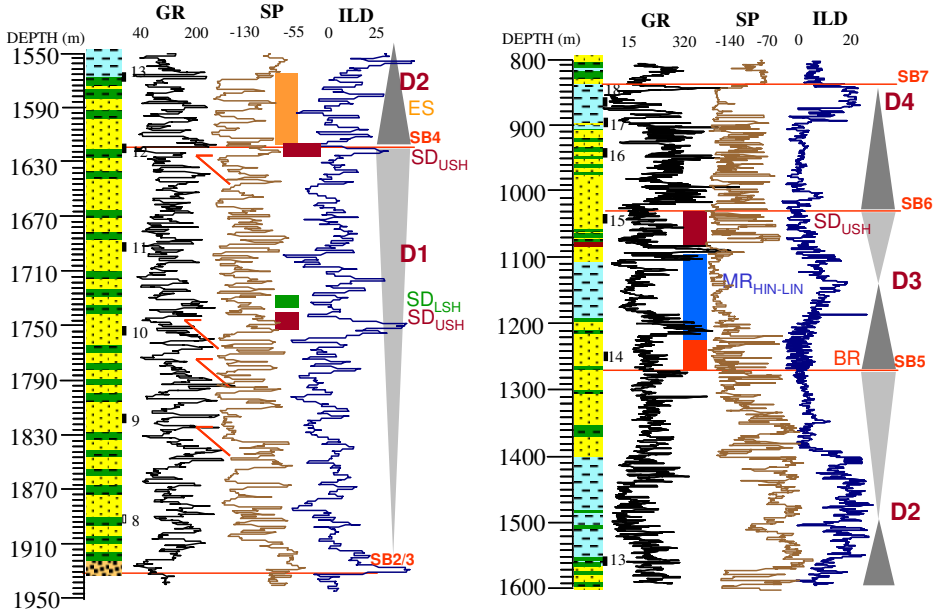
GR
SP
ILD
DEPTH (m)
1550
1590
1630
1670
1710
1750
1790
1830
1870
1910
1950
D2
ES
SB4
SD USH
D1
SD LSH
SD USH
SB2/3
DEPTH (m)
800
900
1000
1100
1200
1300
1400
1500
1600
SB7
D4
SB6
SD USH
MR HIN-LIN
D3
BR
SB5
D2

FIG. 7

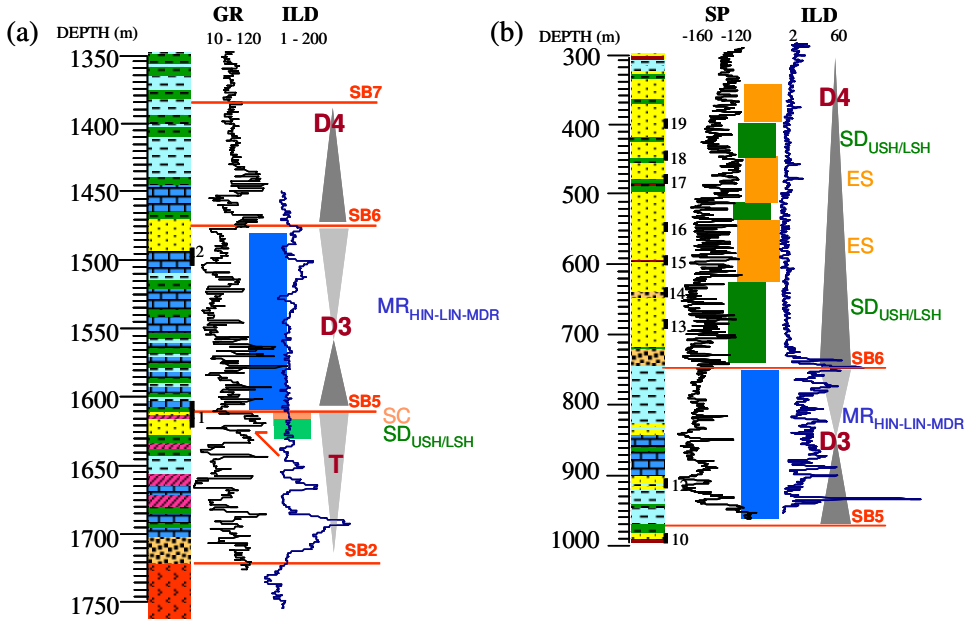
(a)
DEPTH (m)
GR
10 - 120
ILD
1 - 200
1350
1400
1450
1500
1550
1600
1650
1700
1750
SB7
D4
SB6
D3
MR HIN-LIN-MDR
SB5
SC
SD USH/LSH
T
SB2
(b)
DEPTH (m)
SP
-160 -120
ILD
2 60
300
400
500
600
700
800
900
1000
D4
SD USH/LSH
ES
ES
SD USH/LSH
SB6
MR HIN-LIN-MDR
D3
SB5

FIG. 8

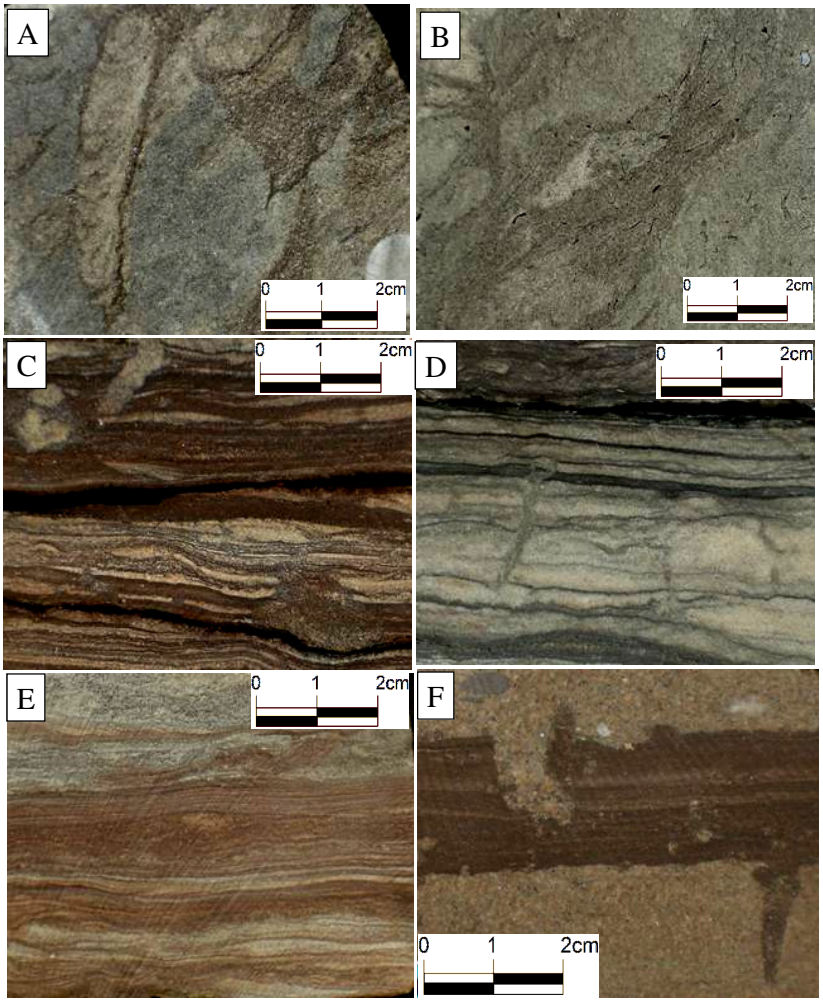
A
B
C
D
E
F
0 1 2cm

FIG. 9

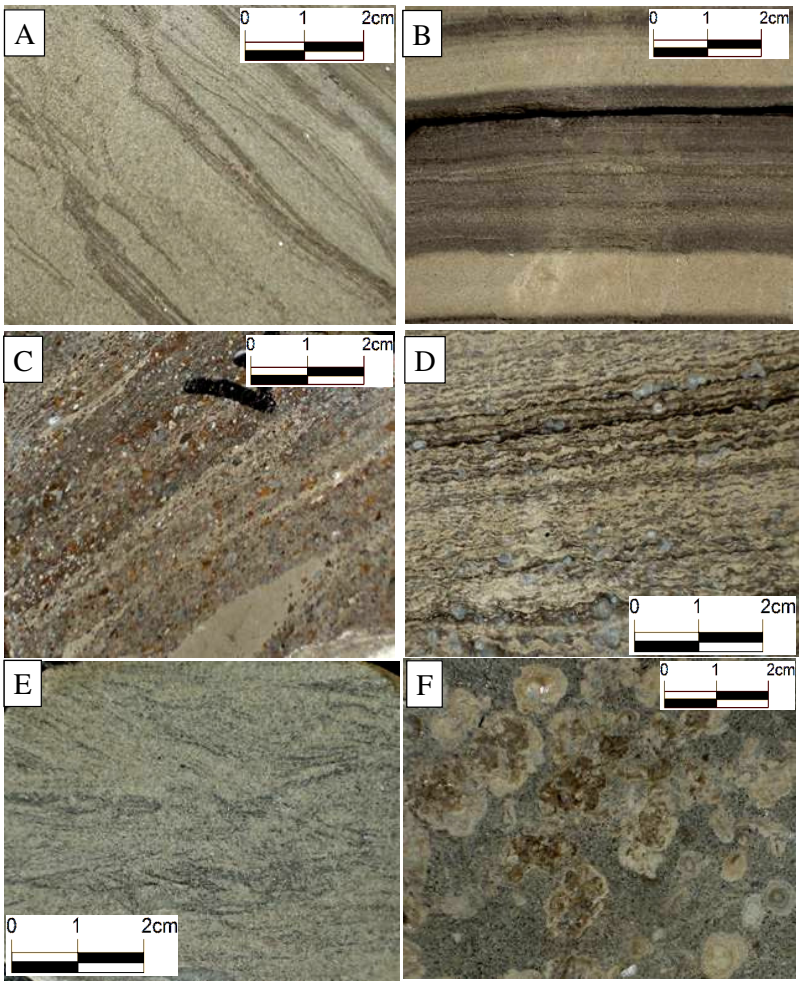
A
B
C
D
E
F
0 1 2cm

FIG. 10

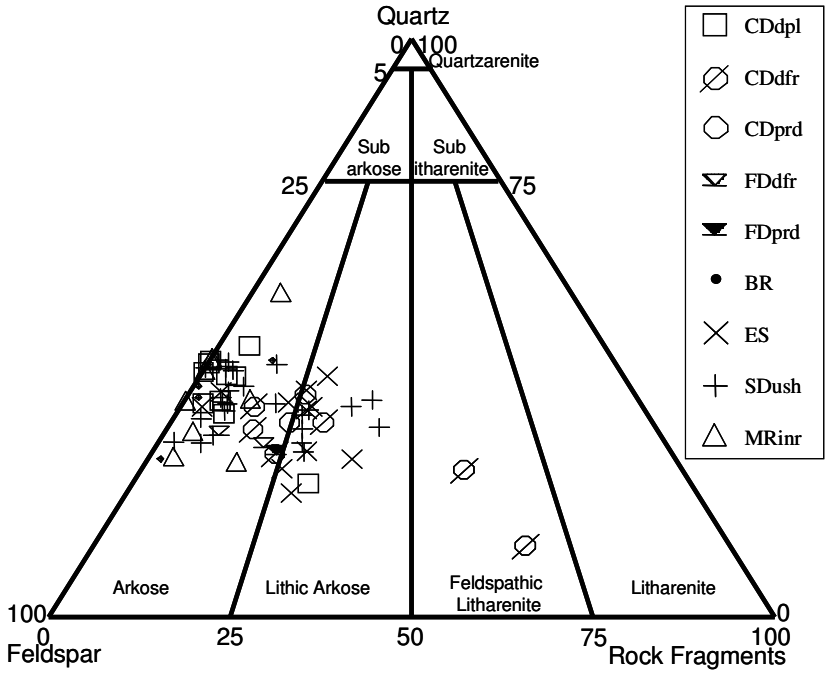
Quartz
0
100
5
Quartzarenite
Sub arkose
Sub litharenite
25
75
Arkose
Lithic Arkose
Feldspathic Litharenite
Litharenite
100
0
25
50
75
100
0
Feldspar
Rock Fragments
CDdpl
CDdfr
CDprd
FDdfr
FDprd
BR
ES
SDush
MRinr

FIG. 11

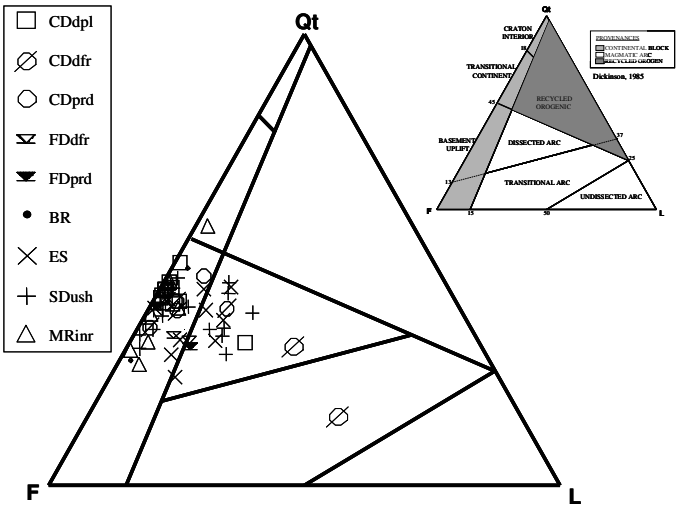
CDdpl
CDdfr
CDprd
FDdfr
FDprd
BR
ES
SDush
MRinr
Qt
F
L
CRATON INTERIOR
TRANSITIONAL CONTINENT
RECYCLED OROGENIC
BASEMENT UPLIFT
DISSECTED ARC
TRANSITIONAL ARC
UNDISSECTED ARC
Dickinson, 1985

FIG. 12

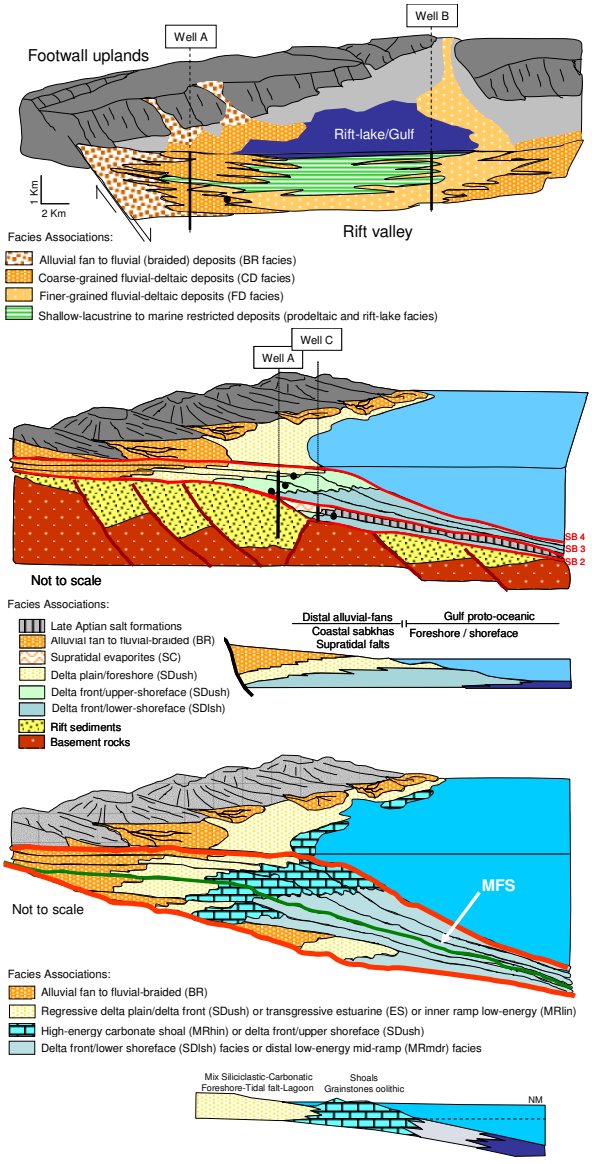
Well A
Well B
Footwall uplands
Rift-lake/Gulf
1 Km
2 Km
Rift valley
Facies Associations:
Alluvial fan to fluvial (braided) deposits (BR facies)
Coarse-grained fluvial-deltaic deposits (CD facies)
Finer-grained fluvial-deltaic deposits (FD facies)
Shallow-lacustrine to marine restricted deposits (prodeltaic and rift-lake facies)
Well C
Well A
SB 4
SB 3
SB 2
Not to scale
Facies Associations:
Late Aptian salt formations
Alluvial fan to fluvial-braided (BR)
Supratidal evaporites (SC)
Delta plain/foreshore (SDush)
Delta front/upper-shoreface (SDush)
Delta front/lower-shoreface (SDlsh)
Rift sediments
Basement rocks
Distal alluvial-fans
Coastal sabkhas
Supratidal falts
Gulf proto-oceanic
Foreshore / shoreface
MFS
Not to scale
Facies Associations:
Alluvial fan to fluvial-braided (BR)
Regressive delta plain/delta front (SDush) or transgressive estuarine (ES) or inner ramp low-energy (MRlin)
High-energy carbonate shoal (MRhin) or delta front/upper shoreface (SDush)
Delta front/lower shoreface (SDlsh) facies or distal low-energy mid-ramp (MRmdr) facies
Mix Siliciclastic-Carbonatic
Foreshore-Tidal falt-Lagoon
Shoals
Grainstones oolithic
NM

FIG. 13

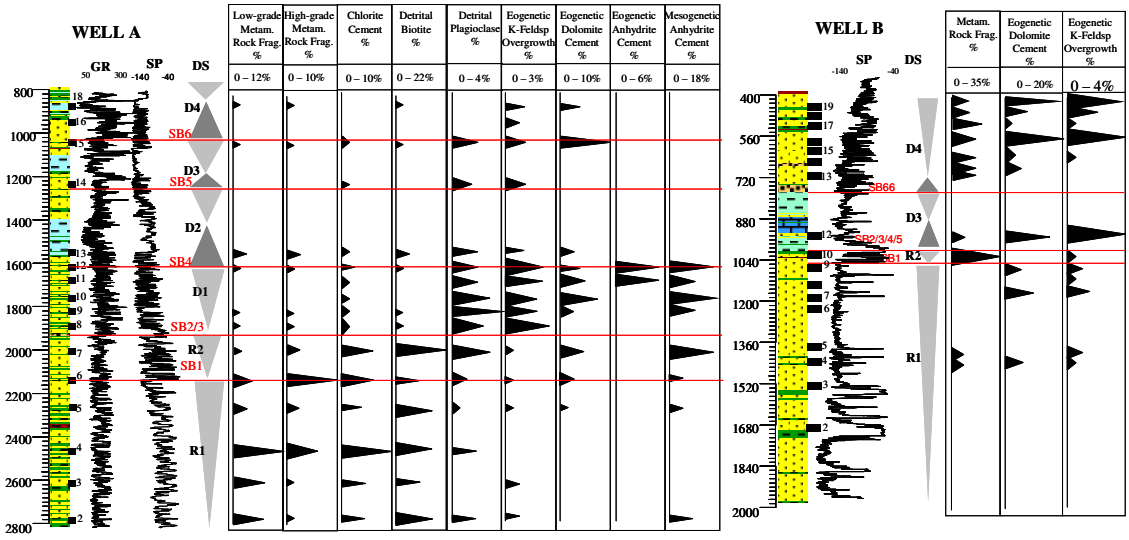
WELL A
GR
SP
DS
Low-grade Metam. Rock Frag. %
High-grade Metam. Rock Frag. %
Chlorite Cement %
Detrital Biotite %
Detrital Plagioclase %
Eogenetic K-Feldsp Overgrowth %
Eogenetic Dolomite Cement %
Eogenetic Anhydrite Cement %
Mesogenetic Anhydrite Cement %
0 – 12%
0 – 10%
0 – 10%
0 – 22%
0 – 4%
0 – 3%
0 – 10%
0 – 6%
0 – 18%
D4
D3
D2
D1
R2
R1
SB6
SB5
SB4
SB2/3
SB1
WELL B
SP
DS
Metam. Rock Frag. %
Eogenetic Dolomite Cement %
Eogenetic K-Feldsp Overgrowth %
0 – 35%
0 – 20%
0 – 4%
D4
D3
R2
R1
SB66
SB2/3/4/5
SB1

FIG. 14

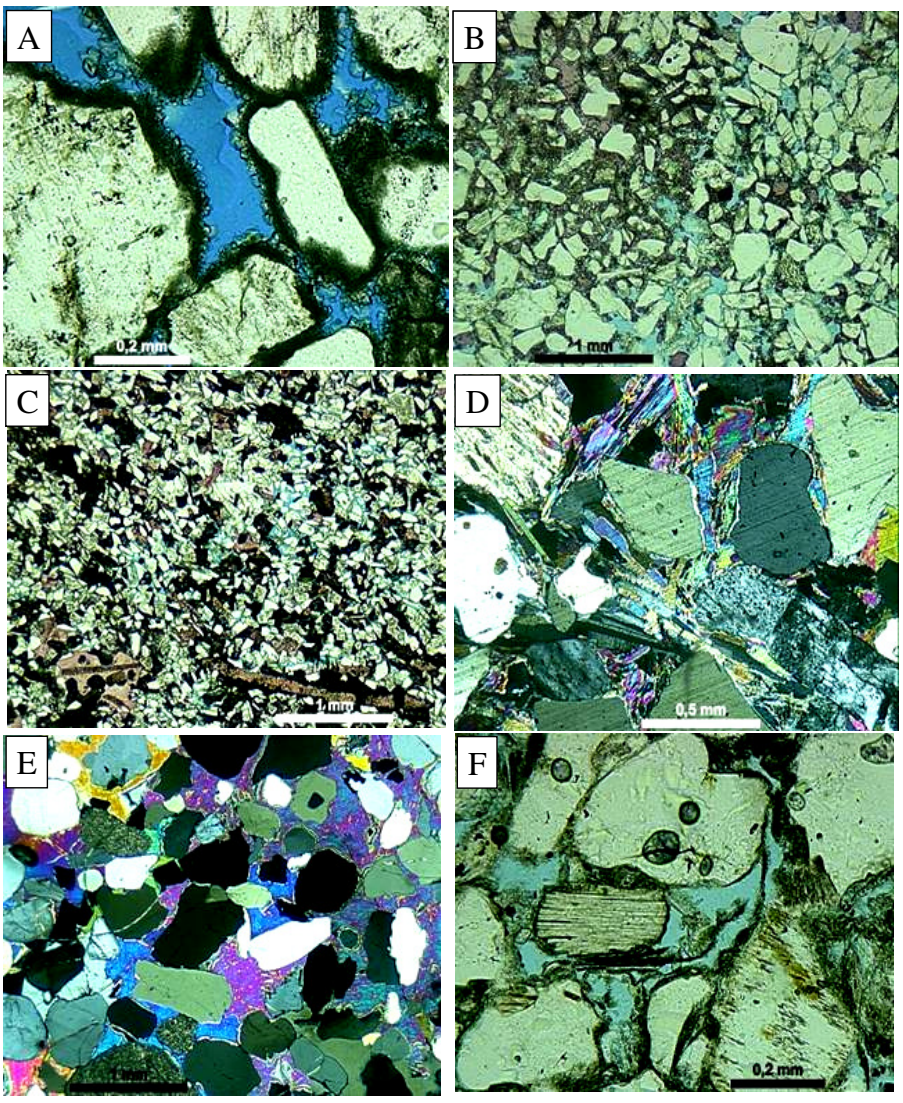
A
0,2 mm
B
1 mm
C
1 mm
D
0,5 mm
E
1 mm
F
0,2 mm

FIG. 15

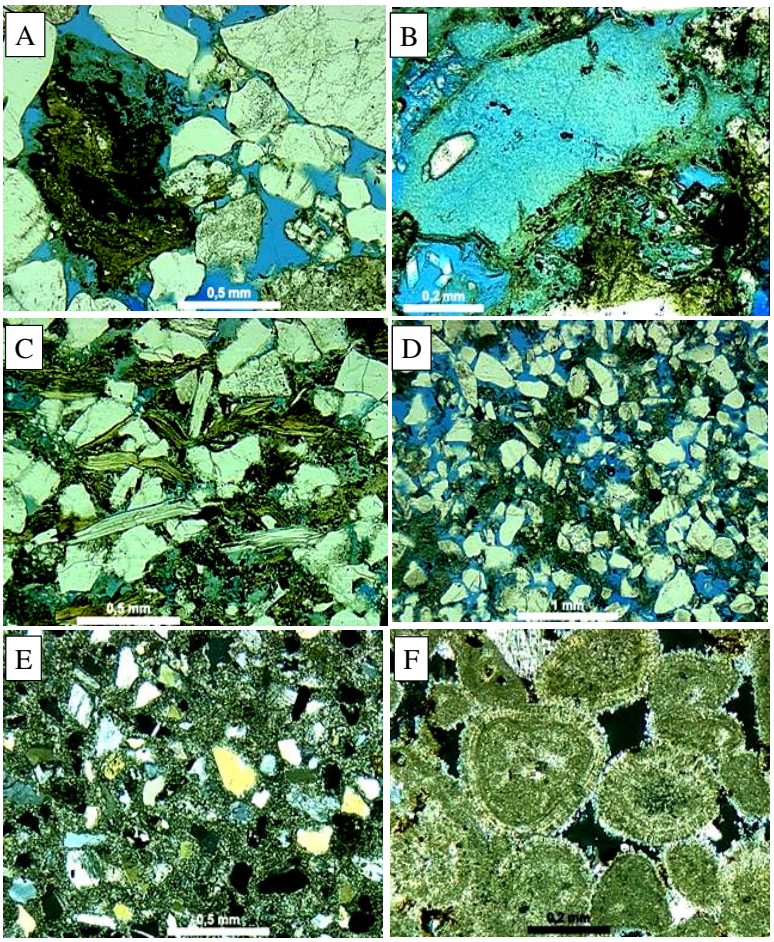
A
B
C
D
E
F
0,5 mm
0,2 mm
0,5 mm
0,2 mm
0,5 mm
0,2 mm

FIG. 16

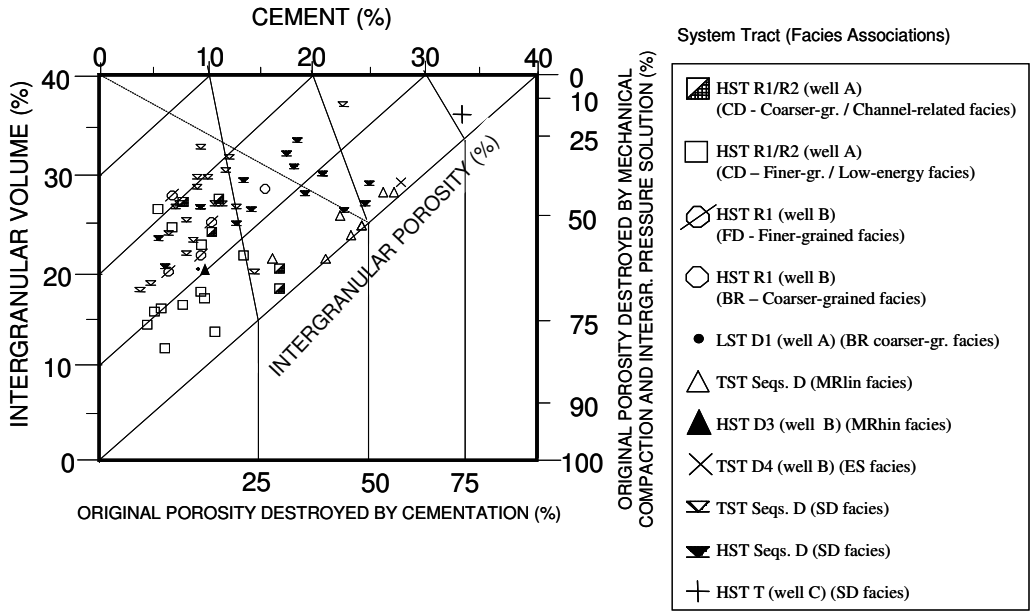
CEMENT (%)
0
10
20
30
40
INTERGRANULAR VOLUME (%)
40
30
20
10
0
INTERGRANULAR POROSITY (%)
25
50
75
ORIGINAL POROSITY DESTROYED BY CEMENTATION (%)
ORIGINAL POROSITY DESTROYED BY MECHANICAL COMPACTION AND INTERGR. PRESSURE SOLUTION (%)
0
10
25
50
75
90
100
System Tract (Facies Associations)
HST R1/R2 (well A)
(CD - Coarser-gr. / Channel-related facies)
HST R1/R2 (well A)
(CD – Finer-gr. / Low-energy facies)
HST R1 (well B)
(FD - Finer-grained facies)
HST R1 (well B)
(BR – Coarser-grained facies)
LST D1 (well A) (BR coarser-gr. facies)
TST Seqs. D (MRlin facies)
HST D3 (well B) (MRhin facies)
TST D4 (well B) (ES facies)
TST Seqs. D (SD facies)
HST Seqs. D (SD facies)
HST T (well C) (SD facies)

FIG. 17a

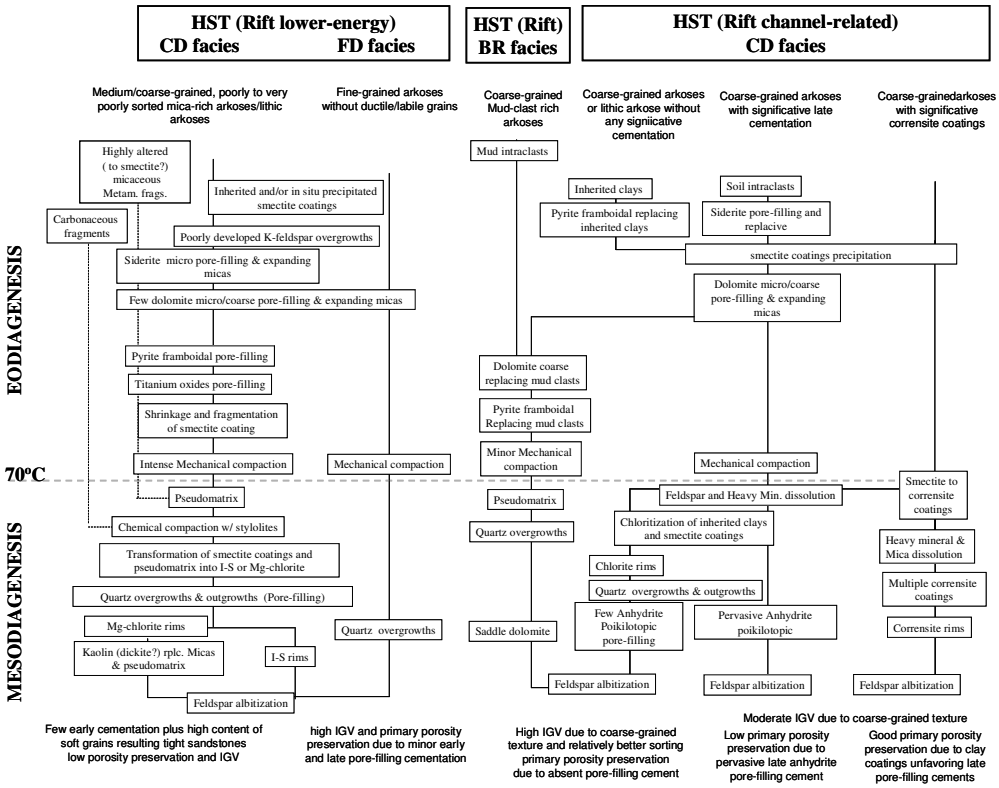

FIG. 17b

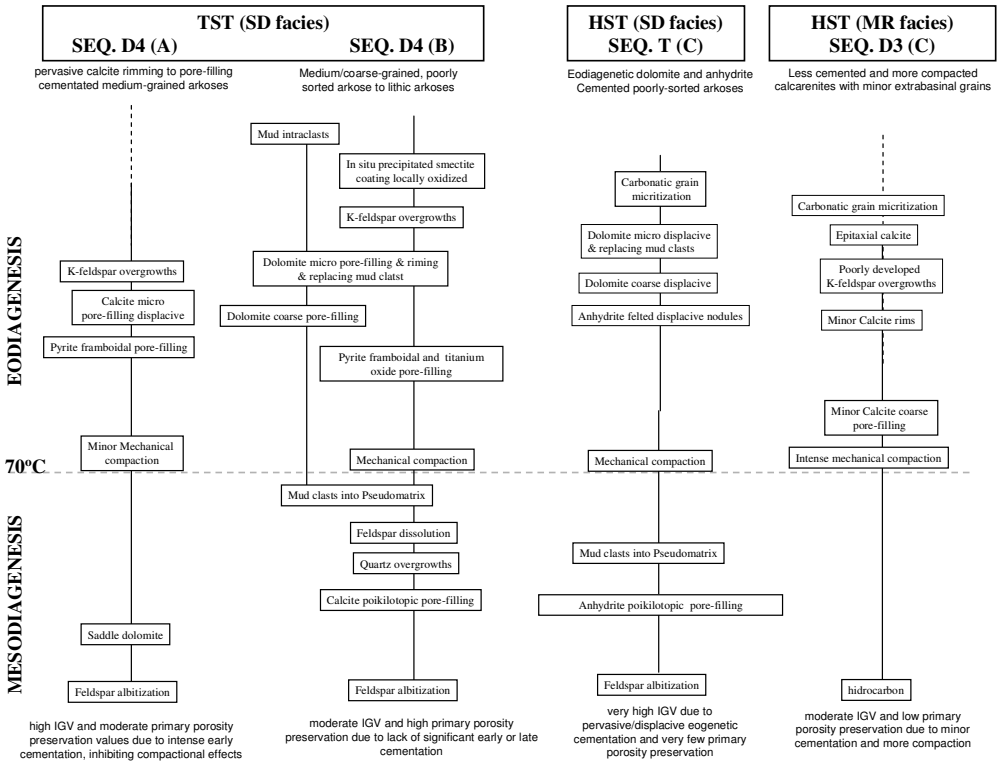

FIG. 17c

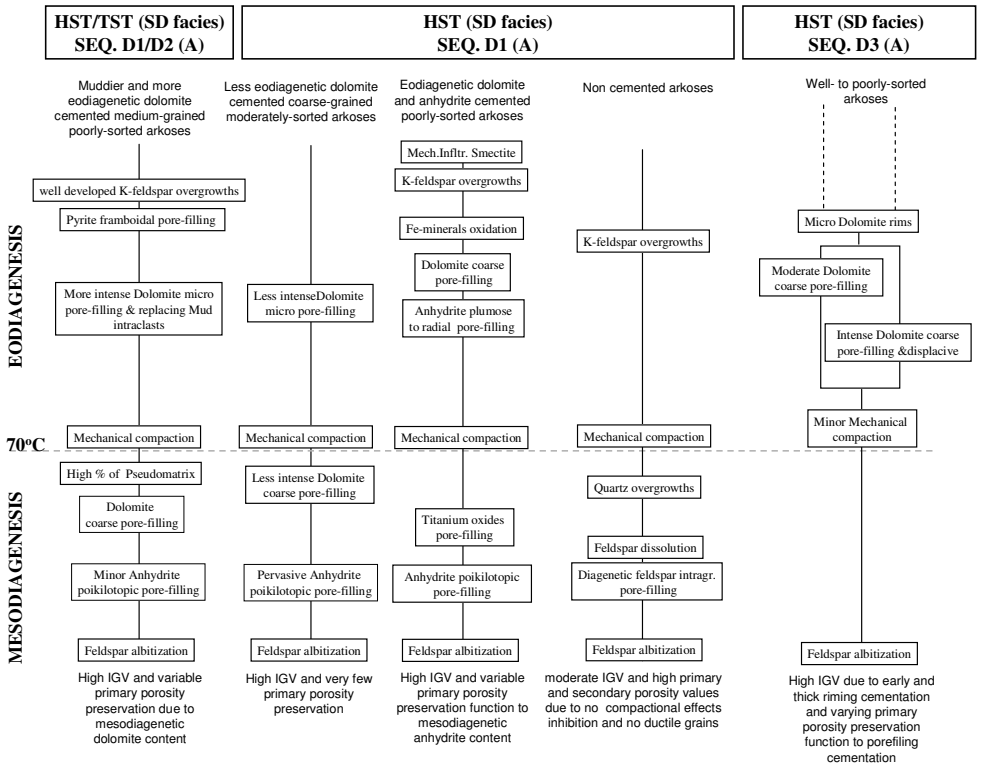

FIG. 17d

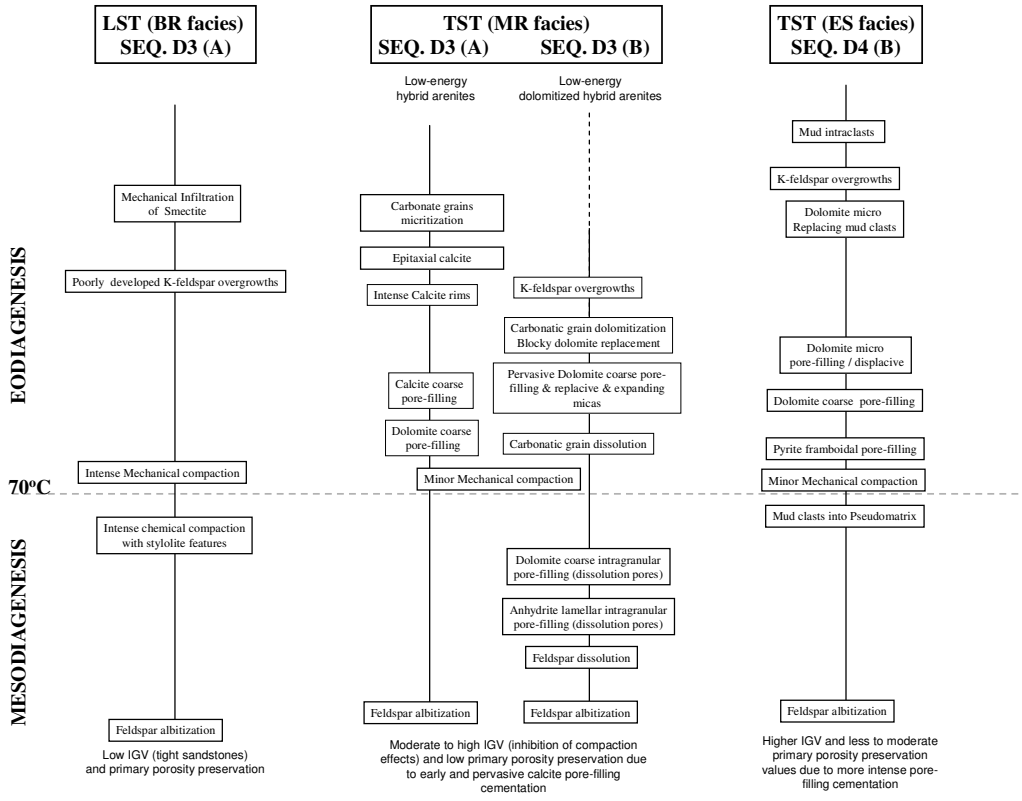

FIG. 18

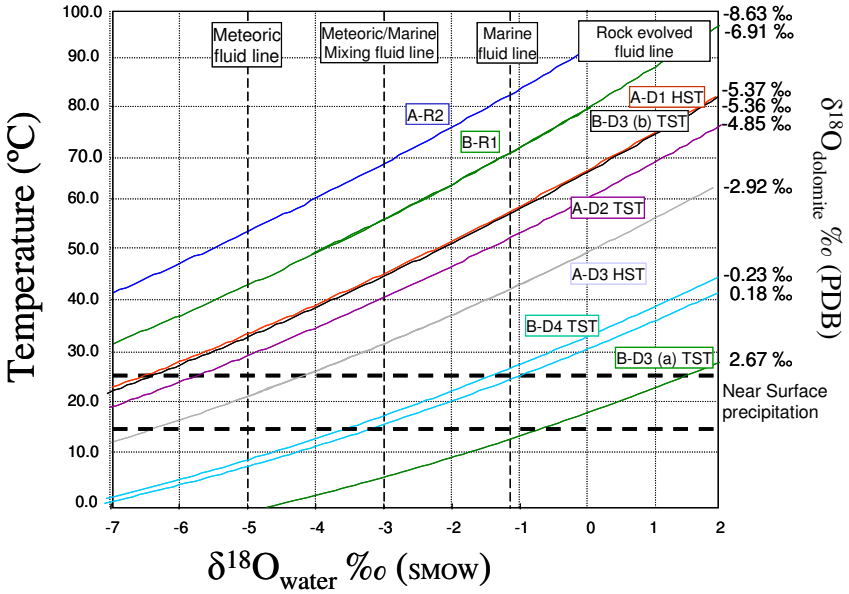
Temperature (°C)
100.0
90.0
80.0
70.0
60.0
50.0
40.0
30.0
20.0
10.0
0.0
-7
-6
-5
-4
-3
-2
-1
0
1
2
δ18Owater ‰ (SMOW)
Meteoric fluid line
Meteoric/Marine Mixing fluid line
Marine fluid line
Rock evolved fluid line
A-R2
B-R1
A-D1 HST
B-D3 (b) TST
A-D2 TST
A-D3 HST
B-D4 TST
B-D3 (a) TST
-8.63 ‰
-6.91 ‰
-5.37 ‰
-5.36 ‰
-4.85 ‰
-2.92 ‰
-0.23 ‰
0.18 ‰
2.67 ‰
Near Surface precipitation
δ18Odolomite ‰ (PDB)

FIG.19

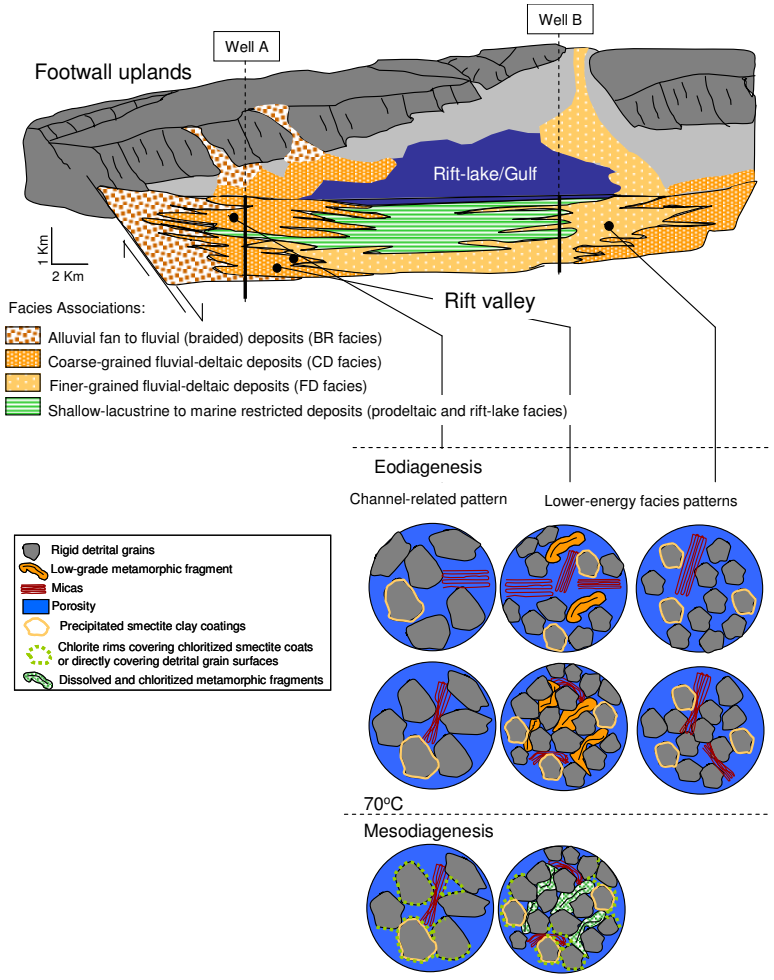
Well A
Well B
Footwall uplands
Rift-lake/Gulf
1 Km
2 Km
Rift valley
Facies Associations:
Alluvial fan to fluvial (braided) deposits (BR facies)
Coarse-grained fluvial-deltaic deposits (CD facies)
Finer-grained fluvial-deltaic deposits (FD facies)
Shallow-lacustrine to marine restricted deposits (prodeltaic and rift-lake facies)
Eodiagenesis
Channel-related pattern
Lower-energy facies patterns
Rigid detrital grains
Low-grade metamorphic fragment
Micas
Porosity
Precipitated smectite clay coatings
Chlorite rims covering chloritized smectite coats or directly covering detrital grain surfaces
Dissolved and chloritized metamorphic fragments
70°C
Mesodiagenesis

FIG.20

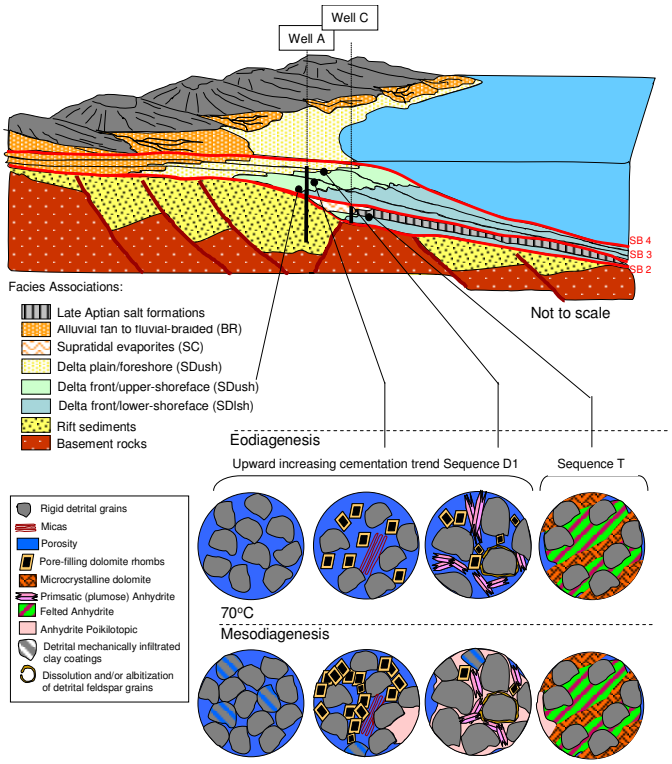
Well C
Well A
SB 4
SB 3
SB 2
Not to scale
Facies Associations:
Late Aptian salt formations
Alluvial fan to fluvial-braided (BR)
Supratidal evaporites (SC)
Delta plain/foreshore (SDush)
Delta front/upper-shoreface (SDush)
Delta front/lower-shoreface (SDlsh)
Rift sediments
Basement rocks
Eodiagenesis
Upward increasing cementation trend Sequence D1
Sequence T
Rigid detrital grains
Micas
Porosity
Pore-filling dolomite rhombs
Microcrystalline dolomite
Prismatic (plumose) Anhydrite
Felted Anhydrite
Anhydrite Poikilotopic
Detrital mechanically infiltrated clay coatings
Dissolution and/or albitization of detrital feldspar grains
70°C
Mesodiagenesis

FIG.21

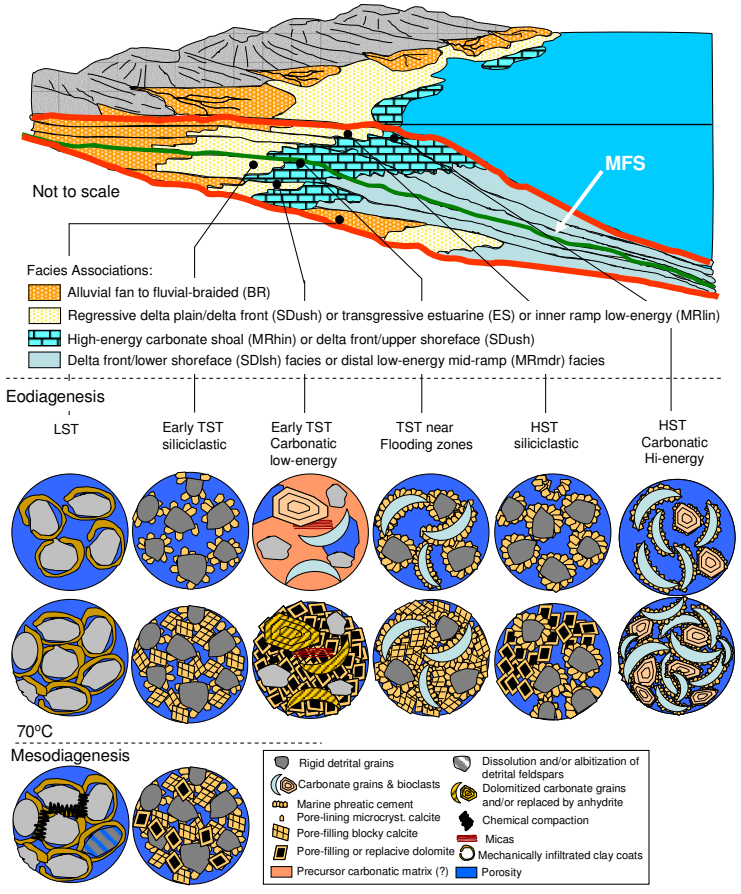
MFS
Not to scale
Facies Associations:
Alluvial fan to fluvial-braided (BR)
Regressive delta plain/delta front (SDush) or transgressive estuarine (ES) or inner ramp low-energy (MRlin)
High-energy carbonate shoal (MRhin) or delta front/upper shoreface (SDush)
Delta front/lower shoreface (SDlsh) facies or distal low-energy mid-ramp (MRmdr) facies
Eodiagenesis
LST
Early TST siliciclastic
Early TST Carbonatic low-energy
TST near Flooding zones
HST siliciclastic
HST Carbonatic Hi-energy
70°C
Mesodiagenesis
Rigid detrital grains
Carbonate grains & bioclasts
Marine phreatic cement
Pore-lining microcryst. calcite
Pore-filling blocky calcite
Pore-filling or replacive dolomite
Precursor carbonatic matrix (?)
Dissolution and/or albitization of detrital feldspars
Dolomitized carbonate grains and/or replaced by anhydrite
Chemical compaction
Micas
Mechanically infiltrated clay coats
Porosity

Table 1 - Lithofacies (LF) types. Facies codes are modified from Miall (1996).

Lithofacies	Description	Interpretation
Gmt	Thickness: 0.2 - 0.6 m. Very poorly sorted, light gray massive conglomeratic sandstones, mostly well-rounded pebbles of sandstones and calcareous rock fragment, displaying fining-upward intervals, with erosional scours.	sudden discharge of sediments to subaqueous dune migration (filling of minor alluvial channels), under high-energy flow conditions
Sl	Thickness: 0.1 - 3 m. Fine- to coarse-grained, locally conglomeratic, poorly sorted, light to dark gray or reddish to pale brown parallel laminated sandstone. Locally micaceous, with mud intraclasts and/or plant fragments, fluidized (dish structures) or wit displacive dolomite cementation (nodules).	deposition in the upper planar bed conditions, under high flow energy conditions
Sr	Thickness: 0.1 - 0.3 m. Fine- to medium-grained, poorly-sorted, light to dark gray or reddish or beige, climbing ripple laminated sandstones (currents), micaceous. Locally showing deformed structures (slumped) and/or moderate bioturbation	migrating wave and current ripples, subaqueous lower planar bottom conditions, at ceasing flow (indicative of waning flow conditions and rapid sediment fallout)
Sm	Thickness: 0.1 - 0.5 m. Fine- to coarse-grained, locally normal graded, poorly-sorted, light gray or whithe-greenish to reddish massive sandstones, micaceous. Locally with load-cast (deformation) structures, dolomite nodules or mud intraclasts	sudden discharge of sediments under high-energy flow conditions (hyperconcentrated flows), or product of intense fluidization and/or bioturbation
Sp	Thickness: 0.2 - 2.0 m. Fine- to coarse-grained, poorly sorted, locally conglomeratic, light to dark gray, planar cross-laminated sandstones. Locally with mud intraclast and plant fragment, or fluidized (dish structures). Finer-grained intervals with moderate bioturbation	migration of subaqueous sediments under low to high flow energy, locally with low (w/ bioturbation) or high sediment input (w/ fluidization)
St	Thickness: 0.1 - 0.7 m. Fine- to coarse-grained, poorly sorted, light gray trough cross laminated sandstones, friable	migration of subaqueous dunes or bars sediments, under low to high flow energy
Sw	Thickness: 0.2 m. Fine-grained, poorly- to well-sorted, light gray wave-rippled cross-laminated sandstones (possible small-scale hummocky cross lamination). Locally micaceous and bioturbated, w/ dolomite nodules (pre-dating oil emplacement) or microfractured (post-dating oil emplacement) filled with anhydrite cement	alteranting flow energy conditions under wave influence, possibly indicating higher-energy conditions (storm waves)
Sb	Thickness: 0.4 - 2.5 m. Fine- to coarse-grained, locally conglomeratic, poorly- to moderately-sorted, white to light gray, highly bioturbated sandstones (no structure preservation). Locally w/ fluidization (dish features)	deposition under low-energy flow conditions and low sedimentation rate to allow intense bioturbation
Sbh	Thickness: 0.1 - 0.8 m. Fine- to medium-grained (locally coarse-grained), poorly to very-poorly sorted, grayish or light yellow to beige bioturbated ooid-, oncoid-, bioclastic-grainstone (hybrid arenite *sensu* Zuffa, 1980). Locally with milimeter-size clay laminae (mud drapes?), vugs filled with calcite cement, or centimeter-size oncoids w/ dissolved nucleii filled by anhydrite cement	deposition under variable energy flow conditions, with some samples showing possible tidal influence
Sc	Thickness: 0.1 - 1.0 m. Fine- to medium-grained, poorly sorted, light to dark gray fluidized sandstone, with dish structures (fluids scape), with intense deformation (convolute bedding) and complete destruction of depositional structures	rapid sediment fallout resulting instability due to liquefaction, leading to disruption of laminae by water escape.
Fl	Thickness: 0.1 - 2 m. Dark gray to black, or reddish to pale brown, laminated mudstone, with varying rates of silt, sand and mud from light gray, very silty or sandier mudstones. Locally micaceous, w/ linsen structures, deformed (convolute structures) and/or with plant fragments	deposition under lower planar bed conditions, with suspended sediments (suspension fallout / waning flood flows), alteranting with sediment migration under low-energy flow conditions
Flc	Thickness: 0.4 - 1.1 m. Light to dark gray carbonate-rich laminated mudstones, with heterolithic texture, alternating layers of light gray carbonatic mud, dark gray micaceous mudstones and very fine-grained sandstones. Locally with slump features (deformation), or brecciated.	low-energy environment with coeval carbonate deposition (carbonate platform)

Table 1 - Cont.

Lithofacies	Description	Interpretation
Ec	Thickness: 0.1 - 1.0 m. Coalesced nodular, chicken-wire bedded anhydrite, alternating with thin layer of yellowish gray to beige carbonate mud (algal-laminated dolomudstone? stromatoliths?).	deposition under fluctuation of the hydrologic setting and salinity, under very arid climatic conditions
H	Thickness: 0.1 - 1 m. Fine-grained, moderately-sorted, micaceous, white to light gray sand-rich heterolith (with mud percentage < 25%) parallel laminated sandstones, alternating with or grading upward into redish to pale brown mud-rich heterolith (with sand percentage < 25%), with linsens or lenses of very fine- to fine-grained light gray sandstones, with varying rates of mud and sand. Sandy intervals showing continuous or discontinuous thin crinkled (i.e. zigzag) laminae composed of mud layers	deposition under low-energy and waning flow conditions, with settling of suspended sediments, with possible tidal influence
He	Thickness: 0.2 - 1 m. Light to dark gray carbonate-rich heteroliths, with alternating layers of light gray carbonatic mud (stromatoliths?) and dark gray micaceous mudstones, with slump (deformation) and brecciated textures (mud crack?). Locally gradding to black rich-organic matter laminated mudstones	deposition under low-energy and waning flow conditions, with settling of suspended sediments, and possible subaerial exposure and semi-arid climatic conditions
Hc	Thickness: 0.4 - 1.1 m. Light to dark gray carbonate-rich laminated mudstones, alternating with dark gray micaceous mudstones and very fine-grained sandstones. Locally with slump features (deformation), with varying content and thickness of sand to carbonate-mud (heteroliths)	deposition under low-energy conditions (settling of suspended sediment), with coeval carbonate (platform) deposition
Csg	Thickness: 0 - 0 m. Light gray or beige millimeter- to centimeter-size bioclasts, ooid- and/or oncoid- grainstones and rudistones, with micaceous terrigenous grains, lithic clasts up to 5 cm wide, showing intense dolomitization. Fractures, vugs, and oncoids (nuclei) filled with anhydrited.	shallow low- to high-energy (wave-reworked?) inner-ramp platform carbonate deposition
Cm	Thickness: 0.1 - 0.3 m. Light gray carbonate mudstone, locally with high terrigenous input, micaceous	low-energy inner- to mid-ramp carbonatic depositional products

Table 1 (cont.)

Table 2. Facies Associations (FA) of studied Jequitinhonha Basin successions.

Facies	Description	Interpretation
CDdpl	Combining the lithofacies: Gmt, Sl, Sp, Sr, Sm, Fl; this facies association consists of fining-upward succession of massive to parallel or planar cross laminated coarse-grained sandstones (locally with conglomeratic base), with possible trough cross-lamination, from fine-grained, climbing rippled cross laminated sandstones, capped by or intercalated with thin (up to 30 cm) massive light gray siltstones to sandy mudstones	Deposits associated with channel-fill migration dunes of shallow fluvial braided streams, with local overbanks deposits, possibly distributary-channel facies of a delta-plain setting, reflecting transition from channelized high- to low-energy flow.
CDdfr	Combining the lithofacies: Sp, Sc; this facies association consists of coarsening-upward succession of medium- to coarse-grained massive to planar cross-laminated sandstones, up to 20 m thick (based upon GR log curves), locally showing convolute structures, associated with slumped or deformed beds. This facies were poorly core sampled.	Deposits associated with subaqueous migrating proximal to distal mouth bars of a delta-front depositional setting.
CDprd	Combining the lithofacies: Sm, Sl, Sb, Fl; this facies association consists of alternation of thick, massive to parallel laminated, black to dark gray mudstones, with thin, massive to parallel laminated, normal graded, fine-grained sandstones.	Mud suspension of distal distributary mouth bar or prodelta deposits to rift-lacustrine setting (high GR well log response), with thin sandy intervals reflecting scattered turbidity flows.
FDdpl	Combining the lithofacies: St, Sl, Sp; this facies association consists of medium- to coarse-grained, poorly sorted, very friable, light gray parallel to planar (locally trough) cross laminated sandstones sets with up to 80 cm thick, locally with high content of mud intraclasts.	Upper most part of a coarsening-upward delta-front to delta-plain fluvial-deltaic succession, comprising subaerial deposition in lowland areas, under high-energy (upper planar bed condition), with mud intraclasts interpreted as product of underlying floodplain sediments erosion due to channel switching. The reduced thickness of interbedded fine-grained facies indicates low-sinuosity streams.
FDdfr	Combining the lithofacies: Sl, Sp, Sr, Sc; this facies association consists of fine- to medium-grained, poorly sorted, light to dark gray climbing ripple laminated sandstones, which pass upwards into parallel and planar cross-laminated sandstones, comprising a coarsening-upward sequence up to 6 m thick, locally with carbonaceous (coal) fragments and mud intraclasts (up to 5 cm wide) and/or showing bioturbation, fluidization (dish structures) and/or deformation (slumped features).	Deposits associated with subaqueous migrating proximal to distal mouth-bars of a delta-front depositional setting, reflecting an interplay of fluvial and lacustrine or restricted gulf environments, with gradual decreasing of grain size toward distal settings.
FDprd	Combining the lithofacies: Fl, Sl; this facies association consists of laminated mudstones alternating or grading upward into light gray, poorly sorted, parallel laminated sandstone, comprising up to 1.5 m thick, locally micaceous and showing bioturbation and/or fluidization (dish structures).	It comprises a relatively stable prodelta setting where mud and fine silt are deposited by fallout from suspension to form quiet well-laminated mudstones and siltstones, unaffected by wave or tidal processes (below lake or restricted gulf environment storm wave base). Locally with slight differences in grain size, probably reflecting fluctuations in river discharges.
BR	Combining the lithofacies: Sl, St, Sr, Fl; this facies association consists of coarse- to medium-grained (thinning-upward succession), poorly sorted, reddish (coarse-grained) to white-greenish (medium-grained) parallel laminated sandstone, into medium-grained, light gray to beije climbing rippled cross laminated sandstones, locally displaying displacive dolomite cementation, preferentially at medium-grained intervals, and topped by reddish to pale brown silty laminated mudstone. Coarser-grained intervals show low preservation (less visible structures). Some samples show high content of mud clast and soil fragments with siderite show erosion of fine grained floodplain or crevasse splay mud during fluvial channel migration, typically deposited as a lag in channel bases.	Subaerial deposition in high-energy (upper planar bed condition) braided river systems, with trough cross-laminated sets interpreted as river-channel shallow braided stream or sheet flood deposits, reflecting areas of more persistent channel flow in the braid plain. Local content of mud clast and soil fragments with siderite interpreted as erosion of fine grained floodplain and crevasse splay mud during fluvial channel migration, as channel base lag-deposits.
SDush	Combining the lithofacies: Sl, Sb, Sc, Sm, Sw; this facies association consists of coarsening-upward succession of medium- to coarse-grained, poorly- to moderately-sorted (locally well-sorted), light to dark gray or reddish to pale brown, parallel laminated or wavy ripple cross laminated sandstones, locally with nodules of dolomite cementation. Intervals with moderate bioturbation and conspicuous deformation (slumped) and convolute bedding.	deltaplain to deltafront settings (upper shoreface) of a coarse-grained coastal deltaic environment (upper shoreface to foreshore facies), under high energy flow conditions, with poorly-sorted intervals interpreted as wave-storm dominated deposits, and better-sorted sands interpreted as wave or longshore currents reworked deposits.

Table 2 - Cont.

Facies	Description	Interpretation
SDlsh	Combining the lithofacies: Sb, Sw, Sr, Hc; this facies association consists of coarsening-upward fine- to medium-grained, poorly to moderately sorted, white-greenish to light gray bioturbated sandstones, locally showing climbing-rippled (or wave-rippled) cross lamination. Fluidization (dish structures) is also observed. Finer facies with light to dark gray carbonate-rich laminated mudstones locally show heterolithic texture, alternating layers of light gray to beije carbonatic mud.	deltafront (lower shoreface) settings of a coarse-grained coastal deltaic environment (lower shoreface facies) deposits, with variable wave-influence, under low energy flow conditions.
ES	Combining the lithofacies: H, Sm, Fl; this facies association consists of fine to coarse-grained, poorly sorted, locally very fine-grained and moderately-sorted, light gray massive sandstones or light brown to reddish massive sandstones, intercalated with layers of fine- to very fine-grained light gray sandstones and reddish to pale brown silty mudstones (rhythmic alternation - heterolithic layers), with varying rates of mud and sand, locally with a sharp change in clay content across sand/mud boundaries, showing load-cast, wavy and linsen features, and crinckled laminae. Heterolithic interval consisting of interlaminated very fine sadnstones, siltstones, and claystones, with an upward decrease in grain size and increase in clay content. Presence of elements of Ichnofauna Skolithos (AT8) and Cruziana (BT17).	Brackish shallow-water tidal influenced inner estuarine settings, reflecting marine-marginal processes of delta plain/delta front (foreshore/upper shoreface) settings. Repetitive sets of mud/sand couplets on a scale of centimeters (and crinkled laminae conformable to ripple bed forms) reflecting intermittent flow-energy (tractive flow alternating with fallout from suspension), indicating wave to tidal intertidal to subtidal mud flat environment setting. Sharp-based coarse-grained sandstone layers overlaping mudstone layers, with possible root marks, interpreted as small tidal-channel deposits, possibly associated with abandoned delta plain (tidal flats or marsh deposits)
SC	Combining the lithofacies: Sl, He, H, Ec; this facies association consists of light to dark gray carbonate-rich mudstone heterolithic facies with millimeter layers of beige, deformed carbonatic mud, w/ in situ breccia (mud crack?) and locally grading to black organic-rich laminated mudstones, intercalated with fine- to medium-grained, moderately-sorted, light gray, sand-rich heterolith (muddy sandstones) or with fine- to coarse-grained, poorly-sorted light gray parallel laminated sandstones with centimeter layers or lenses of beige carbonatic mud. These heterolithic facies occurring vertically associated with coalesced nodular, chicken-wire anhydrite beds, and millimeter-size beige carbonatic mud (possible algal-laminated dolomustones. Stromatoliths?)	The intercalation of carbonatic mud layers (dolomudstones) and heterolithic beds in vertical facies transition to evaporite layers (nodular anhydrite and algal-laminated dolomudstones) suggests deposition on a supratidal flat environment, related to distal progradation of coastal deltaic facies, under reducing accommodation space (highstand conditions) and increasing water circulation restriction, with developing of mudcracks, stromatolites, intraclastic breccias (tepees?), and possible algal laminations, interpreted as supratidal coastal sabkha-salina environment, with sporadic flooding resulting in coarser sediments.
MRhin	Combining the lithofacies: Csg, Sbh; this facies association consists of medium- to coarse-grained, poorly to well-sorted, grayish or light yellow to beige hybrid arenites to skeletal and ooid dolograinstones, with intense carbonate cementation	Deposition under high-energy inner ramp, wave-dominated, shallow marine environment, possibly skeletal/ooid sand shoals, above fair-weather wave base, under continuous wave and current activity
MRlin	Combining the lithofacies: Sbh; this facies association consists of medium-grained, poorly to very-poorly sorted, grayish to beige hybrid arenites to nonlaminated dolomudstones / dolopackstones with centimeter-size oncoids and bioclasts, with pervasive dolomitization with intense diagenetic alteration.	The restricted fauna (dasycladacean algae, mollusks, echinoderms and fusulinids) and interpreted dolomitized carbonate mud, as well as high terrigenous and plant fragments input, suggest deposition under low-energy, shallow-water restricted lagoonal to intertidal or subtidal internal platform setting.
MRmdr	Combining the lithofacies: Flc, Cm; this facies association consists of light gray carbonate mudstone, intercalated with mudstones or light to dark gray carbonate-rich laminated mudstones. Locally showing heterolithic texture (alternation with very fine-grained sandstones) or slumping features (deformation)	Sedimentary structures suggest a carbonatic deposition on stable shelf area, distal carbonate ramp depositional settings, between fair-weather and storm wave base, with local terrigenous influx.

Table 3

Table 3 - Statistical summary of the petrographic parameters of the studied sandstones

Depositional Facies	CD fine-gr.	CD coarse-gr.	BR/FD fine-gr.	BR	SDlsh/ush	SDush	Sdush	BR	MRlin	MRhin	ES
System Tract / Depositional Sequence (Well)	HST/R1-R2	HST/R1-R2	HST / R1	HST / R1	HST / T (C)	HST / D	TST / D	LST / D	TST / D	HST / D	TST / D
Number of samples	n = 12	n = 5	n = 4	n = 1	n = 1	n = 14	n = 19	n = 1	n = 8	n = 1	n = 1
Total	Average	Average	Average	Average	Average	Average	Average	Average	Average	Average	Average
Intergranular Volume	**20.07**	**25.00**	**24.75**	**28.33**	**35.01**	**27.24**	**27.68**	**20.33**	**24.40**	**19.68**	**29.00**
Grain Volume	**79.93**	**75.00**	**75.25**	**71.67**	**64.99**	**72.76**	**72.32**	**79.67**	**75.60**	**80.32**	**71.00**
Cement Volume	**8.50**	**10.23**	**8.58**	**15.67**	**33.67**	**15.41**	**15.47**	**9.67**	**22.81**	**9.68**	**28.33**
Total Extrabasinal Grains	**70.60**	**68.37**	**69.59**	**58.33**	**51.99**	**56.31**	**62.78**	**68.67**	**50.00**	**16.01**	**67.34**
Detrital Quartz	18.77	22.08	21.09	24.00	15.33	20.92	23.56	25.67	17.53	6.00	24.33
Detrital Feldspar	17.30	20.30	26.92	24.34	22.67	23.19	25.22	28.33	22.26	7.34	26.34
Detrital Plagioclase	0.38	0.61	1.09	2.00	0.00	1.01	0.54	0.67	0.20	0.00	0.00
Total Micas	**11.64**	**4.78**	**5.83**	**2.00**	**1.00**	**2.84**	**3.20**	**2.34**	**5.42**	**0.00**	**1.67**
Biotite	8.13	2.86	4.66	1.00	0.67	1.01	1.82	0.67	3.53	0.00	0.67
Chlorite	0.64	0.28	1.00	0.33	0.00	0.26	0.29	0.00	0.57	0.00	1.00
Muscovite	2.86	1.64	1.42	0.67	0.33	1.56	1.09	1.67	1.32	0.00	0.00
Garnet	**1.52**	**3.17**	**1.66**	**2.00**	**1.00**	**2.08**	**2.12**	**3.67**	**0.58**	**0.33**	**2.67**
Total Plutonic Rock Fragment	**5.76**	**12.16**	**5.51**	**4.66**	**8.33**	**3.40**	**2.50**	**4.00**	**1.48**	**2.34**	**4.00**
Total Metamorphic Rock Fragment	**11.93**	**3.44**	**4.75**	**0.33**	**0.00**	**0.40**	**3.14**	**0.00**	**1.07**	**0.00**	**2.00**
Highly altered low-rank metamorphic rock fragment	1.00	0.11	0.00	0.00	0.00	0.00	0.02	0.00	0.00	0.00	0.00
Total Sedimentary Rock Fragment	**1.92**	**0.89**	**1.75**	**0.00**	**3.00**	**1.73**	**1.50**	**0.00**	**0.50**	**0.00**	**0.00**
Dolostone rock fragment	1.27	0.72	1.41	0.00	3.00	1.35	1.21	0.00	0.33	0.00	0.00
Total Intrabasinal Grains	**0.09**	**0.25**	**0.17**	**3.66**	**9.00**	**0.72**	**0.24**	**0.00**	**12.89**	**57.00**	**2.00**
Mud intraclast	0.09	0.17	0.17	3.33	0.00	0.31	0.26	0.00	0.28	0.00	0.00
Carbonate bioclast	0.00	0.00	0.00	0.00	0.00	0.35	0.00	0.00	5.05	8.00	0.00
Carbonate ooid/oncoid/intraclasts	0.00	0.00	0.00	0.00	1.00	0.06	0.00	0.00	7.56	48.67	2.00
Total Diagenetic	**14.21**	**14.28**	**11.67**	**22.33**	**46.02**	**24.60**	**18.46**	**16.01**	**33.45**	**12.68**	**29.66**
K-feldspar Overgrowths	1.01	0.17	0.92	2.33	0.67	1.47	1.57	1.00	0.94	0.67	2.00
Quartz Overgrowths	0.25	0.42	0.50	2.00	0.00	0.13	0.09	0.00	0.00	0.00	0.00
Total Dolomite	**3.57**	**2.28**	**3.33**	**10.34**	**19.00**	**13.70**	**7.04**	**0.00**	**17.47**	**0.00**	**26.34**
Dolomite Coarsely-cryst. Intergr. pore-filling Eodiag.	1.98	1.00	2.50	6.67	5.67	4.21	0.45	0.00	13.06	0.00	20.34
Dolomite Coarsely-cryst. Intergr. pore-filling Mesodiag.	0.00	0.00	0.50	0.00	0.00	0.29	2.56	0.00	0.00	0.00	0.00
Dolomite Coarsely-cryst. replacing Carbonate intraclasts	0.00	0.00	0.00	0.00	0.00	0.00	0.00	0.00	2.93	0.00	0.00
Dolomite Coarsely-crystalline Intergranular displacive	0.00	0.00	0.00	0.67	0.33	2.35	0.00	0.00	0.07	0.00	0.00
Dolomite Coarsely-crystalline Intragranular replacive	1.12	0.94	0.33	3.00	0.00	1.55	0.55	0.00	0.30	0.00	6.00
Dolomite Microcrystalline Intergranular pore-filling Eodiag.	0.08	0.17	0.00	0.00	3.67	0.16	1.12	0.00	0.00	0.00	0.00
Dolomite Microcrystalline repalcing Mud Intraclast	0.06	0.00	0.00	0.00	7.00	0.00	0.00	0.00	0.00	0.00	0.00
Dolomite Microcrystalline replacing Marine Calcite Cement	0.00	0.00	0.00	0.00	0.00	4.00	0.00	0.00	0.00	0.00	0.00
Total Calcite	**0.11**	**0.00**	**0.00**	**0.00**	**0.00**	**0.00**	**6.03**	**0.00**	**9.05**	**8.01**	**0.00**
Calcite Coarsely-crystalline Intergranular pore-filling	0.00	0.00	0.00	0.00	0.00	0.00	1.24	0.00	4.28	2.67	0.00
Calcite Microcrystalline Intergranular displacive	0.00	0.00	0.00	0.00	0.00	0.00	4.11	0.00	0.00	0.00	0.00
Total Siderite	**0.28**	**0.39**	**0.00**	**0.00**	**0.00**	**0.00**	**0.00**	**0.00**	**0.00**	**0.00**	**0.00**
Total Albite	**1.49**	**1.08**	**2.17**	**3.67**	**1.67**	**1.18**	**0.92**	**0.67**	**0.83**	**0.00**	**0.66**
Albite Replacing Detrital K-feldspar	0.87	0.75	1.33	1.00	1.00	0.61	0.54	0.67	0.32	0.00	0.33
Albite Replacing Detrital plagioclase	0.61	0.33	0.84	2.67	0.67	0.61	0.37	0.00	0.51	0.00	0.33
Total Anhydrite	**0.00**	**5.15**	**0.00**	**0.00**	**20.67**	**4.97**	**0.22**	**0.00**	**0.03**	**2.00**	**0.00**
Anhydrite Poikilotopic Intergranular pore-filling Mesodiag.	0.00	2.37	0.00	0.00	10.00	1.70	0.00	0.00	0.00	0.00	0.00
Anhydrite Lamella Intergranular pore-filling Eodiagenetic	0.00	0.00	0.00	0.00	10.67	0.92	0.00	0.00	0.00	0.00	0.00
Anhydrite Lamella replacing Carbonate intraclasts	0.00	0.00	0.00	0.00	0.00	0.00	0.00	0.00	2.17	0.00	0.00
Diagenetic Clay Inherited	**0.60**	**0.69**	**0.33**	**0.00**	**0.00**	**0.00**	**0.32**	**0.00**	**0.00**	**0.00**	**0.00**
Pseudomatrix	**0.00**	**0.00**	**0.00**	**3.67**	**0.00**	**0.01**	**0.22**	**0.00**	**0.00**	**0.00**	**0.00**
Mechanically Infiltrated Smectite Clay	**0.00**	**0.00**	**0.00**	**0.00**	**0.00**	**0.10**	**0.00**	**7.67**	**0.00**	**0.00**	**0.00**
Diagenetic iron oxide	**0.00**	**0.00**	**0.00**	**0.00**	**0.00**	**0.38**	**0.02**	**4.34**	**0.10**	**0.00**	**0.00**
Total Chlorite	**2.63**	**1.42**	**0.25**	**0.00**	**0.00**	**0.42**	**0.33**	**1.00**	**0.00**	**0.00**	**0.00**
Chlorite Rim Intergr. pore-lining covering previous clays	0.17	0.44	0.00	0.00	0.00	0.00	0.00	0.00	0.00	0.00	0.00
Chlorite Microcryst. replacing metamorphic rock frag.	0.33	0.11	0.00	0.00	0.00	0.00	0.00	0.00	0.00	0.00	0.00
Total Corrensite	**0.00**	**1.45**	**0.00**	**0.00**	**0.00**	**0.00**	**0.00**	**0.00**	**0.00**	**0.00**	**0.00**
Total Smectite In situ precipitated	**0.19**	**0.34**	**1.59**	**0.00**	**0.00**	**0.00**	**0.37**	**0.00**	**0.00**	**0.00**	**0.00**
Total Illite-Smectite	**0.70**	**0.00**	**0.00**	**0.00**	**0.00**	**0.00**	**0.21**	**0.00**	**0.00**	**0.00**	**0.00**
Illite Fibrous Intergranular pore-filling	0.33	0.00	0.00	0.00	0.00	0.00	0.00	0.00	0.00	0.00	0.00
Illite Fibrous Intragranular replacing metamorphic rock frag.	0.17	0.00	0.00	0.00	0.00	0.00	0.00	0.00	0.00	0.00	0.00
Total Pyrite	**1.58**	**0.56**	**1.33**	**0.33**	**1.67**	**0.40**	**0.39**	**0.33**	**1.58**	**0.00**	**0.67**
Pyrite Framboid Intergranular pore-filling	1.58	0.22	1.33	0.33	1.67	0.38	0.39	0.33	0.74	0.00	0.67
Total Titanium mineral	**1.34**	**0.95**	**1.25**	**0.00**	**0.00**	**0.31**	**0.35**	**1.00**	**0.00**	**0.00**	**0.00**
Macroporosity Volume	**15.60**	**17.45**	**18.09**	**16.34**	**1.33**	**18.48**	**18.06**	**16.00**	**3.31**	**14.33**	**2.34**
Intergranular Primary	**11.57**	**14.78**	**15.17**	**12.67**	**1.33**	**11.82**	**12.21**	**10.67**	**1.59**	**8.33**	**0.67**
Intragranular by dissolution of Detrital-Constituent	**4.03**	**2.67**	**2.92**	**3.67**	**0.00**	**6.64**	**5.85**	**5.33**	**1.72**	**4.33**	**1.67**
Intragranular by dissolution of Detrital K-feldspar	0.75	0.83	0.42	0.33	0.00	1.66	1.96	3.33	0.71	0.00	0.00
Moldic by dissolution of Detrital-Constituent	**0.74**	**0.11**	**0.42**	**0.67**	**0.00**	**2.93**	**3.08**	**2.00**	**0.13**	**0.00**	**0.67**

Table 4

Table 4. Isotopic ratios of representative carbonate and sulphate cements and depositional sulphate phases (salt formations).

Sample - well Core (Depth)	Cement and (detrital) phases	$\delta^{13}C_{PDB}$	$\delta^{34}S_{CDT}$	$\delta^{18}O_{SMOW}$	$\delta^{18}O_{PDB}$	Occurrence
A-5 (2290.4m)	Anhydrite poik. Mesodiag.	-	1.9	-	-	delta plain - HST Seq.R1
A-7 (2011.35m)	Anhydrite poik. Mesodiag.	-	-2.9	-	-	delta plain - HST Seq.R2
A-7 (2010.5m)	Dolomite microcryst./blocky Mix?	-5.98	-	22.01	-8.36	delta plain - HST Seq.R2
A-9 (1828.3m)	Dolomite microcryst./blocky Mix?	-1.9	-	25.37	-5.37	delta front - HST Seq.D1
A-10 (1759.4m)	(evaporite intraclast)	-	21.3	-	-	delta plain - HST Seq.D1
A-10 (1759.4m)	Anhydrite poik. Mesodiag.	-	0.2	-	-	delta plain - HST Seq.D1
A-12 (1626.4m)	Anhydrite poik. Mesodiag.	-	-0.4	-	-	delta front - HST Seq.D1
A-13 (1558.5m)	Dolomite microcryst./blocky Mix?	0.15	-	25.91	-4.85	delta plain - TST Seq.D2
A-15 (1038.0m)	Dolomite microcryst./blocky Mix?	-2.1	-	27.89	-2.92	delta plain - HST Seq.D3
B-8 (1165.8m)	Dolomite microcryst./blocky Mix?	-1.47	-	23.78	-6.91	fluvial braided - HST Seq.R1
B-12a (931.45m)	Dolomite microcryst./blocky Mix?	2.22	-	33.66	2.67	Platform internal - TST Seq. D3
B-12b (931.45m)	Dolomite blocky Intragranular	2.29	-	25.38	-5.36	Platform internal - TST Seq. D3
B-12c (931.45m)	Anhydrite lamellar Intragranular	-	16.8	-	-	Platform internal - TST Seq. D3
B-16 (547.2m)	Dolomite microcryst. Eodiag.	-3.26	-	31.09	0.18	Estuarine - TST Seq.D4
B-19 (400.5m)	Dolomite microcryst. Eodiag.	-3.42	-	30.67	-0.23	Estuarine - TST Seq.D4
C (1645.0m)	(salt formations - Itaunas Formation)	-	21.5	-	-	Supratidal flat - HST Seq. T
C-1 (1647.5m)	Anhydrite lamellar /felted Eodiag.	-	19.8	-	-	delta front - HST Seq.T

Assunto:	RE: Manuscript submission
Data:	Thu, 13 Mar 2008 11:32:14 -0000
De:	"Christopher Tiratsoo" <ct@jpg.co.uk>
Para:	"celso jardim" <celsomourajardim@yahoo.com.br>

Hello Mr Jardim:
Today the UK courier delivered the package with your letter and two copies on paper of the MS "Jequitinhonha Basin....". This looks to be a strong and well illustrated MS, thank you very much for sending it to the JPG. We shall check over it as soon as we can and then I shall write to you again with preliminary editorial comments before we initiate the external review process. Owing to pressure of work here, I regret that this may not be for several weeks.
with best regards
Christopher Tiratsoo

-----Original Message-----
From: celso jardim [mailto:celsomourajardim@yahoo.com.br]
Sent: 07 March 2008 10:12
To: Christopher Tiratsoo
Subject: Manuscript submission

Dear Mr. Tiratsoo and members of Editorial Board,

I am pleased to inform you that I have submitted the manuscript entitled ***Reservoir quality assessment and petrofacies of the Lower Cretaceous siliciclastic, carbonate and hybrid arenites from the Jequitinhonha Basin, Eastern Brazil,*** co-authored with L.F. De Ros and J.M.M Ketzer, to your appreciation. The two paper copies were posted on March 28th and, according to the postmaster, they should be arriving in three to five days.

I would be glad if you could acknowledge receipt of these copies as soon as possible (addressed to my Yahoo e-mail, if possible).

Yours sincerely,

Mr. Celso Jardim

Reservoir quality assessment and petrofacies of the Lower Cretaceous siliciclastic, carbonate and hybrid arenites from the Jequitinhonha Basin, Eastern Brazil

Celso Moura Jardim[1], Luiz Fernando De Ros[2], João Marcelo Ketzer[3]

[1] PETROBRAS, Av. Republica do Chile, 65/1302 Rio de Janeiro, RJ, 20031-975, Brazil; celsomj@petrobras.com.br

[2] Instituto de Geociências, Universidade Federal do Rio Grande do Sul, Av. Bento Gonçalves, 9500, Porto Alegre, RS, 91501-970, Brazil; lfderos@inf.ufrgs.br

[3] Instituto do Meio-Ambiente, Pontifícia Universidade Católica do Rio Grande do Sul - PUC-RS, Av. Ipiranga, 6681, Porto Alegre, RS, 90619-900, Brazil; marcelo.ketzer@pucrs.br

ABSTRACT

A study of the rift to early drift phase, fluvial, deltaic, and shallow-marine, Lower Cretaceous (Upper Aptian to Lower Albian) siliciclastic sandstones, hybrid arenites and calcarenites from the Jequitinhonha Basin, eastern Brazilian margin, reveals that the distribution of diagenetic alterations and of related reservoir quality evolution can be constrained within a sequence stratigraphic framework. Description of cores, wireline logs, thin sections, and petrophysical porosity and permeability analyses were integrated in order to unravel the genetic aspects that controlled the complex patterns of diagenesis of these rocks, and hence of reservoir quality distribution. The results of this study are relevant to the exploration of rift and early drift successions in Atlantic-type, passive margin settings, and demonstrate the influence of factors such as depositional systems (i.e. sedimentary facies) and detrital composition (provenance) on the diagenetic evolution for the characterization and prediction of reservoir quality and heterogeneity. The integrated interpretation and reservoir quality assessment performed in this paper was accomplished using the concept of reservoir petrofacies. Reservoir petrofacies are defined by the combination of the main attributes affecting reservoir quality (e.g. depositional structures, textures, primary composition, diagenetic processes and products, pore types). This paper demonstrates the practical use of the reservoir petrofacies concept as a tool for the systematic recognition of the attributes that control petrophysical porosity and permeability, seismic and log signatures, in order to reduce the exploration risks.

Keywords: depositional systems, sequence stratigraphy, diagenesis, petrofacies, reservoir quality, petroleum exploration

INTRODUCTION

The prediction of the quality of hydrocarbon reservoirs, which can be defined mostly in terms of porosity and permeability values, is a key parameter of any petroleum prospect. The distribution of reservoirs, seals and source rocks (controlled by depositional facies) and depositional-related reservoir quality can be constrained within a sequence stratigraphic context. The sequence stratigraphy approach is based on the interplay between sediment supply, basin-floor physiography and changes in the relative sea level (cf. Van Wagoner et al., 1990; Posamentier and Allen, 1993). Similarly, the spatial and temporal distribution of near-surface diagenetic alterations in siliciclastic successions can also be constrained within a sequence stratigraphic context (sequence stratigraphic surfaces and systems tracts), based on variations in depositional facies, climatic conditions and significant changes in detrital composition, residence time under specific geochemical conditions, and porewater chemistry (cf. Morad et al., 2000; Ketzer et al., 2002; Ketzer et al., 2003a/b). These, in turn, may exert significant and complex controls on burial diagenetic alterations, resulting in an improvement or deterioration of primary porosity. An integrated approach between diagenesis and sequence stratigraphy enables the prediction of the post-depositional evolution of reservoir quality, which ultimately is the goal of any petroleum exploration activity.

The present study aims to integrate petrological, wireline log, petrophysical and geophysical data of the Lower Cretaceous (Upper Aptian to Lower Albian) siliciclastic sandstones, calcarenites and hybrid arenites from the Jequitinhonha Basin, eastern Brazilian margin. The target is to demonstrate that significant reduction of the exploratory risks can be achieved by characterizing the types, distribution and evolution of the diagenetic processes, and their relationships with depositional facies and sequence stratigraphic surfaces and system tracts. These tasks were performed through description of cores, wireline logs, thin sections, and petrophysical porosity and permeability analyses on core samples from three onshore and shallow offshore wells from the Jequitinhonha Basin (Fig.1). The basin has good potential for oil and natural gas, with several blocks under exploration.

The reservoir quality assessment performed in this paper was accomplished using the concept of reservoir petrofacies *sensu* De Ros & Goldberg (2007), defined by the combination of the main intrinsic attributes affecting the quality of reservoir rocks, comprising: (i) depositional structures, textures and composition; (ii) diagenetic processes and products (volume or intensity, habits and distribution); and (iii) pore types and distribution. These attributes ultimately control petrophysical properties (i.e. porosity and permeability values), and seismic and log signatures. The interpreted petrofacies were put into a stratigraphic context with aid of seismic sections, allowing a better understanding and prediction of the effects of depositional characteristics, tectonic and diagenetic evolution on reservoir quality distribution.

The definition of diagenetic stages used in this paper are *sensu* Morad et al. (2000), including: (i) eodiagenesis (i.e. 0-2 km of burial depth; < 70^{o}C), with pore-water chemistry controlled mainly by the depositional environment; and (ii)

mesodiagenesis (i.e. > 2 km of burial depth; > 70°C), with diagenetic alterations mediated mainly by formation waters evolved through water-rock interactions.

GEOLOGICAL SETTING

The origin and evolution of the Jequitinhonha basin, located at the Eastern Brazilian continental margin, was a result of the rifting Gondwana and opening of the South Atlantic ocean during Mesozoic and Cenozoic times (cf. Asmus and Ponte, 1973; Ojeda, 1982; Chang et al, 1988) (Fig. 1). The basement of the Jequitinhonha basin is composed mostly of Pre-Cambrian granites, gneisses, granulites and low-grade meta-sediments. The stratigraphic section can be divided into four units (cf. Chang et al, 1988; Cainelli & Mohriak, 1999):

(i) Neocomian to Early Aptian sin-rift unit, consisting of continental fluvial to lacustrine-deltaic conglomerates and sandstones associated with organic-rich lacustrine shales of the Mariricu Formation. These rocks were deposited under rapid subsidence, filling N-S to SW-NE half-grabens. The uppermost limit of this unit is represented by an unconformity that marks the onset of a tectonic quiescence, showing the cessation of stretching and rifting of the continental crust (Cainelli & Mohriak, 1999).

(ii) Late Aptian to Early Albian transitional unit, consisting of fluvial-deltaic sandstones deposited in a shallow-water, proto-oceanic environment, capped by evaporitic beds of Itaunas Member (Mariricu Formation). There is an upward-increasing marine influence and arid to semi-arid climate conditions. At the end of the Aptian (period of high aridity), the presence of volcanic barriers to the south (cf. Kumar and Gamboa, 1979) formed a restricted gulf area, allowing the deposition of an evaporite package along the Brazilian continental margin, composed of mainly halite at the base and anhydrite at the top..

(iii) Albian to Paleocene drift transgressive unit, dominated by open marine conditions. At the start of the drift phase, during the Albian-Cenomanian coarse-grained alluvial and coastal sandstones of the São Mateus Formation were deposited, grading offshore into shallow-water carbonates and basinal marls and shales of the Regência Formation. During the Senonian transgression, the Regência carbonates were covered by basinal shales and turbidites of the Urucutuca Formation. The Aptian evaporites were extensively deformed and slided downslope by halokynetic movements, promoting lystric faulting of the post-salt sequences.

(iv) Paleocene to Recent drift regressive sequence, characterized by the progradation of coarse-grained coastal sandstones of the Rio Doce Formation grading offshore towards shallow-water carbonates of the Caravelas Formation. Paleocene-Eocene volcanics and volcaniclastic sediments of the Abrolhos Formation occur at the Royal Charlotte Volcanic Complex, south of the basin.

SAMPLES AND METHODS

The studied Upper Aptian to Lower Albian succession was cored irregularly in three wells drilled in the onshore and shelf part of the basin (Fig. 2). The study was carried out on 140-metre, discontinuous well core data of the three wells (Fig. 3), representing the late rift phase and the passage from evaporitic (transitional) to the onset of the drift phase. The cores were described in detail (lithologies, textures, structures, vertical trends) in order to identify lithofacies (adapted from Miall, 1996) and to interpret facies associations and their successions (*sensu* Walker, 1992) (Table 1), which were compared with well-recognized sedimentary models (e.g. Galloway and Hobday, 1983; Collinson, 1996; Johnson & Baldwin, 1996; Kendall & Harwood, 1996; Reading & Collinson, 1996; Bhattacharya, 2006), and used as the building blocks for the reconstruction of depositional environments and sequence stratigraphic framework (Jardim et al., submitted). The cores were sampled within a depth range of 400 to 2800 m. Sixty-seven thin sections prepared from blue epoxy resin-impregnated samples were described in detail with polarized light microscopes. Petrographic modal analyses were performed using the Petroledge® system (De Ros et al., 2007) by counting 300 points per thin section, recording the relationships between detrital and authigenic components and porosity. The percentage of detrital and diagenetic constituents and types of pores is expressed in relation to bulk rock volume. Sorting was estimated by comparison with the standard charts of Beard and Weyl (1973). Carbonate cements were stained with Alizarin red-S in order to distinguish calcite from other carbonate cements. Available petrophysical porosity and permeability data from the analysed cores were integrated to the stratigraphic and petrologic data.

The paragenetic sequence of diagenetic processes and products was interpreted from the textural relationships obtained from optical and electronic microscopy, aided by X-ray diffraction analyses (Jardim et al., submitted). Scanning electron microscopy (SEM) was performed in a Phillips XL-30 microscope, equipped with an EDAX energy-dispersive spectrometer (EDS). X-ray diffraction analyses of the < 10 µm fraction were performed in 5 oriented samples in a Siemens Bruker AXS D5000 diffractometer, in order to identify the clay mineralogy. The oriented samples were air-dried, ethylene glycol-saturated and heated at 550^{o}C for 2 hours.

DEPOSITIONAL ENVIRONMENT AND STRATIGRAPHIC FRAMEWORK

The stratigraphic framework of Jequitinhonha basin discussed in this paper was based on the interpretation of wireline logs and of facies successions defined from core lithological descriptions (Table 1). The interpreted stratigraphic framework comprises 7 sequences as follows (Fig. 2): two rift phase sequences (R1 and R2); one transitional sequence (T), and four drift phase sequences (D1 to D4) (Jardim et al., submitted).

The clastic continental deposits of the Aptian rift phase sequences are interpreted as a complex interplay of fluvial-deltaic and lacustrine depositional

environments. Three distinct depositional settings were interpreted: **(1)** medium- to coarse-grained braided-stream and deltaic deposits (CD facies associations; Figs. 4, 5), present at Sequence R1 of well A. These deposits are characterized by a poorly developed *spontaneous potential* (SP) – *gamma ray* (GR) coarsening-upward log pattern; **(2)** fine- to medium-grained, poorly- to moderately-sorted deltaic deposits (FD facies associations; Fig. 5), present at Sequence R1 in well B. These deposits are characterized by a typical SP log signature of a deltaic progradation with a coarsening-upward succession; (funnel-shaped log signature); and **(3)** fining-upward successions of coarse- to fine-grained, poorly- to very poorly-sorted sandstones, interpreted as high-energy fluvial braided (BR facies association; Fig. 5), characterized by a box SP/GR pattern, with high sonic (DT) log values, such as at Sequences R1 of well B.

The rift phase sediments were deposited in deep, asymmetric half-grabens under active rift tectonism and increasing marine influence (cf. Kuchle et al., 2005). Aptian braided streams and lacustrine-deltaic deposits present in wells A and B are interpreted as rift sequences R1 and R2, separated by sequence boundary 1 (SB1). Sequence R1 in well A presents coarse-grained fluvial-deltaic deposits (CD facies) that are compositionally and texturally less mature than equivalent finer-grained fluvial-deltaic deposits (FD facies) present in well B, showing high content of ductile metamorphic rock fragments and detrital mica (Fig. 6). Such differences are interpreted as resulted from diverse relative position to basin margin faults and distinct provenance (cf. De Ros et al., 2005). CD facies deposits are interpreted as proximal to basin margin faults, showing significant content of ductile grains and poorer sorting sediments. The more mature and quartz-feldspathic composition of FD facies, on the other hand, reflect more developed transport and erosion.

SB1 implies in little change of sedimentary regime and subsidence patterns, but its time is marked by a sharp shift of facies (mainly primary detrital composition; i.e. source area). It shows a clear shift between wells A and B. The transition of Sequence R1 to R2 in well B, for instance, and conversely to well A, shows a sharp increase of metamorphic rock fragments (decrease maturity of sediments, regarding Sequence R1), with large meta-sandstone and sandstone fragments (Fig. 6). Facies succession from sequences R1 to R2 in well A, and along Sequence R1 in well B shows a thickening-upward delta-front/delta-plain facies corresponding to a coarsening-upward SP trend, with continuous trend of sedimentation rate exceeding creation of accommodation space, locally overlain by braided river systems (continuous low SP signature), such as in the uppermost interval Sequence R1 of well B (Fig. 5). Such trend supports a highstand system tract for Sequence R1. Sequence R2 is poorly preserved in well B, and, therefore rendering a precise stacking pattern interpretation.

The interpreted depositional environments for the Late Aptian to Early Albian transition and Albian stage correspond to an extensive, shallow water, restricted marine, homoclinal ramp, showing an interplay of four differentiated depositional settings (Table 1): **(1)** shallow-water, coarse-grained deltaic deposits (e.g. Bhattacharya, 2006), assigned here to SD facies associations (Figs. 4, 5, 7). This clastic coastal system intertongues basiward and along strike with

carbonate deposits of open-shelf environments (mixed ramp facies discussed below), and landward with fluvial braided facies. This facies locally show a coarsening-upward GR and SP log pattern from delta front (lower to upper-shoreface) to delta plain (foreshore) facies; **(2)** fining upward deposits consisting of coarse-grained sandstone layers alternating with heterolithic (sand/mud) layers (ES facies association; Figs. 4, 5) (e.g. Weimer et al., 1982). This facies occurs vertically associated with SD facies, and are interpreted as brackish water environments (estuaries, lagoons, bays or tidal flats) of low relief and relatively low energy and protected areas along the coast; **(3)** supratidal-coastal sabkha evaporative deposits (SC facies association; Fig. 7). These deposits occur overlying SD deltaic deposits in response to increasing marine influence and arid climatic conditions during the transition of Late Aptian to Early Albian stage; and **(4)** Hybrid arenites (*sensu* Zuffa, 1980) or calcarenite mixed-ramp deposits (MR facies associations; Figs. 4, 5, 7), reflecting the development of extensive shallow water restricted marine mixed siliciclastic-carbonatic ramp depositional environment (e.g. Wright & Burchette, 1996), with coeval supply (intertongue landward) of coarse-grained siliciclastic sources (SD facies).

The Late Aptian to Early Albian gradual transition from continental (fluvial-lacustrine) to marine settings, are characterized by the Transitional sequence - T (well C) and early Drift Sequence D1 (well A), consisting of prograding coarse-grained coastal-deltaic systems (SD facies), which were deposited into a basinal environment grading from a narrow gulf into a progressively open marine conditions, and under arid climatic conditions, capped by sabkha and coastal salina supratidal facies environments (Sequence T). Sequence D1 deposits reflect the high supply of siliciclastics (no indication of coeval carbonate deposition during Sequence D1). The lack of muddy sediments (pro-deltaic facies) observed in the coarse-grained coastal deposits is interpreted as a consequence of the very shallow-water depositional setting (cf. Reading & Collinson, 1996), resulting in high-energy conditions with widespread dispersal of suspended sediment by wave-reworking (cf. Galloway and Hobday, 1983). The occurrence of plant fragments is probably related to the proximal fluvial sediment supply. The SD facies deposits of Sequence D1 show high content (up to 4%) of detrital plagioclase. The high average K-feldspar content (47-50%) suggests rapid erosion and transportation from mountainous source-areas, under arid or semiarid climate. The compositional trends of wells A and B show a gradual decrease of lithic contribution towards Albian samples (Fig. 6). This is especially clear in well A from a lithic composition of rift sequences (R1 and R2) to feldspathic drift Sequence D1, with corresponding decrease of average grain size.

Albian drift phase sequences D2 to D4 reflect the development of an extensive shallow marine mixed siliciclastic-carbonatic ramp depositional environment (cf. Wright & Burchette, 1996). Such environment was characterized by the simultaneous supply of proximal siliciclastics (SD facies), comprising sets of paralic sedimentation, which intertongue basinward with hybrid arenites (*sensu* Zuffa, 1980) or carbonate-dominated deposits, assigned herein to mixed ramp (MR) facies, which are differentiated into three facies associations: high-energy inner ramp (MRhin) and low-energy inner ramp (MRlin), and mid ramp

(MRmdr). Sequences boundaries SB5 and SB6, setting the bottom limit of Sequences D3 and D4 respectively, are characterized by small changes in sedimentary regime, and by alternation of siliciclastic and carbonate deposition. This alternation is herein interpreted as product of relative eustatic sea-level (RSL) fluctuations, coupled with variable sediment input rates (cf. Shew, 1991), with mixed deposition resulted from siliciclastics reworking by longshore and storm processes (cf. Lomando & Harris, 1991). Conversely to the other wells, the transgressive system tract of Sequence D4 in well B is characterized by an alternation of siliciclastic-dominated deltaic succession (SD facies) and restricted estuarine deposits (ES facies). This interval shows distinct detrital composition from other drift sequences, consisting of high content of meta-sedimentary rocks, and plant fragments, suggesting fast and short transportation from source areas, and higher sediment accommodation in comparison with transgressive system tract of wells A and C, resulting unfavourable conditions for carbonate deposition.

DETRITAL TEXTURE, COMPOSITION AND PROVENANCE IMPLICATIONS

The samples analysed range from fine to very coarse, conglomeratic sandstones, with predominance of medium to coarse-grained sandstones, to hybrid arenites (*sensu* Zuffa, 1980) and calcarenites. The sorting is usually poor and the grains are mostly subrounded. The quantitative petrographic results are presented in Table 2 as average values of the reservoir petrofacies defined ahead. The sandstones are dominantly arkoses (av. $Q_{38}F_{56}L_{6}$) and subordinately lithic arkoses (av. $Q_{33}F_{46}L_{21}$) and feldspathic litharenites (av. $Q_{18}F_{30}L_{52}$) *sensu* Folk,1968 (Fig. 8). The dominant immature feldspathic and lithic detrital composition (Fig. 9) is consistent with provenance from uplifted basement terrains (uplifted blocks along the rift margins), characterized by plutonic magmatic and high-grade metamorphic rocks, and from recycled orogenic terrains of sedimentary and low-grade meta-sedimentary rocks (Dickinson, 1985).

The quartz grains are essentially monocrystalline (av. 18%) and detrital feldspars are dominantly orthoclase (av. 17%). Plutonic (av. 4.7%) and low-grade metamorphic (av. 4.2 %) rock fragments are more common in the poorer-sorted, coarser-grained and conglomeratic facies. Sedimentary rock fragments (av. 1.7%) consist mainly of dolostones and related monocrystalline dolomite grains. Intrabasinal grains (av. 2.3%) consist dominantly of mud intraclasts and carbonaceous fragments (plant debris), except for some Albian samples (drift sequences D2 to D4), which are classified as hybrid arenites (*sensu* Zuffa, 1980), contain abundant carbonate intrabasinal grains (ooliths, oncoliths, bioclasts and intraclasts). Bioclastic hybrid arenites and calcarenites occur in the transgressive to highstand deposits of drift sequences, consisting mostly of benthic foraminifers, echinoderms and molluscs (bivalves and gastropods), with increasing number and variety towards the younger sequences (cf. Cordoba, 1994). Pre-salt sandstones of the Transitional Sequence (well C) contain scarce, completely dolomitized bioclasts (ostracodes), ooids and intraclasts.

The average K-feldspar content (47-50%) suggests rapid erosion and transportation, under arid or semiarid climate. Biotite (av. 3.4%) is the main accessory detrital constituent. Garnet (av. 2%) is the second most abundant.

DIAGENETIC CONSTITUENTS

Dolomite. This is the most abundant diagenetic constituent in the studied sandstones (av. 7.0% of bulk volume). Dolomite occurs as intergranular pore-filling (Figs. 10a, 10c) or grain rimming (Fig. 10b) microcrystalline to coarsely-crystalline rhombs (20 to 450 μm, av. 120 μm), locally displacive, and pre-dating other intergranular pore-filling cements, except K-feldspar overgrowths. Microcrystalline rhombs (< 60 μm) occur replacing mud intraclasts and high-Mg calcite rim marine cement. Coarsely-crystalline burial dolomite replaces feldspars, micas and rock fragments, as well as the microcrystalline eogenetic phase. In some samples, euhedral crystals up to 450 μm show wavy extinction and curved faces, characteristic of the "saddle" dolomite type (Fig. 10d).

Calcite. This cement (av. 1.5 % of bulk volume) occurs as microcrystalline, grain-rimming and pore-filling cement in siliciclastic sandstones (Fig. 10e), and replacing early, pore-filling microcrystalline $CaCO_3$ cement in hybrid arenites and calcarenites (Fig. 10f), as well as syntaxial overgrowths on echinoid bioclasts (Fig. 11a). Post-compaction, intergranular pore-filling and grain-replacive, coarsely-crystalline (av. 150 μm) calcite cement is distributed as patches in a few arkoses and lithic arkoses.

Anhydrite. This is the second most abundant diagenetic constituent in the studied sandstones (av. 2.5 % of bulk volume). Anhydrite occurs with two diverse distribution modes. Pre- to syn-compactional, lamellar or prismatic/ plumose (divergent) crystals (from 120 to 500 μm; av. 170 μm) or as felted (fibrous) crystals (Fig. 11b), engulf and thus post-date K-feldspar overgrowths and microcrystalline dolomite. Post-compactional, poikilotopic pore-filling cement (Fig. 11c) with crystal size from 0.3 to 2.4mm (av. 0.9mm) is the common habit (absent along grain contacts – post-compaction?), occurring in some samples mixed with earlier lamellar phase. Large crystals (up to 4.2mm wide) of anhydrite replace large carbonate bioclasts and oncoliths. Anhydrite cement distribution is commonly heterogeneous and patchy, but locally pervasive.

K-feldspar. Potassic feldspar overgrowths are conspicuous in the studied sandstones (av. 1.6 % of bulk volume). The overgrowths are euhedral (sanidine habit), epitaxial, thick (up to 200 μm) and continuously cover detrital orthoclase and microcline grains, and are covered by, thus pre-dating all other intergranular pore-filling authigenic phases, except mechanically infiltrated smectite coatings (syn-precipitated).

Quartz. Quartz cement (av. 0.5%) occurs as euhedral, syntaxial, up to 60 μm thick overgrowths on quartz grains. Quartz overgrowths engulf K-feldspar overgrowths and clay coatings, and are covered by anhydrite poikilotopic cement in some samples. Some rift samples with discontinuous clay coatings

show expressive precipitation of prismatic crystals (outgrowths) with average size of 30 μm (Fig. 11d), locally occupying mouldic pores, post-dating grain dissolution. However, the deepest samples of Sequence R1 (well A) show large amount of discrete, pore-filling quartz outgrowths, while adjacent quartz grains surfaces show no clay coatings or overgrowths. Significant volume (> 2%) of quartz overgrowths and outgrowths is observed only in some of the deeper samples (rift phase sequences of well A).

Smectite. Smectite clays occur in the following habits: (i) as discontinuous coatings, thicker (up to 15 μm) along the concave portion of grain surfaces (scattered occurrence, in most sequences); (ii) as thin (av. 5 μm), pre-compaction, continuous and isopachous coatings (Fig. 11e); (iii) as thick (up to 60 μm; av. 12 μm) continuous and anisopachous, pre-compaction coatings (Fig. 11f), covering most of detrital grains; and (iv) as rims of honeycombed aggregates, covering the coatings in some samples. Shrinkage and fragmentation features are commonly observed, especially in the thicker coatings. X-ray diffraction analyses indicate the preservation of smectite in samples presently buried deeper than 1200 m.

Corrensite. Corrensite clays (regular mixed-layer chlorite-smectite) occur in one sample of Sequence R2 (well A) with the following habits: (i) thick (av. 8 μm), locally multiple (concentric), anisopachous coatings (Figs. 12a, 12b), displaying shrinkage and fragmentation features (Figs. 12c, 12d); and (ii) well developed rims, covering the coatings. Multiple corrensite coatings are observed around dissolved heavy minerals (mainly garnet) indicating recurrent precipitation and dissolution. Corrensite rims post-date the shrinkage of coatings and the expansion of micaceous grains (Fig. 12e), and pre-date grain dissolution (thicker along intergranular space).

Chlorite. Chlorite clays occur replacing detrital biotite and ferro-magnesian heavy mineral grains, mud intraclasts and metamorphic rock fragments (Fig. 12f) and smectite coatings (transformation) (Fig. 13a), as well as directly precipitated (neoformed) as continuous, isopachous (up to 10 μm thick; av. 7 μm) rims made of thin platelets arranged perpendicularly to grains surfaces (Fig. 13b). Chlorite also occurs replacing partially to totally dissolved (locally transformed into pseudomatrix) metamorphic rock fragments. Double rims were formed along both sides of coatings detached due to shrinkage or grain dissolution.

Other diagenetic minerals. Illite-smectite occurs in few Sequence R1 (well A) samples, as intergranular pore-lining or pore-filling (Figs. 11e, 13c), radiated aggregates of fibrous crystals (up to 15 μm), locally covering chloritized coatings or chlorite rims, and also bridging across pores. Pyrite occurs as disseminated intergranular and intraparticle (within bioclasts) pore-filling framboidal aggregates (< 20 μm), and also replacing carbonaceous fragments, micas, clay coatings mud intraclasts and derived pseudomatrix. Siderite occurs as microcrystalline or spherulitic aggregates (up to 20 μm; av. 9 μm), replacing mud intraclasts. Kaolin booklets (up to 80 μm) and pseudomorphic, lamellar crystals occur replacing micas and micaceous fragments. Small, prismatic

crystals of diagenetic titanium oxides (av. 25 μm) replace heavy mineral and biotite grains, and occur as discrete, intergranular pore-filling cement. Diagenetic albite heterogeneously replaces feldspar grains in all depositional facies and systems tracts (av. 1.0% of bulk volume).

COMPACTION AND POROSITY

The degree of compaction undergone by the studied sandstones, as well as the evaluation of the relative role played by compaction and cementation in porosity reduction, were analysed in a diagram plotting the intergranular volume versus intergranular cements volume (cf. Ehrenberg, 1989; Fig. 14). The wide range of intergranular volume (12 to 38%; av. 24.2%) reflects the variable timing and intensity of cementation and compaction of studied samples. Conversely to lithic and poorly-cemented rift samples, sandstones with abundant pre-compaction carbonate or sulphate cementation, such as in transgressive deltaic (SDush) facies of drift sequences or highstand system tracts of transitional sequence, suffered limited compaction, as indicated by their larger intergranular volume. Hybrid arenites of low-energy settings (MRlin) and deltaic (SDush) facies underlying supratidal sandstones of Sequence T suffered pervasive eodiagenetic carbonate and/or sulphate cementation also preserved large intergranular values, but with minor porosity preservation (< 1.5%).

Secondary intragranular porosity (av. 4.3%) resulted mainly from the dissolution of feldspar grains (av. 2.1%) and subordinately from metamorphic rock fragments, heavy minerals and intrabasinal carbonate grains, being more significant in the coarser-grained sandstones of rift sequences and transgressive siliciclastic (SD/TST) samples of drift Sequence D4 of well B, which is characterized by high content of mouldic porosity.

DISCUSSION

The patterns of diagenetic processes distribution in relation to the depositional environments and stratigraphic sequences were analysed in this paper with the aid of reservoir petrofacies concept (*sensu* De Ros and Goldberg, 2007). Reservoir petrofacies are defined by the combination of primary attributes (such as depositional structure, texture, fabric and major primary compositional constituents), with most the influential diagenetic processes, i.e. the main petrographic attributes that control porosity and permeability values, as well as log and seismic signatures. According to this methodology, the samples were first grouped according to their primary petrographic attributes that control original porosity and permeability characteristics. Afterwards, these groups were superimposed with the main diagenetic processes and their paragenetic relationships, in order to differentiate groups which have undergone equivalent modification of the original porosity and permeability.

Reservoir petrofacies characterization and diagenetic evolution of the sandstones

The diversity of original composition and diagenetic alterations, reflecting the varying depositional settings (such as fluvial, deltaic, gulf/lagoon, and shallow marine platform) has resulted into the definition of fourteen reservoir petrofacies (Figs. 15a-c; Table 2):

1. CmpctMica (well A, Seqs. R1-R2, and well B, Seq. R1) petrofacies consists of very poorly to poorly sorted, medium- to coarse-grained arkoses to lithic arkoses, characterized by lack of significant pore-filling cementation, combined with the presence of soft grains, such as monocrystalline micaceous grains (av. 14.5%; Fig. 13d), and subordinate low-rank metamorphic rock fragments and/or mud intraclasts, most deformed into pseudomatrix (Figs. 12f, 13e), resulting in significant mechanical compaction and intergranular porosity reduction (av. 9.7%). The log signature of this petrofacies is characterized by low SP (av. -85.1), GR (av. 82.6) and induction-log resistivity (av. 2.7) values (Fig.16 – cores A5, A7). The seismic signature is characterized by minor seismic impedance contrast, probably reflecting the limited cementation (Fig. 4). The main diagenetic phases (Fig. 15a) include the precipitation of chlorite rims (Fig. 13a), kaolin (dickite) replacing micas and pseudomatrix (Fig. 13b), intergranular pore-lining to pore-filling fibrous illite-smectite (I-S) rims (Fig. 13c), and quartz outgrowths as pore-lining and pore-filling cement (Fig. 13c). Available petrophysical porosity values are 3 to 5% higher than petrographic macroporosity, indicating the occurrence of significant microporosity. Permeability values range from 0.3 to 81mD, due mostly to the heterogeneous distribution of clay coatings and rims.

2. FineA (well B, Seq.R1) petrofacies consists of poorly to moderately-sorted, fine- to medium-grained arkoses. This petrofacies differs from CmpctMica samples by its minor content of detrital mica, which combined with lack of pore-filling cementation has resulted in relatively larger intergranular porosity preservation (av. 15.7%). The log signature of this petrofacies is characterized by low SP (av. -166.6) and induction-log resistivity (av. 1.3) values (Fig. 5), reflecting porous and sandy intervals. The main diagenetic phases are shown in Figure 15a.

3. MudClstA (well B, Seq.R1) petrofacies consists of coarse-grained, poorly-sorted arkoses, characterized by high content of mud intraclasts (av. 7%), partially deformed into pseudomatrix, resulting in intergranular porosity reduction (av. 12.7%). Mud intraclasts and pseudomatrix show preferential replacement by dolomite. This petrofacies shows log signatures characterized by low SP (av. -135.7) and high resistivity logs (av. 4.1) values (Fig.16 – core B7), possibly reflecting the high mud intraclast and dolomite cement content. The main diagenetic phases (Fig. 15a) include replacive dolomite crystals (up to 450 μm), with wavy extension, distinctive of “saddle” dolomite (Fig. 10d).

4. CemA (well A, Seq. R2, and well C, Seq. T) petrofacies consists of poorly- to moderately-sorted, fine- to coarse-grained arkoses, characterized pervasive, intergranular, pore-filling: (i) anhydrite cementation, as locally grain-displacive,

eodiagenetic prismatic-radial (plumose) and/or as mesodiagenetic poikilotopic cement (Figs. 11c, 13f); or (ii) eodiagenetic felted anhydrite and microcrystalline dolomite cementation (Fig. 11b), locally displacive. Felted anhydrite commonly occurs along the stratification with a nodular pattern. Resulting intergranular porosity values are less than 4%. This petrofacies shows log profiles characterized by low SP (av. -54.3) and GR (av. 92.8) values, and high induction-log resistivity (av. 3.6) values (Fig.16 – cores A7, A10, C1). The seismic signature is characterized by strong amplitude values (high seismic impedance contrast). At Sequence D1 this signature is interpreted as result of intense and varying cementation content (alternation with porous petrofacies) (Fig. 4). At Sequence T, is interpreted as reflecting abundant cementation at the upper part of a coarsening-upward GR profile, with upward increase of sonic and resistivity log values towards the evaporitic intervals (Fig. 7). No specific seismic signature was recognized for this petrofacies along Sequence R2, probably due to limited vertical (time) resolution The main diagenetic phases are shown in Figure 15b.

5. PorsCoars (well A, Seqs. R1-R2-D1) petrofacies consists of poorly- to moderately, coarse-grained arkoses to lithic arkoses, characterized by large values of intergranular porosity (av. 13.7%) due to minor content of ductile grains, as well as limited intergranular pore-filling cementation by dolomite and anhydrite. Lithic arkoses contain mostly high-rank metamorphic rock fragments, resulting in minor grain deformation. The log signature of this petrofacies is characterized by relatively low SP (av. -91.7), GR (av. 97.6) and induction-log resistivity (av. 2.8) values (Fig.16 – cores A5, A9). The seismic signature along Sequence D1 is characterized by strong amplitude values (high seismic impedance contrast), interpreted as result of alternation of porous and strongly cemented intervals (CemA samples), vividly contrasting with the poorly-cemented underlying interval of the NonCemA petrofacies (Fig. 4). The main diagenetic phases (Fig. 15b) include the precipitation of smectite coatings and their transformation into corrensite (Figs. 12a), or chlorite (Fig. 17a). Available petrophysical porosity values are up to 5% higher than petrographic macroporosity, in a sample with abundant corrensite, reflecting high microporosity values. Permeability range from 22 to 114mD suggesting a minor impact of clay cements.

6. NonCemA (well A, Seq. D1) petrofacies consists of medium-grained, poorly sorted arkoses, characterized by a lack of pore-filling cementation. These sandstones show large intergranular porosity values (av. 15.7%) due to absence of ductile grains, and high values of intragranular porosity (av. 10%), due dissolution of detrital feldspar (high content – av. 31%). This petrofacies shows log signatures characterized by low SP (-96.1), and induction-log resistivity (av. 2.5) values, and moderate GR (av. 120.1) values. The seismic signature is characterized by minor seismic impedance contrast, probably reflecting the limited cementation (Fig. 4). The main authigenic phases are shown in Figure 15c.

7. MicrDoloA (well A, Seqs. D1/D2) petrofacies consist of poorly to moderately sorted arkoses, locally bioturbated, and with carbonaceous fragments (with stylolitization along grains contacts) and mud intraclasts (partially or totally

deformed into pseudomatrix; Fig. 17b). This petrofacies is characterized by high content of eodiagenetic microcrystalline dolomite (av. 15.7%) and minor anhydrite cementation, resulting in low intergranular porosity values (av. 6.7%). The log profiles are characterized by low SP (av. -101.8) and GR (95.5) values and high induction-log resistivity (av. 5.4) values (Fig.16 – cores A9, A10). The seismic signature is characterized by strong amplitude, interpreted as product of the heterogeneous cementation along Sequence D1 (Fig. 4). Main diagenetic phases are shown in Figure 15b.

8. InfClaysA (well A, Seq. D3) petrofacies consists of coarse-grained, poorly-sorted arkoses, characterized by conspicuous coatings (av. 7.7%) of mechanically infiltrated smectite clays (cf. Moraes & De Ros, 1990; Moraes & De Ros, 1992), which inhibited later cementation (Fig. 11f). This resulted in compacted sandstones with relatively small intergranular porosity values (10.7%). The log signature of this petrofacies is characterized by low SP -GR and induction-log resistivity values (Fig.16 – core A14). No specific seismic signature was recognized for this petrofacies. The main diagenetic phases are shown in Figure 15c.

9. DoloRimA (well A, Seq.D3) petrofacies consists of coarse-grained, well-sorted arkoses, characterized by thick and continuous cryptocrystalline dolomite rims (Fig. 15c), probably formed by replacement of a precursor high-Mg calcite marine cement), covered by microcrystalline pore-lining dolomite (Fig. 10b). Some poorer-sorted samples show less grain-rimming dolomite and abundant, (locally displacive) intergranular pore-filling coarsely-crystalline dolomite cementation (Fig. 10c), reflected in small values of intergranular volume and porosity (Fig. 14). The log signature of this petrofacies is characterized by low SP (av. -117.2) and induction-log resistivity (av. 1.5) values, and moderate GR (124.0) values. No specific seismic signature was recognized for this petrofacies.

10. MicrCalcA (well A, Seq. D4) petrofacies consists of medium-grained, poorly sorted arkoses, characterized by eogenetic calcite cementations continuous microcrystalline rims , and as coarsely-crystalline, intergranular pore-filling, cement. The locally displacive and patchy nature of this calcite cement (Fig. 10e) is evidenced by floating grains and by relatively high intergranular porosity values (av. 14.67%). No specific log and seismic signatures were recognized for this petrofacies. However, seismic signature is characterized by less seismic impedance contrast than hybrid arenite petrofacies (discussed below), probably reflecting less-cemented conditions (Fig. 4). The main diagenetic phases are shown in Figure 15b.

11. CalcHA (well A, Seq. D4) petrofacies consists of fine-grained, poorly to very poorly sorted hybrid arenites (*sensu* Zuffa, 1980), with high content (up to 30%) of intrabasinal carbonate grains, consisting of micritized bioclasts, ooids and carbonate intraclasts. This petrofacies is characterized by early microcrystalline calcite rims (probably after an aragonite or high-Mg calcite marine cement), followed by pervasive epitaxial calcite overgrowths on echinoid bioclasts (Fig. 11a), which obliterated almost totally the original porosity (< 5%). The log signature of this petrofacies is characterized by a box pattern, with low SP (av. -

132.4) and GR (av. 45.2) values, and high induction-log resistivity (av. 11.6) values, reflecting the high carbonate/siliciclastic sand ratio. Seismic signature is characterized by high amplitude contrast due to intense cementation (Fig. 4). The main diagenetic phases are shown in Figure 15a.

12. CmpctOoGr (well C, Seq.D3) petrofacies consists of calcarenites, with high content (av. 57%) of intrabasinal carbonate grains (micritized bioclasts, ooids and intraclasts), and coarse-grained, moderately sorted, quartz-feldspathic extrabasinal sand (av. 16%). This petrofacies is characterized by less intense early cementation than CalcHA samples, showing stronger compaction (lower IGV), reflected by concave/convex grain contacts (Fig. 10f). The less pervasive pore-filling cementation resulted in slightly larger macroporosity values than CalcHA petrofacies (8.3%). The log signature of this petrofacies is similar to CalcHA petrofacies, with exception of relatively lower induction-log resistivity (av. 2.3) values, probably reflecting the more limited cementation (Fig. 7). The seismic signature is characterized by high amplitude contrasts, attesting the high carbonate content. The main diagenetic phases are shown in Figure 15c.

13. PoorCemMet (well B, Seqs. R2 and D4) petrofacies consists of medium- to coarse-grained (in places conglomeratic), poorly to moderately sorted lithic arkoses to feldspathic litharenites, characterized by lack of significant intergranular pore-filling cementation phases, showing moderate to high intergranular porosity values (av. 16.8%; Fig. 17c). The surprisingly limited deformation of sedimentary and low-grade metamorphic rock fragments of the feldspathic litharenites resulted in substantial macroporosity preservation (Fig. 17e), and loose to moderate packing (Fig. 17d). Intragranular, moldic and oversized pores formed by the dissolution of feldspars, heavy minerals and metamorphic rock fragments are locally observed. The log signature of this petrofacies is characterized by an irregular (high frequency oscillation) pattern of low SP (av. -141.9) values and low to moderate induction-log resistivity (av. 3.3) values (Fig.16 – core B19). The main diagenetic constituents (Fig. 15c) include thin and isopachous smectite coatings (Fig. 11e), which are locally thicker around completely dissolved grains (possibly heavy minerals). One available petrophysical data indicate high total porosity (26.7%), similar to petrographic macroporosity (indicating minor to absent microporosity), and high permeability (222mD).

14. DoloAHA (well B, Seq.D2 and D4) petrofacies consists of medium-grained, poorly sorted arkoses or conglomeratic hybrid arenites with up to 25% of intrabasinal carbonate grains. Extrabasinal grains (av. 57.3%), comprise high content of detrital biotite. This petrofacies is characterized by eogenetic, pervasive dolomitization, as intergranular microcrystalline pore-filling and/or grain-replacive (mud intraclasts and pseudomatrix) cementation (Fig. 10a), resulting in complete obliteration of primary porosity (< 1%). Centimetre-size carbonate bioclasts and oncoliths (Fig. 17f) are replaced by coarsely-crystalline dolomite (up to 0.9mm rhombs) and lamellar anhydrite (up to 3.5mm). The log signature of this petrofacies shows similar values than CalcHA petrofacies, being characterized by an irregular and low SP (av. -142.0) values, probably due to varying carbonate/siliciclastic sand ratio, and high induction-log resistivity (av. 19.7) values, reflecting the intense cementation (Fig.16 – cores B12, B19).

One available petrophysical data indicate total porosity value of 10% higher than macroporosity, suggesting significant microporosity contained in the microcrystalline dolomite cementation. Permeability value of 0.1mD attests the intense primary porosity occlusion and poor connection of remaining pore network. The main diagenetic phases are shown in Figure 15a.

Reservoir petrofacies as a tool for reservoir quality prediction

The reservoir quality of studied sandstones, evaluated by their reservoir petrofacies characteristics, reflects the nature of their facies associations, sequence stratigraphic-related diagenetic evolution, depth of burial and tectonic setting. Compaction and cementation were both important in porosity reduction for most system tracts (Fig. 14). The petrofacies characterization, however, highlights the main factors affecting their reservoir quality.

Rift sequences petrofacies are poorly differentiated by logs and seismic profiles (Figs. 4, 5), probably owing to subtle petrophysical and geophysical proprieties variations and/or reduced thicknesses, below seismic resolution (rift CemA samples, for instance). Furthermore, all petrofacies of rift sequences (mainly CmpctMica and PoarsCoars) show compaction as the main process in porosity reduction, which is interpreted as product of intense sediment accumulation rates, resulting in unfavourable conditions for significant eodiagenetic cementation (cf. De Ros, 1996). Consequently, primary composition is the key factor for reservoir quality.

The petrofacies of rift sequences may be separated into two groups, according to their macroporosity values (Figs. 14, 18). A first group, comprising better-sorted, mica-poor FineA samples, with lack of ductile grains, and PoarsCoars and MudClastA samples, mainly corresponding to channel-fill related deltaplain to braided facies, enriched in rigid and stable grains. These petrofacies show high macroporosity values (8 to 19%; av. 13.7%), locally favoured by the presence of Mg-chlorite and corrensite coatings, which probably inhibited subsequent quartz cementation by shielding nucleation sites (cf. Bloch et al., 2002). A second group, comprising poorer-sorted CmpctMica samples, enriched in ductile grains, such as micas and low-rank metamorphic rock fragments, is mainly associated with lower energy settings (shallow/small channels, delta-front to prodelta facies, or overbank and floodplain sediments). This petrofacies, despite similar moderate packing of rigid grains, shows low macroporosity values (3 to 20%; av. 9.7%) due to more intense compaction of ductile grains (Figs. 11d, 13e), and consequently poor reservoir quality. Furthermore, the filling of intergranular pores by massive pore-filling chlorite or I-S aggregates, locally containing Ti-oxides, interpreted as product of pervasive transformation of pseudomatrix derived from the compaction of mud intraclasts, altered metamorphic rock fragments or ferromagnesian heavy mineral grains (Figs. 12f, 13b), as well as the chlorite or illite-smectite rims, contributed to permeability reduction and increased microporosity.

The conspicuous pore-lining and pore-filling chlorite and I-S cementation of CmpctMica samples is herein interpreted as favoured by eodiagenetic precipitation of precursor smectite clay coatings (Fig. 13a), probably as a

product of alteration of ferro-magnesian silicates, such as biotite (cf. Bjorlykke et al., 1989), mud intraclasts, heavy minerals and low-rank metamorphic rock fragments. Conversely, PorsCoars samples, with minor content of such detrital constituents, show scarce clay cementation.

The stratigraphic location of CemA petrofacies above SB1 and below SB4 in well A (Fig. 4) suggests that SB1 and SB2/3 unconformities may have acted as a possible pathway of mesodiagenetic anhydrite-precipitating fluids, with flow enhancement along the more permeable channel-related facies. However, SB1 is a key surface for reservoir quality prediction for rift sequences in areas with provenance similar to well A, considering the distribution of ductile grains, because it separates poor reservoir quality intervals (porosity < 12% and low permeability) of Sequence R1 from overlying Sequences R2 and D1, with larger porosity (12 to 20%) and permeability values, plotting as two separated clusters: tight compaction-dominated and porous compaction and cementation-dominated clusters (Fig. 14).

Conversely to what is observed in well A, the transition of sequences R1 to R2 in well B shows an opposite trend regarding the lithic content (Fig. 6). Sequence R2 (poorly preserved) is characterized by PoorCemMet samples, showing an anomalously high porosity preservation values for a feldspathic litharenite with high content of ductile grains (Fig. 17e). This porosity preservation is herein interpreted as product of limited burial of Sequence R2 in well B area. The Tmax value of 427°C and thermal alteration index of 2.8 of Aptian sediments up to 1000 m below the interval of the PoorCemMet petrofacies corroborate the interpretation of limited burial for these samples (Petrobras unpublished internal report). There is no evidence of a partial cementation that may have inhibited the compaction of this petrofacies, and overpressure is an unlikely mechanism in the sandy succession considered.

The sample of CemA petrofacies in Sequence T (well C), associated with late highstand deltafront-deltaplain sediments overlain by supratidal coastal sabkha deposits, shows substantial porosity reduction by eogenetic felted anhydrite and microcrystalline dolomite cements (Fig. 11b). This characteristic is interpreted as a product of intense evaporitic conditions towards the top of the sequence (Fig. 19). Early character of the cementation is attested by the high intergranular volume and low macroporosity values of this sample, which plots in the tight cementation-dominated cluster of Fig. 14.

The interpreted shallowing-upward facies succession of Sequence D1 shows an upward increase in cementation (Fig. 19), mainly by mesodiagenetic pore-filling anhydrite. This is fairly correlated with the seismic pattern (Fig. 4), which shows strong amplitude reflections, corresponding to the variable content of cement (alternation of CemA and PorsCoars samples), contrasting with the minor seismic impedance of the poorly-cemented NonCemA petrofacies. The good match of reservoir petrofacies with seismic signature suggests that the seismic profile can be used here as a good porosity indicator, conversely to what was observed in the rift sequences. The nodular distribution of anhydrite cementation (Fig. 13f) promotes a more intense impact on porosity reduction than on permeability.

Despite undistinguishable by their seismic signature, the cemented intervals of Sequence D1 (CemA and MicrDoloA samples) can be differentiated by their log signatures, which allow a fair distinction between poorly and pervasively cemented intervals (Fig. 4). The interpreted progradation of deltafront to deltaplain (SDlsh/SDush) facies, possibly grading upward to fluvial braided deposits, is show by a typical coarsening-upward GR log trend. This allows the identification of MicrDoloA samples preferentially associated with deltafront (upper to lower-shoreface) sandstones, whereas CemA samples are preferentially associated with coarser-grained delta plain to possibly fluvial braided deposits. Deltafront (upper to lower-shoreface) sandstones had a poor depositional reservoir quality, due to the admixing of sand and mud through bioturbation. Their reservoir quality was further decreased by preferential cementation by eodiagenetic microcrystalline and mesodiagenetic coarsely-crystalline dolomite, what corresponds to low induction-log resistivity values. Coarser-grained deltaplain sandstones, which had larger original porosity and permeability, were preferentially percolated by fluids responsible for late anhydrite cementation (Fig. 11c), resulting in poorer reservoir quality (Fig. 19). Such samples plot in the tight mixed/compaction-cementation-dominated cluster of Figure 14, showing high induction-log resistivity values.

The lowstand system tract deposits of Sequence D2, characterized by InfClaysA petrofacies, are represented by fluvial braided deposits with high depositional permeability. These deposits suffered, however, abundant mechanical infiltration of detrital smectitic clays under subaerial, hot and arid depositional conditions (cf. Moraes & De Ros, 1992), as irregular coatings (Fig. 11f). The early clay infiltration prevented later cementation, what resulted in intense mechanical compaction (Fig. 14), and in deteriorated reservoir quality (Fig. 20).

The transgressive system tracts of drift Albian sequences D2 to D4 in well A show increasing induction-log resistivity values towards the vicinity of the interpreted condensed sections (Fig. 4). This trend is interpreted as a product of increasing eodiagenetic carbonate cementation, and consequently reservoir quality deterioration in response to increasing influence of marine pore-waters and to the source and nucleation provided by the larger amount of carbonate intrabasinal grains (cf. Morad et al., 2000; Ketzer et al., 2002; Ketzer et al., 2003b; Al-Ramadan et al., 2006). This trend can be observed in MicrCalcA to CalcHA petrofacies (Fig. 20), and is characterized by decreasing of SP-GR values (Fig. 4).

The increase of induction-log resistivity values and of seismic impedance contrast (seismic horizons with high amplitudes), with typical amplitude saturation, at the top of carbonates corresponds to the increase of density and sonic velocity at the carbonate-rich intervals (Fig. 4), vividly contrasting with adjoining siliciclastic-dominated intervals.

MicrCalcA petrofacies, associated with high-energy, siliciclastic-dominated, transgressive deltaic (SDush) settings, show scattered nodular, displacive calcite cementation, which helped to preserve large intergranular volumes,

plotting in the porous mixed/cementation-compaction-dominated cluster of Figure 14. High-energy, carbonate-dominated settings are characterized by the CmpctOoGr petrofacies, showing low, and high content of ooids (Fig. 10f) and ooid aggregates. The subordinate content of extrabasinal grains is mostly coarse-grained and well-sorted. The limited abundance of early carbonatic pore-lining and pore-filling cementation is probably related to a more distal position regarding the condensed section. This resulted in stronger compaction.

Conversely to high-energy deposits, CalcHA and DoloAHA, associated with low-energy, carbonate-dominated, internal platform, lagoonal or estuarine settings, show a more pervasive carbonate cementation. CalcHA samples show intense stratabound microcrystalline rims and epitaxial calcite cementation, plotting in the tight mixed/cementation-dominated cluster (Fig. 14). DoloAHA petrofacies show poor reservoir quality due to pervasive, eodiagenetic, intergranular, microcrystalline dolomite cementation (Figs. 10a), plotting in the tight mixed/cementation-dominated cluster (Fig. 14).

PoorCemMet petrofacies of Sequence D4 (well B), likewise Sequence R2 (well B) samples, are characterized by a siliciclastic-dominated succession, with high content of low-grade metamorphic and sedimentary rock fragments. Despite this, they show good macroporosity (13 to 22.7%; av. 16.8%) values (Figs. 17c, 17d), interpreted as product of limited burial, plotting in the porous compaction-dominated cluster (Fig. 14).

The Siliciclastic-dominated highstand intervals of Albian drift sequences D2 to D4 (Fig. 20) are characterized by DoloRimA petrofacies (well A), with good to moderate reservoir quality, resulted from early cementation by thick dolomite rims (probably replacing a precursor marine cement), inhibiting compaction (Fig. 10b). Local eodiagenetic pore-filling cementation resulted in porosity deterioration (Fig. 10c). Better-sorted samples, interpreted as product of wave-reworking by longshore currents, show less intergranular pore-filling cementation (i.e. better reservoir quality) than poorer-sorted samples. These samples plot in porous compacted/mixed cluster (Fig. 14).

CONCLUSIONS

The spatial and temporal distribution of eodiagenetic alterations (and associated mesodiagenetic processes), as well as their impact on the reservoir quality of the studied Jequitinhonha Basin sandstones, hybrid arenites and calcarenites can be constrained within a sequence-stratigraphic framework. The stratigraphic evolution, related tectonic settings and depositional systems (i.e. sedimentary facies) played an important role on the diagenetic evolution.

The rift phase sediments, deposited in deep, asymmetric half-grabens under active tectonism, consist of braided fluvial and lacustrine-deltaic deposits, which present variable composition and maturity (i.e. ductile grains content) interpreted as resulted from diverse relative position to basin margin faults and distinct source terrains.

The transitional to drift phase sediments, on the other hand, shows the interplay of the simultaneous supply of poorly-sorted, coarser-grained proximal siliciclastic and/or evaporite deposits and shelf hybrid arenites and calcarenites. The former reflect rapid erosion and transportation from elevated source-areas, under arid or semiarid climate. The later correspond to lower-energy internal platform and higher-energy shoal systems of a carbonate ramp. Such complex depositional environment shows variable depositional porosity values and eodiagenetic patterns, mainly reflecting variations in the intrabasinal carbonate content and climatic conditions.

Despite the complexity of diagenetic patterns studied, the characteristics of each reservoir petrofacies reflect the strong influence of depositional processes and eodiagenesis, resulting in distinct reservoir quality, which have been recognized along the stratigraphic succession.

The heterogeneous fluvial-deltaic deposits of rift sequences were characterized by the combination of petrofacies CmpctMica and FineA, defined by their differential detrital composition, resulting in the increased compactional porosity and permeability deterioration of the micaceous petrofacies. Such differentiation allows better reservoir quality estimation for Sequence R1 in well B area.

Reservoir quality distinction between fluvial-deltaic deposits of rift sequences R1 and R2 of well A were also characterized by the distinction among CmpctMica and PorsCoars petrofacies, which were defined by their texture and content of ductile grains (micas and metamorphic rock fragments), with resulting diagenetic alterations. The influence of compaction on porosity and permeability reduction was more important in the fine-grained, lower-energy sandstones, owing to their larger content in micaceous grains, than the coarse-grained channel sandstones.

The distinct trends along SB1 in wells A and B reflect the complex provenance and drainage pattern of sediment inflow to a rift basin, attesting the importance of reservoir petrofacies characterization for porosity prediction in such complex scenarios.

Depositional features, such as detrital composition and texture, influenced the course of diagenetic evolution, determining the degree of interconnectivity between sand bodies, fluid flow pathways and rates. The limited anhydrite cementation in MicrDoloA (larger mud content) relative to CemCoarsA petrofacies is attributed to fluid flow restriction.

The match of seismic amplitude and resistivity-log patterns with cement content and cement-type, respectively, detected in petrofacies NonCemA, MicrDoloA and CemCoarsA of highstand system tract of Sequence D1 (well A) attests the utility of reservoir petrofacies as a tool for reservoir quality prediction.

Increasing carbonate intrabasinal content, corresponding to the onset of the mixed siliciclastic-carbonate platform depositional setting, is observed in the Albian drift sequences, with consequent increased impact on the distribution of eodiagenetic dolomite and calcite cements. This is recognized by observing the

reservoir petrofacies interpreted as transgressive system tract deposits, such as MicrCalcA towards CalcHA (i.e. towards condensed sections). The aid of seismic amplitude and resistivity-log patterns allowed the recognition of such stratabound carbonate cementation.

This paper demonstrates that *reservoir petrofacies concept* is a powerful tool for modelling the distribution of depositional-related diagenetic processes that control reservoir quality.

ACKNOWLEDGEMENTS

The authors thank PETROBRAS, in special M. V. Galvão, A. Grassi, J. A. Cupertino and Paulo de Tarso Guimarães, for access to samples, data, information, and for the license to publish this work. We acknowledge the support of the Institute of Geosciences of Rio Grande do Sul Federal University – UFRGS, and the Environmental Institute of the Pontifical Catholic University of Rio Grande do Sul - PUC-RS. Suggestions by reviewers ..... and ..... helped to improve the manuscript. Special thanks to Dr S. Morad, from Uppsala University, for improving the original manuscript. K. Goldberg, C.M. Scherer and L.A.C. Lopez are also acknowledged for commenting on previous versions of the manuscript and its illustrations.

REFERENCES

AL-RAMADAN, K., 2006. Impact of diagenetic alterations on reservoir quality and heterogeneity of paralic and shallow marine sandstones: link to depositional facies and sequence stratigraphy. Acta Universitatis Upsaliensis, Digital Comprehensive Summaries of Uppsala Dissertations from the Faculty of Science and Technology 195, 57pp.

ASMUS, H.E. and PONTE, F.C., 1973. The Brazilian marginal basins. In: NAIRM, A.E.M. and STEHILI, F.G. (Eds.): The ocean basins and margins. New York, Plenum, v.1, 87-133.

BEARD, D.C. and WEYL, P.K., 1973. Influence of texture on porosity and permeability of unconsolidated sand. *AAPG Bull.*, 57, 349-369.

BHATTACHARYA, J.P., 2006. Deltas. In: POSAMENTIER, H.W., WALKER, R.G. (Eds.): Facies models revisited. *SEPM Spec. Publ.*, **84**, 237-292.

BLOCH, S., LANDER, R.H., and BONNELL, L., 2002. Anomalously high porosity and permeability in deeply buried sandstone reservoirs: Origin and predictability. *AAPG Bull.*, 86, 301-328.

CAINELLI, C and MOHRIAK, W.U., 1999. Some remarks on the evolution of sedimentary basins along the Eastern Brazilian continental margin. Episodes, 22 (3), 206-216

CHANG, H.K., KOWSMANN, R.O. and FIGUEIREDO, A.M.F., 1988. New concepts on the development of East Brazilian marginal basins. *Episodes*, 11 (3), 194-202.

COLLINGS, J.D., 1996. ALLUVIAL SEDIMENTS. In: READING, H.G. (Ed.): Sedimentary environments: processes, facies and stratigraphy, London, Blackwell, p. 37-82.

CÓRDOBA, V.C., 1994. The Development of an Albian-Cenomanian Carbonate ramp as a first marine record in the Jequitinhonha Basin In: 14th International Sedimentological Congress, Recife, Abstracts, 2pp.

DE ROS, L.F.S., MORAD, S. and PAIM, P.S.G., 1994. The role of detrital composition and climate on the diagenetic evolution of continental molasses: evidence from the Cambro-Ordovician Guaritas Sequence, southern Brazil. *Sed. Geol.*, 92, 197-228.

DE ROS, L.F., 1996. Compositional controls in sandstones diagenesis. Acta Universitatis Upsaliensis, Comprehensive Summaries of Uppsala Dissertations from the Faculty of Science and Technology 198, 24pp.

DE ROS, L.F., REMUS, M.V.D., VIGNOL-LELARGE, M.L.M., CHEMALE JR., F. and BAITELLI, R. (2005) Sandstone provenance of BM-J-3 Block, Jequitinhonha Basin, BA. Petrobras-Statoil unpublished report.

DE ROS, L.F., GOLDBERG, K., 2007. Reservoir petrofacies: a tool for quality characterization and prediction, AAPG Annual Conference and Exhibition: The American Association of Petroleum Geologists, Long Beach, CA, USA, Extended Abstracts CD, 6pp.

DE ROS, L.F., GOLDBERG, K., ABEL, M., VICTORINETTI, F., MASTELLA, L. and CASTRO, E., 2007. Advanced Acquisition and Management of Petrographic Information from Reservoir Rocks Using the PETROLEDGE® System. AAPG Annual Conference and Exhibition. The American Association of Petroleum Geologists, Long Beach, CA, USA, Extended Abstracts CD, 6pp.

DICKINSON, W. R., 1985. Interpreting provenance relations from detrital modes of sandstones. In: ZUFFA, G. G. (Ed.): Provenance of Arenites. *NATO Advanced Science Series C*, 148, 333-361.

EHRENBERG, S.N., 1989. Assessing the relative importance of compaction processes and cementation to reduction of porosity in sandstones: discussion; Compaction and porosity evolution of Pliocene sandstones, Ventura Basin, California: discussion. *AAPG Bull.*, 73, 1274-1276.

FOLK, R.L., 1968. Petrology of sedimentary rocks. Austin, Texas, Hemphill's Pub., 107pp.

GALLOWAY, W.E. and HOBDAY, D.K., 1983. Terrigenous clastic depositional systems: applications to petroleum, coal, and uranium exploration. Springer-Verlag Inc., Heidelberg, 489pp.

JARDIM, C.M, KETZER, J.M. and DE ROS, L.F., (submitted). Depositional controls on the diagenetic patterns of Lower Cretaceous sandstones from the Jequitinhonha Basin, Eastern Brazil, Sedimentology, 25pp.

JOHNSON, H.D. and BALDWIN, J.T., 1996. Shallow clastic seas, In: Reading, H.G. (Ed.): Sedimentary environments: processes, facies and stratigraphy, London, Blackwell, 232-280.

KENDALL, A.C. and HARWOOD, G.M., 1996. Marine evaporates: arid shorelines and basins, In: Reading, H.G. (Ed.): Sedimentary environments: processes, facies and stratigraphy, London, Blackwell, 281-324.

KETZER, J.M., MORAD, S., EVANS, R. and AL-AASM, I.S., 2002. Distribution of diagenetic alterations in fluvial, deltaic and shallow marine sandstones within a sequence stratigraphic framework: evidence from the Mullaghmore Formation (carboniferous), NW Ireland. *J. Sed. Res.,* 72 (6), 760-774.

KETZER, J. M., MORAD, S. and AMOROSI, A., 2003a. Predictive diagenetic clay-mineral distribution in siliciclastic rocks within a sequence stratigraphic

framework. In: WORDEN, R. and MORAD, S. (Eds.): Clay Mineral Cementation in Sandstones, *Int. Assoc. Sedimentol. Spec. Publ.,* 34, 42-59.

KETZER, J.M., HOLZ, M. and MORAD, S., 2003b. Sequence stratigraphic distribution of diagenetic alterations in coal-bearing, paralic sandstones: evidence from the Rio Bonito Formation (early Permian), southern Brazil. *Sedimentology*, 50, 855-877.

KÜCHLE, J., HOLZ, M., BRITO, A.F. and BEDREGAL, R.P., 2005. Análise estratigráfica de bacias rifte: aplicação de conceitos genéticos nas bacias de Camamu-almada e Jequitinhonha (Tr. Stratigraphic analysis of rift basins: applications of genetic concepts in Camamu-Almada and Jequitinhonha basins). *Boletim de Geociências da Petrobrás*, 13(1), 227-244.

KUMAR, N. and GAMBOA, L.A.P., 1979. Evolution of the São Paulo plateau (southeastern Brazilian margin) and the implications for the early history of the South Atlantic. *Geol. Soc. Am. Bull.,* 90, part 1, 281-293.

LOMANDO, A.J. and HARRIS, P.M., 1991. Mixed Carbonate-Siliciclastic Sequences (Eds.), Dallas, TX, SEPM (Society for Sedimentary Geology), 569pp.

MIALL, A. D., 1996. The geology of fluvial deposits: sedimentary facies, basin analysis and petroleum geology. Springer-Verlag Inc., Heidelberg, 582pp.

MORAES, M.A.S. and L.F. De Ros, 1990. Infiltrated clays in fluvial Jurassic sandstones of Reconcavo basin, northeastern Brazil. *J. Sed. Petrol.*, 60, 809-819.

MORAES, M.A.S. and DE ROS, L.F., 1992. Depositional, infiltrated and authigenic clays in fluvial sandstones of the Jurassic Sergi Formation, Reconcavo basin, northeastern Brazil. *SEPM Spec. Publ.*, 47, 197-208.

MORAD, S., KETZER, J.M. and DE ROS, L.F., 2000. Spatial and temporal distribution of diagenetic alterations in siliciclastic rocks: implication for mass transfer in sedimentary basins. *Sedimentology*, 47, 95-120.

OJEDA, H.A., 1982. Structural framework, stratigraphy and evolution of Brazilian marginal basins. *AAPG Bull.,*, 66, 732-749.

POSAMENTIER, H.W. and ALLEN, G.P., 1993. Variability of the sequence stratigraphic model: effects of local basin factors. *Sed. Geol.*, 86, 91-109.

READING, H.G. and Collins, J.D., 1996. Clastic coasts, In: Reading, H.G. (Ed.): Sedimentary environments: processes, facies and stratigraphy, London, Blackwell, 154-231.

SHEW, R. D., 1991. Upward-shoaling sequence of mixed siliciclastics and carbonates from the Jurassic Smackover Formation of Central Mississippi, In: LOMANDO, A. J. and HARRIS, P. M. (Eds.): Mixed Carbonate-Siliciclastic Sequences, Dallas, TX, SEPM (Society for Sedimentary Geology), 135-167.

VAN WAGONER, J. C., MITCHUM, R. M., CAMPION, K.M. and RAHMANIAN, V.D., 1990. Siliciclastic sequence stratigraphy in well logs, cores and outcrops: concepts for high resolution correlation of time and facies. AAPG Methods in Exploration Series, 7, 55pp.

WALKER, R.G., 1992. Facies, facies models and modern stratigraphic concepts. In: WALKER, R.G. and JAMES, N.P. (Eds.): Facies models: Response to sea level change. Geological Association of Canada, 1-14.

WRIGHT, V.P. and BURCHETTE, T.P., 1996. Shallow-water carbonate environments. In: READING, H.G. (Ed.): Sedimentary environments: processes, facies and stratigraphy, London, Blackwell, 325-394.

ZUFFA, G. G., 1980, Hybrid arenites: their composition and classification. *J. Sed. Petrol.*, 50, 21-29.

FIGURE CAPTIONS

Figure 1. Location map of the studied wells and stratigraphic summary of Jequitinhonha sedimentary basin (source Brazilian National Petroleum Agency).

Figure 2. Wireline log (gamma-ray and spontaneous potential) correlation cross-section of studied wells (Jardim et al., submitted), with indication of depositional sequences and sequence boundaries (cored intervals not to scale).

Figure 3. Selected cores with identified facies associations and reservoir petrofacies (cores not sampled for this study were omitted here). Modified from Jardim et al. (submitted).

Figure 4. Seismic and wireline log signatures of Aptian rift and Albian drift sequences of well A, their facies associations and interpreted reservoir petrofacies (core details are shown in figure 3). Red arrows indicate interpreted fluvio-deltaic coarsening-upward successions. Modified from Jardim et al. (submitted).

Figure 5. Wireline log signatures of Aptian rift and Albian drift sequences of well B, their facies associations and interpreted reservoir petrofacies (core details are shown in figure 3). Red arrows indicate interpreted fluvio-deltaic coarsening-upward successions. Modified from Jardim et al. (submitted).

Figure 6. Compositional trends of wells A and B regarding selected diagnostic detrital and diagenetic constituents (Jardim et al., submitted).

Figure 7. Seismic and wireline log signatures of Aptian/Albian transitional and Albian drift sequences of well C, their facies associations and interpreted reservoir petrofacies (core details are shown in figure 3). Red arrows indicate interpreted fluvio-deltaic coarsening-upward successions. Modified from Jardim et al. (submitted).

Figure 8. The original detrital composition of 67 representative samples of Jequitinhonha Basin sandstones plotted on Folk (1968) classification diagram.

Figure 9. Compositional indication of the tectonic provenance setting of the studied sandstones plotted on Dickinson (1985) diagram.

Figure 10. Optical photomicrographs. A) DoloAHA petrofacies sample with intense intergranular, locally displacive, micro- to coarsely-crystalline dolomite cementation. Crossed polarizers (XP). B) and C) DoloRimA petrofacies samples with pore-lining small dolomite rhombs. Uncrossed polarizers (//P). D) MudClastA petrofacies sample with coarsely-crystalline saddle dolomite replacing precursor dolomite cement (replacing mud intraclasts) (XP). E) MicrCalcA petrofacies transgressive upper-shoreface sample with locally

displacive calcite cementation (//P). F) CmpctOoGr petrofacies sample of highstand sample with compaction of carbonate ooids and intraclasts (XP).

Figure 11. Optical micrographs and backscattered electrons (BSE) images. A) CalcHA petrofacies sample in the vicinity of condensed section (Seq. D3), with calcite overgrowths around bioclasts, and macroporosity due to limited carbonate cementation (//P). B) CemA petrofacies sample of highstand system tract of Sequence T with intergranular porosity obliteration due to eodiagenetic microcrystalline dolomite and felted anhydrite cements (XP). C) CemA petrofacies sample of highstand of Sequence D1 with intense burial anhydrite cementation and low porosity (c. 2%) (XP). D) BSE image of CmpctMica petrofacies sample with quartz outgrowths and I-S fibrous rims. E) BSE image of PoorCemMet petrofacies sample with smectite coatings around grains (thicker around possibly heavy mineral dissolved grains). F) InfClaysA petrofacies sample of the lowstand of Sequence D3 with mechanically infiltrated smectite coatings inhibiting later cementation, resulting in intense compaction and minor macroporosity preservation (c.11%) (//P).

Figure 12. Optical micrographs and backscattered electrons (BSE) images. A) PorsCoars petrofacies sample with multiple corrensite coatings, precipitated during grain dissolution, later covered by corrensite rims, favouring macroporosity preservation (//P). B to D) BSE images of the same sample with corrensite rims on both sides of coatings (thicker along intergranular side), probably from the transformation of precursor smectite coatings. E) BSE image of PorsCoars petrofacies sample with corrensite expanding micas. F) CmpctMica petrofacies sample with dissolved low-rank metamorphic rock fragment replaced by chlorite (chlorite rims and micaceous fragments) (//P).

Figure 13. Optical micrographs and backscattered electrons (BSE) images. A) BSE image of PorsCoars petrofacies sample with chlorite coatings (chloritized precursor smectite coatings?) covered by chlorite rims around dissolved grain. B) BSE image of CmpctMica petrofacies sample with Mg-chlorite rims and K-feldspar overgrowths and intergranular dickite cement (replacing pseudomatrix derived from metamorphic rock fragment dissolution and compaction). C) BSE image of CmpctMica petrofacies sample with I-S rims covering micas and quartz outgrowths). D) CmpctMica petrofacies sample with intense mechanical compaction (//P). E) BSE image of the same petrofacies with chlorite and micaceous fragments occupying intergranular (also as pseudomatrix) and intragranular (post-dissolution) pores. F) CemA petrofacies sample with late poikilotopic anhydrite cementation (//P).

Figure 14. Plot of cement volume versus intergranular volume (cf. Ehrenberg, 1989), illustrating the preferential mechanisms of porosity reduction in the studied samples.

Figures 15a to 15c. Diagrams with interpreted paragenetic evolution with main diagenetic alterations of each reservoir petrofacies.

Figure 16. Reservoir petrofacies with diagnostic log signatures associated with petrographic attributes (see text for details).

Figure 17. Optical micrographs and backscattered electrons (BSE) images. A) BSE image of PorsCoars petrofacies sample with chlorite rims covering partially dissolved garnet grain; dolomite expanding micas. B) BSE image of MicrDoloA petrofacies sample with heterogeneous macroporosity due to sorting and mud intraclast content variation; intraclasts, micas and K-feldspar overgrowths. C) PoorCemMet transgressive petrofacies sample with moderate values of macroporosity (c. 17%) (//P). D) BSE image of the same sample with minor compaction despite the high content of low-grade metamorphic fragments; early K-feldspar overgrowths. E) PoorCemMet petrofacies sample showing high content of low-rank metamorphic grains, limited compaction and anomalously high macroporosity (//P). F) DoloAHA petrofacies sample with mesodiagenetic anhydrite replacing oncoliths and intraclasts within a strongly dolomitized framework, with high biotite content (XP).

Figure 18. Schematic model showing the spatial and temporal distribution of diagenetic alterations and variations in the diagenetic evolution pathways of rift sequences sandstones. Modified from Jardim et al. (submitted).

Figure 19. Schematic model showing the spatial and temporal distribution of diagenetic alterations and variations in the diagenetic evolution pathways of Transitional and D1 sequences. Modified from Jardim et al. (submitted).

Figure 20. Schematic model showing the spatial and temporal distribution of diagenetic alterations and variations in the diagenetic evolution pathways of drift sequences. Modified from Jardim et al. (submitted).

Table 1. Facies Associations (FA) of studied Jequitinhonha Basin successions.

Table 2. Statistical summary of the petrographic parameters of studied sandstones.

FIG. 1

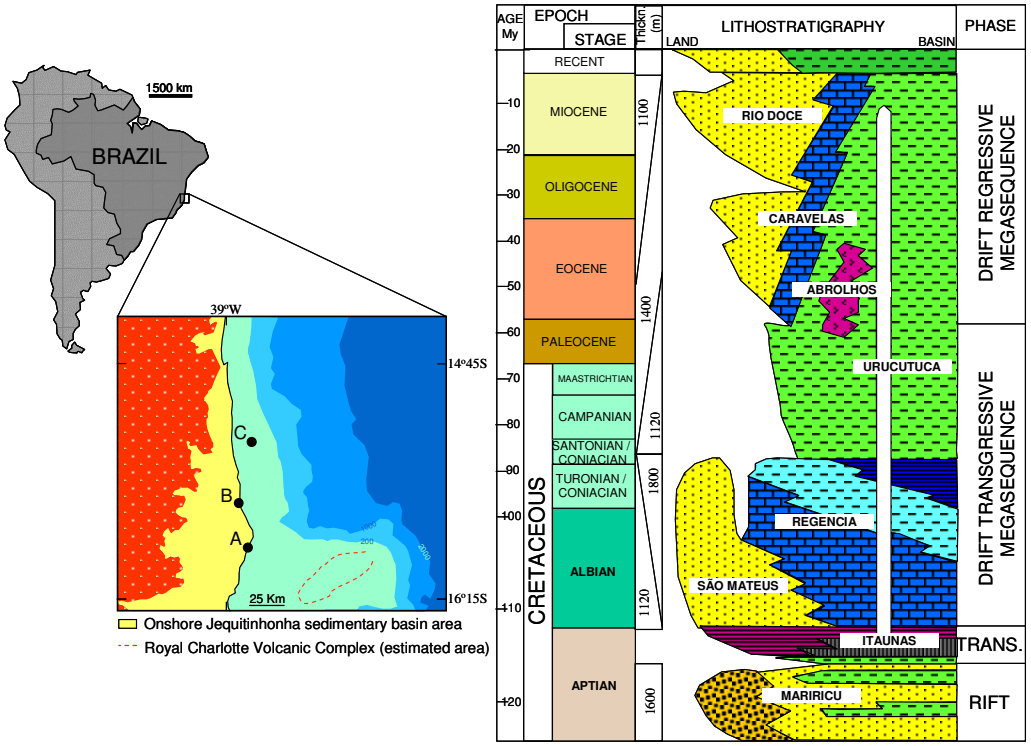
1500 km
BRAZIL
39°W
14°45S
16°15S
25 Km
A
B
C
Onshore Jequitinhonha sedimentary basin area
Royal Charlotte Volcanic Complex (estimated area)
AGE My
EPOCH
STAGE
Thickn (m)
LITHOSTRATIGRAPHY
LAND
BASIN
PHASE
RECENT
MIOCENE
OLIGOCENE
EOCENE
PALEOCENE
MAASTRICHTIAN
CAMPANIAN
SANTONIAN / CONIACIAN
TURONIAN / CONIACIAN
ALBIAN
APTIAN
CRETACEOUS
1100
1400
1120
1800
1120
1600
RIO DOCE
CARAVELAS
ABROLHOS
URUCUTUCA
REGENCIA
SÃO MATEUS
ITAUNAS
MARIRICU
DRIFT REGRESSIVE MEGASEQUENCE
DRIFT TRANSGRESSIVE MEGASEQUENCE
TRANS.
RIFT

FIG. 2

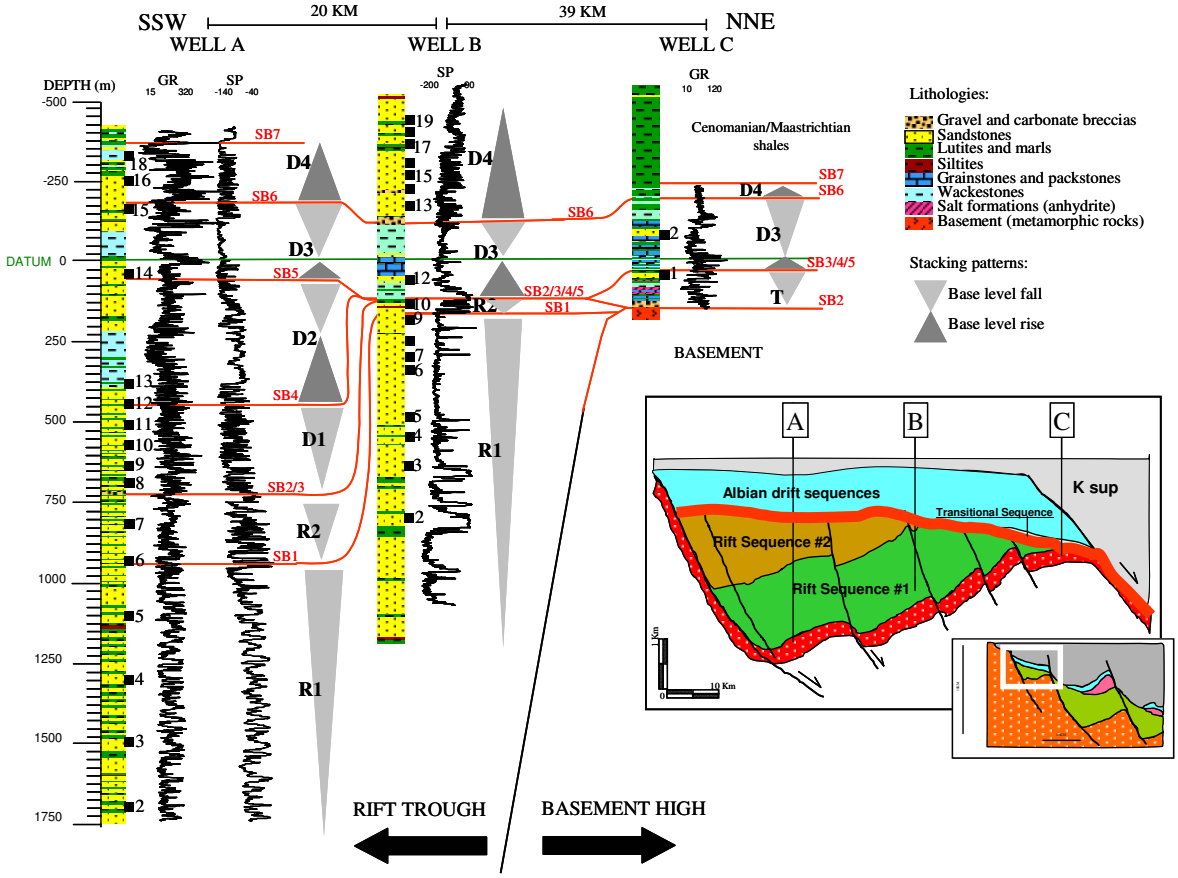
SSW
20 KM
39 KM
NNE
WELL A
WELL B
WELL C
DEPTH (m)
GR
SP
DATUM 0
SB7
SB6
SB5
SB4
SB2/3
SB1
SB2/3/4/5
SB3/4/5
SB2
D1
D2
D3
D4
R1
R2
T
Cenomanian/Maastrichtian shales
BASEMENT
RIFT TROUGH
BASEMENT HIGH
Lithologies:
Gravel and carbonate breccias
Sandstones
Lutites and marls
Siltites
Grainstones and packstones
Wackestones
Salt formations (anhydrite)
Basement (metamorphic rocks)
Stacking patterns:
Base level fall
Base level rise
A
B
C
Albian drift sequences
K sup
Transitional Sequence
Rift Sequence #2
Rift Sequence #1
10 Km

FIG. 3

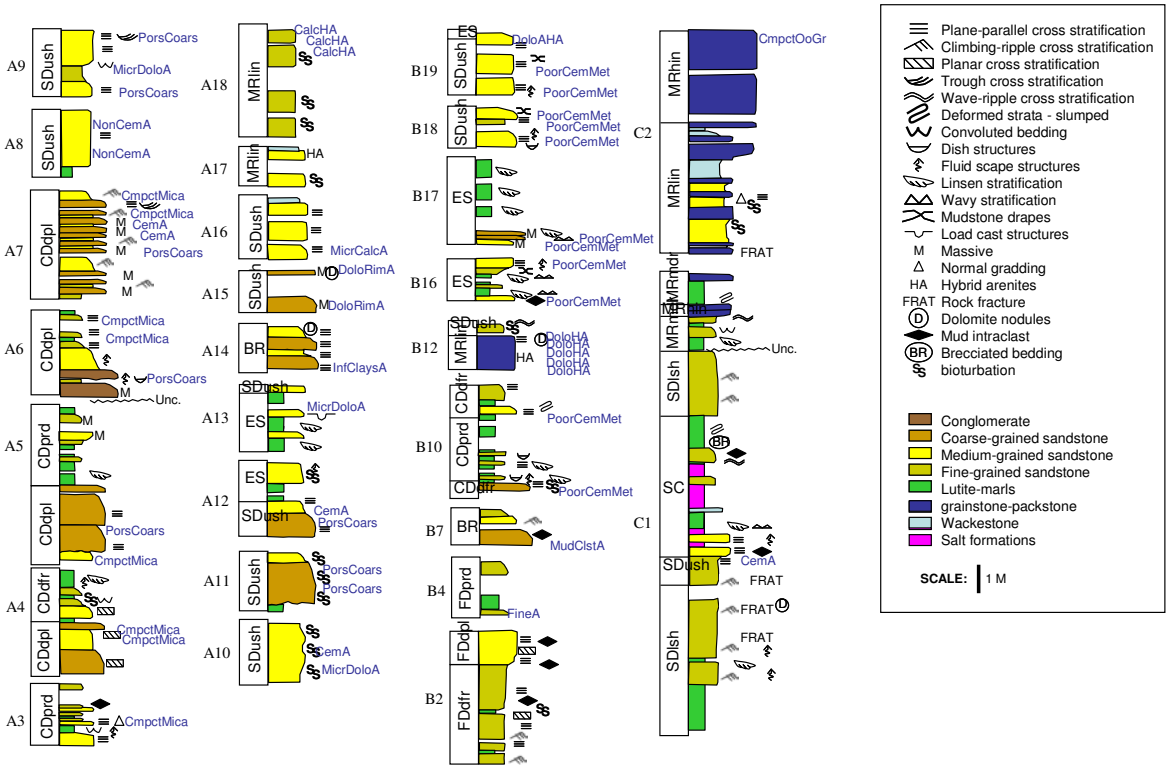
A9
SDush
PorsCoars
MicrDoloA
PorsCoars
A8
SDush
NonCemA
NonCemA
A7
CDdpl
CmpctMica
CmpctMica
CemA
CemA
PorsCoars
A6
CDdpl
CmpctMica
CmpctMica
PorsCoars
Unc.
A5
CDprd
CDdpl
PorsCoars
CmpctMica
A4
CDdfr
CDdpl
CmpctMica
CmpctMica
A3
CDprd
CmpctMica
A18
MRlin
CalcHA
CalcHA
CalcHA
A17
MRlin
HA
A16
SDush
MicrCalcA
A15
SDush
DoloRimA
DoloRimA
A14
BR
InfClaysA
A13
SDush
ES
MicrDoloA
A12
ES
SDush
CemA
PorsCoars
A11
SDush
PorsCoars
PorsCoars
A10
SDush
CemA
MicrDoloA
B19
SDush
ES
DoloAHA
PoorCemMet
PoorCemMet
B18
SDush
PoorCemMet
PoorCemMet
PoorCemMet
B17
ES
PoorCemMet
PoorCemMet
B16
ES
PoorCemMet
PoorCemMet
B12
MRlin
SDush
DoloHA
DoloHA
DoloHA
DoloHA
DoloHA
HA
B10
CDdfr
CDprd
CDdfr
PoorCemMet
PoorCemMet
B7
BR
MudClstA
B4
FDprd
FineA
B2
FDdpl
FDdfr
C2
MRhin
MRlin
MRndr
SDish
SDush
CmpctOoGr
FRAT
Unc.
BR
SC
C1
SDush
CemA
FRAT
FRAT
FRAT
SDish
Plane-parallel cross stratification
Climbing-ripple cross stratification
Planar cross stratification
Trough cross stratification
Wave-ripple cross stratification
Deformed strata - slumped
Convoluted bedding
Dish structures
Fluid scape structures
Linsen stratification
Wavy stratification
Mudstone drapes
Load cast structures
M Massive
Normal gradding
HA Hybrid arenites
FRAT Rock fracture
D Dolomite nodules
Mud intraclast
BR Brecciated bedding
bioturbation
Conglomerate
Coarse-grained sandstone
Medium-grained sandstone
Fine-grained sandstone
Lutite-marls
grainstone-packstone
Wackestone
Salt formations
SCALE: 1 M

FIG. 5

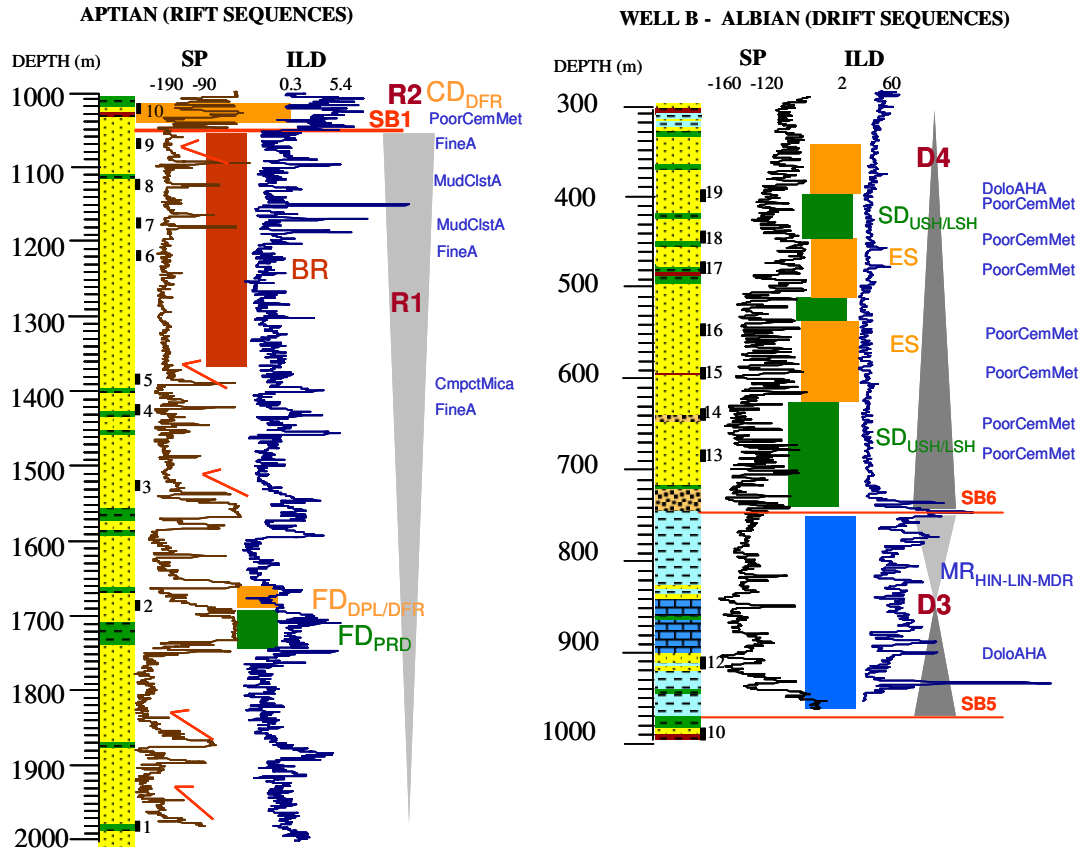
APTIAN (RIFT SEQUENCES)
DEPTH (m)
SP
-190 -90
ILD
0.3 5.4
1000
1100
1200
1300
1400
1500
1600
1700
1800
1900
2000
10
9
8
7
6
5
4
3
2
1
R2
CDDFR
SB1
PoorCemMet
FineA
MudClstA
MudClstA
FineA
BR
R1
CmpctMica
FineA
FDDPL/DFR
FDPRD
WELL B - ALBIAN (DRIFT SEQUENCES)
DEPTH (m)
SP
-160 -120
ILD
2 60
300
400
500
600
700
800
900
1000
19
18
17
16
15
14
13
12
10
D4
DoloAHA
PoorCemMet
SDUSH/LSH
PoorCemMet
ES
PoorCemMet
ES
PoorCemMet
PoorCemMet
SDUSH/LSH
PoorCemMet
SB6
MRHIN-LIN-MDR
D3
DoloAHA
SB5

FIG. 4

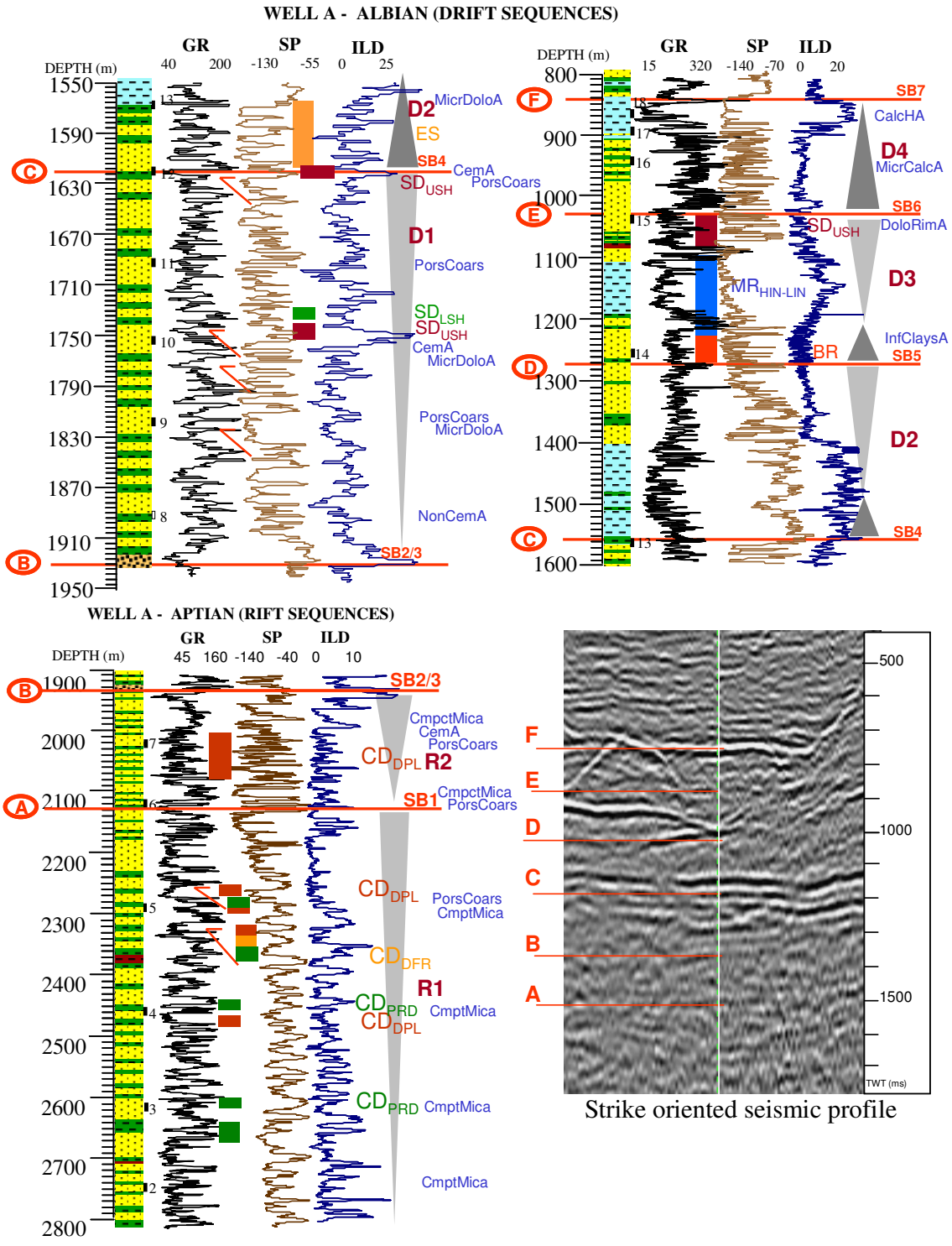

Strike oriented seismic profile

FIG. 6

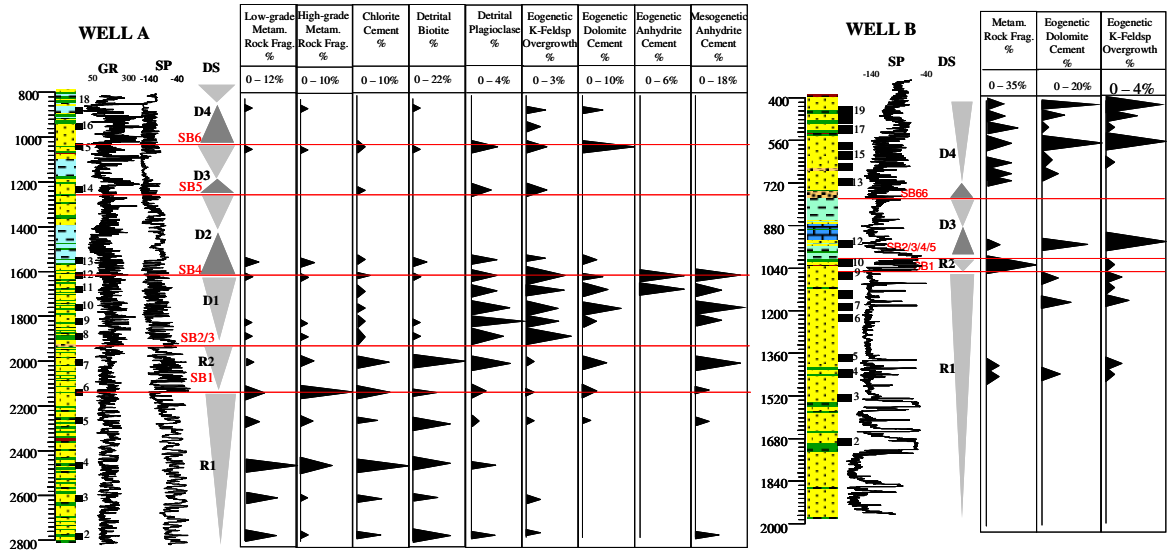
WELL A
GR
SP
DS
D4
SB6
D3
SB5
D2
SB4
D1
SB2/3
R2
SB1
R1
Low-grade Metam. Rock Frag. %
High-grade Metam. Rock Frag. %
Chlorite Cement %
Detrital Biotite %
Detrital Plagioclase %
Eogenetic K-Feldsp Overgrowth %
Eogenetic Dolomite Cement %
Eogenetic Anhydrite Cement %
Mesogenetic Anhydrite Cement %
0 – 12%
0 – 10%
0 – 10%
0 – 22%
0 – 4%
0 – 3%
0 – 10%
0 – 6%
0 – 18%
WELL B
SB66
SB2/3/4/5
SB1
Metam. Rock Frag. %
Eogenetic Dolomite Cement %
Eogenetic K-Feldsp Overgrowth %
0 – 35%
0 – 20%
0 – 4%

FIG. 7

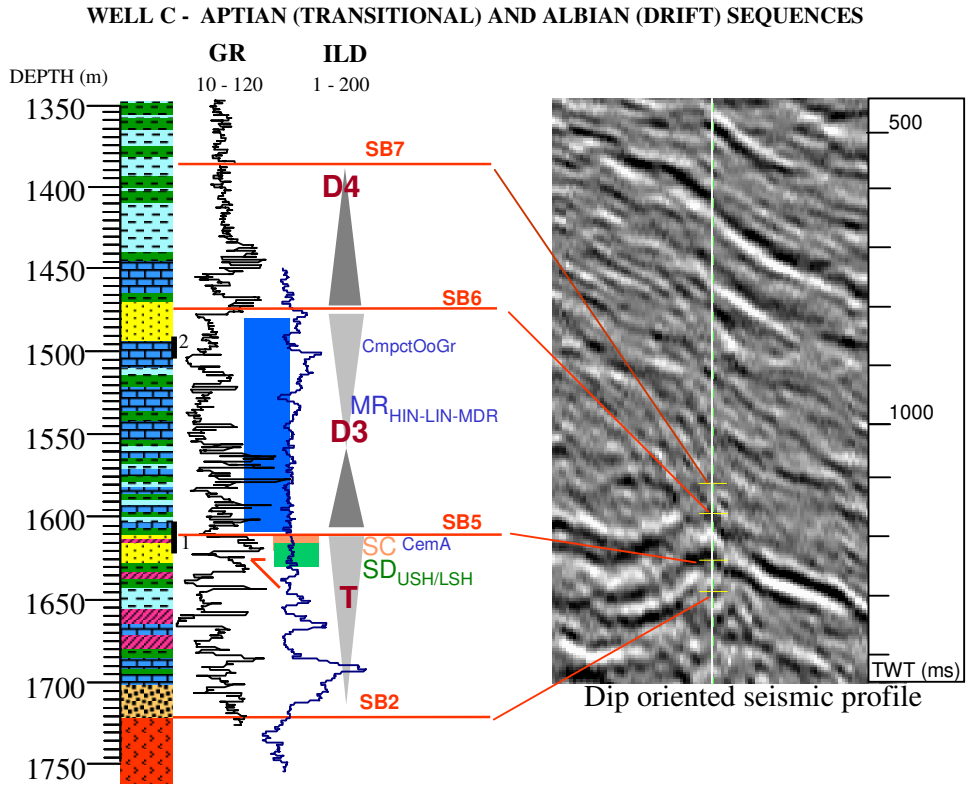
WELL C - APTIAN (TRANSITIONAL) AND ALBIAN (DRIFT) SEQUENCES
DEPTH (m)
GR
10 - 120
ILD
1 - 200
SB7
D4
SB6
CmpctOoGr
MR HIN-LIN-MDR
D3
SB5
SC CemA
SD USH/LSH
T
SB2
Dip oriented seismic profile
TWT (ms)

FIG. 8

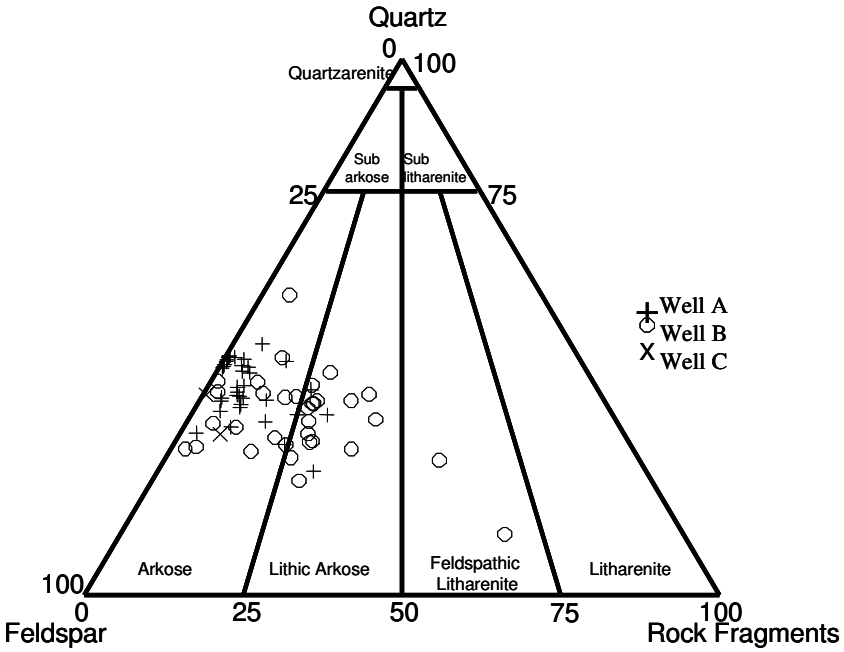
Quartz
0
100
Quartzarenite
Sub arkose
Sub litharenite
25
75
Well A
Well B
Well C
Arkose
Lithic Arkose
Feldspathic Litharenite
Litharenite
100
0
25
50
75
100
Feldspar
Rock Fragments

FIG. 9

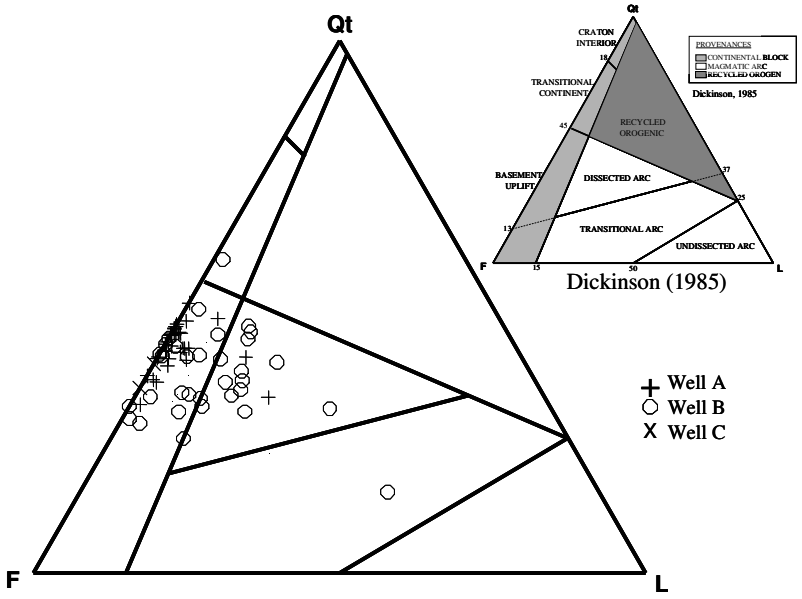
Qt
F
L
Well A
Well B
Well C
CRATON INTERIOR
TRANSITIONAL CONTINENT
RECYCLED OROGENIC
BASEMENT UPLIFT
DISSECTED ARC
TRANSITIONAL ARC
UNDISSECTED ARC
PROVENANCES
CONTINENTAL BLOCK
MAGMATIC ARC
RECYCLED OROGEN
Dickinson, 1985
Dickinson (1985)

FIG. 10

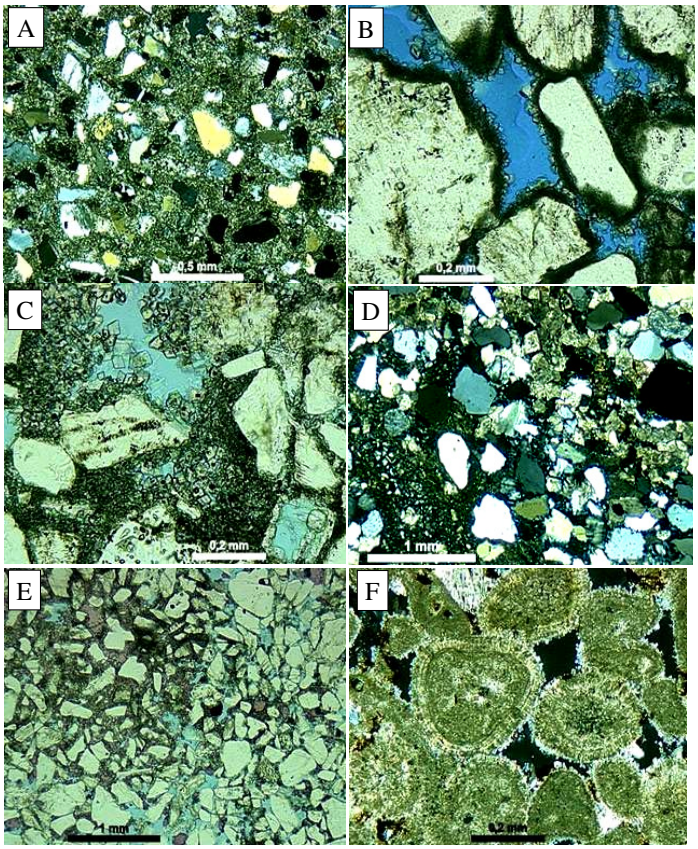

FIG. 11

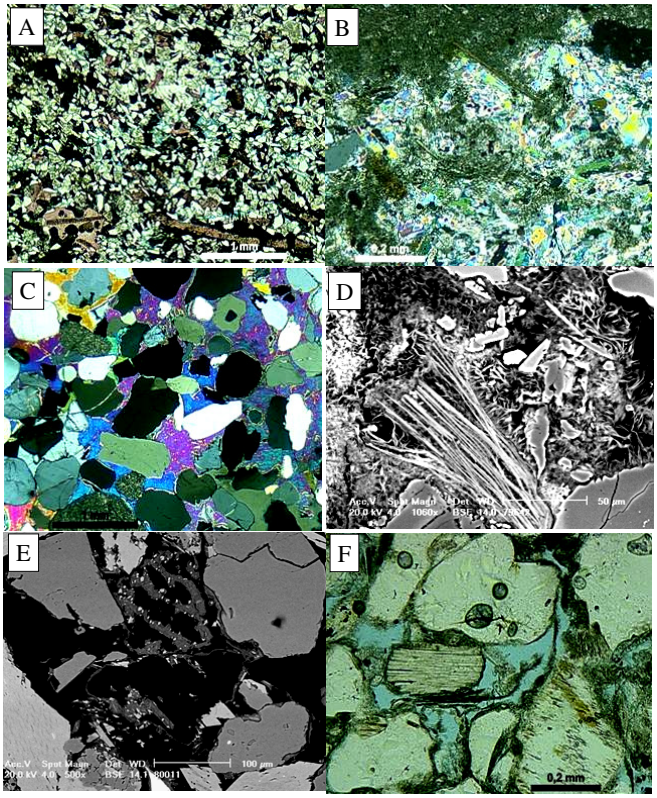

FIG. 12

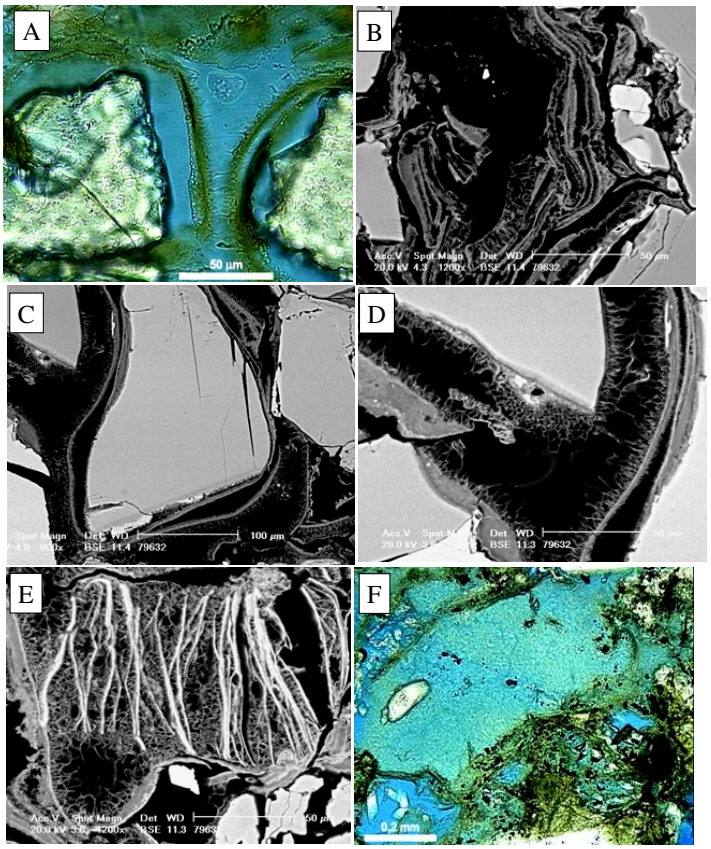

FIG. 13

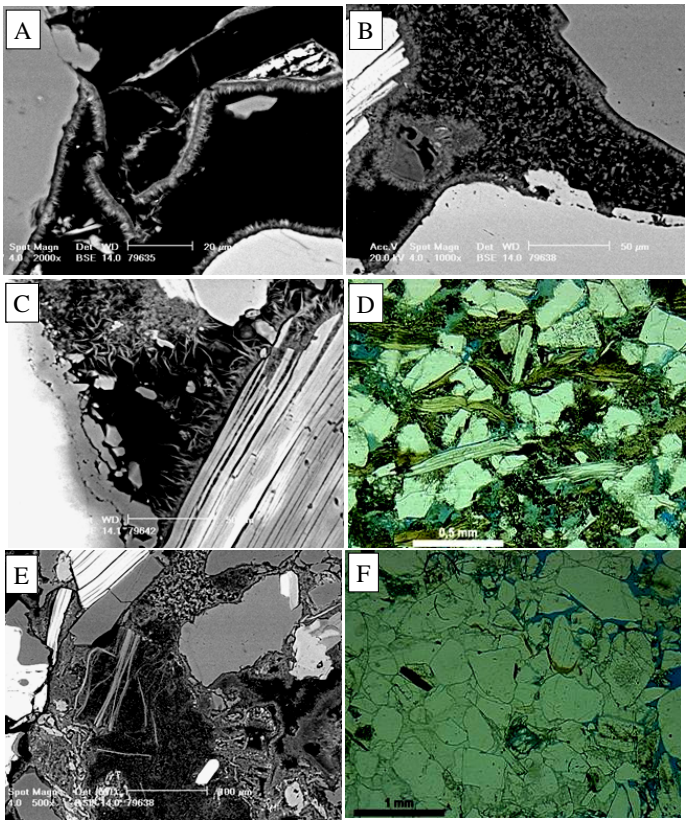

FIG. 14

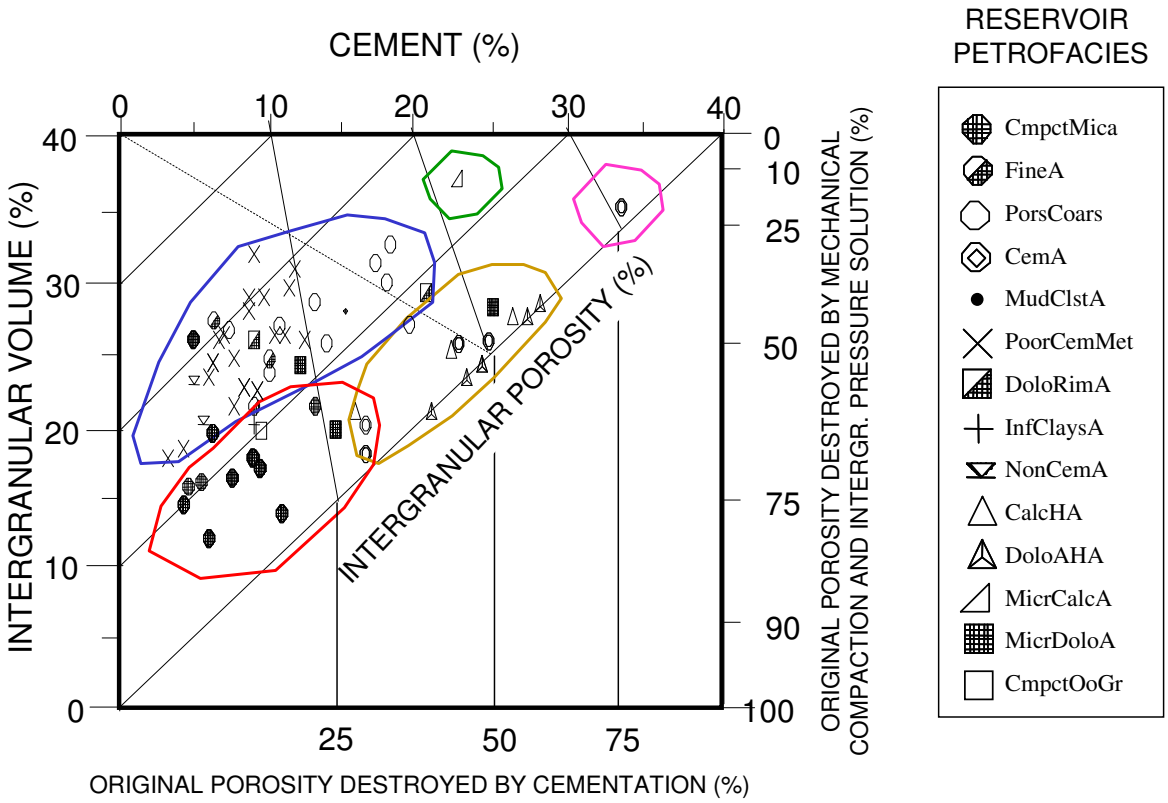

FIG. 15a

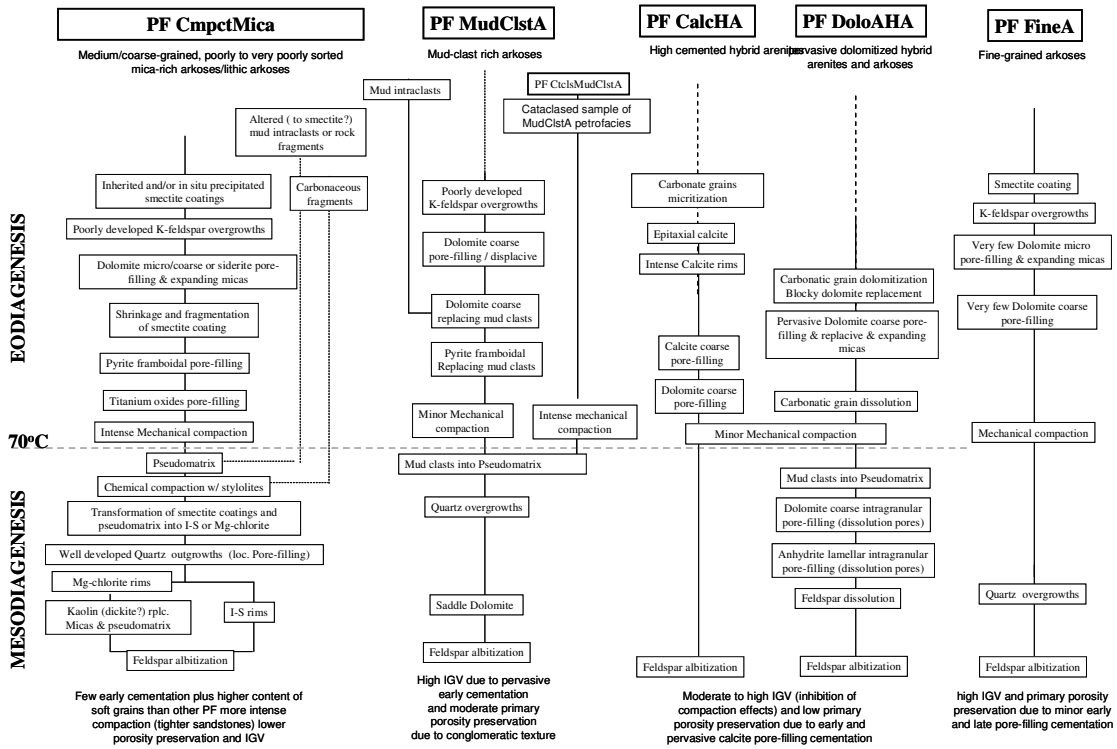

FIG. 15b

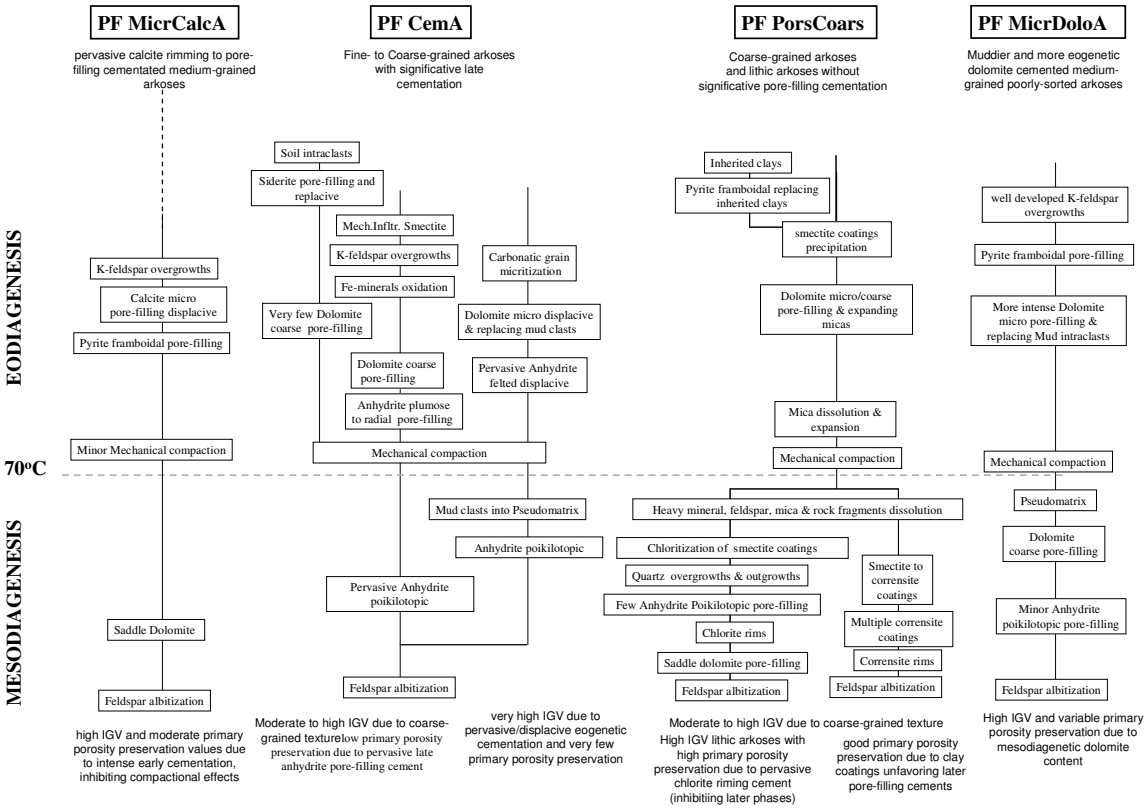

FIG. 15c

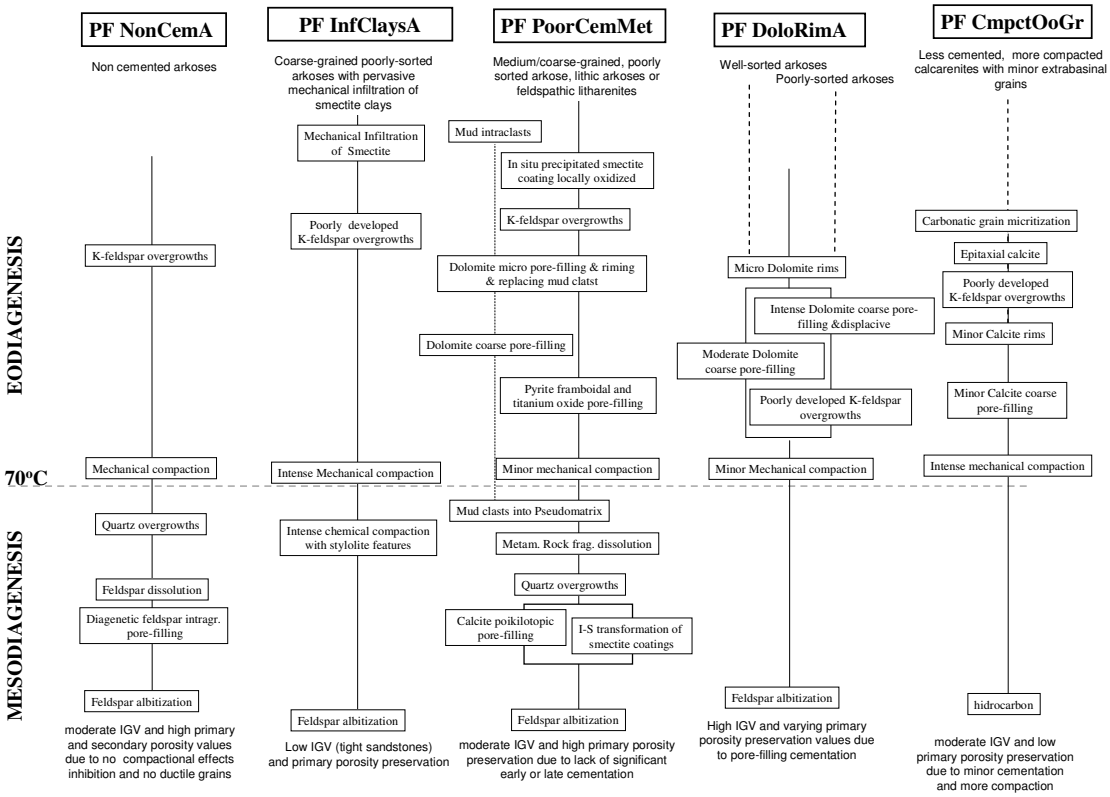

FIG. 16

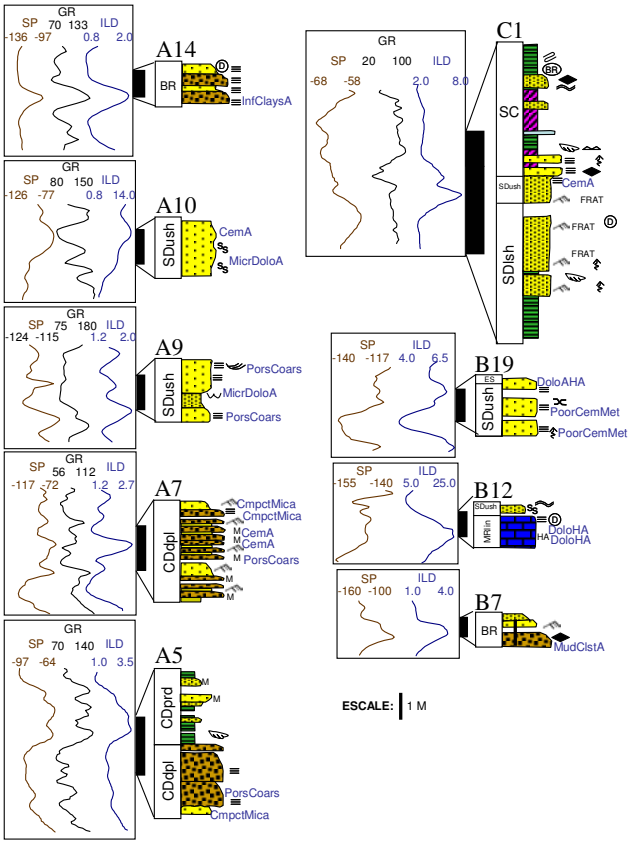
GR
SP 70 133 ILD
-136 -97 0.8 2.0
A14
BR
InfClaysA
GR
SP 80 150 ILD
-126 -77 0.8 14.0
A10
SDush
CemA
MicrDoloA
GR
SP 75 180 ILD
-124 -115 1.2 2.0
A9
SDush
PorsCoars
MicrDoloA
PorsCoars
GR
SP 56 112 ILD
-117 -72 1.2 2.7
A7
CDdpl
CmpctMica
CmpctMica
CemA
CemA
PorsCoars
GR
SP 70 140 ILD
-97 -64 1.0 3.5
A5
CDprd
CDdpl
PorsCoars
CmpctMica
GR
SP 20 100 ILD
-68 -58 2.0 8.0
C1
SC
SDush
SDlsh
CemA
FRAT
FRAT
FRAT
SP ILD
-140 -117 4.0 6.5
B19
SDush
DoloAHA
PoorCemMet
PoorCemMet
SP ILD
-155 -140 5.0 25.0
B12
SDush
MRIm
DoloHA
DoloHA
SP ILD
-160 -100 1.0 4.0
B7
BR
MudClstA
ESCALE: 1 M

FIG. 17

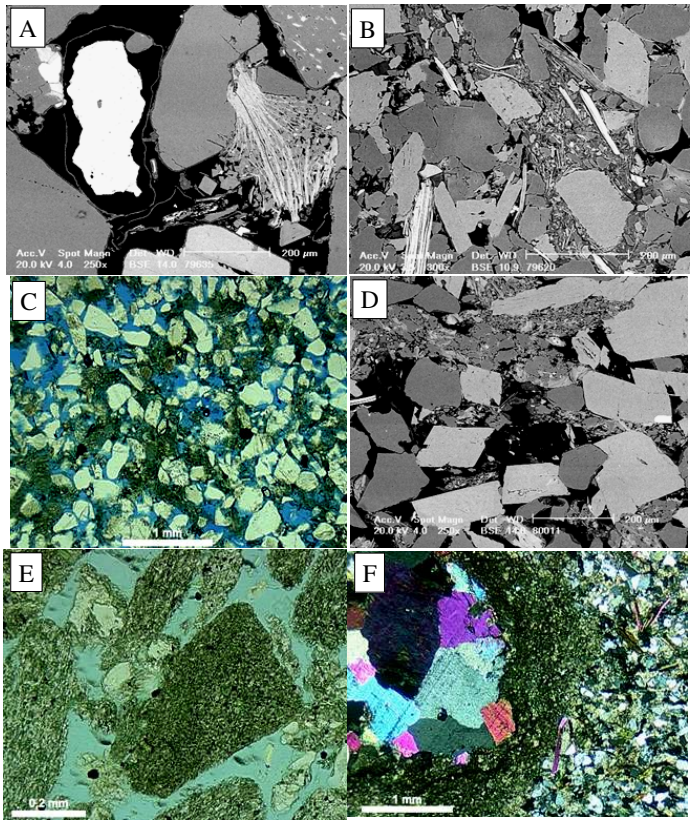
A
B
C
D
E
F
1 mm
1 mm

FIG. 18

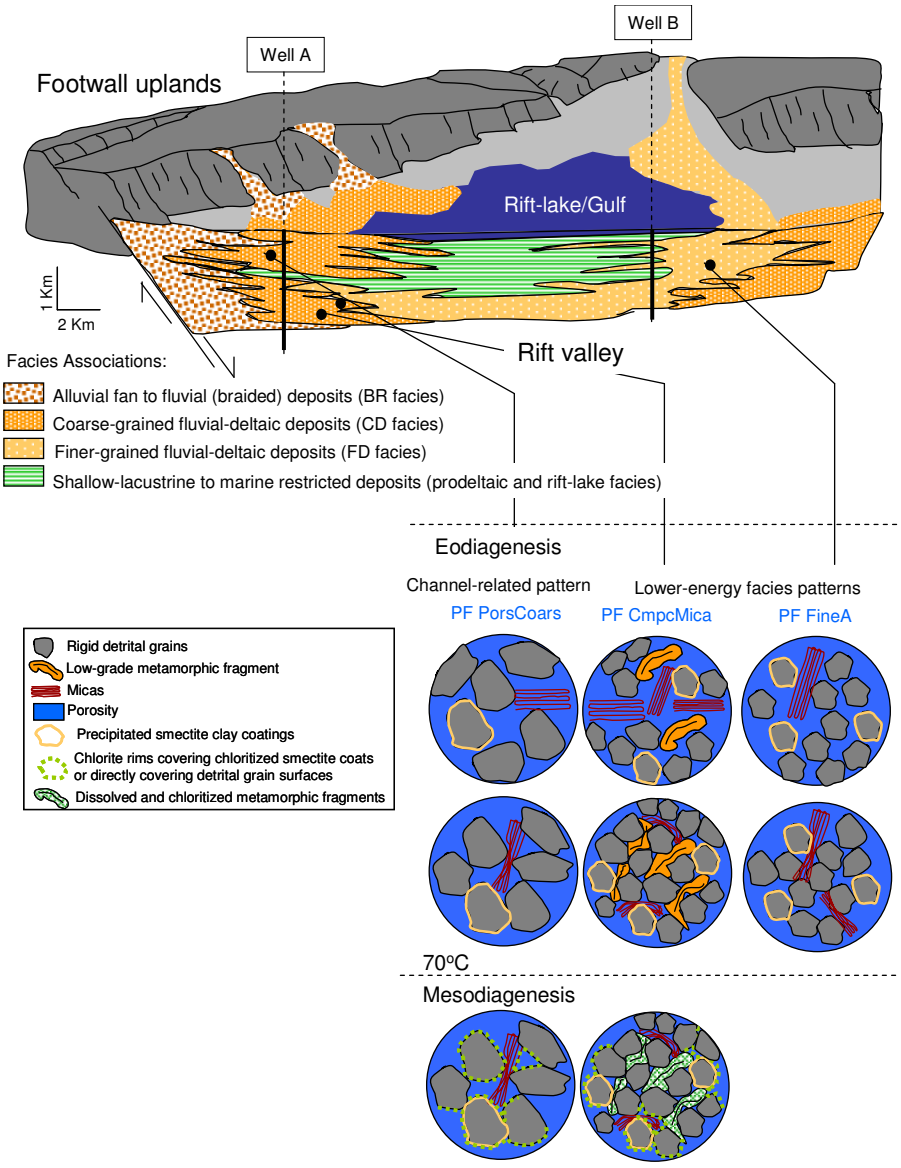
Well B
Well A
Footwall uplands
Rift-lake/Gulf
1 Km
2 Km
Rift valley
Facies Associations:
Alluvial fan to fluvial (braided) deposits (BR facies)
Coarse-grained fluvial-deltaic deposits (CD facies)
Finer-grained fluvial-deltaic deposits (FD facies)
Shallow-lacustrine to marine restricted deposits (prodeltaic and rift-lake facies)
Eodiagenesis
Channel-related pattern
Lower-energy facies patterns
PF PorsCoars
PF CmpcMica
PF FineA
Rigid detrital grains
Low-grade metamorphic fragment
Micas
Porosity
Precipitated smectite clay coatings
Chlorite rims covering chloritized smectite coats or directly covering detrital grain surfaces
Dissolved and chloritized metamorphic fragments
70ºC
Mesodiagenesis

FIG. 19

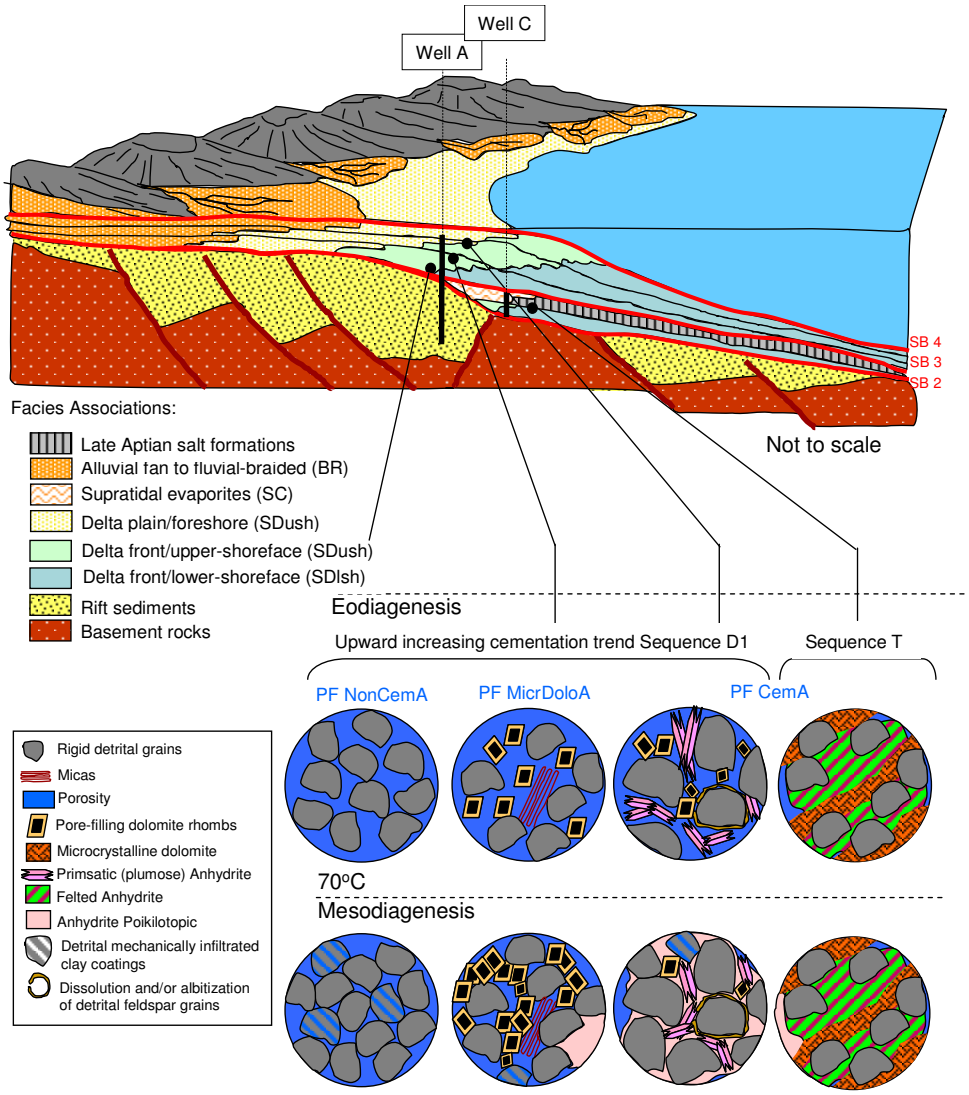
Well C
Well A
SB 4
SB 3
SB 2
Not to scale
Facies Associations:
Late Aptian salt formations
Alluvial fan to fluvial-braided (BR)
Supratidal evaporites (SC)
Delta plain/foreshore (SDush)
Delta front/upper-shoreface (SDush)
Delta front/lower-shoreface (SDlsh)
Rift sediments
Basement rocks
Eodiagenesis
Upward increasing cementation trend Sequence D1
Sequence T
PF NonCemA
PF MicrDoloA
PF CemA
Rigid detrital grains
Micas
Porosity
Pore-filling dolomite rhombs
Microcrystalline dolomite
Prismatic (plumose) Anhydrite
Felted Anhydrite
Anhydrite Poikilotopic
Detrital mechanically infiltrated clay coatings
Dissolution and/or albitization of detrital feldspar grains
70ºC
Mesodiagenesis

FIG. 20

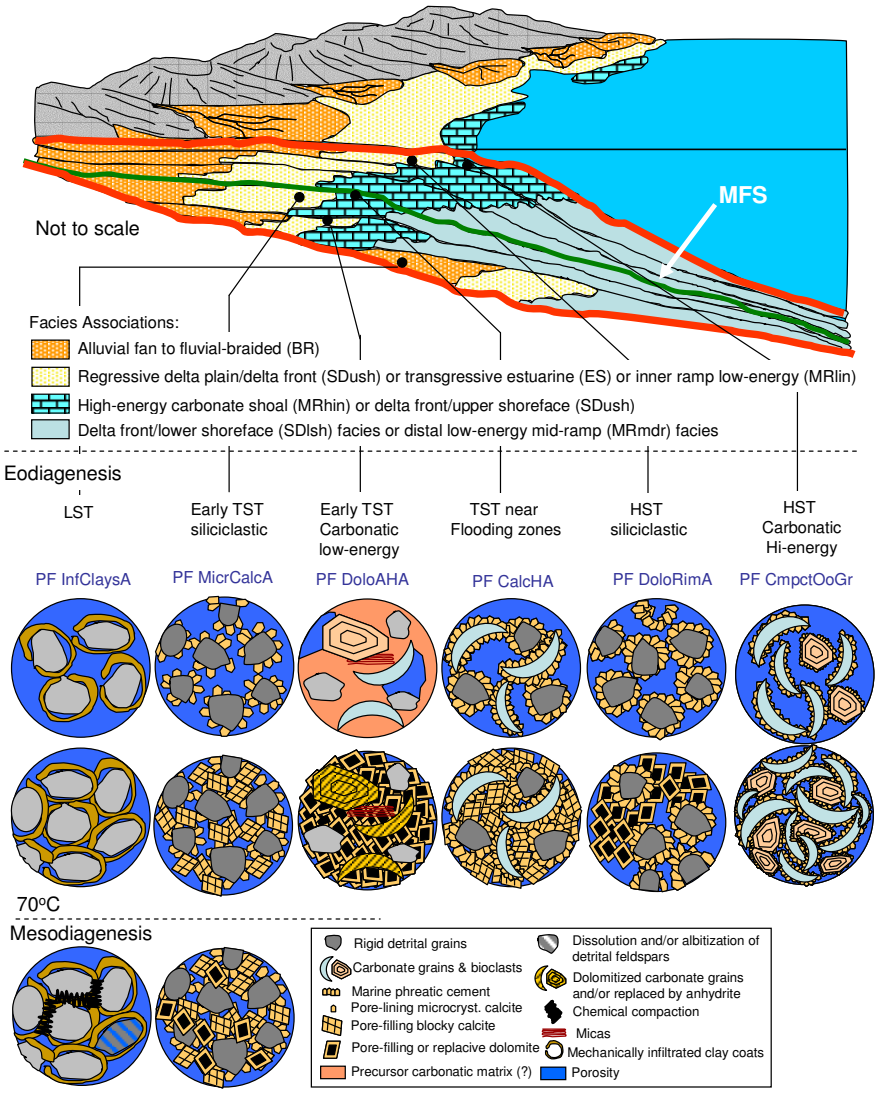
MFS
Not to scale
Facies Associations:
Alluvial fan to fluvial-braided (BR)
Regressive delta plain/delta front (SDush) or transgressive estuarine (ES) or inner ramp low-energy (MRlin)
High-energy carbonate shoal (MRhin) or delta front/upper shoreface (SDush)
Delta front/lower shoreface (SDlsh) facies or distal low-energy mid-ramp (MRmdr) facies
Eodiagenesis
LST
Early TST siliciclastic
Early TST Carbonatic low-energy
TST near Flooding zones
HST siliciclastic
HST Carbonatic Hi-energy
PF InfClaysA
PF MicrCalcA
PF DoloAHA
PF CalcHA
PF DoloRimA
PF CmpctOoGr
70°C
Mesodiagenesis
Rigid detrital grains
Carbonate grains & bioclasts
Marine phreatic cement
Pore-lining microcryst. calcite
Pore-filling blocky calcite
Pore-filling or replacive dolomite
Precursor carbonatic matrix (?)
Dissolution and/or albitization of detrital feldspars
Dolomitized carbonate grains and/or replaced by anhydrite
Chemical compaction
Micas
Mechanically infiltrated clay coats
Porosity

Table 1. Facies Associations (FA) of studied Jequitinhonha Basin successions (Jardim et al., submitted).

Facies	Description	Interpretation
CDdpl	This facies association consists of fining-upward succession of massive to parallel or planar cross laminated coarse-grained sandstones (locally with conglomeratic base), with possible trough cross-lamination, from fine-grained, climbing rippled cross laminated sandstones, capped by or intercalated with thin (up to 30 cm) massive light gray siltstones to sandy mudstones	Deposits associated with channel-fill migration dunes of shallow fluvial braided streams, with local overbanks deposits, possibly distributary-channel facies of a delta-plain setting, reflecting transition from channelized high- to low-energy flow.
CDdfr	This facies association consists of coarsening-upward succession of medium- to coarse-grained massive to planar cross-laminated sandstones, up to 20 m thick (based upon GR log curves), locally showing convolute structures, associated with slumped or deformed beds. This facies were poorly core sampled.	Deposits associated with subaqueous migrating proximal to distal mouth bars of a delta-front depositional setting.
CDprd	This facies association consists of alternation of thick, massive to parallel laminated, black to dark gray mudstones, with thin, massive to parallel laminated, normal graded, fine-grained sandstones.	Mud suspension of distal distributary mouth bar or prodelta deposits to rift-lacustrine setting (high GR well log response), with thin sandy intervals reflecting scattered turbidity flows.
FDdpl	This facies association consists of medium- to coarse-grained, poorly sorted, very friable, light gray parallel to planar (locally trough) cross laminated sandstones sets with up to 80 cm thick, locally with high content of mud intraclasts.	Upper most part of a coarsening-upward delta-front to delta-plain fluvial-deltaic succession, comprising subaerial deposition in lowland areas, under high-energy (upper planar bed condition), with mud intraclasts interpreted as product of underlying floodplain sediments erosion due to channel switching. The reduced thickness of interbedded fine-grained facies indicates low-sinuosity streams.
FDdfr	This facies association consists of fine- to medium-grained, poorly sorted, light to dark gray climbing ripple laminated sandstones, which pass upwards into parallel and planar cross-laminated sandstones, comprising a coarsening-upward sequence up to 6 m thick, locally with carbonaceous (coal) fragments and mud intraclasts (up to 5 cm wide) and/or showing bioturbation, fluidization (dish structures) and/or deformation (slumped features).	Deposits associated with subaqueous migrating proximal to distal mouth-bars of a delta-front depositional setting, reflecting an interplay of fluvial and lacustrine or restricted gulf environments, with gradual decreasing of grain size toward distal settings.
FDprd	This facies association consists of laminated mudstones alternating or grading upward into light gray, poorly sorted, parallel laminated sandstone, comprising up to 1.5 m thick, locally micaceous and showing bioturbation and/or fluidization (dish structures).	It comprises a relatively stable prodelta setting where mud and fine silt are deposited by fallout from suspension to form quiet well-laminated mudstones and siltstones, unaffected by wave or tidal processes (below lake or restricted gulf environment storm wave base). Locally with slight differences in grain size, probably reflecting fluctuations in river discharges.
BR	This facies association consists of coarse- to medium-grained (thinning-upward succession), poorly sorted, reddish (coarse-grained) to white-greenish (medium-grained) parallel laminated sandstone, into medium-grained, light gray to beije climbing rippled cross laminated sandstones, locally displaying displacive dolomite cementation, preferentially at medium-grained intervals, and topped by reddish to pale brown silty laminated mudstone. Coarser-grained intervals show low preservation (less visible structures). Some samples show high content of mud clast and soil fragments with siderite show erosion of fine grained floodplain or crevasse splay mud during fluvial channel migration, typically deposited as a lag in channel bases.	Subaerial deposition in high-energy (upper planar bed condition) braided river systems, with trough cross-laminated sets interpreted as river-channel shallow braided stream or sheet flood deposits, reflecting areas of more persistent channel flow in the braid plain. Local content of mud clast and soil fragments with siderite interpreted as erosion of fine grained floodplain and crevasse splay mud during fluvial channel migration, as channel base lag-deposits.
SDush	This facies association consists of coarsening-upward succession of medium- to coarse-grained, poorly to moderately-sorted (locally well-sorted), light to dark gray or reddish to pale brown, parallel laminated or wavy ripple cross laminated sandstones, locally with nodules of dolomite cementation. Intervals with moderate bioturbation and conspicuous deformation (slumped) and convolute bedding.	deltaplain to deltafront settings (upper shoreface) of a coarse-grained coastal deltaic environment (upper shoreface to foreshore facies), under high energy flow conditions, with poorly-sorted intervals interpreted as wave-storm dominated deposits, and better-sorted sands interpreted as wave or longshore currents reworked deposits.

Table 1 - Cont.

Facies	Description	Interpretation
SDlsh	This facies association consists of coarsening-upward fine- to medium-grained, poorly to moderately sorted, white-greenish to light gray bioturbated sandstones, locally showing climbing-rippled (or wave-rippled) cross lamination. Fluidization (dish structures) is also observed. Finer facies with light to dark gray carbonate-rich laminated mudstones locally show heterolithic texture, alternating layers of light gray to beije carbonatic mud.	deltafront (lower shoreface) settings of a coarse-grained coastal deltaic environment (lower shoreface facies) deposits, with variable wave-influence, under low energy flow conditions.
ES	This facies association consists of fine to coarse-grained, poorly sorted, locally very fine-grained and moderately-sorted, light gray massive sandstones or light brown to reddish massive sandstones, intercalated with layers of fine- to very fine-grained light gray sandstones and reddish to pale brown silty mudstones (rhythmic alternation - heterolithic layers), with varying rates of mud and sand, locally with a sharp change in clay content across sand/mud boundaries, showing load-cast, wavy and linsen features, and crinckled laminae. Heterolithic interval consisting of interlaminated very fine sadnstones, siltstones, and claystones, with an upward decrease in grain size and increase in clay content. Presence of elements of Ichnofauna Skolithos (AT8) and Cruziana (BT17).	Brackish shallow-water tidal influenced inner estuarine settings, reflecting marine-marginal processes of delta plain/delta front (foreshore/upper shoreface) settings. Repetitive sets of mud/sand couplets on a scale of centimeters (and crinkled laminae conformable to ripple bed forms) reflecting intermittent flow-energy (tractive flow alternating with fallout from suspension), indicating wave to tidal intertidal to subtidal mud flat environment setting. Sharp-based coarse-grained sandstone layers overlaping mudstone layers, with possible root marks, interpreted as small tidal-channel deposits, possibly associated with abandoned delta plain (tidal flats or marsh deposits)
SC	This facies association consists of light to dark gray carbonate-rich mudstone heterolithic facies with millimeter layers of beige, deformed carbonatic mud, w/ in situ breccia (mud crack?) and locally grading to black organic-rich laminated mudstones, intercalated with fine- to medium-grained, moderately-sorted, light gray, sand-rich heterolith (muddy sandstones) or with fine- to coarse-grained, poorly-sorted light gray parallel laminated sandstones with centimeter layers or lenses of beige carbonatic mud. These heterolithic facies occurring vertically associated with coalesced nodular, chicken-wire anhydrite beds, and millimeter-size beige carbonatic mud (possible algal-laminated dolomustones. Stromatoliths?)	The intercalation of carbonatic mud layers (dolomudstones) and heterolithic beds in vertical facies transition to evaporite layers (nodular anhydrite and algal-laminated dolomudstones) suggests deposition on a supratidal flat environment, related to distal progradation of coastal deltaic facies, under reducing accommodation space (highstand conditions) and increasing water circulation restriction, with developing of mudcracks, stromatolites, intraclastic breccias (tepees?), and possible algal laminations, interpreted as supratidal coastal sabkha-salina environment, with sporadic flooding resulting in coarser sediments.
MRhin	This facies association consists of medium- to coarse-grained, poorly to well-sorted, grayish or light yellow to beige hybrid arenites to skeletal and ooid dolograinstones, with intense carbonate cementation	Deposition under high-energy inner ramp, wave-dominated, shallow marine environment, possibly skeletal/ooid sand shoals, above fair-weather wave base, under continuous wave and current activity
MRlin	This facies association consists of medium-grained, poorly to very-poorly sorted, grayish to beige hybrid arenites to nonlaminated dolomudstones / dolopackstones with centimeter-size oncoids and bioclasts, with pervasive dolomitization with intense diagenetic alteration.	The restricted fauna (dasycladacean algae, mollusks, echinoderms and fusulinids) and interpreted dolomitized carbonate mud, as well as high terrigenous and plant fragments input, suggest deposition under low-energy, shallow-water restricted lagoonal to intertidal or subtidal internal platform setting.
MRmdr	This facies association consists of light gray carbonate mudstone, intercalated with mudstones or light to dark gray carbonate-rich laminated mudstones. Locally showing heterolithic texture (alternation with very fine-grained sandstones) or slumping features (deformation)	Sedimentary structures suggest a carbonatic deposition on stable shelf area, distal carbonate ramp depositional settings, between fair-weather and storm wave base, with local terrigenous influx.

Table 2

Table 2 - Statistical summary of the petrographic parameters of the studied sandstones

PETROFACIES	CalcHA	MicrCalcA	DoloRimA	InfClaysA	NonCemA	CmpctMica	CemA	FineA	PorsCoars	PoorCemMet	MicrDoloA	DoloAHA	MudClstA	CmpctOoGr
Number of samples	3	1	2	1	2	11	5	3	9	19	3	6	1	1
Total	Average	Average	Average	Average	Average	Average	Average	Average	Average	Average	Average	Average	Average	Average
Intergranular Volume	**24.67**	**37.34**	**27.66**	**20.33**	**21.51**	**18.15**	**25.14**	**24.78**	**28.26**	**25.83**	**24.23**	**24.94**	**28.33**	**19.68**
Grain Volume	**75.33**	**62.66**	**72.34**	**79.67**	**78.49**	**81.85**	**74.86**	**75.22**	**71.74**	**74.17**	**75.77**	**75.06**	**71.67**	**80.32**
Cement Volume	**21.56**	**22.67**	**14.99**	**9.67**	**5.84**	**8.12**	**23.00**	**9.11**	**14.52**	**9.05**	**17.56**	**24.78**	**15.67**	**9.68**
Total Extrabasinal Grains	**42.67**	**50.02**	**52.33**	**68.67**	**66.07**	**70.33**	**65.59**	**69.67**	**61.53**	**67.02**	**60.68**	**58.99**	**58.33**	**16.01**
Detrital Quartz	17.33	22.00	19.84	25.67	25.27	21.27	22.86	21.78	21.30	20.46	23.23	18.83	24.00	6.00
Detrital Feldspar	19.45	21.01	21.51	28.33	30.93	18.85	23.94	27.22	22.60	23.53	23.90	25.28	24.34	7.34
Detrital Plagioclase	0.00	0.00	0.99	0.67	0.67	0.67	0.93	1.00	1.11	0.56	0.77	0.33	2.00	0.00
Total Micas	**2.55**	**1.67**	**3.34**	**2.34**	**2.51**	**14.46**	**3.40**	**5.78**	**2.81**	**2.09**	**3.33**	**7.18**	**2.00**	**0.00**
Biotite	1.44	0.67	1.17	0.67	0.67	11.67	1.93	3.11	1.33	0.47	1.89	4.79	1.00	0.00
Chlorite	0.00	0.00	0.34	0.00	0.00	0.21	0.07	0.89	0.33	0.96	0.11	1.11	0.33	0.00
Muscovite	1.11	1.00	1.83	1.67	1.84	3.03	1.40	1.78	1.15	0.65	1.33	1.28	0.67	0.00
Garnet	**0.56**	**1.00**	**1.66**	**3.67**	**1.84**	**2.00**	**2.07**	**1.89**	**3.11**	**2.16**	**3.33**	**0.95**	**2.00**	**0.33**
Total Plutonic Rock Fragment	**1.55**	**2.67**	**2.83**	**4.00**	**3.01**	**8.09**	**9.20**	**5.01**	**5.96**	**2.74**	**1.78**	**1.83**	**4.66**	**2.34**
Total Metamorphic Rock Fragment	**0.00**	**0.00**	**0.17**	**0.00**	**0.84**	**3.58**	**0.87**	**3.89**	**2.07**	**11.30**	**0.33**	**2.11**	**0.33**	**0.00**
Highly altered low-rank metamorphic rock fragment	0.00	0.00	0.00	0.00	0.00	1.64	0.00	0.00	0.07	0.05	0.00	0.00	0.00	0.00
Total Sedimentary Rock Fragment	**0.00**	**0.00**	**1.67**	**0.00**	**0.17**	**0.64**	**1.87**	**1.89**	**1.74**	**3.33**	**2.22**	**0.83**	**0.00**	**0.00**
Dolostone rock fragment	0.00	0.00	1.00	0.00	0.17	0.46	1.60	1.89	1.74	2.37	2.22	0.56	0.00	0.00
Total Intrabasinal Grains	**25.78**	**0.00**	**1.00**	**0.00**	**0.00**	**0.21**	**2.40**	**0.00**	**0.30**	**0.04**	**0.78**	**0.33**	**3.66**	**57.00**
Mud intraclast	0.55	0.00	0.34	0.00	0.00	0.21	0.20	0.00	0.22	0.09	0.56	0.00	3.33	0.00
Carbonate bioclast	10.11	0.00	0.67	0.00	0.00	0.00	0.00	0.00	0.00	0.00	0.22	0.00	0.00	8.00
Carbonate ooid/oncoid/intraclasts	15.11	0.00	0.00	0.00	0.00	0.00	0.40	0.00	0.07	0.00	0.00	0.33	0.00	48.67
Total Diagenetic	**26.22**	**26.34**	**26.49**	**16.01**	**8.54**	**15.37**	**29.47**	**11.89**	**20.76**	**11.11**	**25.23**	**38.83**	**22.33**	**12.68**
K-feldspar Overgrowths	0.22	0.67	0.50	1.00	3.51	0.36	1.14	1.22	1.59	2.97	0.78	1.72	2.33	0.67
Quartz Overgrowths	0.00	0.00	0.00	0.00	0.84	0.24	0.73	0.67	0.15	0.25	0.11	0.00	2.00	0.00
Total Dolomite	**4.66**	**5.33**	**22.99**	**0.00**	**0.00**	**3.91**	**4.73**	**2.78**	**4.04**	**3.04**	**15.67**	**29.61**	**10.34**	**0.00**
Dolomite Coarsely-cryst. Intergr. pore-filling Eodiag.	4.66	0.00	5.83	0.00	0.00	1.85	1.93	2.00	2.59	1.42	2.44	21.28	6.67	0.00
Dolomite Coarsely-cryst. Intergr. pore-filling Mesodiag.	0.00	0.00	0.00	0.00	0.00	0.00	0.00	0.67	0.00	0.00	7.22	0.00	0.00	0.00
Dolomite Coarsely-cryst. replacing Carbonate intraclasts	0.00	0.00	0.00	0.00	0.00	0.00	0.00	0.00	0.00	0.00	0.00	4.89	0.00	0.00
Dolomite Coarsely-cryst. Intergranular displacive	0.00	0.00	4.66	0.00	0.00	0.00	0.07	0.00	0.00	0.00	0.22	0.11	0.67	0.00
Dolomite Coarsely-cryst. Intragranular replacive	0.00	0.00	2.34	0.00	0.00	1.42	0.13	0.11	0.89	0.04	2.11	1.50	3.00	0.00
Dolomite Microcrystalline Intergranular pore-filling Eodiag.	0.00	0.00	0.00	0.00	0.00	0.09	0.73	0.00	0.11	0.04	3.67	0.00	0.00	0.00
Dolomite Microcrystalline repalcing Mud Intraclast	0.00	0.00	0.00	0.00	0.00	0.06	1.40	0.00	0.00	0.00	0.00	0.00	0.00	0.00
Dolomite Microcrystalline replacing Marine Calcite Cement	0.00	0.00	8.00	0.00	0.00	0.00	0.00	0.00	0.00	0.00	0.00	0.00	0.00	0.00
Total Calcite	**18.11**	**17.33**	**0.00**	**0.00**	**0.00**	**0.18**	**0.00**	**0.00**	**0.00**	**0.69**	**0.00**	**0.00**	**0.00**	**8.01**
Calcite Coarsely-cryst. Intergranular pore-filling	8.55	3.33	0.00	0.00	0.00	0.00	0.00	0.00	0.00	0.35	0.00	0.00	0.00	2.67
Calcite Microcrystalline Intergranular displacive	0.00	12.33	0.00	0.00	0.00	0.00	0.00	0.00	0.00	0.00	0.00	0.00	0.00	0.00
Total Siderite	**0.00**	**0.00**	**0.00**	**0.00**	**0.00**	**0.27**	**0.93**	**0.00**	**0.00**	**0.04**	**0.00**	**0.00**	**0.00**	**0.00**
Total Albite	**1.00**	**1.67**	**1.00**	**0.67**	**1.84**	**1.37**	**1.27**	**2.33**	**1.26**	**0.86**	**0.55**	**0.67**	**3.67**	**0.00**
Albite Replacing Detrital K-feldspar	0.44	1.00	0.50	0.67	0.84	0.85	0.80	1.44	0.71	0.37	0.56	0.22	1.00	0.00
Albite Replacing Detrital plagioclase	0.56	0.67	0.50	0.00	1.01	0.52	0.47	0.89	0.56	0.49	0.55	0.45	2.67	0.00
Total Anhydrite	**0.00**	**0.00**	**0.00**	**0.00**	**0.00**	**0.00**	**18.16**	**0.00**	**8.53**	**0.00**	**2.23**	**0.06**	**0.00**	**2.00**
Anhydrite Poikilotopic Intergranular pore-filling Mesodiag.	0.00	0.00	0.00	0.00	0.00	0.00	12.29	0.00	1.19	0.00	0.00	0.00	0.00	0.00
Anhydrite Lamella Intergranular pore-filling Eodiag.	0.00	0.00	0.00	0.00	0.00	0.00	3.20	0.00	1.04	0.00	0.00	0.00	0.00	0.00
Anhydrite Lamella Intragranular replacive	0.00	0.00	0.00	0.00	0.00	0.00	1.07	0.00	0.96	0.00	0.33	0.00	0.00	0.33
Anhydrite Lamella replacing Carbonate intraclasts	0.00	0.00	0.00	0.00	0.00	0.00	0.00	0.00	0.00	0.00	0.00	3.61	0.00	0.00
Diagenetic Clay Inherited	**0.00**	**0.67**	**0.00**	**0.00**	**0.00**	**0.54**	**0.46**	**0.00**	**0.11**	**0.33**	**0.00**	**0.00**	**0.00**	**0.00**
Pseudomatrix	**0.00**	**0.00**	**0.00**	**0.00**	**0.00**	**0.00**	**0.00**	**0.00**	**0.07**	**0.00**	**0.22**	**0.00**	**3.67**	**0.00**
Mechanically Infiltrated Smectite Clay	**0.00**	**0.00**	**0.00**	**7.67**	**0.00**	**0.00**	**0.07**	**0.00**	**0.15**	**0.00**	**0.00**	**0.00**	**0.00**	**0.00**
Diagenetic iron oxide	**0.00**	**0.00**	**0.00**	**4.34**	**0.00**	**0.00**	**0.27**	**0.00**	**0.56**	**0.05**	**0.00**	**0.17**	**0.00**	**0.00**
Total Chlorite	**0.00**	**0.00**	**0.17**	**1.00**	**0.67**	**3.82**	**0.54**	**0.00**	**1.08**	**0.00**	**0.67**	**0.00**	**0.00**	**0.00**
Chlorite Rim Intergranular pore-lining covering previous clays	0.00	0.00	0.00	0.00	0.00	0.27	0.13	0.00	0.26	0.00	0.00	0.00	0.00	0.00
Chlorite Microcryst. replacing metamorphic rock frag.	0.00	0.00	0.00	0.00	0.00	0.55	0.00	0.00	0.07	0.00	0.00	0.00	0.00	0.00
Total Corrensite	**0.00**	**0.00**	**0.00**	**0.00**	**0.00**	**0.00**	**0.00**	**0.00**	**0.96**	**0.00**	**0.00**	**0.00**	**0.00**	**0.00**
Total Smectite In situ precipitated	**0.00**	**0.00**	**0.00**	**0.00**	**0.00**	**0.30**	**0.00**	**2.11**	**0.07**	**1.00**	**0.00**	**0.00**	**0.00**	**0.00**
Total Illite-Smectite	**0.00**	**0.00**	**0.00**	**0.00**	**0.00**	**1.15**	**0.00**	**0.00**	**0.00**	**0.56**	**0.00**	**0.00**	**0.00**	**0.00**
I-S Fibrous Intergranular pore-filling	0.00	0.00	0.00	0.00	0.00	0.55	0.00	0.00	0.00	0.00	0.00	0.00	0.00	0.00
I-S Fibrous within intragranular porosity (low-rank metam. rock frag.)	0.00	0.00	0.00	0.00	0.00	0.27	0.00	0.00	0.00	0.00	0.00	0.00	0.00	0.00
Total Pyrite	**1.56**	**0.67**	**0.17**	**0.33**	**0.34**	**1.12**	**0.80**	**1.33**	**0.63**	**0.70**	**0.78**	**1.45**	**0.33**	**0.00**
Pyrite Framboid Intergranular pore-filling	0.67	0.67	0.17	0.33	0.34	1.12	0.80	1.33	0.56	0.70	0.44	0.78	0.33	0.00
Total Titanium mineral	**0.00**	**0.00**	**0.00**	**1.00**	**0.50**	**1.12**	**0.27**	**1.44**	**0.93**	**0.51**	**0.67**	**0.00**	**0.00**	**0.00**
Macroporosity Volume	**5.22**	**22.34**	**19.51**	**16.00**	**25.92**	**14.46**	**4.33**	**19.00**	**18.27**	**21.74**	**12.45**	**1.56**	**16.34**	**14.33**
Intergranular Primary	**3.11**	**14.67**	**12.67**	**10.67**	**15.73**	**9.67**	**2.14**	**15.67**	**13.71**	**16.77**	**6.67**	**0.17**	**12.67**	**8.33**
Intragranular by dissolution of Detrital-Constituent	**2.11**	**7.67**	**6.84**	**5.33**	**10.20**	**4.79**	**2.20**	**3.34**	**4.52**	**4.97**	**5.78**	**1.39**	**3.67**	**4.33**
Intragranular by dissolution of Detrital K-feldspar	1.22	2.67	1.17	3.33	3.84	1.00	0.67	0.44	1.33	0.53	1.78	0.17	0.33	0.00
Moldic by dissolution of Detrital-Constituent	**0.00**	**5.00**	**4.34**	**2.00**	**0.34**	**1.06**	**0.33**	**0.56**	**1.63**	**2.63**	**1.67**	**0.33**	**0.67**	**0.00**

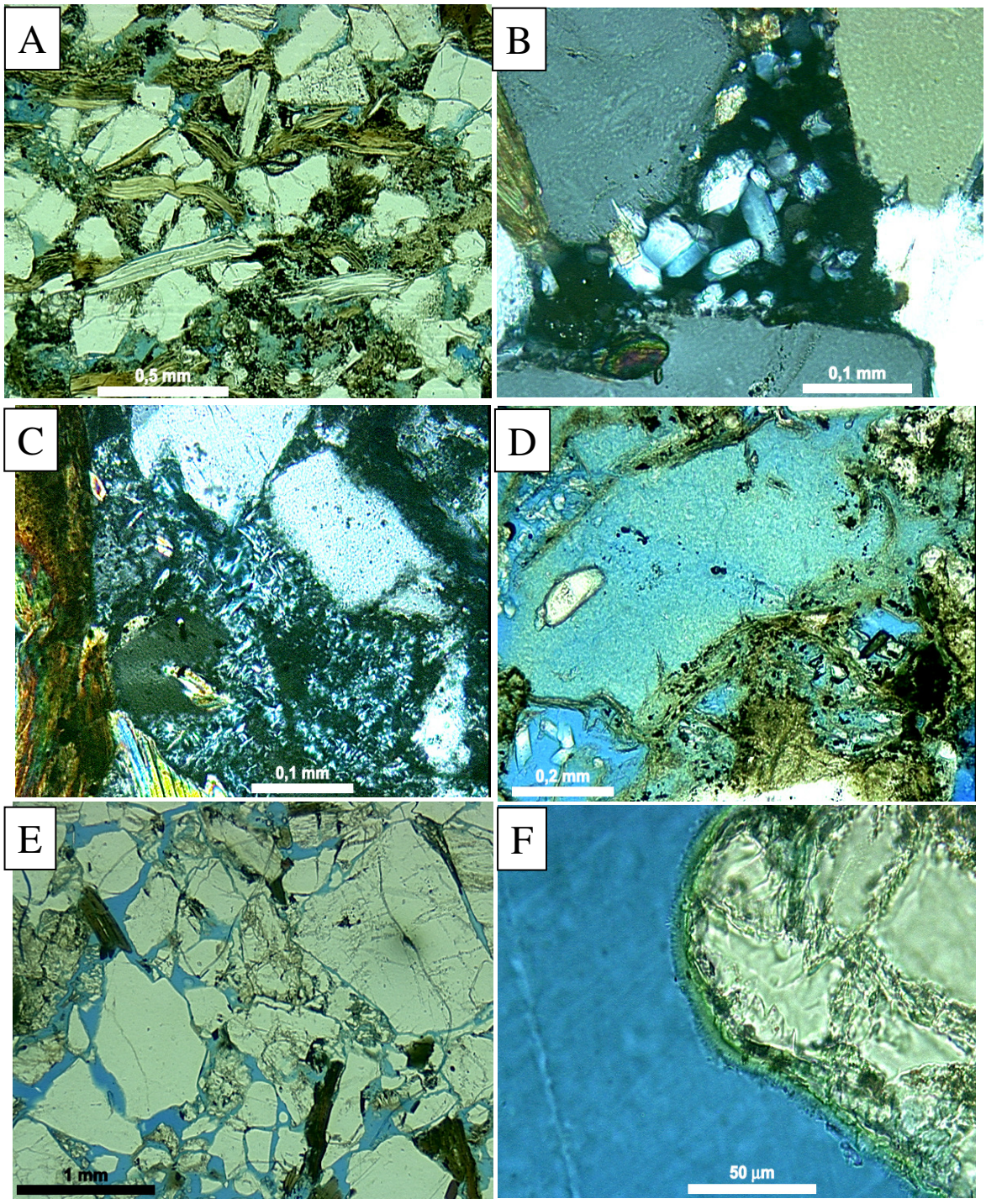

Anexo B-1. Fotomicrografias óticas mostrando: A e B) Petrofácies CmpctMica (2624.8m) com alta compactação mecânica de grãos micaceous (polarizadores descruzados - //P) e com projeções prismáticas de quartzo com caráter *pore-filling* (polarizadores cruzados - XP). C) Petrofácies CmpctMica (2786.0m) com cimentação tardia por franjas de I-S (XP). D) Petrofácies CmpctMica (2476.8m) com alteração e deformação de possíveis fragmentos de rocha metamórfica de baixo grau, ou intraclastos lamosos, com impacto nas propriedades permo-porosas (//P). E) Petrofácies PorsCoars (2290.4m) com reduzida cimentação intergranular com impacto nos valores de porosidade. F) Petrofácies PorsCoars (2149.9m) com cimentação por clorita na forma de franjas recobrindo cuticulas eodiageneticas, consistindo em neoformacao de cuticulas precursoras de esmectita (//P).

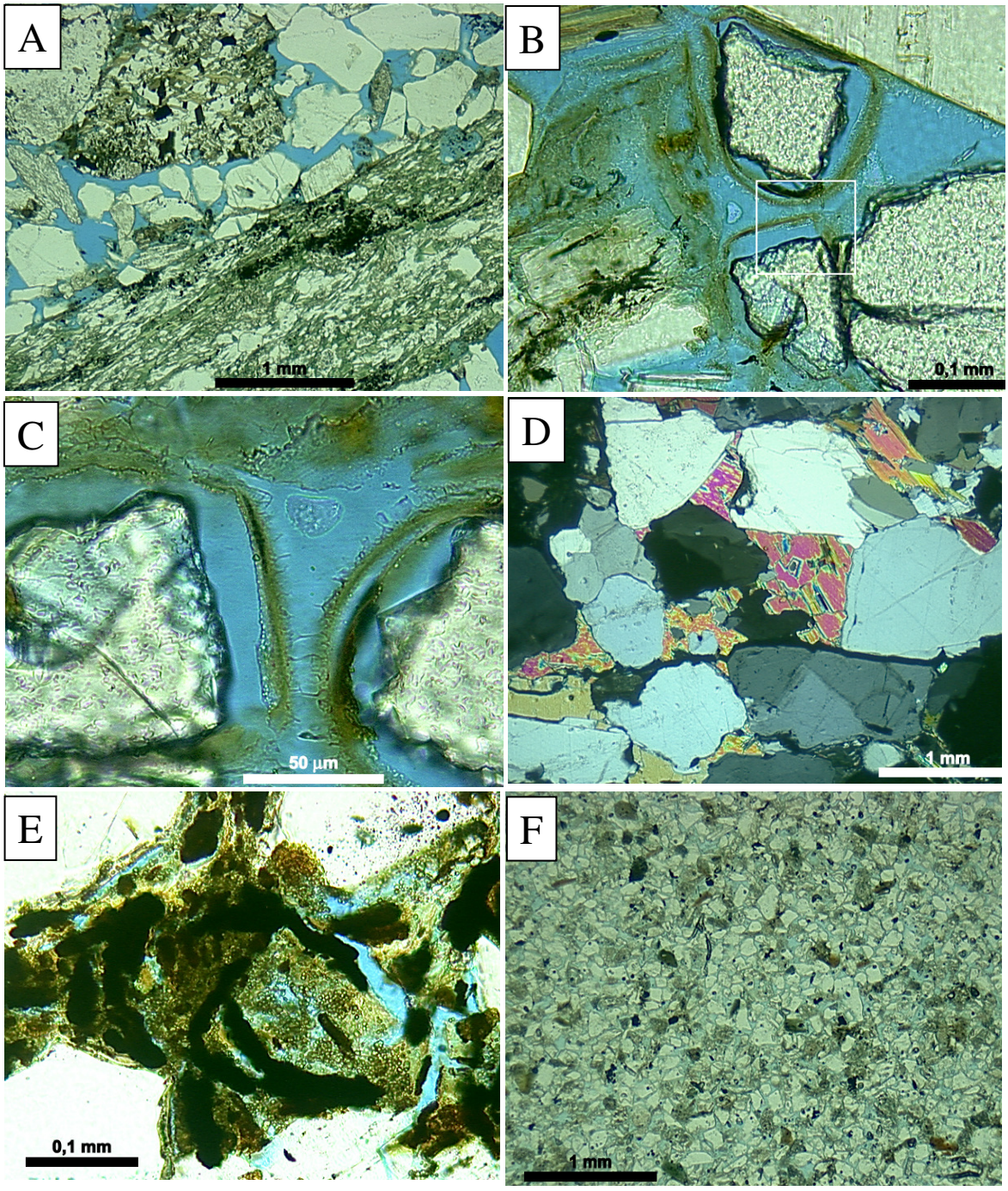

Anexo B-2. Fotomicrografias óticas mostrando: A) Petrofácies PorsCoars (2149.9m) com fragmentos metamórficos de alto grau (pouca deformação), com boa macroporosidade (c.16%) (//P). B e C) Petrofácies PorsCoars (2012.7m) com múltiplas cutículas de corrensita, localmente pré-compactacionais (transformação esmectita?), recobertas por franjas (favos) de corrensita (//P). D) Petrofácies CemA (2012.0m) com cimentação pós-compactacional por anidrita poiquilotopica (XP). F) Petrofácies CemA (2011.3m) com presença de intraclastos (solos?), com intensa cimentação por siderita microcristalina (//P). Petrofácies FineA (1434.5m) com seleção moderada e baixo conteúdo em grãos dúcteis, resultando boa preservação de porosidade primaria (c.14%) (//P).

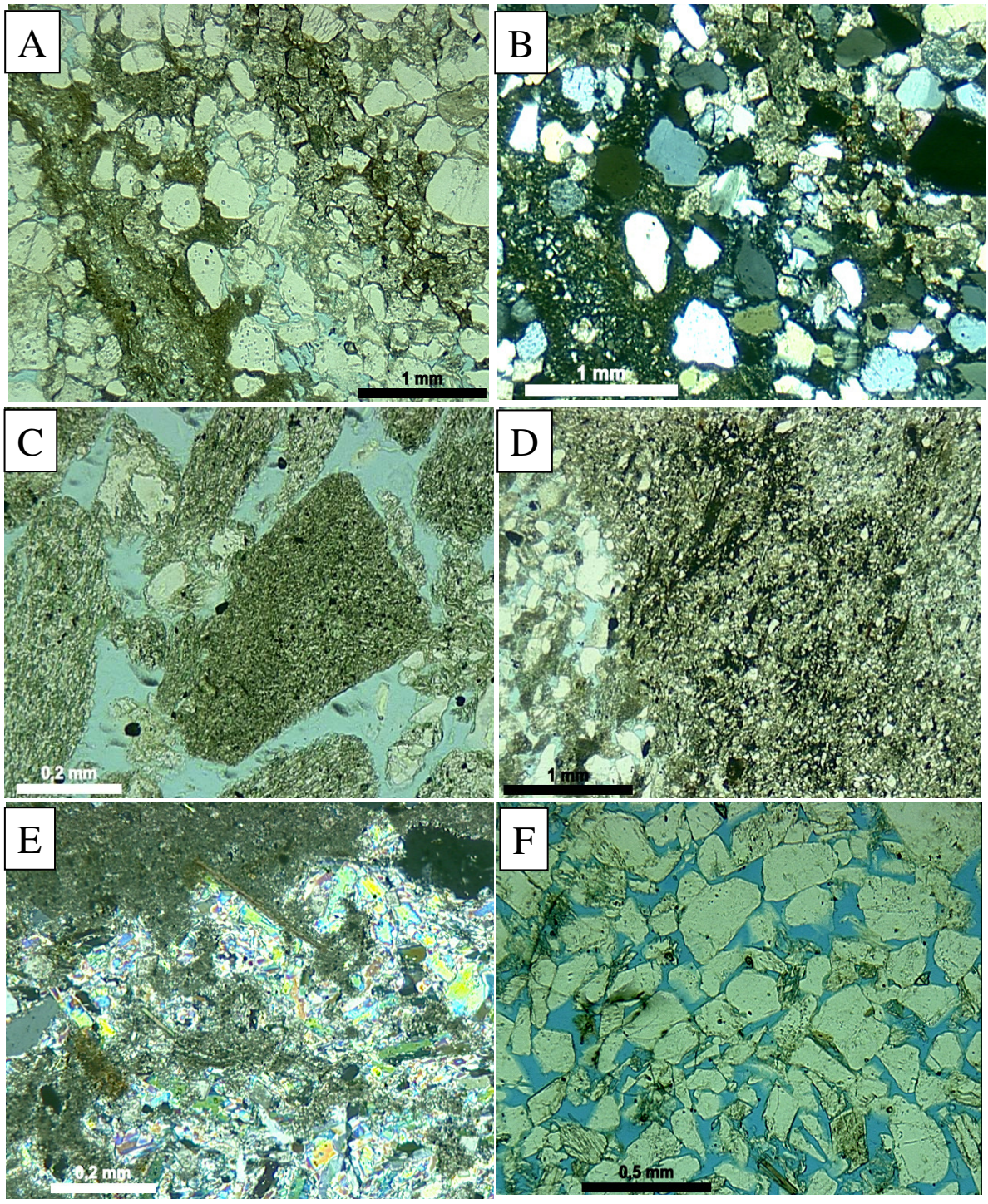

Anexo B-3. Fotomicrografias óticas mostrando: A e B) Petrofácies MudClastA (1168.5m) com alto conteúdo em intraclastos lamosos e formação de pseudomatriz (//P), e intensa cimentação por dolomita microcristalina intergranular e substituindo intraclastos lamosos, e fases tardias (megacristais – dolomita tipo *saddle*), substituindo fases precoces (XP). C) Petrofácies PoorCemMet (1016.0m) com alto conteúdo em fragmentos de rocha metamórfica de baixo grau, e preservação anômala de porosidade primaria (//P). D) Petrofácies PoorCemMet (1011.8m) com fragmentos de arenito com pouca litificação (//P). E) Petrofácies CemA (1647.5m) com cimentação precoce e intensa por dolomita microcristalina e anidrita tipo feltro , e, localmente, com hábito lamelar (XP). F) Petrofácies NonCemA (1893.5m) com boa porosidade face caráter quartzo-feldspático da composição primária e ausência de cimentação intergranular expressiva (//P).

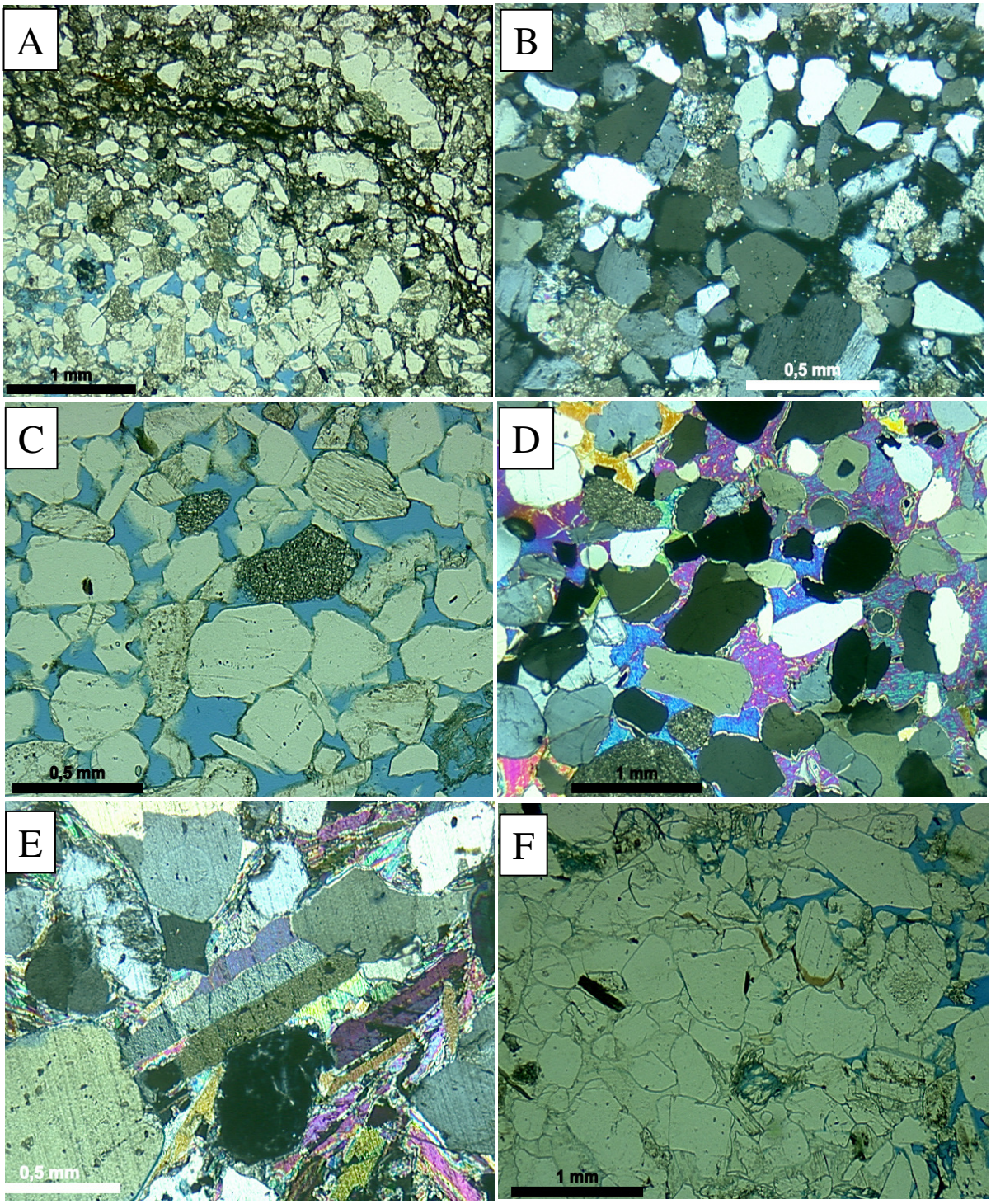

Anexo B-4. Fotomicrografias óticas mostrando: A e B) Petrofácies MicrDoloA (1828.3m) com intervalos ricos em intraclastos lamosos, preferencialmente cimentados por dolomita eodiagenética (//P), e com cimentação por dolomita intergranular, com possível mistura de fases pré-compactacional microcristalina e pós-compactacional blocosa (XP). C) Petrofácies PorsCoars (1827.2m) com variável macroporosidade em função da seleção e granulometria (//P). D) Petrofácies CemA (1759.4m) com intervalo com baixa preservação de porosidade devido intensa cimentação tardia por anidrita poiquilotópica (XP). E e F) Petrofácies CemA (1626.3m) com cimentação eodiagenética (deslocante?) por anidrita com hábito prismático (XP), e caráter nodular da cimentação tardia anidrita, resultando redução localizada de porosidade, com impacto menor na permeabilidade (//P).

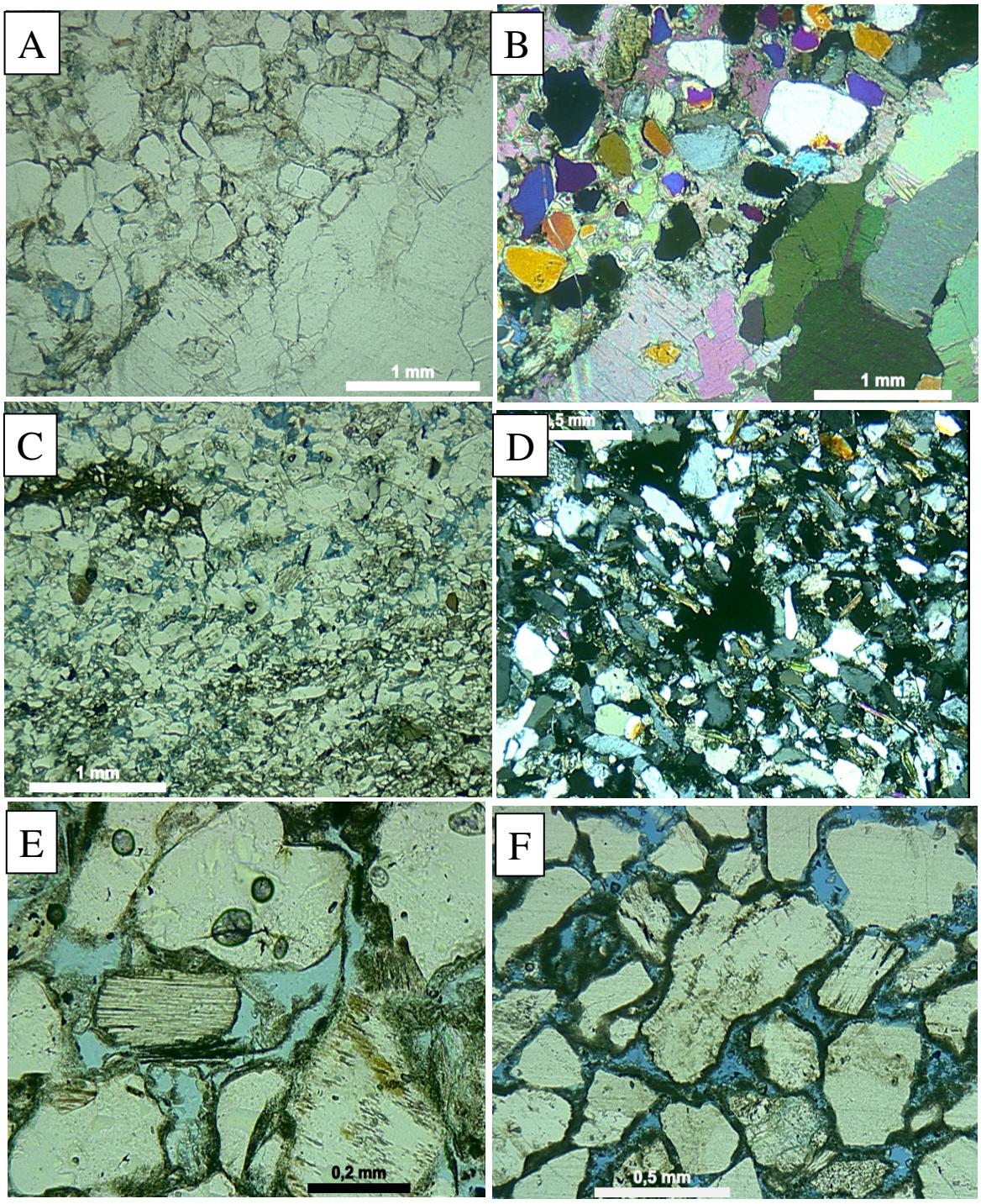

Anexo B-5. Fotomicrografias óticas mostrando: A e B) Petrofácies CemA (1759.4m - lâmina 50 µm) com intraclasto evaporítico (//P e XP). C e D) Petrofácies MicrDoloA (1558.5m) com cimentação eodiagenética por dolomita microcristalina (XP) e presença de intraclastos (//P). E) Petrofácies InfClaysA (1250.0m) com infiltração mecânica de argilas esmectitas (espessura variável espessura, e feições de desidratação e descolamento. Caráter precoce inibindo cimentos posteriores, resultando alta compactação mecânica e química, e baixos valores de preservação de porosidade (c.11%) (//P). F) Petrofácies DoloRimA (1035.0m) com envelope micritico e franjas de dolomita microcristalina, favorecendo a preservação de porosidade primaria, inibindo colapso do arcabouço frente à compactação mecânica (//P), e detalhe das franjas (XP).

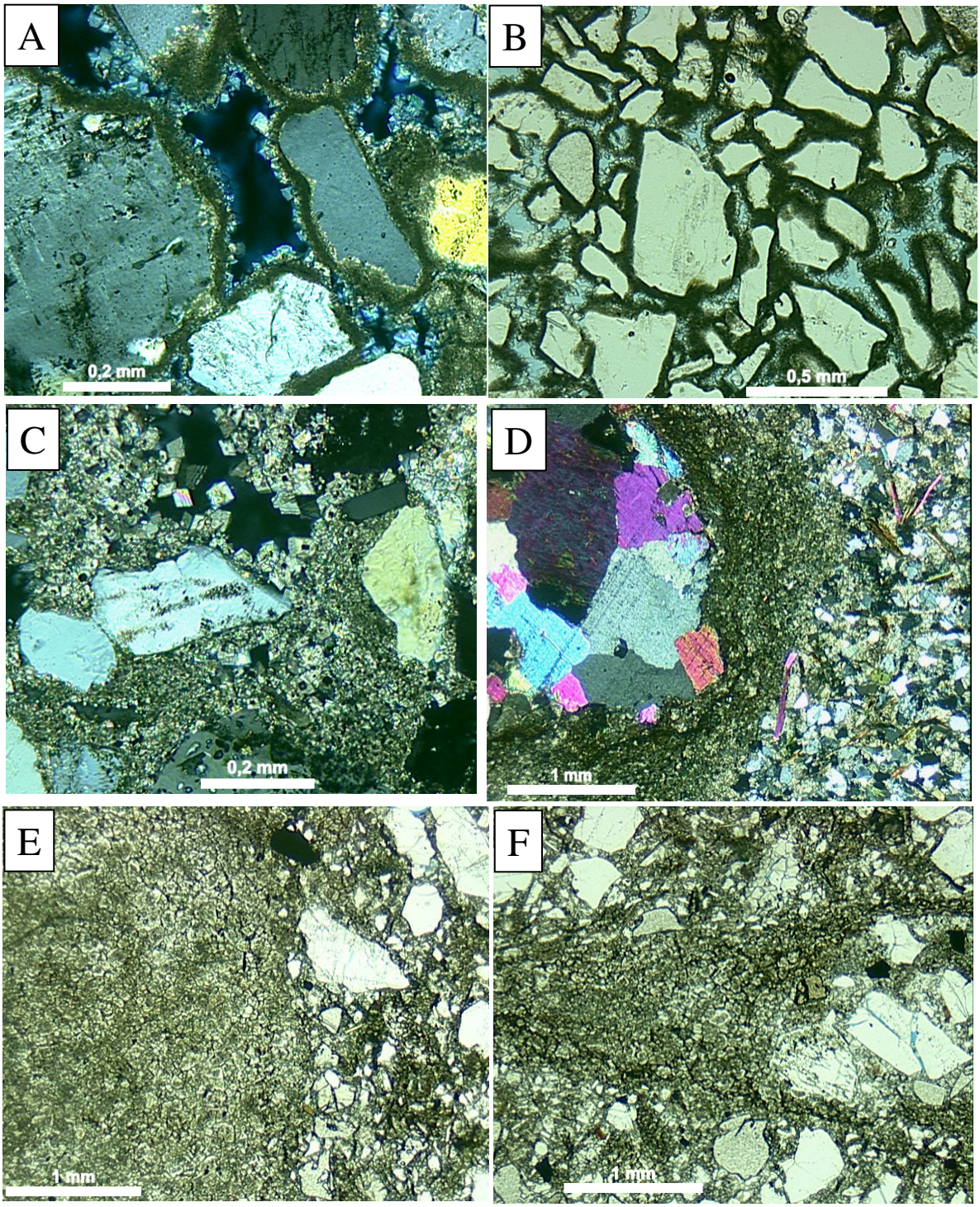

Anexo B-6. Fotomicrografias óticas referente à Petrofácies DoloAHA, mostrando: A) Petrofácies DoloRimA (1035.0m) detalhe das franjas (XP). B) Petrofácies DoloRimA (1038.5m) aumento no percentual de cimentação intergranular *pore-filling* (cristais com núcleos dissolvidos), localmente deslocante, resultando menor preservação da porosidade primaria (//P). C) Petrofacies DoloRimA (1038.5m) detalhe cimentação *pore-filling* (XP). C) Petrofácies MicrCalcA com cimentação eodiagenética, deslocante, por calcita microcristalina (//P). D) Cimentação intergranular por dolomita microcristalina a blocosa e dissolução dos grãos carbonáticos (oncolitos), com posterior cimentação intragranular por dolomita blocosa (cristais euédricos e megacristais de anidrita) (931.4m) (XP). E e F) Detalhe dos grãos carbonáticos e bioclastos carbonáticos dolomitizados (931.2m) (//P).

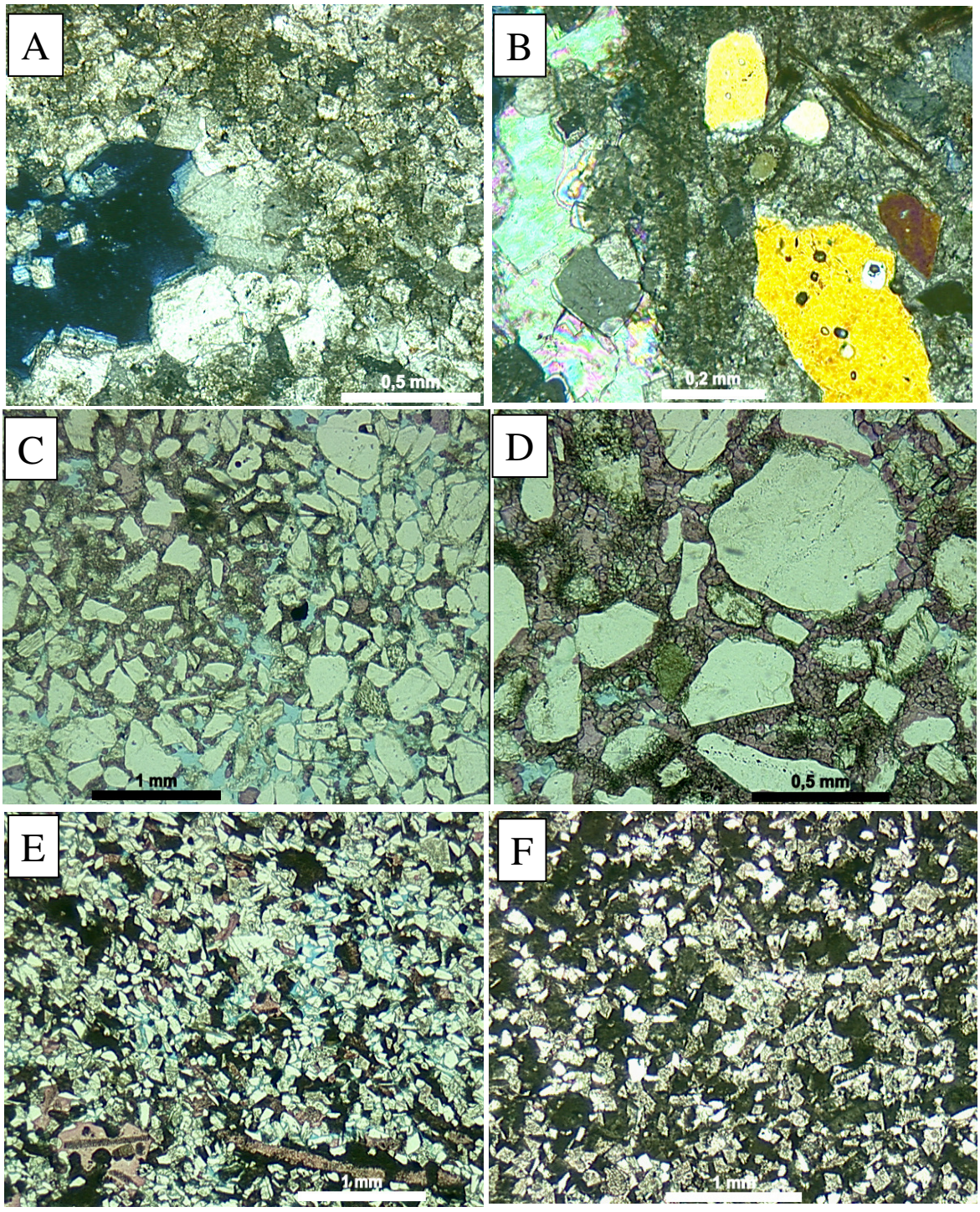

Anexo B-7. Fotomicrografias óticas mostrando: A e B) Petrofácies DoloAHA (931.4m) lâmina 50 µm com detalhe da cimentação intragranular por dolomita e anidrita (XP). C e D) Petrofácies MicrCalcA (940.0m) com cimentação eodiagenética, deslocante, por calcita microcristalina (//P) e detalhe do cimento calcita intergranular (//P). E) Petrofácies CalcHA (853.8m) com cimentação eodiagenética por calcita microcristalina tipo *pore-lining* (envelope micritico) e *pore-filling,* localmente com ocorrência de calcita epitaxial (crescimento secundário) ao redor de grãos de equinodermas (//P). F) Petrofácies CalcHA (854.0m) com intensa cimentação por dolomita blocosa pós-datando calcita (XP).

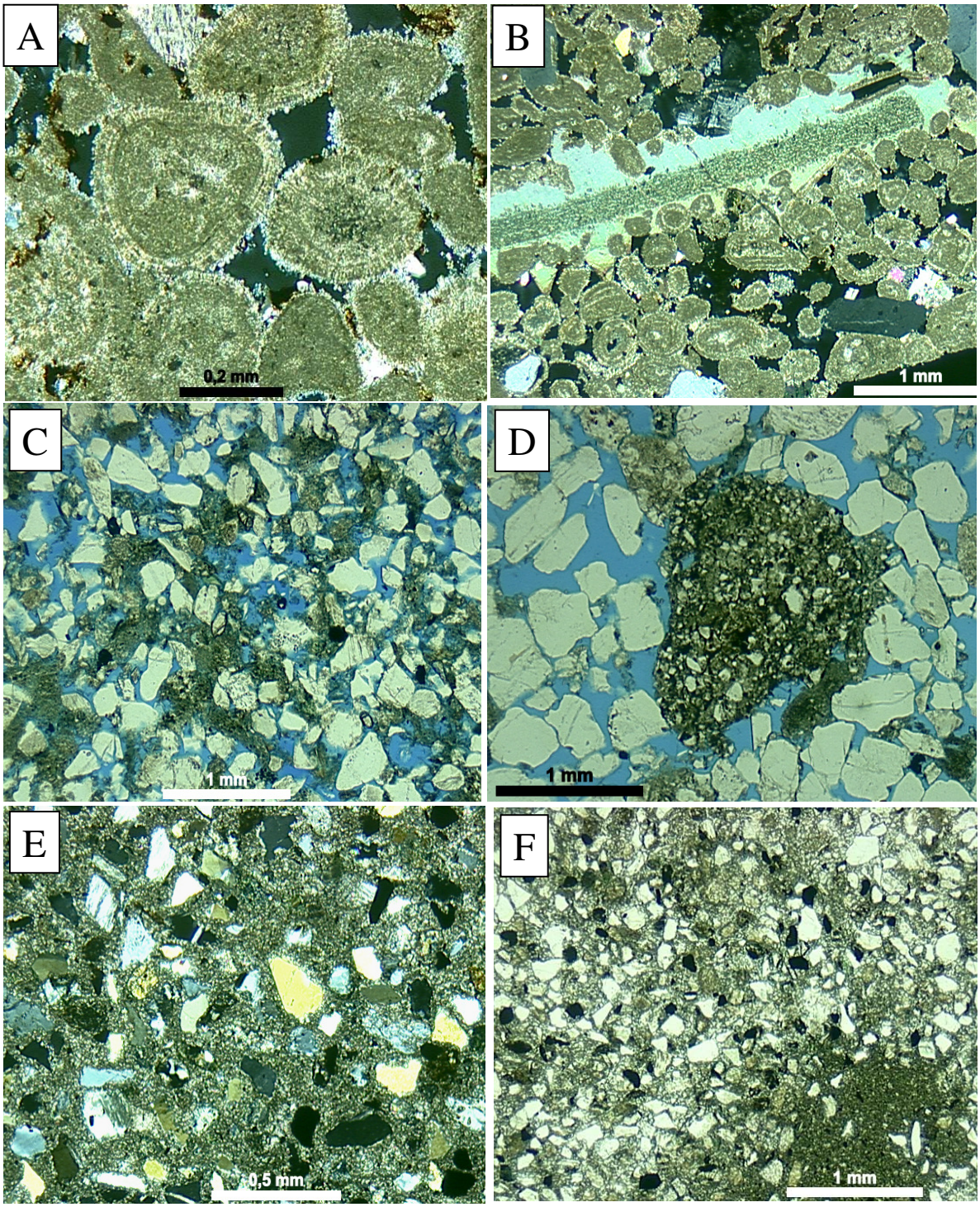

Anexo B-8. Fotomicrografias óticas mostrando: A e B) Petrofácies CmpctOoGr (1525.5m) com cimentação eodiagenética por calcita microcristalina tipo *pore-lining* (envelope micrítico menos espesso que petrofácies CalcHA, resultando maior compactação), e crescimento sintaxial calcita ao redor de equinodermas (XP). C) Petrofácies PoorCemMet (497.3m) com alto percentual em fragmentos de rochas metamórficas de baixo grau, com variáveis valores de preservação de porosidade (//P). D) Petrofácies PoorCemMet (611.1m) com grandes fragmentos de arenitos indicando pouco transporte (//P).C e D) Petrofácies DoloAHA (400.5m) com cimentação por dolomita microcristalina, deslocante, relativamente grossa (multi-fase?) com obstrução completa da porosidade primaria (XP), localmente com presença de intraclastos e formação de pseudomatrix (//P).

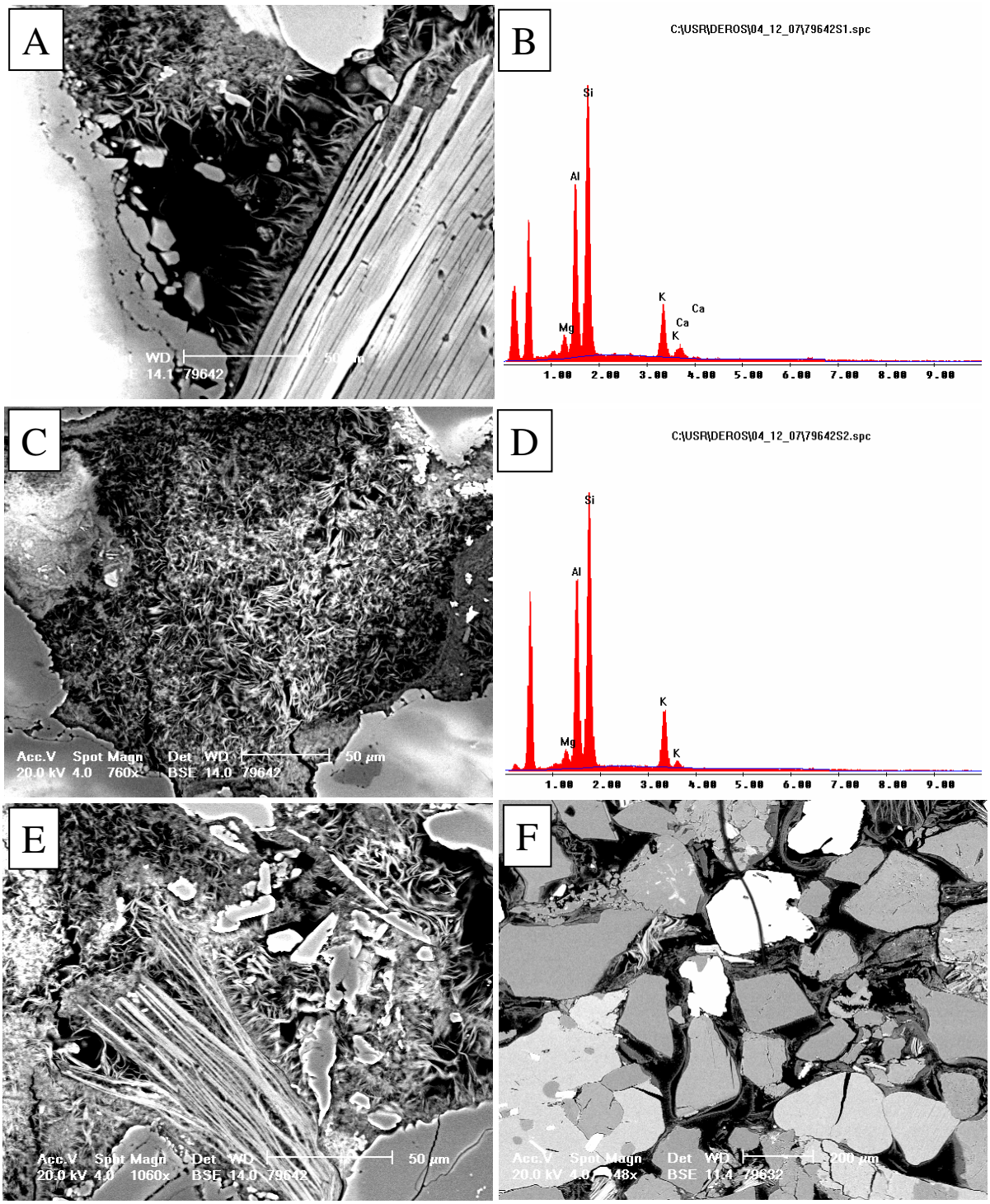

Anexo C-1. Fotomicrografias de microscopia eletrônica (*Backscattering*) mostrando: A) Petrofácies CmpctMica (2786.0m) com franjas de ilita-esmectita (I-S) sobre micas e crescimentos secundários (*outgrowths*) de quartzo. B) Espectro EDS das franjas de I-S. C) Dissolução de grão, possível micáceo em origem, substituído por I-S. D) Espectro EDS das franjas de I-S. E) Franjas de I-S, crescimentos secundários de quartzo e transformação de micas. F) Petrofácies PorsCoars (2012.7m), vista geral de cutículas e franjas descoladas de corrensita.

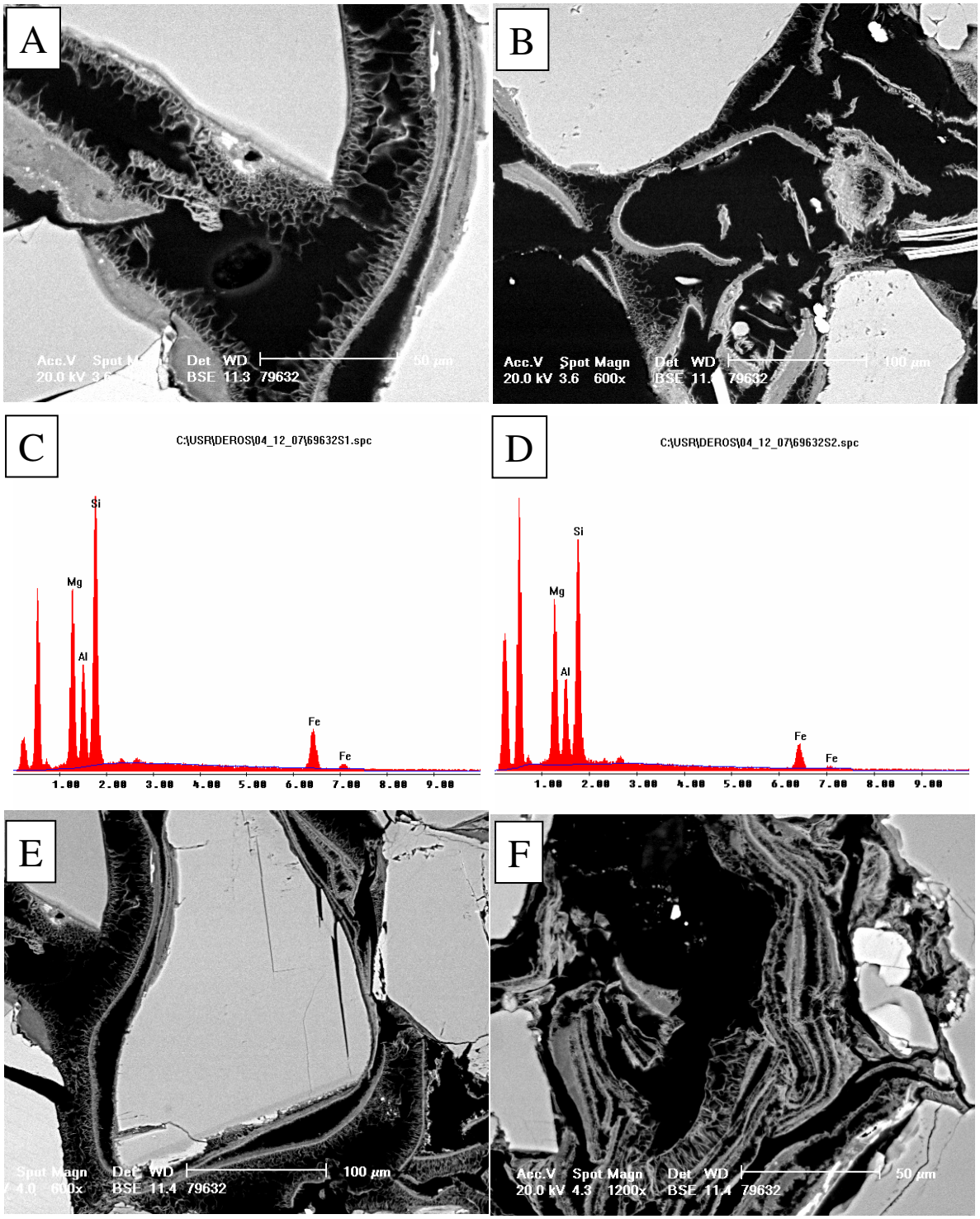

Anexo C-2. Fotomicrografias de microscopia eletrônica (*Backscattering*) mostrando: A) Petrofácies PorsCoars (2012.7m) com franjas de corrensita, morfologia em favo. B) Grãos dissolvidos com espessas cutículas (minerais pesados?). C) Espectro EDS das cutículas pré-compactacionais de corrensita (magnesianas, índices muito superior ao Al). Provável transformação de esmectitas magnesianas precursoras. D) Espectro EDS da franja neoformada de corrensita. E e F) cutículas múltiplas, descoladas, localmente com franjas duplas, mais espessas no lado intergranular. Dissolução de grãos, em especial de minerais pesados, como possível fonte para precipitação de cutículas de esmectitas. Multiplas cutículas com possível origem a partir de continuada dissolução. Recobrimento das cutículas por franjas como produto de diagênese profunda.

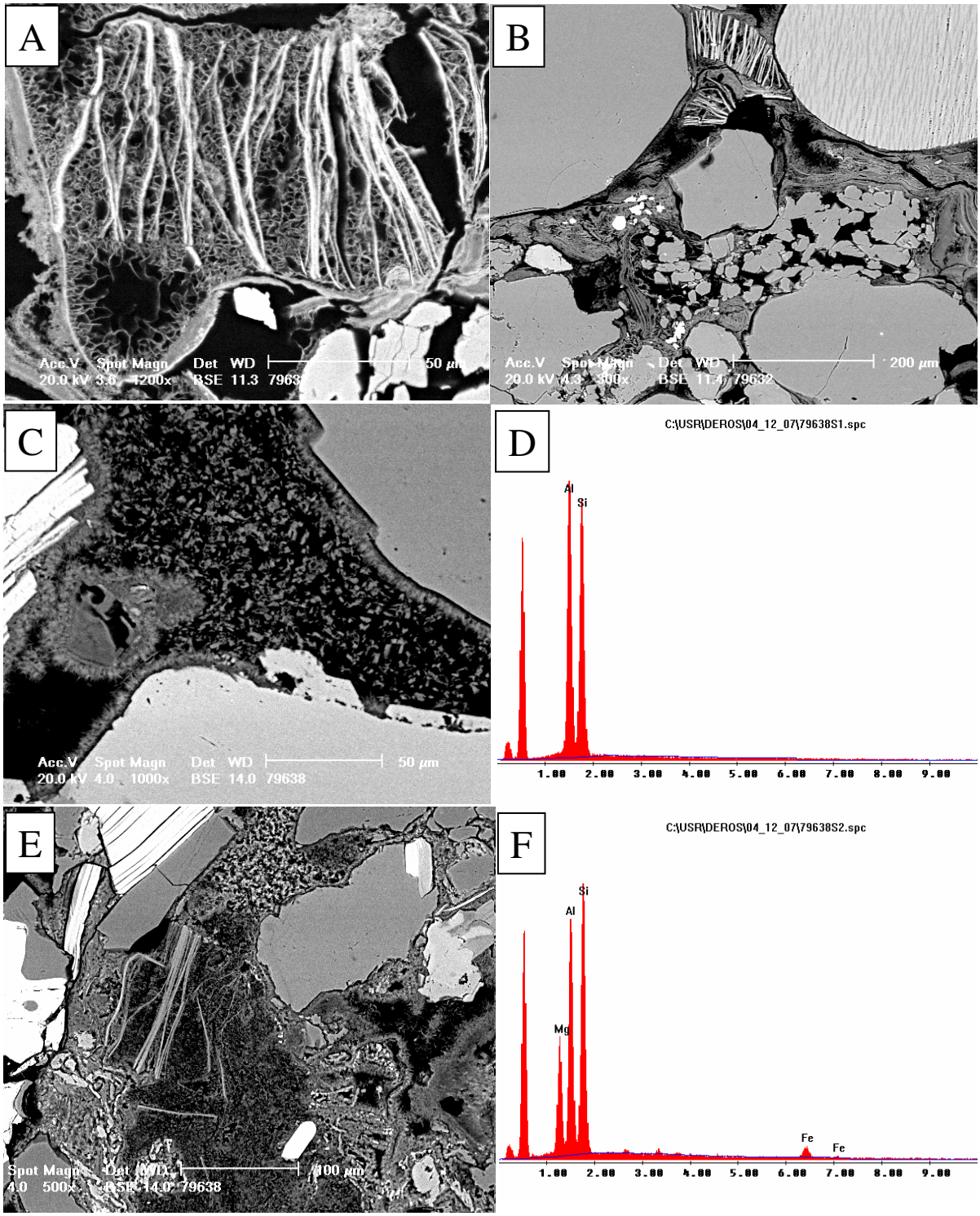

Anexo C-3. Fotomicrografias de microscopia eletrônica (*Backscattering*) mostrando: A) Petrofácies PorsCoars (2012.7m) com mica expandida por corrensita. B). Grãos dissolvidos e substituídos (fragmentos de rocha com quartzo diagenético), e micas expandidas. C) Petrofácies CmpctMica (2476.8m) com franja de clorita competindo com crescimento de feldspato. D) Espectro EDS de caulin (dickita?) *pore-filling*. E) Restos micáceos com clorita. F) Espectro EDS de franja de clorita magnesiana.

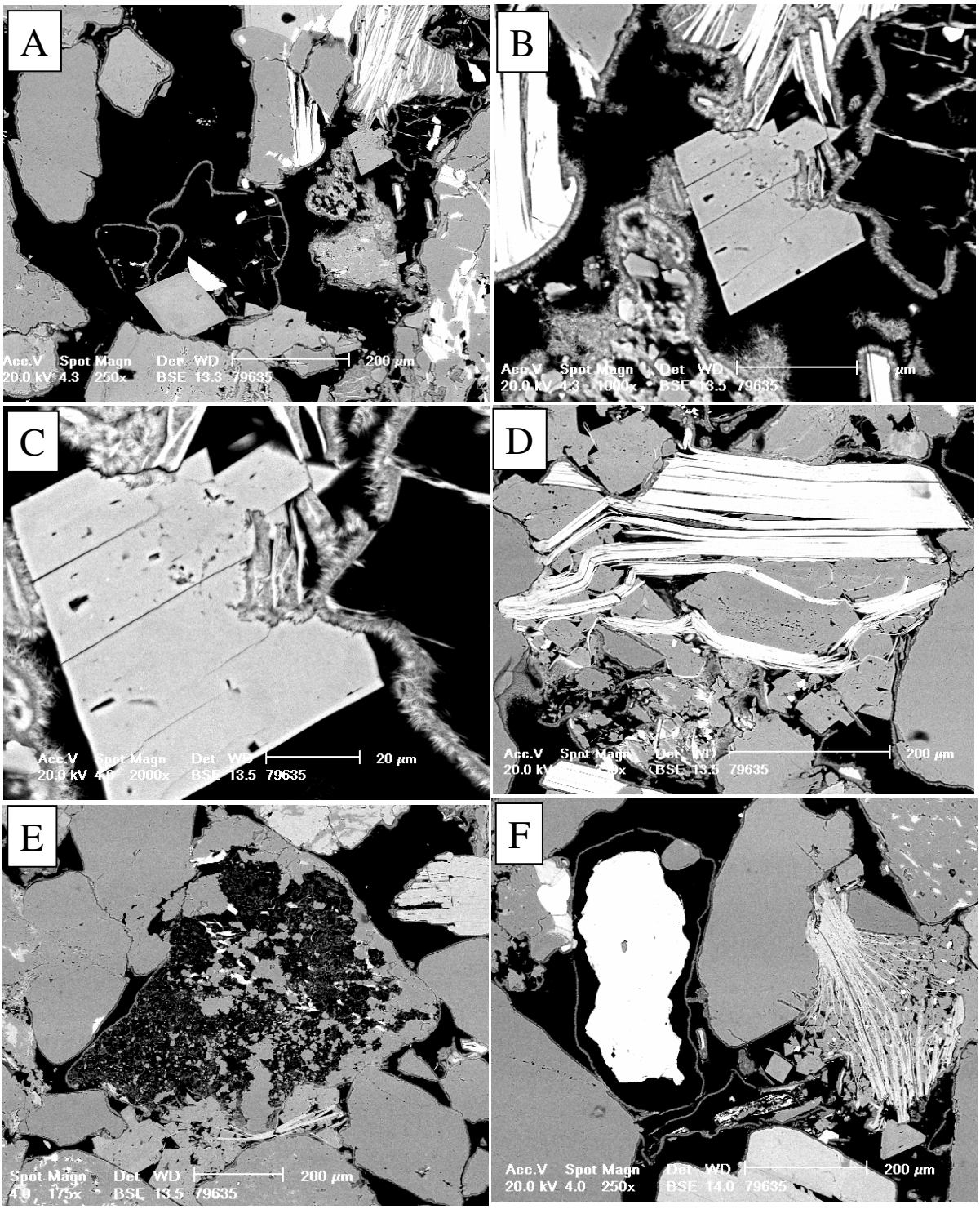

Anexo C-4. Fotomicrografias de microscopia eletrônica (*Backscattering*) da petrofácies PorsCoars (2149.9m) mostrando: A) Franjas de clorita em torno de grãos dissolvidos; cristais de dolomita e fragmento rocha metamórfica. B) Detalhe franjas de clorita e cristal de dolomita. C) Detalhe foto anterior. D) Dolomita expandindo micas (biotita). E) Fragmento meta-sedimentar dissolvido e cloritizado. F) Franja de clorita sobre granada parcialmente dissolvida e micas expandidas por dolomita.

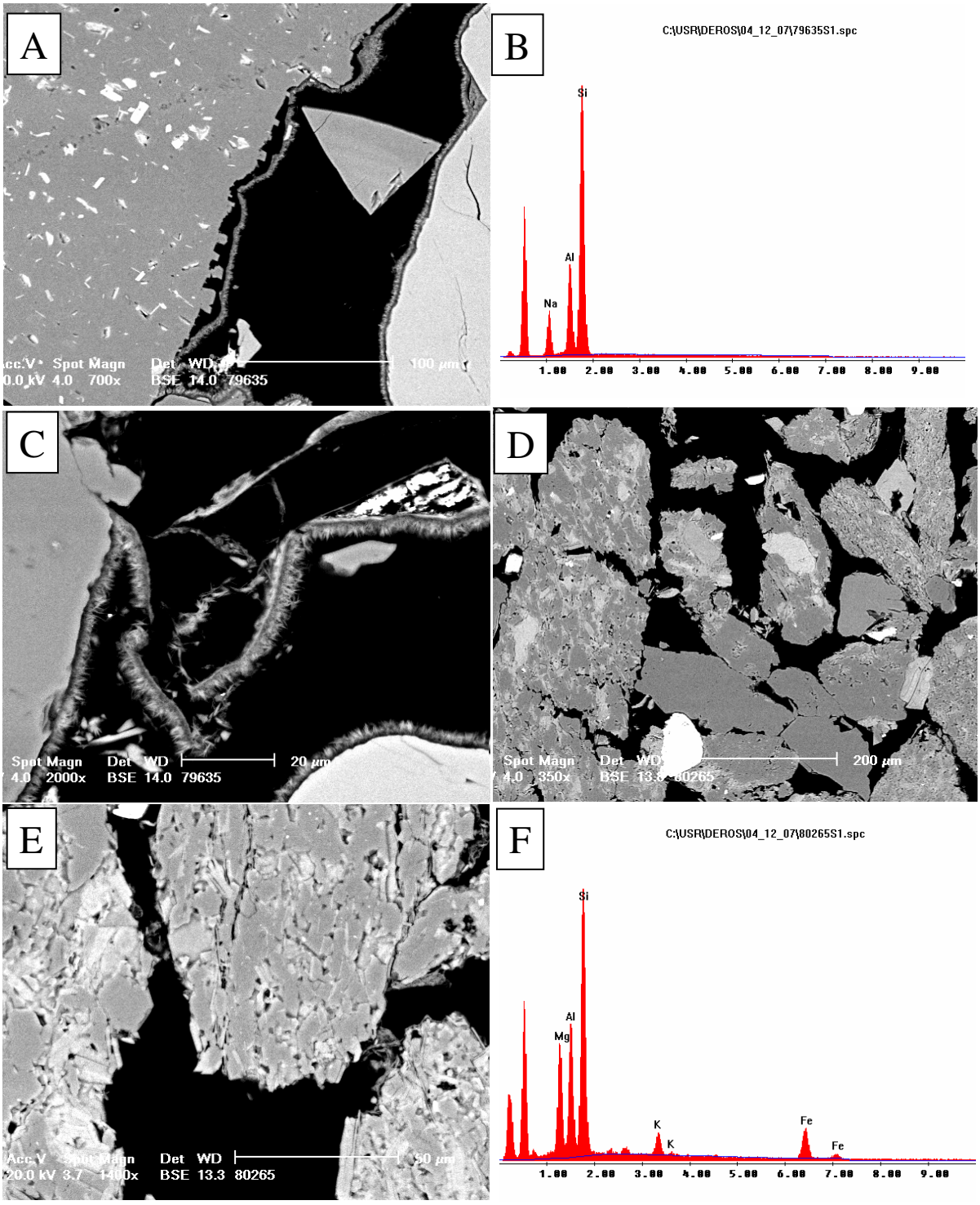

Anexo C-5. Fotomicrografias de microscopia eletrônica (*Backscattering*) mostrando: A) Petrofácies PorsCoars (2149.9m) com fragmento de rocha metamórfica com albita *pore-lining*, pós-datando descolamento da cutícula, franja de clorita e cristal de dolomita “em sela”. B) Espectro EDS da altiba microcristalina abaixo da franja de clorita. C) Detalhe cutículas precursoras e franjas de clorita; grão dissolvido. D) Petrofácies PoorCemMet (1016.0m) fragmentos de rocha metamórficas pouco compactados (com algum fraturamento). E) Fragmentos metamórficos e cimentação por cutículas de I-S. F) Espectro EDS da cimentação intergranular por I-S.

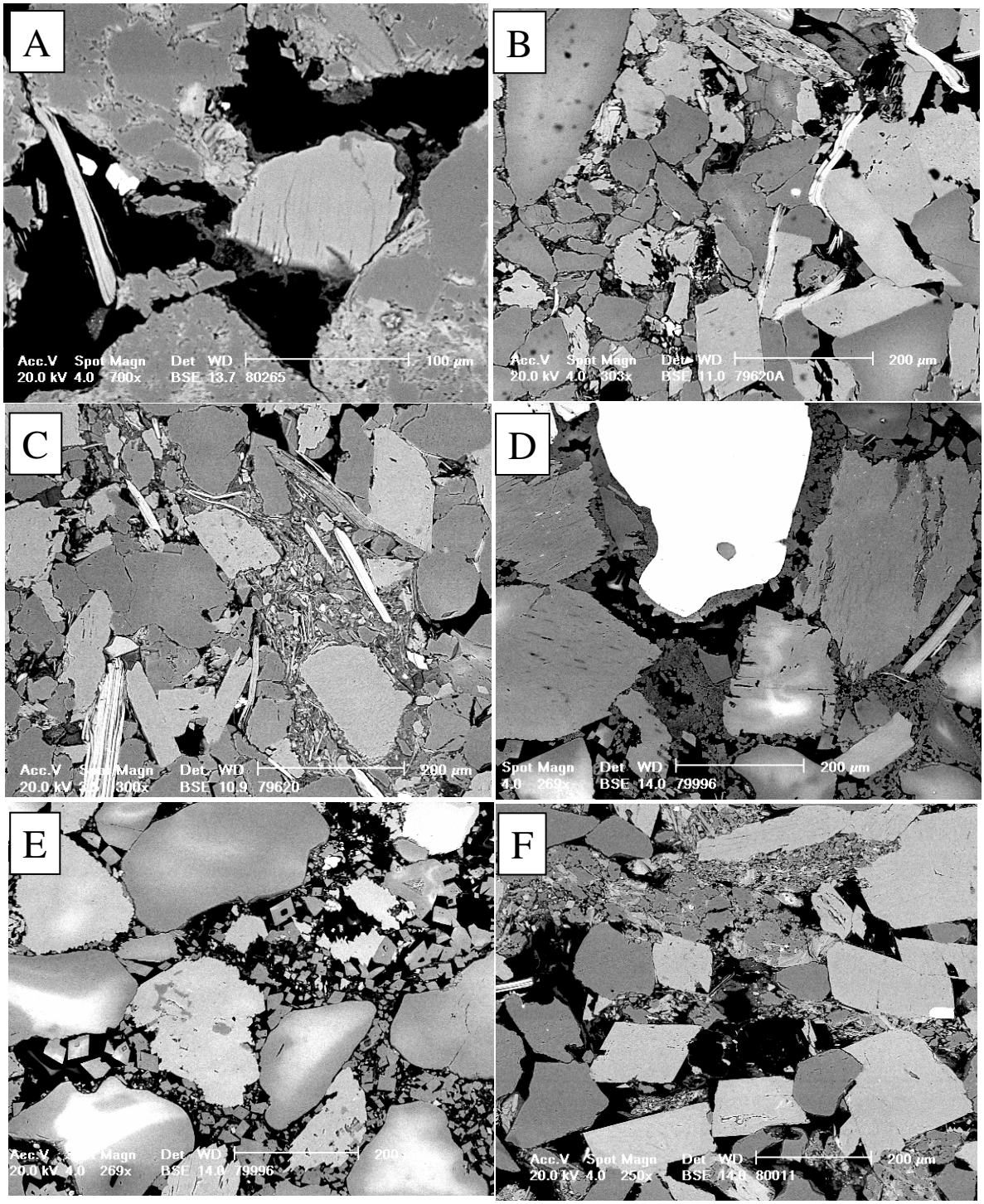

Anexo C-6. Fotomicrografias de microscopia eletrônica (*Backscattering*) mostrando: A) Petrofácies PoorCemMet (1016.0m) com cutículas irregulares de I-S. B) Petrofacies MicrDoloA (1558m) com crescimentos de feldspatos e quartzo, micas e intraclastos, localmente dissolução. C) Intraclastos e micas. D) Petrofácies DoloRimA (1038.0m) com franjas descontínuas em torno dos grãos. E) Dolomita *pore-filling* com alguns núcleos dissolvidos. C) Petrofácies PoorCemMet (497.5m), alto percentual em líticos metamórficos pouco compactados, e grandes crescimentos de feldspatos precoces.

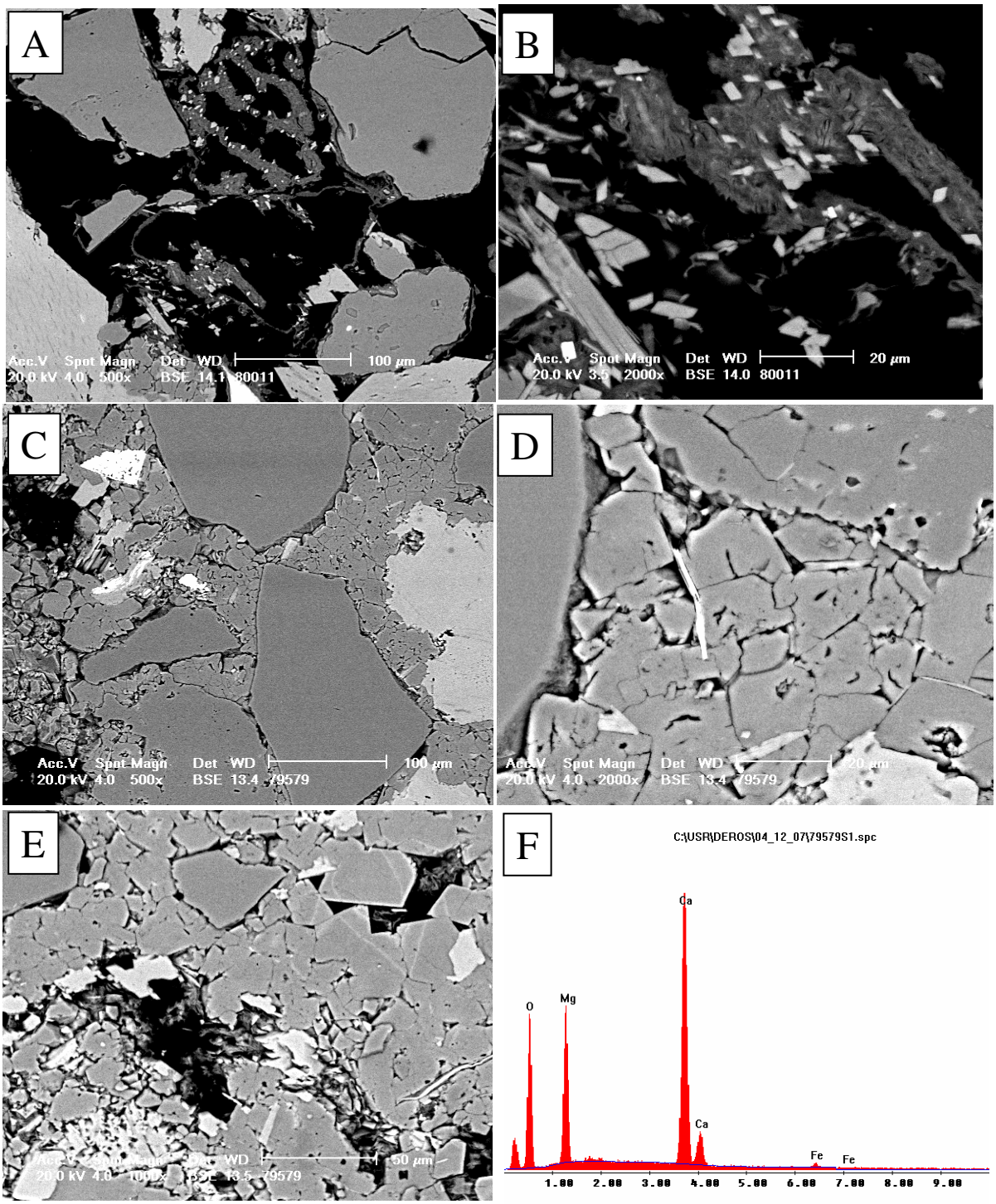

Anexo C-7. Fotomicrografias de microscopia eletrônica (*Backscattering*) mostrando: A) Petrofácies PoorCemMet (497.5m) com cutículas irregulares em torno de grãos de minerais pesados dissolvidos. B) micro cristais de K-feldspato imersos em fase mineral argilosa. C) Petrofácies DoloAHA (400.5m), cimento *pore-fill* dolomita microcristalina a blocosa. D) Detalhe cimento dolomita, com leve zonação (porção externa mais ferrosa). E) Cimentação dolomita com variável cristalinidade (dois tamanhos). F) Espectro EDS do cimento dolomita (levemente ferrosa).

DXR – Sequência R1 (Poço A)

Petrofácies Reservatório CmpctMica

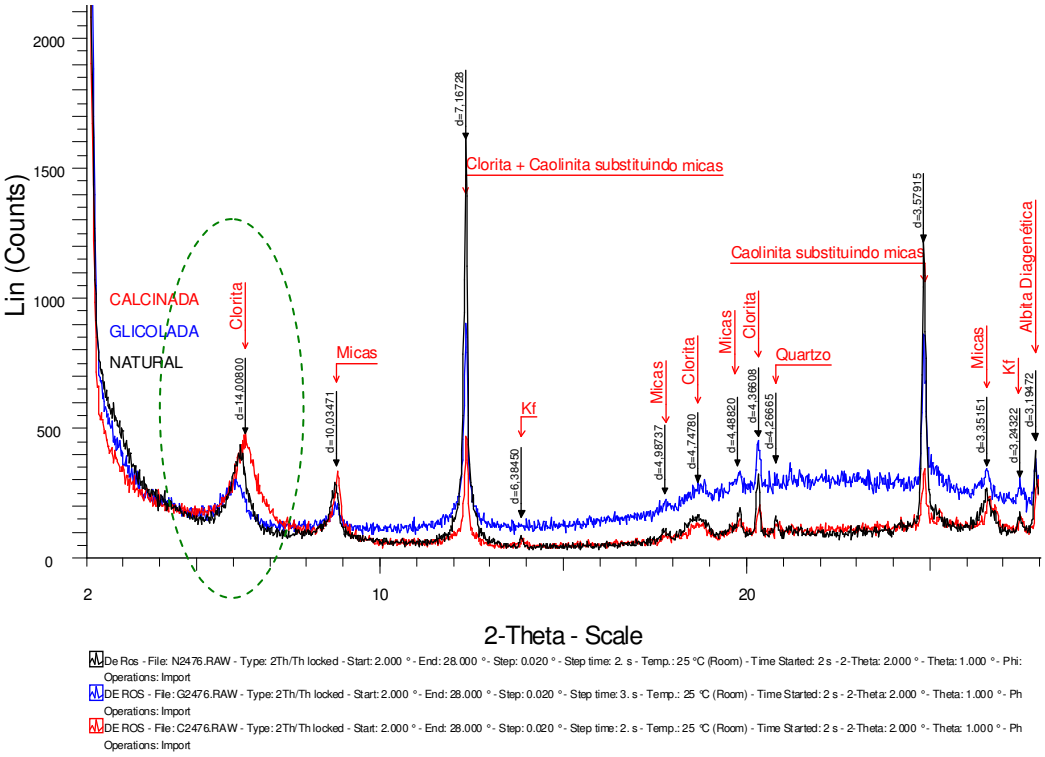

Feições mais significativas:

• Primeiro pico da clorita (14 Å), sem indicação de esmectita, sugerindo completa neoformação (cloritização) das cutículas pré-compactacionais de esmectitas.

• Segundo pico da clorita (7 Å) com valor maior que o primeiro pico (?!), sugrerindo sobreposição com primeiro pico de caulim (7 Å). A presença de caulim é dada pela redução na amostra calcinada. Vê-se presença de caulim (dickita?) em substituição de micas. Espectro de EDS via MEV (Anexo C) identifica dickita em substituição a produto de alteração compondo pseudomatrix (possível fragmento metamórfico micáceo).

Anexo D-1

DXR – Sequência R2 (Poço A)

Petrofácies Reservatório PorsCoars

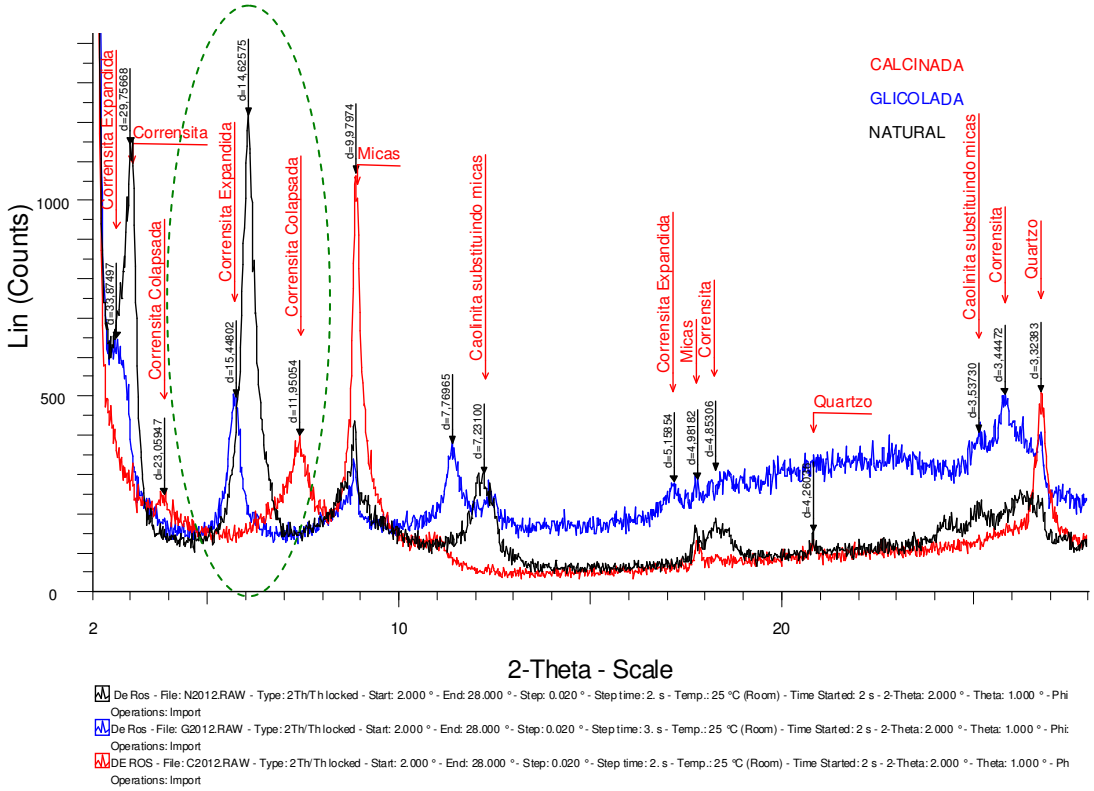

Feições mais significativas:

• Pico da corrensita bem destacado na amostra natural, com pouca expansão (amostra glicolada).

• Picos de ilita (10 Å) interpretados como micas detriticas

Anexo D-2

DXR – Sequência D3 (Poço A)

Petrofácies Reservatório InfClaysA

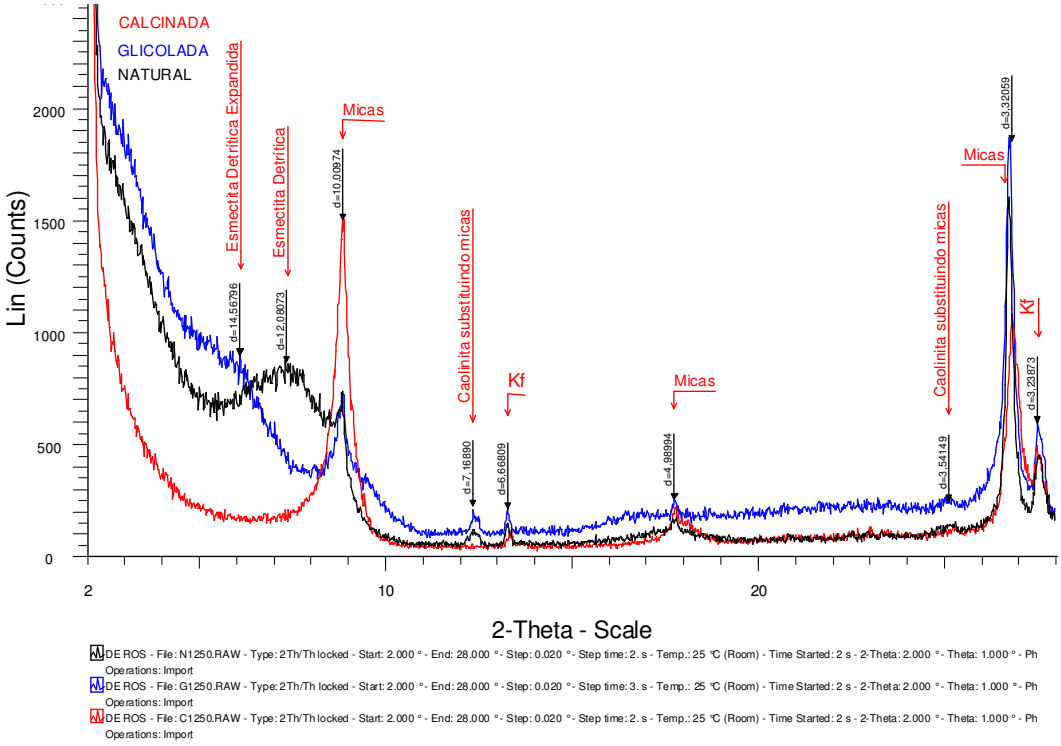

Feições mais significativas:

• Picos de esmectita associados à presença de cutículas de esmectitas detriticas (mecanicamente infiltradas), com pouca expansão (amostra glicolada).

• Picos de ilita (10 Å) interpretados como micas detriticas.

Anexo D-3

DXR – Sequência D4 (Poço B)

Petrofácies Reservatório PoorCemMet

Amostra 1

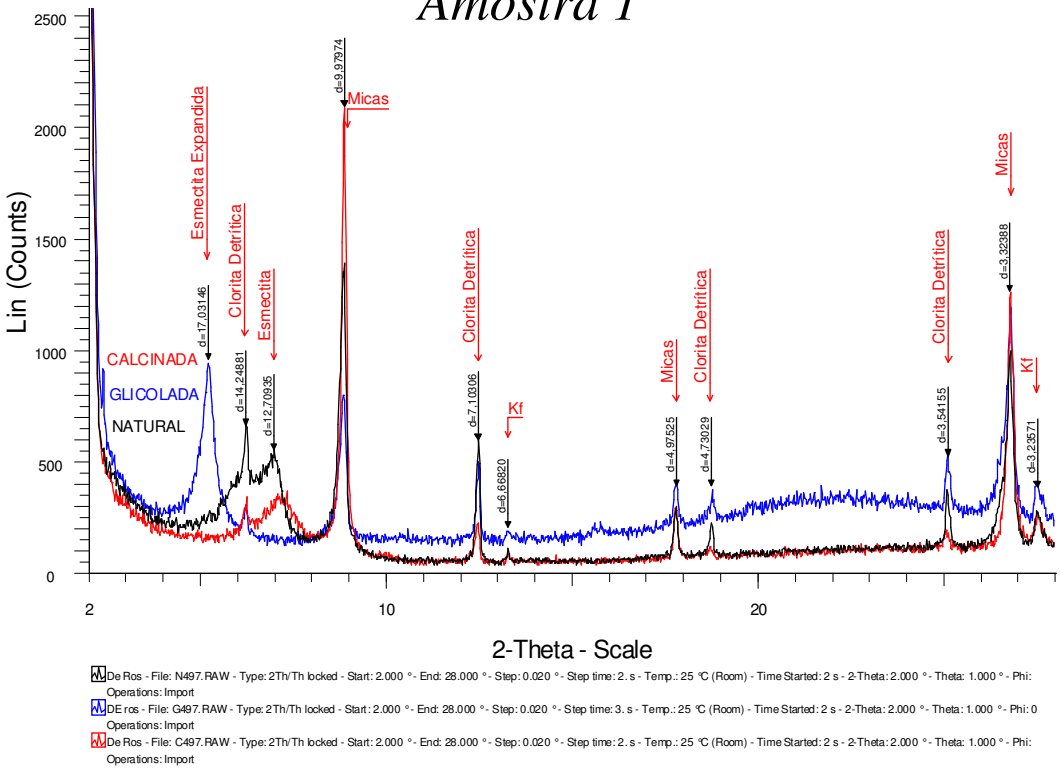

Feições mais significativas:

• Bem destacados os picos da clorita (14 Å) e da esmectita (12 Å), indicando haver as duas espécies, sem presença de interestratificados (C-S).

• Presença dispersa de cutículas de esmectita precipitadas (*in situ*), resultando pico da esmectita.

• A ausência de clorita autigênica na amostra sugere contaminação de clorita detrítica.

Anexo D-4

DXR – Sequência D4 (Poço B)

Petrofácies Reservatório PoorCemMet

Amostra 2

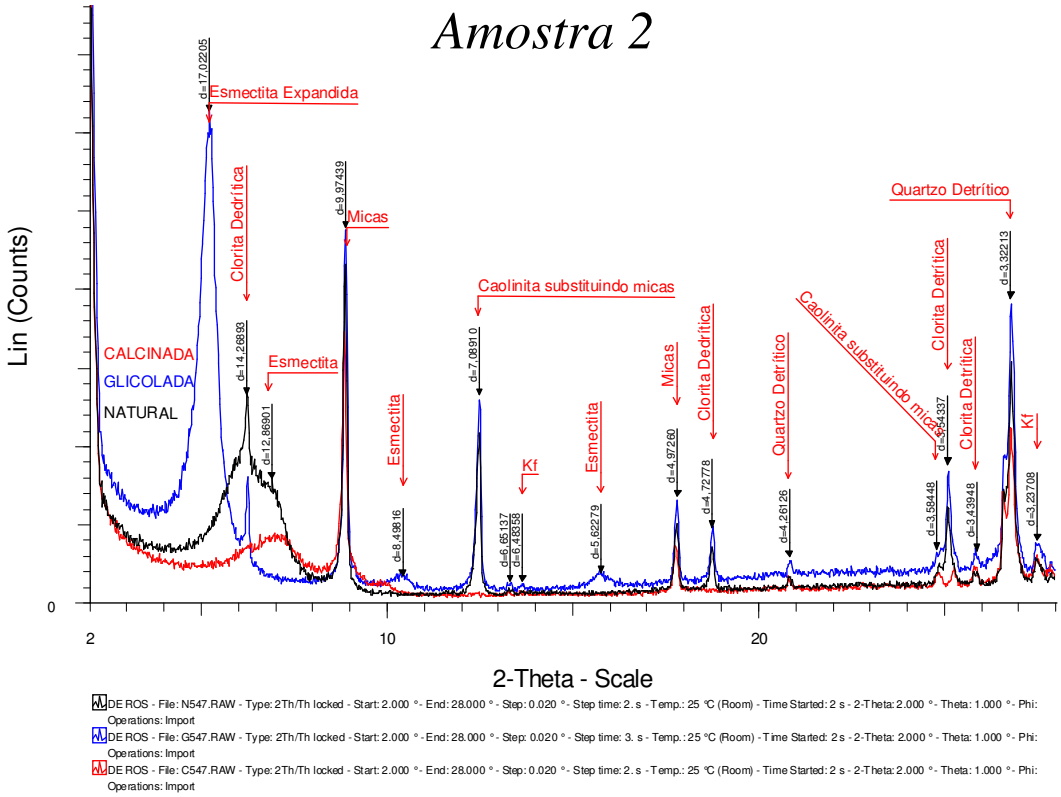

Feições mais significativas:

• Presença de cutículas de esmectitas autigenicas, precipitadas in situ, bem destacadas nos picos das amostras natural e glicolada (alta expansão refletindo estrutura perfeita, em contraste com a estrutura das esmectitas infiltradas).

• Picos da ilita (10 Å) interpretados como contaminação de micas.

• Picos da caolinita (10 Å) resultante da caolonita substituindo micas.

• Picos da clorita interpretado como contaminação de clorita detrítica.

Anexo D-5